REPORT DOCUMENTATION PAGE

AFRL-SR-AR-TR-04-

0459

1. REPORT DATE (DD-MM-YYYY)	2. REPORT TYPE	3. DATES COVERED (From - To)
August 31, 2004	Final	Feb 1, 2003 - May 31, 2004

4. TITLE AND SUBTITLE
Passage of Energetic Particles Through Matter

5a. CONTRACT NUMBER
F49620-03-C-0016

5b. GRANT NUMBER

5c. PROGRAM ELEMENT NUMBER

6. AUTHOR(S)
N. J. Carron

5d. PROJECT NUMBER

5e. TASK NUMBER

5f. WORK UNIT NUMBER

7. PERFORMING ORGANIZATION NAME(S) AND ADDRESS(ES)

ATK Mission Research
Corporation
735 State Street
Santa Barbara, CA 93101

8. PERFORMING ORGANIZATION REPORT NUMBER

MRC-R-1686

9. SPONSORING / MONITORING AGENCY NAME(S) AND ADDRESS(ES)

Air Force Office of Scientific Research
4015 Wilson Blvd
Arlington, VA 22203-1954

NE

10. SPONSOR/MONITOR'S ACRONYM(S)
AFOSR

11. SPONSOR/MONITOR'S REPORT NUMBER(S)

12. DISTRIBUTION / AVAILABILITY STATEMENT

UNLIMITED DISTRIBUTION /AVAILABILITY

DISTRIBUTION STATEMENT A
Approved for Public Release
~~Distribution Unlimited~~

13. SUPPLEMENTARY NOTES

14. ABSTRACT

This report collects cross sections for photons passing through matter. A thorough discussion of the background physics is provided, together with graphs for many processes. This material, together with additional similar material for electrons, heavy ions (protons and heavier) and neutrons, is to be published by IOP Publishing, in late 2004 or early 2005.

20040910 056

15. SUBJECT TERMS
Photon, cross section, electron, stopping power, energy loss, scattering

16. SECURITY CLASSIFICATION OF:			17. LIMITATION OF ABSTRACT	18. NUMBER OF PAGES	19a. NAME OF RESPONSIBLE PERSON
a. REPORT	b. ABSTRACT	c. THIS PAGE			N. J. Carron
U	U	U	UNLIMITED		19b. TELEPHONE NUMBER (include area code) (805) 963-8761

THE PASSAGE OF ENERGETIC PARTICLES THROUGH MATTER

This is the final report on contract F49620-03-C-0016, "The Passage of Energetic Particles Through Matter". More material than presented here has been prepared, and will appear as a book published in late 2004 or early 2005 by Institute of Physics Publishing, Ltd., the publishing arm of the British Institute of Physics, Bristol, England.

OBJECTIVES

The work is to collect in one place relevant material on the passage of energetic particles (photons, neutrons, electrons, protons, α particles, and heavier ions) through matter that researchers continually need: charged particle stopping powers and ranges, neutral particle cross sections, mean free paths, dose, fluence-to-dose conversions, etc.

For decades researchers have made use of data on photon cross sections (photoelectric effect, Compton effect, pair production at higher energies) and photon mean free paths; on electron stopping power and ranges in different materials; and on, say, proton range, stopping powers and straggling in solids and gases. These quantities are needed in many areas of importance to defense. Some are:

- Nuclear EMP (photon Compton scattering in air).
- Nuclear SGEMP (X-ray effects on satellites)
- Radiation effects on electronics.
- Spacecraft shielding.
- Designing satellites and exo-atmospheric missiles to survive radiation belts and nuclear bursts.
- Shielding of laboratory neutron, X-ray, or β sources.
- Ionization produced in gases and solids by the passage of energetic particles.
- Damage to vacuum windows by beam transmission.

The immediate objective was to prepare a manuscript, suitable for presentation to a commercial book publisher, that contains an appropriate level of theoretical discussion, formulae when available, graphs (many never published before nor available anywhere else), and numerical data on a CD-ROM, on the useful parameters of photons, electrons, neutrons, protons, and alpha particles passing through matter. The intent is to provide in one place an authoritative discussion and data for the needed cross sections, mean free paths, stopping powers, ranges, dose, fluence-to-dose conversions, etc. constantly required by researchers.

The principal intended audience is the community of physics and engineering workers in the fields of aerospace research, engineering, and design; spacecraft and missile shielding (military, AF; as well as civilian, NASA); charged and neutral particle beam research; the nuclear weapons

effects community; the design of earth-orbit and interplanetary space craft; and the many disciplines involving nuclear physics, such as nuclear particle detectors. The academic community should also find it of interest, as may the large field of radiological health, but they are not the primary targets.

FEATURES OF THE WORK

Although much of the material is available somewhere in the literature, there is value in collecting it in one place, to save much time searching. In addition, some material is new. Some examples are

1. Plots of a cross section *vs Z* for selected energies. Web-based data makes it possible to plot data this way. Figure 2.5 shows the standard plot of, say, photo-electric cross section in seven elements as a function of photon energy. Figure 2.6 plots the same cross section as a function of *Z* for selected photon energies. Although similar plots for some quantities have appeared in the literature, it is not common to think of cross sections as a function of *Z*. It is useful when seeking a material with desired properties.
2. Quantities of interest (cross sections, ranges, etc.) are, of course, functions of incident particle energy *E* for each element. They are therefore actually functions of *Z* and *E*, and so contour plots of cross sections, ranges, stopping powers, and mean free paths as functions of *Z* and *E* can be constructed. For example, Figure 2.52 shows photon total cross section for all elements at all energies. This plot compresses all 92 tables (for the 92 elements) of cross section *vs E* for each element into one plot. This is also useful when seeking materials with desired properties, for spotting trends, and for making quick calculations on any material.
3. Introduction of the useful concept of (electron) Bremsstrahlung photon number yield, as used in the Al penetration problem. This is an extension of the discussion in Mission Research Corporation report N-1079, which treats the number of photons continuously emitted by a live electron with instantaneous energy *E*, during its life while slowing down.

Another reason to put all this into one place is that researchers experienced in the use of these concepts for defense purposes are getting older. Their expertise will be lost if it isn't documented. New workers need a place to learn. The easier we make if for them the better.

The full document is comprised of five chapters:

Chapter 1: Introduction
Chapter 2: Photons
Chapter 3: Electrons
Chapter 4: Protons and Heavier Ions
Chapter 5: Neutrons

The present document is Chapter 2, Photons.

CHAPTER 2

PHOTONS

CHAPTER 2

PHOTONS

Circumstances arise in which one has need to study the passage through matter of photons with wavelength λ from as long as hundreds of kilometers or more (radio waves, photon energies $\lesssim 10^{-11}$ eV) to as short as the size of a nucleus (γ rays, energies $\gtrsim$ 100 MeV). Not surprisingly, over this 19 or more orders of magnitude in photon energy, the physics of the interactions between photon and matter varies widely. Somewhat surprisingly, there are only about four basic processes that control the entire span of energies. At long wavelengths photons interact with bulk matter as a whole; a classical description parameterizing the matter with a conductivity, dielectric constant, and magnetic permeability applies. As wavelength decreases individual photon-atom interactions dominate, and photoelectric absorption, Compton scattering, and pair production become successively the dominant process. Pair production remains the dominant process for all photon energies above about 100 MeV.

For interactions with matter in bulk, the primary focus of the subject matter in this book, a first distinction can be made based on the photon wavelength compared with the size of an atom. All atoms are of order one Angstrom (1 Å = 10^{-8} cm) in radius, and the distance d between atomic planes in (ordered) solids is of order a few Angstroms. In the interaction with condensed matter this leads to a basic difference between the cases in which photon wavelength is much less than or much greater than about one Angstrom. The distinction is important, especially at long wavelengths, because most atomic cross section data bases, such as those used to construct graphs in this book, are the cross sections for photons interacting with free, isolated atoms at a very low temperature, i.e., neglecting thermal effects and changes in atomic structure due to interaction with neighboring atoms.

2.1 LONG WAVELENGTHS

When λ is long compared with d (photon energies roughly less than a few keV), the photon interacts coherently with many atoms and with many atomic planes. In ordered solids, such as crystals, phase coherence is preserved, and gives rise to interference which reflects the lattice structure. However, in liquids or amorphous solids phase coherence is lost because of the random positions of the scattering atoms. With such long wavelengths compared to the target (atom) size, the photon is not fruitfully thought of as a particle, so far as its interaction with the material target is concerned. Instead, the wave nature of the photon dominates its behavior, and the long wavelength photon appears to be propagating through a "continuous" medium. Classical electromagnetics then allows the target medium to be characterized with electromagnetic parameters different from vacuum (dielectric constant ϵ, magnetic permeability μ, conductivity σ). The transmission can be treated by a conventional (complex) index of refraction $n = n_r + in_i$ as a function of photon energy $E = h\nu$ or of wavelength $\lambda = c/\nu$. The real and imaginary parts of the index of refraction can vary wildly with wavelength, due to resonances arising from atomic or molecular levels

comparable with the photon energy.

In some plasma or astrophysical applications, and when the gas is mono-atomic rather than molecular, the material density can be, or course, far below that of conventional solids. In such cases a photon does interact independently with each atom as it traverses the medium, and individual photon–atom cross sections are the appropriate parameters for describing the passage of photons through this gaseous matter.

Likewise, in diatomic or polyatomic gases, a restriction similar to that applying to condensed matter holds. At relatively long wavelength ($\lambda \gtrsim$ a few Angstroms, $E \lesssim$ a few keV), the photon interacts with the molecule as a whole, not with its individual constituent atoms. The photon–molecule scattering cross section is not the incoherent sum of free atom cross sections. Molecular rotational and vibrational modes, and molecular electronic levels, are completely absent in free atom cross sections, and absorption edges or ionization potentials are changed in the molecule. For example, the ionization potential of the H atom is 13.598 eV, and that of atomic O is 13.618 eV, while that of an isolated H_2O molecule is only 12.61 eV. For understanding the propagation of long wavelength photons through polyatomic gases, one needs the correct photon–molecule cross sections. While these can be computed approximately, they are best obtained from experimental measurements.

The fact that low energy photons do not interact with solids, liquids, and polyatomic gases the same as they do with free, isolated atoms, is no surprise, and is well appreciated. A quantitative comparison to demonstrate the actual differences as a function of energy is worthwhile. One can see at what energies the use of free atom cross sections becomes inaccurate. Below these energies, more accurate photon propagation models or, better yet, actual data on photon attenuation, must be used.

Limits of Applicability of Free Atom Cross Sections in Condensed Media at Long Wavelength

In condensed matter atoms are closely packed so that their atomic orbitals and energy states are distorted from their free atom configurations by the effects of neighboring atoms. In metals the distortion is so great that the outer electrons normally bound in an isolated atom become unbound and free to move as conduction electrons throughout the solid. In Al, for example, the three M-shell electrons of the isolated atom become the free conduction electrons in the solid.

The actual scattering cross section from each atom therefore differs from that when the atom is isolated. In addition, photons may interact with solids, and be scattered or absorbed, by non-atomic processes altogether, such as phonon excitation or plasmon excitation [Ly85, Mi85]. These facts limit the applicability of photon–free atom cross sections to condensed media. These limits can be demonstrated by comparing calculations based on free atom cross sections with experimental data on the passage of relatively long wavelength photons through solids and liquids.

A point of comparison is usefully made via the measured total photon attenuation through solids or liquids at room temperature. Experimental attenuation is obtained from tabulated indices of refraction.

With this one can compare the attenuation that would be predicted using photon–free atom scattering.

Long wavelength photons are often characterized by their wavelength λ rather than their energy $E=h\nu$. The connection, of course, is

$$E(\text{eV}) = h\nu = hc/\lambda = 12{,}398/\lambda(\text{Å}).$$

The experimental real and imaginary parts of the index of refraction, n_r and n_i respectively, in many materials as a function of wavelength are tabulated in [Pa98]. The attenuation is obtained from them as follows.

The electric field of a plane electromagnetic wave of vacuum wavelength λ and wavenumber $k = 2\pi/\lambda$ behaves as

$$E = E_0 e^{inkx} = E_0 e^{in_r kx} e^{-n_i kx} \tag{2.1}$$

as it propagates through the material with index of refraction $n=n_r+in_i$ in the $+x$ direction. Its amplitude decays exponentially with depth x as $\exp(-n_i k x)$, and its intensity, proportional to E^2, decays as $\exp(-2n_i kx)$. These are the amplitude and intensity of the remaining propagating wave. Its energy has been lost to nonconservative processes, parameterized by n_i which represents a possible electrical conductivity and/or imaginary part of the dielectric constant $\epsilon = n^2$.

It is common to introduce the parameter

$$\alpha = 2n_i k = 4\pi n_i/\lambda \ , \tag{2.2}$$

so that the intensity depth dependence may be written $\exp(-\alpha x)$. α has the dimensions of an inverse length, and is the *attenuation coefficient*. Its inverse, $1/\alpha$, is the *attenuation length*, the distance at which the intensity drops to $1/e$ of its initial value. From experimental data on n_i, one constructs α via Eq(2.2).

On the other hand, in the free atom picture, we consider a photon flux of intensity I (say, ergs/cm^2/sec) passing through a tenuous material where photon–free atom cross sections are applicable. Let N be the density of scattering atoms, and σ the total scattering cross section. $N\sigma$ (cm^{-1}) is the scattering cross section per unit volume. In a distance dx the unscattered intensity of this photon beam, I, is reduced by

$$dI = -IN\sigma dx \tag{2.3}$$

and so the intensity at depth x is

$$I(x) = I_0 \exp(-N\sigma x) \ , \tag{2.4}$$

where I_0 is the original intensity. Then $1/N\sigma$ is the distance at which the intensity drops to $1/e$ of its initial value. This $N\sigma$, where σ is the photon–free atom total cross section, may be compared with the α, Equation(2.2), determined from the experimental index of refraction. They will agree to the extent that photon–free atom cross sections are applicable.

We show two examples of this comparison, in Aluminum and in water. First consider Al.

Long Wavelength Photon Attenuation in Metallic Aluminum

The upper graph in Figure (2.1) shows n_i vs $E = h\nu = hc/\lambda$, constructed from measurements of n_i vs λ or the imaginary part of $\epsilon=n^2$ vs λ presented by Smith, Shiles, and Inokuti [Sm85]. The Al K-edge at 1.56 keV is evident. From n_i we construct α, Eq(2.2), which is shown in the lower graph (solid line).

This α is to be compared with $N\sigma$. σ is the photon-free Al atom total cross section. For it we use the value tabulated by Lawrence Livermore National Laboratory in the EPDL97 data base, which extends from 1 eV to 100 GeV. The quantity $N\sigma$ is plotted as the dashed line in the same graph. Were the photon-free atom cross sections applicable to solid Aluminum, the two curves should agree. In fact, they agree only above about 500 eV. Below this energy, and especially below about 50 eV, they differ by up to an order of magnitude. (Cross sections below 100 eV compiled in EPDL97 are not to be believed with great accuracy. See discussion in section 2.11 below. Nevertheless, the point to be made here is clear.)

The free atom Al L-edges (L_1=119.05 eV, L_2=81.2 eV, L_3=80.7 eV) are seen in the dashed line. In the data, solid line, they are distorted, and the lowest L edge has been down-shifted about 8 eV to approximately 72.6 eV. (The Al M1-edge is at about 10.16 eV.)

Below about 15 eV the actual absorption is nearly an order of magnitude greater than that implied by free atom cross sections. The reason has to do with Al valence electrons.

In metallic Al of mass density $\rho = 2.698$ gm/cm^3, the atomic number density is

$$N = N_A\rho/A = 6.022\times10^{22} \text{ atoms/cm}^3,$$

where

$$N_A = 6.022\,142\times10^{23} \text{ per mole}$$

is Avogadro's number, and $A = 26.982$ is the atomic weight. Al releases three valence electrons per atom, which are the "free" electrons that are responsible for its electrical conductivity. Thus the free electron density in metallic Al is $N_e = 1.807\times10^{23}$ elec/cm^3. The plasma frequency of these electrons is $\omega_p = (4\pi e^2N_e/m)^{½} = 2.398\times10^{16}$ rad/sec, or $f_p = \omega_p/2\pi = 3.817\times10^{15}$ Hz.

Now a collisionless plasma is opaque to electromagnetic radiation of frequency less than the plasma frequency. For Al the corresponding photon energy is $E = hf_p = 15.78$ eV. Photons of lesser energy cannot propagate in metallic Al. The actual attenuation is not infinite because the electrons are not truly free; they suffer collisions with the background ions, which permits some propagation of the incident wave. The collisions result in only finite attenuation, as shown in the data, where the solid line rises from about 10^5 cm^{-1} to 10^6 cm^{-1} suddenly as E drops below 15.78 eV. No comparable sudden rise is seen in the free-atom cross section calculation, although the photo-electric cross section is rising as E decreases. This attenuation is due

to a bulk plasma effect, entirely non-atomic, and is completely unaccounted for by ordinary photon–atom scattering. A similar plasma attenuation is seen in all metals at their plasma frequency.

Thus free atom cross sections reliably account for photon propagation through metallic Al only for photon energies above about 500 eV.

Long Wavelength Photon Attenuation in Water

A similar comparison can be made in a dielectric, say water.

In Figure (2.2) the solid line shows α for liquid water, constructed as in Eq(2.2) with n_i taken from data presented by Querry, Wieliczka, and Segelstein [Qu91]. The dashed line is the attenuation coefficient calculated from free atom cross sections from EPDL97, as $N(\mathrm{H})\sigma(\mathrm{H}) + N(\mathrm{O})\sigma(\mathrm{O})$, where $N(\mathrm{x})$ is the density of species x, and $\sigma(\mathrm{x})$ is the free atom total cross section. These authors present data only up to 120 eV. Again agreement is poor below at least 120 eV. As the atomic cross sections go virtually to zero below the H K-edge (13.56 eV), the free atom cross sections predict essentially no attenuation below that energy, whereas actual attenuation is substantial.

In liquid water free atom cross sections reliably account for photon propagation only for photon energies above a few hundred eV.

Comparisons in other materials could easily be made. Although many cross section graphs in this book go down to 10 eV, the reader must use judgment when applying them to condensed matter below a few hundred eV. As discussed in Section 2.11, data on the CD-ROM is presented only above 100 eV.

In this long wavelength region, several references are useful:

- The treatment by Ward [Wa94] is a good introduction to the theory of propagation of light through matter (the term "light" is used generically, and includes IR, visible, UV, etc.).

- The three volume set edited by Palik [Pa98] contains thorough data on the real and imaginary parts of the index of refraction of many solids for wavelengths $10^{-4}\,\mu\mathrm{m} \lesssim \lambda \lesssim 1000\,\mu\mathrm{m}$ ($10^{-3}\,\mathrm{eV} \lesssim h\nu \lesssim 10\,\mathrm{keV}$).

- The venerable *IR Handbook* [Wo85] is a storehouse of theory and data on the transmission through materials for wavelengths in the IR (roughly 1 – 100 μm).

- The compilation edited by Klocek [Kl91] includes IR properties of other materials than the *IR Handbook*.

- J. H. Weaver, C. Krafka, D.W. Lynch, and E.E. Koch, *Physics Data: Optical Properties of Metals*, Volumes I and II, No. 18-1 and 18-2. Fachinformationzentrum, Karlsruhe, Germany (1981).

• S.S. Ballard, J.S. Browder, and J.F. Ebersole, Chapters 6b and 6c in D. E. Gray, editor, *American Institute of Physics Handbook*, 3rd Edition, McGraw-Hill, New York, 1972.

• A short table of the index of refraction and absorption coefficients of metals is in the *CRC Handbook of Chemistry and Physics*, e.g., 75th Edition (1994) CRC Press, Boca Raton, Florida.

• The two volume *Handbook of Optics*, Michael Bass, ed., 2nd Edition, McGraw-Hill, New York (1995) contains a wealth of information concerning theory and data on transmission of optical wavelengths through materials.

2.2 SHORT WAVELENGTHS

When wavelengths are comparable with or less than atomic dimensions (i.e., photon energies greater than a few keV), the particle nature of the photon dominates in the interaction with each atom (although, of course, when computing the interaction, its wave nature is used in quantum mechanics)[1]. Then one can think of a particle of light passing through matter, undergoing more or less independent interactions with atoms on the way. Under these circumstances index of refraction is a less useful concept, for the photon does not merely elastically scatter, although an index of refraction can always be defined in terms of the complex scattering amplitude [Ne66].

Rather, each photon in the beam has a certain probability of interacting with an atom, measured by the cross section. For a given atom density, this translates into a certain probability per unit path length of interacting with the bulk material. It can interact with an atom in one of several distinct ways. It may be absorbed by photoelectric absorption, ejecting an electron. It may also elastically scatter from the atom, being a coherent scattering from all atomic electrons, leaving the atom undisturbed in its original state (called *coherent* scattering, or *Rayleigh* scattering). It may Compton scatter from a bound atomic electron, ejecting the electron and scattering off at longer wavelength. (This may be off any electron, leaving the atom in different states, and so is called *incoherent* scattering). Or, in the electric field of the nucleus or the atomic electrons, it may disappear in the production of an electron-positron pair.

In any of these four ways (and other minor ways mentioned below), the original photon is removed from the incident beam. This higher energy range is the subject of this book.

Photons of energy greater than some tens of keV are sometimes referred to as *penetrating radiation.* This historical term derives from the particle's ability to penetrate thin sheets of material, such as Aluminum,

---

[1] The concept of a photon (but not the name) as a "quantum of electromagnetic radiation" was introduced early in the 20th century. Physicists struggled with its meaning, and it was only in 1923 when A. H. Compton did the critical experiment on scattering of light off particles at high energy, and the kinematics were seen to be consistent with those of a (zero mass) particle, that physicists took seriously the concept of a particle of light. The name *photon* was assigned in 1926 by American chemist Gilbert N. Lewis. The story is beautifully told in Pais, *Inward Bound* [Pa86].

and refers in general to radiations that penetrate to some macroscopic distance. Dental and medical X-rays fall in this class, as do nuclear γ rays. Sometimes very energetic charged particles also fall in the class of penetrating radiation. However charged ions (protons, α particles, etc.) must be at higher energies, for the range of a 10 MeV proton in, say, water or polyethylene, is only about 0.1 cm, and the range of higher mass ions is even less. A 10 MeV electron has a range of about 6 cm in polyethylene, and so may qualify as "penetrating".

2.3 PHOTON INTERACTIONS

As mentioned, in general a photon interacts with an atom primarily in one of four ways:

• Elastic scattering in which the atom is left in its original state and a photon of the original energy continues on at a different angle (*Rayleigh* or *coherent* scattering). The photon loses no energy.

• Inelastic scattering in which an electron is ejected and a lower energy photon is emitted (*Compton* or *incoherent* scattering). The photon loses some of its energy.

• *Photo-electric absorption* in which the photon is absorbed, kicking out an electron. The electron shell vacancy is then filled by an outer electron dropping down; the transition may emit a photon (*fluorescence*), or emit a different outer electron (*Auger* effect). Alternatively, its energy may be taken up by the medium by collisional quenching or phonon excitation. (Since fluorescence and Auger emission are so fast ($\lesssim 10^{-11}$ sec) collisional quenching, while possible, is seldom the dominant process). The original photon loses all energy.

• The destruction of the photon and the creation of an electron-positron pair. This occurs in the Coulomb field of the nucleus (*nuclear pair production*) or of an atomic electron (*electronic* pair production, also called *triplet* production). The photon loses all its energy.

These are the dominant four processes. Other possible processes in which the photon interacts with the atomic *electrons*, always small compared with the above four, are

• *First Order Photo-excitation.* In this process the photon is *absorbed* by an electron in a low shell, say the *K* shell, and excited to a high, vacant, bound state of the atom. The recoiling atom provides for momentum conservation. Subsequent de-excitation of the atom may be by emission of another photon (the *Electronic Raman* effect, being a form of fluorescence), Auger emission, phonon excitation (in solids), or by collisional quenching. As vacant, high, atomic states are relatively closely spaced, often by only a few eV, this process is energetically possible only when the photon energy is just a few eV below the *K* edge (or *L* edge, ...). It is manifested in small oscillations in the total absorption cross section just below the *K* edge [Sa88]. Otherwise it is seldom important, partly because such finely defined incident X-rays are seldom encountered in practice. It is, however, more important for absorption of visible and UV photons (from the *L*, *M*, ... shells). At those energies, Electronic Raman scattering can be a useful diagnostic. It is a fairly new subject of research; it is employed, for example, in studying the electronic structure of superconductors [De00]. A

review is in [Te97].

• *Second Order Photo-excitation.* In this process the photon is *scattered* by an electron in a low shell, raising the electron to a high, vacant, bound state of the atom, while the reduced energy photon exits the interaction region (which also defines this as an electronic Raman effect). This is similar to Compton scattering except that the electron is given insufficient energy to be ejected. And, unlike first-order photo-excitation, the incident photon may have any energy. A review of this inelastic X-ray scattering without ionization is given by Åberg and Tulkki [Åb85].

Still other processes, in which the photon interacts with the atomic *nucleus*, also small compared with the primary four processes, are

• *Nuclear Thomson* scattering. This is elastic scattering from the nuclear charge. As it leaves the atom unchanged, it is coherent with Rayleigh scattering. The scattering amplitude for Thomson scattering from a single electron is, to order of magnitude, $r_o = e^2/mc^2$ (see Eq(2.12)). The amplitude for coherent, Rayleigh scattering from the Z electrons in an atom is, to order of magnitude, e^2F/mc^2, where $F(q)$ is the elastic scattering form factor, a function of the momentum transferred to the atom, q (see Eq(2.14)). For small q, $F \sim Z$, but for large q, F is much smaller. However, the amplitude for Thomson scattering from the nucleus is of order $(Ze)^2/Mc^2$, where M is the mass of the nucleus. The nuclear Thomson amplitude is smaller than the electronic contribution by the factor Z^2m/MF. This ratio is about $(Z^2/A)/1837F$, where A is the nuclear atomic weight. At low energies and small momentum transfer, this is of order 3×10^{-4} for all elements, and nuclear Thomson scattering is almost always negligible compared with scattering from atomic electrons. But at high energies (~ 1 MeV), the momentum transfer is also large, F can be less than or of order 0.001, and the ratio can be several percent or more, especially for high Z. At energies greater than or of order 1 MeV in heavy elements nuclear Thompson scattering can interfere with atomic Rayleigh scattering.

• *Non-elastic Nuclear* scattering. This includes the giant dipole resonance, photo-disintegration, photo-pion production, and all non-elastic events. Figure (2.3) shows the non-elastic photo-nuclear cross section on four major isotopes. It is largest at 15-20 MeV, and is usually less than about 5% of the atomic cross section. In Pb^{208}, for example, the photo-nuclear cross section is seen to peak near 14 MeV at about 0.6 barn. At the same energy, the total atomic cross section is about 19 barn (due primarily to pair production). In this example the photo-nuclear cross section is only some 3% of the atomic cross section.

Several countries have constructed photo-nuclear cross section libraries (U.S., S. Korea, China, Japan, Russia). All of these are available at the International Atomic Energy Agency [IAEApn]. At energies near the peak of the giant resonance they agree quite well, but at other energies they can differ substantially from one another. The cross sections plotted in Figure (2.3) are recommended ones. In the figure, only Fe^{56} is shown beyond 150 MeV. The sudden rise at 140 MeV is due to the onset of pion production.

• *Delbrück* scattering from the nuclear field. This is elastic photon scattering from the Coulomb electric field surrounding the nucleus. The incident photon scatters from virtual electron-positron pairs, and is effectively a radiative correction to Compton scattering off the nucleus. Enormous electric fields are

necessary for it to occur with any appreciable probability; the unscreened electric field at $r = 10^{-11}$ cm from a Pb nucleus is 1.2×10^{19} V/m. Like the preceding two nuclear effects, it is never the dominant photon-atom interaction process. But it can be important if attention is restricted to photon elastic scattering from atoms. In high Z atoms at a few MeV incident energy there can be strong interference among atomic Rayleigh, nuclear Thomson, and Delbrück scattering [Ki85].

Below 10 to 100 keV, depending on Z, photons are primarily absorbed by the photoelectric effect. From tens of keV to ~ 10 MeV, the dominant process is Compton scattering. Above this energy pair production is largest.

The scope of magnitude is illustrated in Figure (2.4) which shows individual and total cross sections in Aluminum as a function of incident photon energy $E = h\nu_o$, from 10 eV to 10^5 MeV. Data are taken from LLNL's Evaluated Photon Data Library, EPDL97. They are plotted in units of cm^2/gram, the cross section of 1 gram of Al atoms ($= N_A/A = 2.23\times10^{22}$ atoms). This cross section is related to the individual atom cross section σ(barn/atom) by

$$\sigma(\text{cm}^2/\text{gm}) = 10^{-24}\frac{N_A}{A}\,\sigma(\text{barn/atom}) \qquad (2.5)$$

where N_A is Avogadro's number defined on page 4, and A is the atomic weight (26.98 for Al). For Al, 1 cm^2/gm = 44.80 barn/atom.

Similar cross section plots for other elements are in Section 2.8.

Standard tables of photon cross sections and related material parameters are widely available, and listed below in Section 2.11.

We discuss photoelectric absorption first, in Section 2.4, then coherent Rayleigh scattering in Section 2.5. Section 2.6 presents a fairly thorough set of graphs for Compton scattering.

Section 2.7 briefly discusses pair production, and Section 2.8 summarizes all processes for selected elements, and presents total cross section and mean-free path contour plots for all elements at all energies.

We remark that a popular pocket book , the "X-ray Data Booklet" has recently been re-issued, and is available free of charge from http://xdb.lbl.gov. It contains useful summary information on atomic X-ray properties, synchrotron radiation, electron binding energies, etc.

2.4 PHOTO-ELECTRIC ABSORPTION

Photoelectric absorption is the most probable interaction for photon energies $E \lesssim 10$ keV (for $Z \lesssim 4$), or $E \lesssim 100$ keV (for $Z \lesssim 30$), or $E \lesssim 700$ keV (for $Z \lesssim 90$). It is discussed by Heitler [He54], by Evans [Ev55], and by Bethe [Be53]; thorough plots are in [Pl75].

Remembering that

$$1 \text{ barn} \equiv 1 \text{ b} = 10^{-24} \quad (\text{cm}^2) \tag{2.6}$$

a convenient cross section unit is the Thomson cross section

$$\sigma_T = \frac{8\pi}{3} r_o^{\,2} = 0.665246 \text{ b} \tag{2.7}$$

where $r_o \equiv e^2/mc^2 = 2.818 \times 10^{-13}$ cm is the classical electron radius.

Kinematically a free electron cannot absorb a photon, but an electron bound in an atom can. The less tightly bound it is, the less likely it will absorb. Therefore the atomic photoelectric cross section is largest when photon absorption takes place from the K shell. The K shell binding energy E_K is approximately proportional to Z^2, and the cross section behaves roughly as a power of E_K, making the cross section approximately proportional to a power of Z, roughly between Z^4 and Z^5.

Likewise, the more energetic the photon the more nearly free does the electron appear, causing the cross section to decrease with increasing photon energy.

The calculation of photoelectric absorption is simple only in the Born approximation. In this case, and when the ejected electron is nonrelativistic ($h\nu \ll mc^2$), the photoelectric cross section per atom from the K shell is calculated to be [He54]

$$\sigma_K = 2\sqrt{8}\,\alpha^4 Z^5 \sigma_T \left(\frac{mc^2}{h\nu}\right)^{7/2}, \tag{2.8}$$

when photon energy is not too close to the K edge, where $\alpha = e^2/\hbar c = 1/137$ is the fine structure constant. The factor 2 is because there are two electrons in the K shell. Some distance from the K edge is required for the validity of this equation so the outgoing electron is energetic enough for the Born approximation to be valid.

Being simple absorption, one might expect the cross section for the photo-electric effect to be proportional to the square of the coupling constant e. But, as Thomson scattering is a second order process, $\sigma_T \propto e^4$, and $\alpha \propto e^2$, σ_K is seen to be proportional to e^{12}. The interaction Hamiltonian is, of course, of first order in e. However, the initial state (K shell) wave function contains e in its radial dependence $\exp(-Zr/a_o)$, where $a_o = \hbar^2/me^2 = 0.529$ Å is the Bohr radius. The other powers of e beyond 2 in (2.8) for σ_K arise then from initial state normalization and from evaluation of the matrix element integral itself, which brings a_o down from the exponent into an overall factor, making σ_K proportional to a high power of e.

For very relativistic energies, when $h\nu \gg mc^2$,

$$\sigma_K = \frac{3}{2}\alpha^4 Z^5 \sigma_T \left(\frac{mc^2}{h\nu}\right), \tag{2.9}$$

and the cross section drops off only as $1/h\nu$. A more general formula holds in the moderately relativistic

case $h\nu \sim mc^2$ [He54]. These expressions also hold only for sufficiently small Z (again for the Born approximation to be valid).

The strong dependence on Z means the photoelectric effect can still be important in heavy elements even at energies (~ 1 MeV) where the Compton effect is expected to dominate.

Calculations are simple, and very approximate, only for the elementary cases just mentioned. L and M shells should be added, the Born approximation must be circumvented, and all energies, including near edges and relativistic energies, must be computed, to obtain the actual photoelectric cross section per atom, $\sigma_{pe}(h\nu)$. These calculations are done numerically using Dirac-Hartree-Fock and related sophisticated wave function models.

Absorption in the K shell contributes the dominant amount to the total atom cross section. As a convenient rule of thumb, L, M, and higher shells contribute about 1/4 that of the K shell, so that $\sigma_{pe}(h\nu) \approx (5/4)\sigma_K$. However, over all Z and photon energies $h\nu$ the atom cross section $\sigma_{pe}(h\nu)$ does not behave as a single power of Z or of $h\nu$. Davisson and Evans [Da52] have reviewed theory and experiment for the photoelectric cross section.

Experimental atomic cross sections and theoretical models have been evaluated by NIST, and by Lawrence Livermore National Laboratory. See Section 2.11 below. Their compilations are widely used. We present some of these data here.

Figure (2.5) shows the photo-electric cross section (cm^2/gm) for several elements as a function of E, while Figure (2.6) shows it for selected energies as a function of Z.

Cross Section Contour Plots

For each element the photoelectric cross section $\sigma_{pe}(E)$, or the cross section for any other process, is a function of $E = h\nu$. That is, the photoelectric cross section, or the cross section for any other given process, is a function of Z and E, and so forms a surface in Z, E space. The cross section for all elements at all energies can then be represented by contours in that space, and one can grasp at a glance the behavior with both variables, over all energies and all elements.

Contours in barn/atom

Contours of the photoelectric cross section on a free, isolated atom at rest, $\sigma_{pe}(Z,E)$, in barn/atom, are shown in Figure (2.7). The figure extends down to 100 eV. The user must observe the caveat in Section 2.1 when employing them in condensed media below several hundred eV.

In contour plots, and in graphs of cross sections vs Z such as Figure (2.6), data exist, of course, only at integer Z. Between integral values of Z the curves have no meaning; they serve primarily as an eye guide.

The complete photoelectric cross section on an atom, σ_{pe}, has about the same dependence on Z as σ_K above. While σ_{pe}(b/atom) $\propto Z^4$ to Z^5, if one expresses it as cm^2/gm by multiplying by the number of atoms per gram:

$$N_g = N/\rho = N_A/A\ ,$$

where N(cm^{-3}) is the number of atoms per unit volume, ρ(gm/cm^3) is the target mass density, and A is the element atomic weight, σ_{pe}(cm^2/gm) scales more nearly between Z^3 and Z^4 since ρ is nearly proportional to Z.

Contours in cm^2/gram

In switching from σ_{pe}(b/atom) to

$$\sigma_{pe}(\text{cm}^2/\text{gm}) = 10^{-24}\,\frac{N_A}{A}\,\sigma_{pe}(\text{b/atom})$$

the Z dependence shifts due to the dependence of A on Z. First, the Z dependence shifts down one power of Z as just mentioned. Second, A is not exactly proportional to Z; there are small, local deviations. The atomic weight $A(Z)$ of the elements in their natural isotopic composition is shown in Figure (2.8). The smooth, monotonically increasing dependence on Z is interrupted at Z = 18-19, 27-28, and 52-53, where A momentarily decreases with increasing Z. Other irregular behavior can be seen at different Z in the figure. This irregular dependence causes the irregularities in the contour plot of σ_{pe} (cm^2/gm), Figure (2.9), at those values of Z. The irregularities are not very significant in this figure since they are small compared to the difference between adjacent contour lines. They are more pronounced when contour values are more closely spaced, as in the Compton cross section discussed later, Figure (2.42).

X-ray Edge Energies

Photo-absorption in the K (or L, or M, ...) shell can occur, of course, only for photon energies greater than that shell's absorption edge. Some edges for the elements are shown in Figure (2.10). The K edge in Al is 1.56 keV, that in Pb is 88 keV. The L_1 edge in Al is 119 eV, that in Pb is 15.85 keV. When less than a few hundred eV, edge energies are known less accurately; they may be uncertain by perhaps 10%, and at all energies can be uncertain to an absolute energy of 1 to 3 eV [Ch95c]. A classic compilation of edge energies is that of Bearden and Burr [Be67]. More recent tabulations are at NIST's reference site [NIST], Biémont et al. [Bi99], and in Deslattes et al. [De03].

Angular Distribution of Photoelectrons

The first order interaction Hamiltonian between the electromagnetic field and an electron is $-(e/mc)\vec{p}\cdot\vec{A}$, where $\vec{A} = \hat{e}A$ is the vector potential of the incident photon, $\hat{e}$ the unit vector, and $\vec{p}$ the electron momentum. Thus the matrix element contains the factor $\hat{e}\cdot\vec{p}$. As a result, for very low energy

photons ($\lesssim$ 10 keV), photoelectrons tend to be ejected parallel to the electric field vector $\vec{E} \| \hat{e}$ of the incident photon, and so perpendicular to the photon direction, in a general $\sin^2\theta$ pattern (unpolarized photons), where θ is the angle between the original photon direction and the outgoing electron momentum. At *all* energies the electron never exits in exactly the forward direction, θ=0, where $\hat{e}\cdot\vec{p}$ vanishes.

At higher energies the distribution is shifted forward, significantly so for $E \gtrsim 100$ keV, while remaining zero at θ=0. Non-relativistically, the angular distribution, per unit solid angle, is approximately proportional to $\sin^2\theta/(1-\beta\cos\theta)^4$, where β is v/c of the electron [He54]. A better relativistic expression for $Z/137 \ll 1$, and neglecting electron binding (i.e., photon energy = electron energy) was given by Sauter [Sa31] and summarized by Davisson and Evans [Da52],

$$\frac{d\sigma}{d\Omega} \sim \frac{\sin^2\theta}{(1-\beta\cos\theta)^4}\left\{\frac{1}{\gamma} + \frac{1}{2}(\gamma-1)(\gamma-2)(1-\beta\cos\theta)\right\} \qquad (2.10)$$

where $\gamma = (1-\beta^2)^{-½}$ is the usual electron relativistic factor. A more recent survey of theory and experiments is given by Berkowitz [Be79]. These distributions are plotted in Figure (2.11) as functions of incident photon energy. There is little interest in photo-absorption above about 1 MeV, since in all materials the cross there is dominated by Compton scattering.

Figure (2.11*a*) shows this angular distribution for several photon energies, and Figure (2.11*b*) shows the cumulative angular distribution.

In Figure (2.12) is shown the polar angle (relative to the photon direction) inside of which ½ the electrons are ejected. By E = 1 MeV, half the electrons come out within about 22° of the original photon direction. Ignoring binding energies, the electron kinetic energy $T = E = h\nu$. Then the electron momentum $p = [2mT+T^2]^{½}/c = [1+2mc^2/E]^{½}E/c$ always exceeds the photon momentum E/c; the difference is taken up by the atom recoiling backwards. Also plotted is the fraction of all electrons that emerge in the forward hemisphere, $\theta < \pi/2$. By 100 keV, some 87% of all ejected electrons exit in the forward hemisphere. A recent compilation of photoelectron angular distributions for elements $Z < 54$ is presented in [Tr01]. Deviations from pure dipole behavior are discussed in [De99].

Fluorescence and Auger Electrons

After photoelectric absorption has occurred, a vacancy exists in the shell from which the electron was ejected. That vacancy may be filled by a higher shell electron jumping down, while a photon of energy equal to the difference of the two shells is emitted. Such photons are called *characteristic* X-rays, since their energy is characteristic of that atom's energy levels. This process of characteristic photon emission after photo-absorption is called *fluorescence*.

Alternatively, instead of a photon emission, while one electron jumps down to fill the vacancy a second electron from an outer shell may be emitted. For a vacancy in the K shell, this *Auger* process is the only alternative to fluorescence. The probability that fluorescence will occur is called the *Fluorescence Yield* ω,

and the probability that Auger emission will occur is the *Auger Yield a*. For a *K* shell vacancy, then, $\omega_K + a_K = 1$. Radiative transitions are more probable ($\omega_K > 1/2$) for elements of $Z > 30$, while Auger emission is more probable ($\omega_K < 1/2$) for $Z < 30$.

Fluorescence is important for it affects the locality of incident photon energy deposition. Without it, the entire photon energy would be deposited locally (within the range of the emitted Auger electron). With it, the characteristic X-ray carries off a fraction of the original photon's energy and deposits it some distance away where that X-ray itself is absorbed. The mean free path against absorption of a fluorescence X-ray is many times the range of an electron of the same or lower energy.

The fluorescence photon has an energy just below the X-ray edge of the shell from which the original electron was ejected, for example an energy $E_K - E_L$ if a photon was absorbed by the *K* shell and fluorescence occurred when an *L* shell electron dropped down to the *K* shell. This is a meaningful example, since *K* shell absorption is about 80% of total photo-absorption. At the energies of these fluorescence photons, the photo-absorption cross section is several times smaller than just above the edge. Thus these fluorescence photons have a mean free path in the material several times greater than the original incident photons. Therefore they are more penetrating in the target material than the incident photons, and will deposit energy to much greater depths. Photon transport codes must therefore account for fluorescence. MCNP, ETRAN (ITS), and TART, for example, do indeed include fluorescence models.

Photo-absorption cross sections are large at low to moderate X-ray energies. In Fe, for example, just above the *K* edge (7.08 keV), the absorption cross section is about 3.8×10^4 barn/atom, or 408 cm^2/gm. Photons of this energy have a mean free path against photoelectric absorption of only 2.45×10^{-3} gm/cm^2, or 3.1 μm. But fluorescent photons with energy just below the *K* edge experience a photo-absorption cross section of only 4.8×10^3 barn, and a mean free path of about 25 μm. Thus when Fe or other materials are exposed to X-rays just above their *K* edge, the photons tend to be absorbed very near the surface. But (half of) the fluorescent X-rays produced easily escape back out of the material. Consequently, fluorescence is a useful tool for studying surface composition, contamination, and surface structure. Puri, et al. [Pu95] present a careful analysis of *K* and *L* shell cross sections for fluorescence applications.

Coster-Kronig Transitions

In addition to emitting fluorescence X-rays or Auger electrons, when photo-absorption occurs in a shell with subshells, that is *L* and higher, a third possibility exists. After photo-absorption by an electron in one subshell, the vacancy may be filled by an electron in the same shell but different subshell (of higher energy). These intra-shell transitions are known as *Coster-Kronig Transitions*. For photo-absorption in the *L* shell, the *Coster-Kronig Yields* $f_{1,2}$ and $f_{1,3}$ are the probabilities that a primary vacancy in the L_1 subshell is filled by a transition from subshell 2 or 3, respectively; and $f_{2,3}$ is the probability that a primary vacancy in the L_2 subshell is filled by a transition from subshell 3. L_1 is always the deepest subshell, L_3 the shallowest. Coster-Kronig (C-K) transitions are radiationless, and are accompanied by the emission of another electron either from another subshell within the same shell or from a higher shell.

Thus, by definition, the *Auger yield* a_S is the probability that a vacancy in shell S ($S = K, L, M, ...$) is filled by a non-radiative transition by an electron from a higher shell. The *Coster-Kronig yield* is the probability that a vacancy in a subshell is filled by an electron from another subshell in the same shell, while the emitted electron may come from either the same shell or a higher shell. After the C-K transition to a different subshell, the atom decays by a fluorescence or Auger process from that subshell.

The electron configuration of L subshells, and their approximate levels (eV) in a few atoms are:

Subshell	configuration	$_{13}$Al	$_{26}$Fe	$_{50}$Sn	$_{82}$Pb
L_1	$2S_{1/2}$	119.05	843	4,440	15,847
L_2	$2P_{1/2}$	81.2	734	4,161	15,251
L_3	$2P_{3/2}$	80.73	721	3,927	13,040

In the L shell, it is also possible for an L_1 vacancy to be filled by a radiative transition from L_3. The symbol $f'_{1,3}$ is commonly used for this probability. Radiative transitions within shells higher than L are also possible. For known cases, these radiative probabilities are always much less than non-radiative C-K transitions between the same subshells [Ba72]. For example, $f'_{1,3} \ll f_{1,3}$.

In the absence of C-K transitions, the radiative fluorescence yield for the L and higher shells is defined to be an average of its subshell yields. In the presence of C-K transitions, the average shell fluorescence yield must be defined more carefully. At least two methods have been proposed for this averaging process [Ba72]. K shell yields, and L, M and higher shell average yields are periodically tabulated as new data and calculations become available [Ba72, Kr79, Hu89, Hu94]. The average radiative yield of shell S is denoted by ϖ_S.

For photo-absorption in the L_1 subshell, the C-K transition probability is $f_1 = f_{1,2} + f_{1,3}$. It is larger than the sum of the L_1 subshell fluorescence yield and Auger yield combined for all elements except near Z = 50–60, where it is about equal to the L_1 Auger yield [Kr79].

As K shell absorption is about 80% of all photo-absorptions, that shell's fluorescence and Auger yields are the most important. Figure (2.13) shows K shell fluorescence yield ω_K, and the Auger yield, $a_K = 1 - \omega_K$, as a function of Z. What is actually plotted here is the convenient fit [Hu89]:

$$\omega_K(Z) = \left(\frac{S}{1-S}\right)^4 ;$$

$$S = \sum_{i=0}^{3} c_i Z^i ; \qquad (2.11)$$

$$c_0 = 0.037 , \qquad c_1 = 0.03112 ,$$

$$c_2 = 5.44\times10^{-5} , \qquad c_3 = -1.25\times10^{-6}$$

that represents the data very well [Hu89, Hu94]. Average L shell and M shell fluorescence yields, ϖ_L and ϖ_M, are also shown.

Energy Transfer by the Photo-electric Effect

In addition to the fluorescence yields ω and ϖ, another parameter that is often tabulated, useful in determining energy transfer to charged particles in the photo-electric effect, is the fraction f_{pe} of the incident photon energy that ends up in kinetic energy of ejected electrons, per absorbed photon. This includes the kinetic energy of the primary electron and those of subsequent Auger electrons emitted throughout the entire fluorescence cascade. Conversely one can speak of the fraction of the incident photon energy that goes to fluorescence photons. Let X be the average energy of fluorescence radiation emitted per absorbed photon of energy E. Then the fraction of the incident photon energy that goes to fluorescence photons is X/E, and, by conservation of energy, $E = X + f_{pe}E$, or

$$f_{pe} = 1 - (X/E).$$

X includes the energies of all fluorescence X-rays emitted throughout the entire cascade. Then the energy put into the material in the form of kinetic energy of electrons is $E - X = f_{pe}E$ per absorbed photon.

The energy X is tabulated in the LLNL Evaluated Photon Data Library, EPDL97. In Aluminum, for example, for an incident photon of any energy E above the K edge (1.56 keV), the average fluorescence photon energy X is approximately 49 eV *per photon absorbed*, almost independent of E, and so $f_{pe} \approx 1$. The reason for the small value of X when a photon of energy close to 1.5 keV can be emitted is that the fluorescence yield in Al is only about 0.04, and it is more likely that no photon is emitted at all; the most probable photon energy is zero.

In Au the fluorescence yield is about 0.96, and the K edge is E_K=80.7 keV. There, for a photon of any energy E above E_K, X is about 59 keV, a substantial fraction of E_K, almost independent of E.

A quantitative example at high Z, where the fluorescence yield is large, is shown for W in Figure (2.14) which compares the incident photon energy (dashed curve) with the energy transferred to the material in the form of electron kinetic energy. Just above the K edge the energy deposited drops from the photon energy E to about $0.3E$, that is, to about that due to photo-absorption by the L edge. Since ω_K is so large (~0.95) most of the energy due to K shell absorption is returned to fluorescence photons, and is not deposited "locally". In high Z materials fluorescence makes a big difference in energy deposited for photons above an absorption

edge, especially the K edge.

Energy Transfer Coefficient

Consider a beam of photons, each of energy E, with number fluence $\varphi=\varphi(E)$ (photons/cm^2) incident on a material with atom number density N (atoms/cm^3). The photon energy fluence is $E\varphi$ (MeV/cm^2). The photoelectric cross section is σ_{pe} (cm^2/atom). There are $N\sigma_{pe}\varphi$ photoelectric interactions per cm^3. Each interaction absorbs a photon, so the energy removed from the beam, per unit volume, is $N\sigma_{pe}E\varphi$ (MeV/cm^3).

Each interaction removes an energy E and deposits an energy $f_{pe}E$ near the struck atom in the form of electron kinetic energy. The remaining energy $E - f_{pe}E = X$ exits the atom as other photons. The kinetic energy in charged particles released per unit volume is therefore $f_{pe}EN\sigma_{pe}\varphi$ (MeV/cm^3). Relative to the incident energy fluence $E\varphi$, the energy transferred to the material (as electron kinetic energy) is $f_{pe}N\sigma_{pe}$ (cm^{-1}).

The coefficient

$$\mu_{tr} = f_{pe}\sigma_{pe}N \quad (\text{cm}^{-1})$$

is called the *Linear energy-transfer coefficient*. If the atom number density N is expressed instead as per gram, $N_g = N/\rho = N_A/A$, μ_{tr} can be written as

$$\mu_{tr}/\rho = f_{pe}\sigma_{pe}N_g \quad (\text{cm}^2/\text{gm})$$

and is the *mass energy-transfer coefficient*. When multiplied by the incident photon energy fluence $E\varphi$ it results in the kinetic energy released per gram of material, known as the *kerma*

$$\text{kerma} = (\mu_{tr}/\rho)E\varphi = f_{pe}\sigma_{pe}N_gE\varphi \quad (\text{MeV/gm})$$

Thus the significance of X or f_{pe} lies in its relation to the kerma delivered to the material, and the mass energy-transfer coefficient connects the incident energy fluence to the kerma. The kerma per photon/cm^2 (the *specific kerma*) is therefore

$$\text{kerma-cm}^2 = (\mu_{tr}/\rho)E = f_{pe}\sigma_{pe}N_gE \quad (\text{MeV-cm}^2/\text{gm})$$

This quantity itself, with units often given as MeV-cm^2/gm, is sometimes referred to just as the kerma. As the released electrons with average energy $f_{pe}E$ then travel through the material, they may lose their own energy to ionization, excitation, or to Bremsstrahlung. The energy lost to ionization and excitation is considered "local" energy deposition by the original photon. The part lost to Bremsstrahlung is in the form of other photons, which generally travel a distance large compared with the electron range, and is considered removed from the volume of interest. It deposits some distance away only after the Bremsstrahlung photons

are themselves absorbed.

The energy-transfer coefficient μ_{tr} and kerma are to be distinguished from the *energy-absorption coefficient* and *dose*. μ_{tr} and kerma measure energy immediately created in the form of charged particle kinetic energy out of energy of neutral particles (here photons). However, the energy left in the target material, measured by the energy-absorption coefficient or dose, is the energy of the charged particles that is transferred to ionization and excitation. It is less than the kerma by the amount that is subsequently lost to Bremsstrahlung as the charged particles pass through the medium. It includes only that part of the energy in charged particles that ends up in the form of ionization or excitation. The energy-absorption coefficient and dose connect the incident energy fluence to the energy that is actually deposited by charged particles.

Further discussion of energy deposition is in Section 2.9.

Time Scale for Fluorescence

The term *luminescence* is a general term for emission of radiation. Fluorescence is a special instance of luminescence. Fluorescence is generally understood to mean the stimulated emission of radiation that occurs over times less than or on the order of 10^{-8} sec.

Phosphorescence is another special case of luminescence. It is the stimulated emission of radiation that persists much longer than fluorescence. Its time scale may be microseconds, seconds, days, or months or longer, and occurs primarily in molecular compounds rather than atoms.

Phosphorescence over the longer times may be affected by material temperature, and is the principle of operation of the *thermoluminescent diode*. Here, after exposure to X-rays, absorbed energy is trapped in a metastable molecular state. Upon heating there occurs thermal excitation to a higher, nearby state from which transitions to a much lower state are allowed, thus giving rise to luminescence when the sample is warmed. Its intensity as a function of temperature then reveals how much original X-ray exposure there was. Modern TLDs trap absorbed energy in trapping centers in semiconductors instead of metastable molecular states, but the principle is the same [Kn00].

The fluorescence yield ω_S by itself carries no information about the mean life τ, or width $\Gamma=\hbar/\tau$, against radiative or Auger emission (although it does fix the radiative to Auger mean life ratio τ_R/τ_A). *K* shell radiative mean lives τ_R are less than 10^{-11} sec ($\Gamma_R > 10^{-4}$ eV) and Auger mean lives τ_A are less than 10^{-15} sec ($\Gamma_A \geq 10^{-1}$ eV) for all elements with $Z>5$. At $Z=30$, where $\omega_K \approx a_K$, $\tau_R \approx \tau_A \approx 6\times10^{-16}$ sec ($\Gamma_R \approx \Gamma_A \approx 1$ eV). Both τ_R and τ_A are shorter for $Z>30$, and longer for $Z<30$ [Kr79].

Fluorescence and Auger Cascades

A vacancy in an atomic shell may be created by a number of processes: photo-absorption, Compton scattering, nuclear electron capture or internal conversion, or, in the case of an incident electron, electron

scattering. No matter how the vacancy ("hole") is created, the atom subsequently relaxes by having that vacancy filled either by fluorescence or an Auger process (including possible Coster-Kronig transitions).

If the primary vacancy is in the K shell, an L_2 or L_3 electron may drop down to fill it, and an Auger electron or a photon may then be emitted. If the process is fluorescence, there is now a vacancy in the L shell. If by Auger, there may be two vacancies in the L shell, or one in the L shell and one in a higher shell. These secondary "holes" are now filled again either by fluorescence or by an Auger process. The cascade can continue many times for high Z elements. For a primary K shell vacancy in Uranium, for example, (U has K, L, M, N, O, P, and Q shells consisting of 29 subshells) there can be emitted 154 different X-ray energies, and 2772 different electron energies [Cu95]. As mentioned, for simplicity fluorescence yields and Auger yields are usually computed and tabulated for each shell as averages over the subshells.

Photo-Electron and Auger-electron Energies

Energies of photo-electrons in many elements and selected compounds are available at the NIST X-ray Photoelectron Spectroscopy (XPS) Database, (NIST Standard Reference Database 20) [NIST20]. This database was built from an evaluation of the published literature, and contains over 19,000 photoelectron and Auger-electron lines, together with chemical shifts, doublet splittings, etc. A version is available on-line.

2.5 COHERENT RAYLEIGH SCATTERING

A photon can elastically scatter from the atom as a whole, leaving the atom in its original, unexcited state. As the photon scatters coherently from all the electrons, the process is called *coherent* scattering (while Compton scattering from any one atomic electron is often referred to as *incoherent* scattering)[2]. Evans [Ev55] has a brief but useful treatment. See also the brief discussion in [Ha58].

The differential atomic scattering cross section is conveniently written in terms of the differential cross section for elastic scattering from a single, isolated electron (Thomson scattering). The Thomson cross section for unpolarized light is

$$\frac{d\sigma_T}{d\Omega} = \frac{1+\cos^2\theta}{2} r_o^2 \qquad (2.12)$$

[2] In general one should distinguish between *elastic* scattering and *coherent* scattering. The term elastic generally means that the scattered photon has the same energy as the incident photon. The term coherent means that the amplitudes for all contributing processes are summed, preserving their relative phases, before squaring to obtain a cross section. An elastic process is not necessarily coherent. The term incoherent means that the amplitudes for all contributing processes are squared before being summed to obtain a cross section. One could have, for example, a coherent scattering process that is not elastic. For present purposes, the terms coherent, elastic, and Rayleigh scattering are taken to be synonymous; the incident and scattered photons have the same energy and the atom is left in its original state. And incoherent means Compton scattering, in which the scattered photon has less energy than the incident photon, and an electron is ejected from the atom.

with total cross section

$$\int d\Omega \frac{d\sigma_T}{d\Omega} = \frac{8\pi}{3} r_o^2 \equiv \sigma_T \tag{2.13}$$

whose numerical value was given in Eq(2.7).

To account for the coherent scattering from Z electrons, the cross section for elastic, Rayleigh scattering[3] from a single, isolated atom with (spherically symmetric) electronic charge density $e\rho(r)$ (ρ is the electron number density) is written, as a first approximation,

$$\frac{d\sigma}{d\Omega} = \frac{d\sigma_T}{d\Omega} F(q)^2 \tag{2.14}$$

where

$$F(q) = \int d^3 r e^{i\vec{q}\cdot\vec{r}} \rho(r) = 4\pi \int dr r^2 \frac{\sin(qr)}{qr} \rho(r) \tag{2.15}$$

is the usual atomic form factor for scattering through angle θ while transferring momentum $\hbar\vec{q}$,

$$\vec{q} = \vec{k}_o - \vec{k}' \tag{2.16}$$

to the atom. Here $\hbar\vec{k}_o$ is the incident photon momentum, and $\hbar\vec{k}'$ is the scattered photon momentum. For elastic scattering $k' = k_o$, and

$$q = k_o \sqrt{2[1-\cos\theta]} = 2k_o \sin(\theta/2) = 4\pi \sin(\theta/2)/\lambda \tag{2.17}$$

where $\lambda = 2\pi/k_o$ is the incident wavelength. $F(q)$ is computed in various models for $\rho(r)$. From Eq(2.15), clearly $F(0) = Z$, and F is monotonically decreasing with increasing q. Were it not for further corrections, in the forward direction (q=0) the coherent sum of scattering from each electron would make the atomic differential cross section Z^2 times larger than the Thomson cross section r_o^2.

Equations (2.14) and (2.15) describe scattering from a distributed charge density, and Eq(2.15) is the usual Born approximation for the form factor. This formulation is deficient in two respects. First, no account is taken of the internal energy level structure of the atom, and so no resonances are treated, a serious problem at incident energies comparable to atomic levels and edge energies. The Rayleigh cross section has rapid variation and sharp dips near absorption edges; the simple form factor approximation does not account for this "anomalous" behavior. Second, the form factor is real, meaning the scattering amplitude has no

---

[3] The term "Rayleigh scattering" means different things to different people. See A.T. Young, *Phys. Today* **35**: 42 (January, 1982)

imaginary part and so violates unitarity. When these effects are accounted for the differential cross section in the forward direction is no longer $Z^2 r_o^2$.

Anomalous scattering and an imaginary part of the scattering amplitude are usually taken into account by augmenting the form factor F with the *anomalous scattering factors* f_1 and f_2:

$$F \Rightarrow F + f_1 + if_2 \tag{2.18}$$

so that the cross section for Rayleigh scattering from an atom becomes

$$\begin{aligned} \frac{d\sigma}{d\Omega} &= \frac{1+\cos^2\theta}{2} r_o^2 \, | F(q) + f_1 + if_2 |^2 \\ &= \frac{1+\cos^2\theta}{2} r_o^2 \, [(F(q) + f_1(k_o))^2 + f_2(k_o)^2] \end{aligned} \tag{2.19}$$

The anomalous factors are approximately functions of the incident photon energy only, not of q. Relativistic effects and nuclear Thomson scattering may or may not be included in the anomalous factors [Ch95a]. A good review of the theory is by Kissel and Pratt [Ki85].

Let f_{coh} be the scattering amplitude for elastic scattering, so that the differential coherent cross section is $d\sigma/d\Omega = |f_{coh}|^2$. According to the optical theorem the imaginary part of f_{coh} in the forward direction is related to the total cross section by

$$\text{Im}\, f_{coh}(k_o, \theta=0) = \frac{k_o}{4\pi} \sigma_{Tot}(k_o) \ . \tag{2.20}$$

This means that f_2 is given by the total cross section according to

$$f_2(k_o) = \frac{E}{2hcr_o} \sigma_{Tot}(E) \tag{2.21}$$

where $E = \hbar k_o c$ is photon energy. A common alternate form for this last equation is $\sigma_{Tot}(E) = 2\lambda r_o f_2(k_o)$. Except at higher energies where the Compton cross section contributes, σ_{Tot} may be replaced in this equation by the total photo-electric cross section σ_{pe}.

Recent compilations of form factors and anomalous scattering factors are given by Wang, et al. [Wa93] and by Chantler [Ch95a; available in digitized tabular form at the NIST web sites Ch95b; Ch95c; Ch00]. Henke, et al. [He93] also provides a tabulation. In addition, F, f_1, and f_2 are given in the *Evaluated Photon Data Library* (EPDL) from LLNL (see Section 2.11). The form factor $F(q)$ is fairly well understood and agreed upon, and is not even given in [He93] or [Ch95a]. But recent compilations of f_1 and f_2 vary considerably below a few keV. Figure (2.15) compares three sets of anomalous form factors f_1 and f_2 in Fe, while Figure (2.16) shows the resulting angular distribution and total Rayleigh cross section computed from the same three recent compilations plus EPDL89 of the anomalous scattering factors at 300 eV. $F(q)$ from EPDL97 was used in all four. Computations improve with time, and seem to be converging in the most recent tabulations, but there has been considerable change just since 1989. Agreement is better at higher

energies. A fifth compilation, from 50 keV to 1.5 MeV, can be found in [Ch98]. The earlier 1989 compilation, EPDL89, is included in the figure to demonstrate progress toward convergence. But in all cases, the LLNL 1997 compilation, EPDL97, is to be preferred over EPDL89.

The cross section for coherent scattering is almost never more than 10% of competing cross sections (photo-electric and Compton) at any energy. It is shown as a function of energy in the plots in Section 2.8 of all cross sections for many elements. It is largest (i.e., near 10% of the total) at energies of 10 keV - 100 keV, depending on Z. However the differential cross section is strongly peaked in the forward direction. Figure (2.17) shows the differential Rayleigh cross section for atomic Aluminum as a function of scattering angle θ for several energies, and Figure (2.18) shows the angular distribution on a polar plot. Figures (2.19) and (2.20) show the same for Lead. Figure (2.21) shows the polar angle θ inside of which 50% or 90% of scattered photons emerge, in four elements. In Al, for example, at 100 keV, ½ of scattered photons emerge at less than about 9°. Scattered photons emerge more and more nearly in the forward direction as energy increases and Z decreases.

Thus Rayleigh scattering peaks generally in the forward direction. It will be seen later that Compton scattering from a free electron also peaks generally in the forward direction (although for scattering from atoms it vanishes in a narrow cone immediately around θ=0). Thus, while both coherent and incoherent scattering do (may) scatter photons out of the original beam direction, if one needs accurate calculations of an incident photon beam attenuation, one must consider the angle from incidence inside of which one may consider a scattered photon still to be in the (attenuated) beam.

For the latest developments in photon elastic scattering from atoms, follow the LLNL web site: http://www-phys.llnl.gov/Research/scattering/index.html.

2.6 COMPTON SCATTERING

The Compton effect is the inelastic scattering of a photon from an electron. The electron recoils and is ejected from the atom, the scattered photon emerges with reduced energy, and the atom is left ionized, with a vacancy in the shell that had been occupied by the ejected electron. It is the dominant process for typical energies of nuclear γ rays, hundreds of keV to several MeV.

Bethe and Ashkin [Be53], Evans [Ev55], and Heitler [He55] have excellent discussions of Compton scattering, and useful formulas. More recent work is summarized in [Wi77].

Compton scattering of a photon from electrons bound in an atom differs from scattering from a free electron. The differential cross section for Compton scattering from a single, free electron is the Klein-Nishina formula $d\sigma_{KN}/d\Omega$, Eq(2.30). The differential (in outgoing photon angle) Compton scattering cross section from an atom is sometimes expressed in terms of the Compton scattering from a single electron as

$$\frac{d\sigma_{atom}}{d\Omega} = \frac{d\sigma_{KN}}{d\Omega} S(q,Z) \tag{2.22}$$

where $S(q,Z)$ is the *incoherent scattering function* for that atom. S describes the effects of the different binding energies of electrons in different atomic shells. Here $\hbar q$ is the magnitude of the momentum transferred to the recoil electron,

$$\vec{q} = \vec{k}_o - \vec{k}',$$
$$q = \frac{E}{\hbar c}\left[1 - 2\frac{\nu'}{\nu_0}\cos\theta_\gamma + \left(\frac{\nu'}{\nu_0}\right)^2\right]^{1/2} \tag{2.23}$$

where $E = \hbar k_o c = h\nu_o$ is the incident photon energy, $E' = \hbar k' c = h\nu'$ is the scattered photon energy, and θ_γ is the outgoing angle of the scattered photon relative to the incident photon direction. At high energy or high momentum transfer q, binding energies make no difference, and $S(q\rightarrow\infty, Z) \rightarrow Z$; the cross section is simply the sum of the Compton scatterings for each electron. Cross sections add (rather than amplitudes) because the atom is left in a different state according to which electron is ejected. At very low energies, $\sigma_{KN} \rightarrow \sigma_T$, but S, $d\sigma_{atom}/d\Omega$, and the total cross section $\sigma_{atom} = \int (d\sigma_{atom}/d\Omega) d\Omega$ all approach 0, due to binding energies. The incoherent scattering function on many elements has recently been reviewed by Wang, et al. [Wa93] and by Kahane [Ka98].

For a free electron, kinematics determines E' in terms of θ_γ, so q is a function of only θ_γ *or* E', but not both. The Compton electron takes the remaining energy. But for an atom, the kinetic energy of the ejected electron is smaller than the free electron kinematic expression by the binding energy. If less than the binding energy is transferred to the bound electron, Compton scattering (defined on an atom as ejecting an electron) cannot occur. For incident photon energies well above absorption edges, the binding energy makes little difference, and the angular distribution from an atom will be close to that from a free electron (except very near $\theta_\gamma = 0$; see section below on Compton scattering from atoms).

When one wishes to investigate the detailed energy *and* angle distribution of the outgoing photon from atomic Compton scattering, one works with the doubly differential cross section $d^2\sigma/dE'd\Omega$ [e.g., Be93]. These considerations are usually of interest when one measures the scattered photon and wishes to infer information about the structure of the struck atom. In addition, the velocity of the struck electron in the atom produces a Doppler broadening of the incident photon apparent frequency, resulting in a broadening in outgoing photon energy at a given angle. The shape of this broadened line is the *Compton profile*, and is a current topic of research [e.g., Hu99a and references therein]. The current state of calculations of incoherent scattering have been summarized by Bergstrom and Pratt [Be97].

COMPTON SCATTERING FROM A FREE ELECTRON

Properties such as angular distributions are easier to understand off a free electron, and the differences from atomic scattering are generally small. The major difference is in photon scattering near the forward

direction, discussed separately below in a later section.

Here we present formulae and graphs for Compton scattering from a single, free electron. Atomic (barn/atom) and bulk cross sections (cm^2/gm) and mean free paths in matter are presented in a later section.

Our discussion and graphs are for an unpolarized photon. Formulae for polarized photons, needed much less frequently, can be found in Heitler [He54] and Evans [Ev55].

Figure (2.22) defines scattering angles in the scattering plane. Incident photon energy is $E = h\nu_o$, scattered photon energy is $E' = h\nu'$. The photon scattering angle relative to incident photon direction is θ_γ; the electron scattering angle is θ_e. (Referring to Evans [Ev55], our photon scattering angle θ_γ is Evans' ϑ, our electron scattering angle θ_e is Evans' φ). T is the outgoing electron kinetic energy.

Kinematics

The energy and momentum conservation laws determine all final momenta in terms of one final parameter, often taken as the scattered photon outgoing angle θ_γ. The relations were first worked out by Compton in 1923. Following Davisson and Evans [Da52] and Evans [Ev55], the scattered photon energy is

$$E' = h\nu' = \frac{h\nu_o}{1 + \alpha(1 - \cos\theta_\gamma)} \tag{2.24}$$

which determines the frequency shift $\nu' - \nu_o$ of the scattered radiation, where α is the commonly defined ratio of the incident photon energy to the electron rest energy,

$$\alpha \equiv \frac{h\nu_o}{mc^2} . \tag{2.25}$$

The shift in photon wavelength, from the incident $\lambda_o = c/\nu_o$ to the scattered photon $\lambda' = c/\nu'$ is

$$\lambda' - \lambda_o = \lambda_C(1 - \cos\theta_\gamma) \tag{2.26}$$

where $\lambda_C \equiv h/mc = 2.426\times10^{-10}$ cm is the *Compton wavelength* of the electron (m is the electron rest mass.) In Compton scattering, the wavelength shift depends only on the scattered photon angle, not on the incident photon energy.

The outgoing electron has kinetic energy

$$
\begin{aligned}
T &= h\nu_o - h\nu' \\
&= h\nu_o \frac{\alpha(1-\cos\theta_\gamma)}{1+\alpha(1-\cos\theta_\gamma)} \\
&= h\nu_o \frac{2\alpha\cos^2\theta_e}{(1+\alpha)^2 - \alpha^2\cos^2\theta_e}
\end{aligned}
\tag{2.27}
$$

and its outgoing angle θ_e is related to that of the scattered photon θ_γ by

$$
\cot\theta_e = (1+\alpha)\frac{1-\cos\theta_\gamma}{\sin\theta_\gamma} = (1+\alpha)\tan\frac{\theta_\gamma}{2} \,. \tag{2.28}
$$

or, conversely,

$$
\cos\theta_\gamma = 1 - \frac{2}{(1+\alpha)^2\tan^2\theta_e + 1} \,. \tag{2.29}
$$

For scattering from a free electron $T = h\nu_o - h\nu'$, but in atomic scattering, the outgoing electron kinetic energy is smaller than $h\nu_o - h\nu'$ by its binding energy.

The cross section for scattering numbers of photons through angle θ_γ is the well-known Klein-Nishina cross section (for unpolarized photons)

$$
\frac{d\sigma_{KN}}{d\Omega} = \frac{r_o^2}{2}\frac{1}{[1+\alpha(1-\cos\theta_\gamma)]^2}\left[1+\cos^2\theta_\gamma + \frac{\alpha^2(1-\cos\theta_\gamma)^2}{1+\alpha(1-\cos\theta_\gamma)}\right], \tag{2.30}
$$

where $d\Omega = \sin\theta_\gamma d\theta_\gamma d\varphi_\gamma$ is the direction of the scattered photon.

Only the energy $h\nu'$ has been scattered, while the energy $T = h\nu_o - h\nu'$ has been transferred to the electron. Since $h\nu'$ has been scattered, while $h\nu_o$ was incident, the cross section for scattering photon *energy* through angle θ_γ is $d\sigma_s/d\Omega = (h\nu'/h\nu_o)\, d\sigma_{KN}/d\Omega$. Because of the distinction between scattering numbers of photons and energy of photons, references [Da52] and [Ev55] refer to $d\sigma_{KN}/d\Omega$ as the *collision cross section* and to $d\sigma_s/d\Omega$ as the *scattering cross section*. However, this terminology does not seem to have gained wide acceptance; rather the terms "collision cross section" and "scattering cross section" are regarded as synonymous, both referring to the collision cross section for the scattering of numbers of particles (in this case $d\sigma_{KN}/d\Omega$). If the scattering of energy is intended, it is stated explicitly.

For given incident photon energy $h\nu_o$, $d\sigma_{KN}/d\Omega$ is a function of only θ_γ, but can also be written as

$$\frac{d\sigma_{KN}}{d\Omega} = \frac{r_o^2}{2}\frac{\nu'^2}{\nu_o^2}\left[\frac{\nu_o}{\nu'} + \frac{\nu'}{\nu_o} - \sin^2\theta_\gamma\right]$$
$$= r_o^2\frac{\nu'^2}{\nu_o^2}\left[\frac{1+\cos^2\theta_\gamma}{2} + \frac{(\nu_o-\nu')^2}{2\nu_o\nu'}\right], \qquad (2.31)$$

showing that it differs from the Thomson differential cross section $d\sigma_T/d\Omega$, Eq(2.12), in two ways. First, to the angular dependence $\frac{1}{2}(1+\cos^2\theta_\gamma)$ is added the term $(\nu_o-\nu')^2/2\nu_o\nu'$, which arises from the matrix element. This term vanishes as $h\nu_o \to 0$, since there $\nu' \to \nu_o$. And second, it differs by the overall factor $(\nu'/\nu_o)^2$ whose origin is purely due to phase space, not the matrix element. In concert with the first term, this second factor reduces scattering at large angles, where $h\nu'$ can be much less than $h\nu_o$ (the electron carries off most of the energy). In the forward direction, $\theta_\gamma = 0$, $\nu' = \nu_o$, and the two corrections leave the Thomson differential cross section, r_o^2; at all energies, the Compton differential cross section on a free electron in the forward direction is equal to the Thomson differential cross section, $d\sigma_{KN}/d\Omega(\theta_\gamma=0) = d\sigma_T/d\Omega(\theta_\gamma=0) = r_o^2$.

At low energy, $\nu' \to \nu_o$, and free electron Compton scattering approaches Thomson scattering at all angles, $d\sigma_{KN}/d\Omega \to d\sigma_T/d\Omega$.

Total Compton Cross Section

Integrating $d\sigma_{KN}/d\Omega$ over solid angles, one obtains the Klein-Nishina total cross section for Compton scattering from a single, free electron (and for unpolarized incident and outgoing photons)

$$\sigma_{KN} = 2\pi r_o^2\left\{\frac{1+\alpha}{\alpha^2}\left[\frac{2(1+\alpha)}{1+2\alpha} - \frac{1}{\alpha}\ln(1+2\alpha)\right] + \frac{1}{2\alpha}\ln(1+2\alpha) - \frac{1+3\alpha}{(1+2\alpha)^2}\right\}. \qquad (2.32)$$

It is shown in Figure (2.23). At low energies it approaches the Thomson cross section σ_T.

The Compton cross section for photons scattering from atoms is approximately $Z\sigma_{KN}$. However at low energies it is less than $Z\sigma_{KN}$ for two reasons. First, at energies below an element's K edge, the K electrons cannot be ejected, and so the effective atomic number for Compton scattering is $Z-2$. Below higher edges even fewer electrons can contribute, and so the cross section is reduced again. Of course, this occurs only at energies below X-ray edges, where the Compton effect is much smaller than photo-absorption. Second, as will be seen below, at all energies the Compton differential scattering from an atom is smaller than $Zd\sigma_{KN}/d\Omega$ inside some fairly small angle near the forward direction (and actually vanishes inside a very small angle). When integrated over all solid angles, this forward dip makes the atomic Compton cross section smaller than $Z\sigma_{KN}$, even at energies well above an atom's K edge.

Particle Characteristic Energies

Given an outgoing scattering angle for either the electron or scattered photon, kinematics fixes the energies. For given incident photon energy $h\nu_o$, Figure (2.24) shows the maximum and, averaged over all outgoing angles, the average Compton electron kinetic energies, and the average energy of the scattered photon, as a fraction of $h\nu_o$. From Eq(2.27) at $\theta_\gamma = \pi$, the electron maximum energy T_{max} is

$$T_{max} = \frac{h\nu_o}{1 + 1/(2\alpha)} \tag{2.33}$$

α was defined in Eq(2.25). Maximum scattered photon energy $h\nu'_{max}$ is the incident energy $h\nu_o$.

Compton Electron Energy

The distribution $d\sigma/dT$ of outgoing electron energy T can be obtained by combining the photon angular distribution $d\sigma_{KN}/d\mu = -2\pi d\sigma_{KN}/d\Omega$, where $\mu \equiv \cos\theta_\gamma$, with the relation between T and μ, the second of Eqs (2.27):

$$\begin{aligned} \frac{d\sigma}{dT} &= \frac{d\sigma_{KN}}{d\mu}\frac{1}{dT/d\mu} = -2\pi\frac{d\sigma_{KN}}{d\Omega}\frac{1}{dT/d\mu} \\ &= \frac{\pi r_o^2}{\alpha h\nu_o}\left[1 + \left(1 - \frac{1}{\alpha}\frac{T}{h\nu_o - T}\right)^2 + \frac{T^2}{(h\nu_o - T)h\nu_o}\right] \end{aligned} \tag{2.34}$$

where $dT/d\mu$ was obtained by differentiating the second of Eqs (2.27). Then $(d\sigma/dT)dT$ is the cross section for producing a Compton electron with energy in $(T, T + dT)$.

The maximum energy the Compton recoil electron can have is T_{max} given by Eq(2.33). Eq(2.34) gives the distribution at energies less than or equal to T_{max}. The maximum occurs at an energy

$$E_s = h\nu_o - T_{max} = h\nu_o \frac{1}{1 + \frac{2h\nu_o}{mc^2}} \tag{2.35}$$

below the incident photon energy.

The energy-differential cross section Eq(2.34) is shown in Figure (2.25) (barn/MeV) for the Compton electron, for several incident photon energies. The electron maximum energy T_{max} is also its most probable energy, but its average energy is ~0.5 – 1 times its maximum. The distribution is rather flat at low energies, but rises to a sharp peak at T_{max}.

Figure (2.26) is the Compton electron energy as a function of its outgoing polar angle θ_e (relative to the incident photon direction), for several incident energies $h\nu_o$. It has its maximum energy in the forward direction ($\theta_e = 0$), and ~0 energy if ejected at a right angle. Kinematically, the electron cannot exit in the backward hemisphere.

In the photoelectric effect, when the electron is ejected in the forward direction, its momentum can exceed that of the incident photon. Momentum conservation is assured because the atom recoils backwards, and its momentum balances the total. However in the Compton effect, the photon scatters in the backward direction, carrying sufficient momentum so that no atomic recoil is necessary.

Scattered Photon Energy

Figure (2.27) show the scattered photon energy distribution $d\sigma/dh\nu'$. Since the electron energy $T = h\nu_o - h\nu'$, the photon energy spectrum mirrors that of the electron. The photon, however, may backscatter.

The first and second of Eqs(2.27) readily give the scattered photon energy $h\nu'$ as a function of its scattering angle θ_γ:

$$h\nu' = \frac{h\nu_o}{1+\alpha(1+\cos\theta_\gamma)} \tag{2.36}$$

where α is again given by Eq(2.25).

Figure (2.28) graphs Eq(2.36) for several values of $h\nu_o$. For "back-scattering", say $\theta_\gamma \gtrsim 120°$, the energy is relatively insensitive to θ_γ. For exact back-scattering ($\theta_\gamma = 180°$) the scattered photon energy is

$$h\nu' = \frac{h\nu_o}{1+2\alpha} \qquad (\theta_\gamma = 180°) \tag{2.37}$$

Here, at low energies ($h\nu_o \ll mc^2$), $h\nu' \to h\nu_o$. At high energies ($h\nu_o \gg mc^2$), $h\nu' \to mc^2/2 = 255$ keV. The back-scattered photon energy is always less than $mc^2/2$.

Photon-Electron Angle Relations

Figure (2.29) shows the outgoing electron angle θ_e for given scattered photon angle θ_γ. Zero degrees is the forward direction, 180° is back-scattering.

For $h\nu_o \gtrsim 2$ MeV, the electron strongly prefers to exit near the forward direction; the electron will exit at $\theta_e \lesssim 30°$ so long as the photon scatters at $\theta_\gamma \gtrsim 40°$.

Electron Angular Distribution

The electron differential scattering cross section $d\sigma/d\Omega_e$ (barn/ster) is shown in Figure (2.30*a*), and the distribution in polar angle θ_e, $d\sigma/d\theta_e = 2\pi\sin\theta_e\, d\sigma/d\Omega_e$ (barn/radian) in (*b*). The same quantities are shown in Figure (2.31) in polar plots. Above several MeV, the electron angular distribution is extremely peaked in the forward direction.

Scattered Photon Angular Distribution

The photon differential scattering cross section $d\sigma/d\Omega_\gamma$ (barn/ster) is shown in Figure (2.32*a*), and the distribution in polar angle θ_γ, $d\sigma/d\theta_\gamma = 2\pi\sin\theta_\gamma\, d\sigma/d\Omega_\gamma$ (barn/radian) in (*b*). Again, the same quantities are

shown in Figure (2.33) in polar plots. In the forward direction ($\theta_\gamma = 0$) the photon differential cross section is $r_o^2 = 0.0794$ b at all energies. This is true only for scattering from a free electron. Angular distributions near $\theta_\gamma = 0$ are much different when scattering from an atom, as discussed in the next section.

Cumulative Angular Distributions

Figure (2.34) gives the fraction of all electrons and photons that exit at a polar angle less than θ. At $h\nu_o$ = 3 MeV, half of all Compton electrons come out at less than/greater than about 19°, while half of photons exit at less than/greater than about 47°.

The bottom graph in Figure (2.34) shows the angle inside of which ½ of electrons/photons exit, as a function of $h\nu_o$. For a 2 MeV photon, ½ of all electrons exit at less than 22°, and ½ of the scattered photons exit at less than 51°.

Comment on Angular Distribution

Kinematics requires that the scattered photon and the ejected Compton electron cannot both exit the interaction in the forward direction. If the photon comes out near $\theta_\gamma = 0$, the electron comes out near $\theta_e = 90°$. If the electron comes out near $\theta_e = 0°$, the photon comes out near $\theta_\gamma = 180°$.

Since the photon angular distribution is peaked in the forward direction, one might therefore expect the electron distribution must peak at some large angle, or, at least, could not also peak in the forward direction. In fact, however, both the electron and photon angular distributions do peak in the forward direction.

This does not violate kinematics, since the two particles do not both exit in the forward direction in the same one event.

Kinematically, since electrons cannot backscatter but photons can, scattered photons have available twice the phase space that is available to electrons. The photon need only exit at an angle $\gtrsim 40°$, for example (when $h\nu_o$ = 3 MeV), in order for the electron to exit at an angle $\lesssim 22°$ (Figure 2.29); the electrons tend to be compressed in the forward direction. When scattered at a large angle, the photon has relatively little energy. Momentum conservation then throws the electron forward. Electrons are significantly more compressed at higher energies (see, e.g., Figure (2.30) or (2.31)).

Application to a Gamma Spectrometer

Detectors of high energy photons (gammas) rely on the interaction of the gamma with the material of the detector itself. Bolometers measure the temperature rise of a small mass as it absorbs the energy of some of the photons that enter it. Scintillators are excited to emit light when a photon deposits energy in it. Semiconductor detectors measure the charge of electron-hole pairs created by photon energy deposition.

At nuclear gamma ray energies the Compton effect is usually the most probable process; a gamma entering the detector is more likely to Compton scatter than to be absorbed by the photo-electric effect or undergo pair production. The short-range Compton electron then deposits its energy in the detector.

Eq(2.34) for the Compton electron energy spectrum is therefore useful in studies of the performance of liquid or solid state detectors. A solid scintillator (e.g., NaI, CsI, or Bismuth Germanate (BGO)) senses the energy deposited by the Compton electron (or photo-electron) by measuring the energy in light (essentially visible) emitted when excited and ionized atoms de-excite or recombine. This light enters a photo-multiplier tube which converts it to an electrical pulse, which is then amplified. Except for relatively small non-linearities, the electrical output of the scintillator is proportional to the energy deposited in the crystal [Kn00].

Another common detector is a solid semiconductor (e.g., GaAs, CdTe, CdZnTe (CZT), or HgI_2) in which the energy deposited by the photon creates electron-hole pairs which are collected at electrodes attached to the crystal. The number of pairs, and hence the magnitude of the charge pulse, is proportional to the energy deposited in the crystal by the photon.

The photon deposits its energy by 1) suffering a photo-electric absorption, ejecting a photo-electron which has a short range and deposits its energy by further ionization; 2) undergoing Compton scattering from an atomic electron in the detector, ejecting a short-range Compton electron with a fraction of the original photon energy, while the reduced energy scattered photon continues on;'or 3) undergoing pair production (if the photon energy exceeds 1.02 MeV), ejecting an electron and positron which then ionize further.

Figure (2.35) schematically shows the typical geometry of a semiconductor detector in a metal housing, with three illustrative photons incident normally on the crystal. The upper photon is absorbed in the crystal by the photo-electric effect; essentially all its energy is deposited in the crystal. The second photon passes through the crystal and is Compton back-scattered from solid material in the rear; the back-scattered photon is absorbed in the crystal. The third photon Compton scatters in the crystal; the electron deposits its energy and the scattered photon continues on, here leaving the crystal. These processes are discussed below.

The range of the Compton electron is almost always a small fraction of the detector linear dimensions, and so deposits all its energy in the detector. But the scattered photon continues to much greater distance. If the crystal is not too large, the scattered photon often exits the crystal without interacting again. As detector response is proportional to energy deposited, a Compton event leads to a fraction of the photon energy being registered by the detector, as energy deposited by the Compton electron. The energy deposited is therefore T_{max} or less, and Eq(2.34) gives the pulse height distribution due to Compton electrons when gammas enter the detector material and Compton scatter once. That whole process is quite common, especially for small crystals.

Instead of a single Compton scattering, the gamma ray may be absorbed directly by the photo-electric effect, depositing essentially all its energy $h\nu_o$ in the crystal. For low Z materials the electron binding energy is recovered in the form of Auger electron kinetic energy. But for high Z, electron binding energy is lost to fluorescence photons, so there are counts on the low energy side of the full photon energy (in $Z = 50$, Figure 2.13 shows that if the gamma is photo-absorbed in the K shell 86% of absorptions produce a fluorescence X-ray). Alternatively, once Compton scattered, the lower energy scattered photon may be photo-absorbed before exiting, with the result that again all the initial energy $h\nu_o$ is deposited in the crystal. In either of these cases, or in a number of other processes or sequence of processes, the entire gamma ray energy is deposited

in the crystal. As a result, the detector will measure the full gamma energy $h\nu_o$ and display a peak at that energy. The magnitude of the peak, called the *photo-peak*, is determined by the source intensity. The sharpness of the peak is determined by the energy resolution of the detector; the count rate falls off rapidly away from the center of the peak.

But due to the relatively high probability of a single Compton scattering followed by escape of the scattered photon, at an energy T_{max} (i.e., at an energy E_s below the photo-peak at $h\nu_o$) there will be a relatively sudden rise in the pulse height distribution as the energy of Compton electrons is detected. This rise is called the *Compton edge*. At energies below the edge the pulse height distribution is determined by the cross section Eq(2.34).

Figure (2.36) shows an example of a relatively clean gamma ray spectrum taken by a CdZnTe crystal detector. The crystal is 5mm×10mm×10mm and was exposed for 20 hours to a Cs^{137} source which emits $h\nu_o$ = 661.6 keV gammas. The photons were incident normally on the 10×10 mm face; the longest path available to them was 5 mm. The photo-peak is very pronounced. Natural environmental background gammas were also present, of course, and have not been subtracted from the data.

As one proceeds down in energy below the photo-peak, at an energy T_{max} = 477 keV (or E_s = 184 keV below the peak) the signal rises, registering Compton electrons created when the gamma Compton scattered in the crystal and the scattered photon exited without further interaction; that is the Compton edge. In the figure, along with the measured spectrum, the ideal Compton electron energy spectrum, Eq(2.34), at and below the Compton edge, is drawn (dotted line). This is the spectrum of Compton electrons, and the detector response, that would occur if the gamma scattered from free electrons and there were no detector imperfections or background noise.

The actual shape of the measured spectrum in the vicinity of the Compton edge is not a sharp discontinuity, but is smoothed and rounded. The reasons are: 1) the natural resolution of the detector (here about 3% or about 15 keV) broadens the response to any one energy; 2) thermal drift of the detector calibration during the long measurement spreads the response; 3) Compton scattering on the bound crystal electrons is not the same as scattering from free electrons; and 4) background gammas have not been subtracted in the figure, and they provide a non-uniform background noise. The rounded Compton edge is referred to as the *Compton shoulder.*

To illustrate the effects of the four broadening mechanisms, Eq(2.34) has been filtered through a typical detector resolution function with an 18 keV full width at half maximum (about 3.8% at 477 keV). The result is shown as the dashed line in the figure. Above 500 keV this broadened line falls below the data because the measurements include background noise not represented in the calculation. The shape of the broadened spectrum is quite close to the measured spectrum near the Compton edge at 477 keV. Below that energy, background noise and back- or side-scattering makes the data higher than the computed ideal spectrum.

Also seen in Figure (2.36) is a peak at 190 keV labeled "backscatter peak". Gammas will most likely penetrate the 5 mm thick crystal without interacting at all (the mean free path against any interaction of a 662

keV photon in CdZnTe is 2.1 cm). In the structure there is always some solid material behind and around the crystal. After passing through or nearby the crystal the gamma can Compton scatter from this material through a large angle, and the reduced-energy scattered photon will propagate back to the crystal where it is likely photo-absorbed. From Eq(2.36) the energy of the back-scattered photon is 184 keV or greater, depending on the angle through which it scattered. As this is the minimum energy of a scattered photon, and scattering occurs through a wide range of angles from surrounding material, a broad peak is produced by these scattered photons entering the crystal from many angles and being absorbed. The peak is steep on the low energy side, since 184 keV is the strict minimum photon energy, but the distribution of smaller scattering angles and larger energies gives the peak a wider slope on the high energy side. In CdZnTe, near 190 keV, photo-electric absorption is more probable than Compton scattering, so the full energy of the back-scattered photon is recorded. A back-scatter peak like this is commonly seen in gamma detectors.

Information from both the photo-peak and the Compton shoulder can be used to increase confidence in photo-spectroscopy over a simple measurement of the photo-peak alone. In addition, since the Compton scattered photon can easily be arranged to exit the crystal (by making it small), a second crystal can be positioned to capture some scattered photons. By measuring time coincidence between the two, confident photo-spectroscopy can be performed [Kn00, Si65, Sh64, Qu72].

COMPTON SCATTERING FROM ATOMS

Angular Distribution

The angular distribution of scattered photons in Compton scattering from atoms is given by Eq(2.22) , and is different from the angular distribution in Compton scattering from a free electron. The difference is caused by the binding of electrons, and the incoherent scattering function $S(q)$ is intended to quantify that effect.

At high momentum transfer to the atomic electrons (and so high energy transfer) the binding energy of electrons makes no difference, and the cross section for scattering from an atom of atomic number Z is simply Z times the Klein-Nishina cross section: $d\sigma_{atom}/d\Omega = Zd\sigma_{KN}/d\Omega$. That is, $S(q) = Z$ for large q. But the momentum transfer is very small for forward or near forward photon scattering, even at high incident energy, and in exactly the forward direction ($\theta_\gamma = 0$) one has $q = 0$ for all energies. If there is no momentum transferred to the electrons in the atom, no electron can be ejected, and Compton scattering does not occur. The differential cross section for the outgoing photon direction in Compton scattering from an atom vanishes in the exact forward direction, $d\sigma_{atom}(\theta_\gamma=0)/d\Omega = 0$. (The differential cross section for *electron* ejection in the forward direction does not vanish).

This is illustrated in Figure (2.37) which shows the photon differential cross section in Fe for three incident energies. The solid lines are the atomic cross sections, computed by Eq(2.22) with $S(q)$ taken from Livermore's EPDL97. The dashed lines are Z times the Klein-Nishina cross section, Eq(2.30) or (2.31). The Klein-Nishina cross section peaks smoothly in the forward direction, but the atomic cross sections, while

generally peaking forward, have a sharp dip at small angles and go to zero at θ_γ=0. This behavior is due to the following.

The minimum energy that must be transferred to an electron in order for Compton scattering to occur (i.e., in order for an electron to be ejected) is the atom's ionization potential, roughly of order 10 eV. The minimum energy for Compton scattering to occur on a K shell electron is the K edge energy E_K. Now from Eq(2.27) when the electron receives energy T, the photon scatters at angle θ_γ given by

$$1-\cos\theta_\gamma = \frac{mc^2 T}{(h\nu_o)^2}\,\frac{1}{1-T/h\nu_o} \tag{2.38}$$

For small θ_γ, and for $T \ll h\nu_o$, this becomes

$$\theta_\gamma(h\nu_o, T) = \frac{\sqrt{2mc^2 T}}{h\nu_o} = 10^{-3}\,\frac{\sqrt{T(\text{eV})}}{h\nu_o(\text{MeV})} \tag{2.39}$$

Thus at $E = h\nu_o = 1$ MeV, the photon must scatter through 3.2 mrad = 0.18° in order to impart 10 eV to an electron. A Compton scattered photon cannot exit at an angle smaller than this on an atom with ionization potential 10 eV.

The atomic cross section is not equal to $Zd\sigma_{KN}/d\Omega$ until *every* electron can be ejected, including the most tightly bound electrons; that is, until $T = E_K$. In Fe the K edge is $E_K = 7.08$ keV. Using this value for T in Eq(2.39), $\theta_\gamma(h\nu_o,T)$ at $E = 1$ MeV is 0.084 = 4.8°. Figure (2.37) shows that this is just the angle at which $d\sigma_{atom}/d\Omega$ returns to the value $Zd\sigma_{KN}/d\Omega$. When the energy transfer to an electron, T, exceeds E_K, Compton scattering from an atom reverts to Klein-Nishina scattering at angles greater than $\theta_\gamma(h\nu_o,T)$ given by Eq(2.39).

For fixed incident energy E, the variation with Z of the differential cross section near the forward direction is then controlled merely by the K shell energy $T = E_K(Z)$, as it determines $\theta_\gamma(h\nu_o,T)$. This is illustrated in Figure (2.38) which shows the angular distribution of the scattered photon, at $h\nu_o = 1$ MeV, on Be, Fe, and Pb. The differential cross section has been divided by Z so that they become equal away from the forward direction. The cross sections differ only at angles less than $\theta_\gamma(h\nu_o,T)$.

A scattered photon can indeed emerge at $\theta_\gamma = 0$, but it cannot be accompanied by an ejected electron, and so, by definition, the process is not Compton scattering. Coherent scattering peaks at $\theta_\gamma = 0$, but the scattered photon has the same energy as the incident photon. Inelastic scattering can also occur at $\theta_\gamma = 0$, with the atom left in an excited, un-ionized state.

In contrast to the angular distribution of the scattered photon, the angular distribution of the outgoing electron is essentially the same for an atom as for the single-electron Klein-Nishina formula, at least when $E \gg E_K$. The reason is that when a photon scatters into angles near forward, the electron is ejected near $\theta_e = \pi/2$, with little energy and little range in the material. But whenever the electron is ejected with a substantial energy, the photon must impart substantial momentum to the atom, and scatter through a substantial angle. In these cases, the photon and electron distributions follow the Klein-Nishina distribution.

COMPTON SCATTERING IN THE ELEMENTS

As with all photon interaction cross sections, the Compton cross section in the elements is tabulated in various data bases, as mentioned in Section 2.11.

Total Compton Cross Section

If the angular distribution for atomic Compton scattering were the same as that of the Klein-Nishina formula, that is, if $S(q) = Z$ for all q, the total Compton cross section for scattering from an atom would be just $Z\sigma_{KN}$. But in the differential cross section, the actual deviation of S from Z at small q, as just discussed, makes the atomic Compton cross section less than $Z\sigma_{KN}$, especially at relatively low energies.

The Compton cross section *vs* $E=h\nu_o$ for several elements is shown in Figure (2.39). When expressed in cm^2/gm as in this figure, the approximate proportionality to Z is largely removed, and the bulk cross section is only slowly varying with Z.

The slow variation with Z is also seen in Figure (2.40), which shows the Compton scattering cross section (cm^2/gm) for selected energies as a function of Z. Data are taken from EPDL97.

Collecting these data for the elements, the total atomic Compton interaction cross sections (barn/atom) in all elements for energies from 1 keV to 100 MeV are shown in the contour plot of Figure (2.41). The corresponding bulk total Compton cross sections (cm^2/gm) in all elements are shown in the contour plot in Figure (2.42). Here, because contour values are fairly closely spaced, the variation of atomic weight A with Z makes very visible irregularities in the shape of contour lines. These were first discussed in the context of the photo-electric contour plots, Figures (2.7) and (2.9), where the irregularities are not pronounced because of the relatively large spacing between contour lines.

The atomic Compton cross section is proportional to Z and so essentially to A. Mass density ρ is also proportional to A. Therefore, at energies where the Compton effect dominates, the cross section expressed as cm^2/gm by Eq(2.5) is nearly independent of atomic number. This is clearly seen in Figure (2.42). Near 1 MeV, for example, the Compton cross section is about 0.06 cm^2/gm in all elements. In the vicinity of 1 MeV, Compton scattering is the dominant process; therefore the photon-matter total interaction cross section in all elements is also about 0.06 cm^2/gm. This will be seen again in the total cross section graph of Figure (2.53). It is not true far from 1 MeV where the photo-electric or pair production effects dominate.

2.7 PAIR PRODUCTION

At energies above about 1 MeV another photon-atom process can occur in which the photon disappears and an electron-positron pair emerges from the atom. This pair production occurs by the photon interacting with the (static) electric field surrounding the nucleus or an electron. As is the case for Delbrück scattering, enormous fields are required for this process to occur. As mentioned previously, the static nuclear field at a

distance r=100 fm = 10^{-3} Å from a high-Z nucleus is of order 10^{19} V/m, and at a distance 0.01 Å from an electron is 1.4×10^{15} V/m.

For γ rays of nuclear origin ($\lesssim$ several MeV), pair production is seldom the dominant process. At 3 MeV in Aluminum, for example, the cross section is only 0.002 cm^2/gm, requiring several hundred gm/cm^2 to convert most γ's by pair production, whereas the Compton cross section is about 0.034 cm^2/gm. In Tungsten at the same energy pair production is only 0.01 cm^2/gm. But by 20 MeV in Al, or at only 5 MeV in W, the cross section for pair production is as large as the cross section for Compton scattering. At still higher energies pair production is the dominant process for a photon to interact with matter, and remains so at all higher energies.

Threshold Energies for Pair Production

In pair production in the Coulomb field of a nucleus, the heavy nucleus can recoil, absorbing momentum but essentially no energy. Thus, for all practical purposes, energy is conserved among the incident photon and the two members of the created pair, but momentum is not conserved among those three particles alone (of course both energy and momentum are rigorously conserved among the photon, the nucleus, and the created pair). To create the pair and conserve energy, the photon need have only $2mc^2$ of energy, just sufficient to create both members of the pair at rest. Thus the threshold photon energy for pair production in the field of a nucleus is $2mc^2$ = 1.022 MeV.

Pair production can also occur in the field of an electron in the atom. Here, the created positron and electron, and the struck electron, are all ejected from the atom; the process is referred to as *triplet* production. In this case the recoiling electron absorbs both momentum and energy, and the energy it absorbs is not negligible. As the target electron carries some energy away, the threshold photon energy for pair production in the field of an electron will be greater than $2mc^2$. To obtain the threshold energy, it is convenient to consider the conservation laws in the center-of-momentum frame of reference.

Figure (2.43) sketches the geometry. Results will be obtained for a target particle of any mass M, but we are primarily interested in the threshold when the target particle is an electron, $M = m$.

For the discussion of threshold kinematics we work with units in which $h = c = 1$. In the laboratory frame, where the target mass M is at rest, the photon has energy ν_o. In the center-of-momentum (CM) system, the photon has energy ν_{CM}, and the target mass M has momentum $p_{CM} = -\nu_{CM}$. The target energy is $E_{CM} = \sqrt{(M^2 + p_{CM}^2)} = \sqrt{(M^2 + \nu_{CM}^2)}$.

At the threshold of pair production in the CM system, each member of the pair is created at rest. The photon has energy ν_{CM}^{th} to be determined. Since the total momentum vanishes, the target particle is also at rest, and the only energies are the three rest masses. Consequently, equating the incident system energy to the final energy, the CM threshold photon energy for pair production is given by

$$\nu_{CM}^{th} + \sqrt{M^2 + \nu_{CM}^{th\ 2}} = M + 2m \tag{2.40}$$

or

$$\nu_{CM}^{th} = 2m\frac{M+m}{M+2m} \tag{2.41}$$

To obtain the threshold photon energy ν_o^{th} in the laboratory system, we need now only transform the energy ν_{CM}^{th} back to the lab frame in which M is at rest.

To do this, let the velocity of the CM system, measured in the lab frame, be V. Then in the CM system the photon has energy

$$\nu_{CM} = \nu_o\gamma(1 - V), \tag{2.42}$$

where

$$\gamma = \frac{1}{\sqrt{1-V^2}}\ , \tag{2.43}$$

and the target has velocity $-V$ and momentum $p_{CM} = -\gamma MV$. But by definition, the CM system is the one in which the photon momentum equals in magnitude the target momentum,

$$\nu_{CM} = p_{CM} = \gamma MV. \tag{2.44}$$

Thus V is determined by equating

$$\nu_{CM} = \nu_o\gamma(1-V) = \gamma MV\,, \tag{2.45}$$

from which one obtains

$$V = \frac{\nu_o}{M+\nu_o}\ . \tag{2.46}$$

Inserting this expression for V in Eq(2.42) we express ν_{CM} in terms of ν_o,

$$\nu_{CM} = \nu_o\sqrt{\frac{1-V}{1+V}} = \frac{\nu_o}{\sqrt{1+2\nu_o/M}}\ . \tag{2.47}$$

At threshold, this is to be equated to Eq(2.41), and we have

$$\nu_{CM}^{th} = \frac{\nu_o^{th}}{\sqrt{1+2\nu_o^{th}/M}} = 2m\frac{M+m}{M+2m} \ . \tag{2.48}$$

which is the desired relation determining the laboratory threshold energy ν_o^{th} in terms of the target mass M and electron mass m.

Clearly, if the target is very heavy, $M \gg m$, the threshold energy is $2m$, as stated for pair production in the field of a nucleus. But if the target is an electron, $M = m$, Eq(2.48) becomes

$$\nu_{CM}^{th} = \frac{4}{3}m \ . \tag{2.49}$$

Reverting to normal units, the CM threshold photon energy for pair production in the field of an electron is $(4/3)mc^2$. In the laboratory frame, Eq(2.48) says that the threshold photon energy for pair production is

$$h\nu_o^{th} = 4mc^2 \ . \tag{2.50}$$

Pair production in the field of a nucleus starts at $h\nu_o^{th} = 2mc^2 = 1.022$ MeV, while pair production in the field of an electron starts at $h\nu_o^{th} = 4mc^2 = 2.044$ MeV.

In pair production from an electron, energy and momentum are, of course, conserved among the incident photon, the created pair, and the original electron, but neither energy nor momentum is conserved among just the photon and the created pair.

Z Dependence and Approximate Value of Cross Section

Heitler [He54] contains a thorough derivation of the pair production cross section. Bethe and Ashkin [Be53] and Evans [Ev55] review the theory and experimental basis.

In the Coulomb field of an exposed nucleus the amplitude for the process is proportional to the field magnitude, and so to the nuclear charge Ze, and to the electron-positron charge e. Then the amplitude is proportional to Ze^2, and the pair-production cross section on an unscreened nucleus is proportional to $Z^2 r_o^2$. Screening by atomic electrons is important when both the outgoing positron and electron are relativistic. At these high energies screening makes the Z dependence slightly less than the second power. In general, for all elements and at all incident photon energies above 3 MeV, the total pair production cross section from the (screened) nucleus rises from about 1 to less than about 15 times σ_o as Z increases, where

$$\sigma_o \equiv \alpha Z^2 r_o^2 = 5.795\times10^{-4} Z^2 \ \text{(barn)}.$$

The contribution to the total cross section due to pair production from atomic electrons is proportional to Zr_o^2, so the total (nuclear plus electronic) pair production cross section is approximately proportional to $\alpha Z(Z+1)r_o^2 = (1+1/Z)\sigma_o$, at energies greater than $4mc^2$ where both processes are possible. Again, screening

reduces this value at high energies. Figure (2.44) illustrates the approximate proportionality to $Z(Z+1)$. The reduction at high energies is about a factor of two in high-Z elements.

Heitler [He54] shows that the nuclear pair production cross section $\sigma_{pp}^{nuc}(Z,E)$, at very high photon energies E, approaches a constant value independent of E, given approximately by

$$\sigma_{pp}^{nuc}(E\rightarrow\infty) \rightarrow \frac{28}{9}\left[\ln\left(\frac{183}{Z^{1/3}}\right) - \frac{1}{42}\right]\sigma_o$$

More correctly, above 1 GeV both the nuclear and electronic pair production cross sections from an atom are given by an expression of the form

$$\sigma_\infty + [c_2 + c_3\ln(E)]/E.$$

σ_∞ is the infinite energy cross section. σ_∞ and the coefficients c_2 and c_3 are tabulated for each element in, for example, the EPICSHOW data set distributed with LLNL's TART code.

In Al, the right hand side of $\sigma_{pp}^{nuc}(E\rightarrow\infty)$ is 1.32 barn. The infinite energy number σ_∞ for the nuclear cross section is given by the LLNL data base as 1.3097, very close indeed to the theoretical number. With the contribution from pair production off atomic electrons included, the total pair production cross section at 100 GeV on Al is given in the LLNL data base EPDL97 as 1.428 barn, and on Pb at the same energy as 41.183 b.

The foregoing is the "classic" discussion of pair production. Tsai [Ts74] has summarized more recent developments. He reports that the more accurate calculations put the infinite energy Al pair production cross section at 1.443 b, and that of Pb at 41.72 b. In the LLNL database the infinite energy number $\sigma_\infty^{nuc}+\sigma_\infty^{elec}$ for Al is 1.429, and that for Pb is 41.244 b, slightly less than Tsai's value.

Graphs of Pair Production Cross Sections

Tabulations of pair production cross section data are available separately for the nuclear and electronic processes (e.g., in NIST XCOM, or in EPDL97), but here we plot only their sum, the total pair production cross section.

Figure (2.45) shows cross sections as a function of $E = h\nu_o$ for seven elements, while Figure (2.46) plots the cross sections as a function of Z for selected photon energies.

In Figure (2.47) are contours of the total pair production cross section *vs* Z and E in barn/atom. The variation with both independent variables is, of course, quite smooth.

Again converting to units of cm^2/gm by multiplying by N_A/A, contours are shown in Figure (2.48). The irregularity in these contours introduced by the irregular variation of $A(Z)$ is evident. It is especially pronounced near Z=85–86, where $A(Z)$ has a significant discontinuity (recall Figure 2.8).

2.8 TOTAL PHOTON CROSS SECTIONS

Figures (2.49H) through (2.49U) show photo-electric, Rayleigh (coherent), Compton (incoherent), pair-production and total cross sections *vs* incident photon energy in a number of elements of increasing *Z*. Aluminum was shown in Figure (2.4). Plots such as these, for all elements, are conveniently available in LLNL's display package, EPICSHOW, distributed with the neutron-photon Monte Carlo code TART. Similar graphs can also be generated by the Janis software from the Nuclear Energy Agency. See Section 2.11.

It is worth noting that in Hydrogen Compton scattering is the main process from 3 keV to 70 MeV, essentially the full range of X-rays and gamma rays. Photo-electric absorption doesn't dominate until below 3 keV, and pair production doesn't dominate until above 70 MeV. And between about 10 keV and 10 MeV, Compton scattering is an order of magnitude more probable than any other process. This is significant since H is a major constituent of organic materials; scattering from H is more probable than absorption in H.

Likewise, in Carbon Compton scattering is the main process from about 25 keV to 25 MeV. Low *Z* materials tend to scatter X-rays (if sufficiently energetic) more than absorb them.

Total cross sections for several elements as a function of photon energy *E* are also shown in Figure (2.50), and at selected energies as a function of *Z* in Figure (2.51).

Finally, contours of total cross section (barn/atom) in all elements for all energies are in Figure (2.52), and in (cm^2/gm) in Figure (2.53). Its inverse, the mean free path against any scattering (gm/cm^2), is separately useful; it is in Figure (2.54).

From Figure (2.53) or (2.54) one can see, for example, that in high *Z* materials the largest photon mean free path, that is, the most penetrating radiation, occurs at 3 – 5 MeV, while in low *Z* materials it is somewhat higher, near 10 MeV or more.

Use of Contour Plots in Shielding Applications

Besides conveying an appreciation of overall trends in *E* and *Z*, the contour plots can be useful in applications. For example, they can help in selecting shielding material. If we wish to shield, in general, X-rays of energy $\lesssim$ 100 keV, with the least mass of material, one sees from Figure (2.54) that high *Z* elements are to be favored over low *Z*, for the photoelectric effect dominates with a large cross section and small mean free path.

If we wish to absorb as well as possible, with the least mass of material, all photons with energy less than, say, 80 keV, one should not necessarily merely select the highest *Z*. Figure (2.54) shows that the mean free path of an 80 keV photon in U is 0.3 gm/cm^2, while in Nd (*Z*=60) it is only 0.2 gm/cm^2, because we are above the Nd *K* edge but below the Uranium *K* edge. *Z*=58 to 60 are the best absorbers for the purpose, because at all energies the mean free path is less than 0.2 gm/cm^2. While other elements may be better

absorbers of some energies less than 80 keV, all elements other than 58 – 60 have smaller cross sections for some energy less than 80 keV. Note that elements near W are the best absorbers of 80 keV itself, but they are not the best at, say, 65 keV or below.

If the photon spectrum to be absorbed has a certain feature, other elements may be more appropriate. Even if all energies are below 80 keV, it may be that the energy in the X rays is concentrated in a narrower band of lower energies. In that case, to minimize energy transmission, it may be best to choose elements that best absorb in that narrow band, even though they do not absorb each energy below 80 keV as well as other elements.

If a specific energy photon is to be shielded, one can take good advantage of photo-absorption edges. One tries to select a material with *K* edge just below the energy to be absorbed. Suppose we wish to absorb the 59.54 keV γ from the decay of Am^{241}. The *K* edge of element Z=70 (Yb) is 61.33 keV, while that of element *Z*=69 (Tm) is 59.39 keV[4]. Thus Tm can absorb the photon in its K edge, but Yb cannot. One sees from Figure (2.53) that the absorption cross section in elements ..., 68, 69 is about 12 cm^2/gm, while in elements 70, 71, ... is only 3 cm^2/gm, so for the same mass Tm is four times as good an absorber as Yb. What is not so easy to recognize without a contour plot is that not only are elements ..., 68, 69 better than 70, 71, ... but that no other element of any *Z* is as good as *Z*=69. For absorbing 60 keV, Tm requires less mass than any other element. Figure (2.54) shows that the mean free path in Tm is about 0.08 gm/cm^2, while that in Pb is 0.2. Thus to absorb 99% of the photons (4.6 mean free paths), one would need about 0.37 gm/cm^2 of Tm, but 0.92 gm/cm^2 of Pb.

For final, detailed work, after consulting contour plots for estimates, cross section numbers for the selected elements should be checked in the numerical tables on the accompanying CD-ROM or other sources.

2.9 ATTENUATION, AND ENERGY DEPOSITED IN TARGET MATERIAL

Attenuation of a Beam

An incident photon beam is *attenuated* whenever a photon is absorbed or scattered out of the beam. Thus the intensity $I(E,x)$ of the remaining unscattered photons in a beam of photons of energy E depends on distance penetrated x according to

$$I(E,x) = I_o \exp(-N\sigma_{tot}x)$$

where N is the atom number density (cm^{-3}), or density of scattering centers, I_o is the initial intensity, and

---

[4] These are the numbers on the NIST web site. The LLNL EPDL97 data base uses 61.44 and 59.49 keV, respectively.

$$\sigma_{tot} = \sigma_{tot}(E) = \sigma_{pe} + \sigma_C + \sigma_{Rayl} + \sigma_{pp}$$

is the total cross section for the photon to interact with the atom (or scattering center), the sum of photo-electric absorption σ_{pe}, Compton scattering σ_C, coherent Rayleigh scattering σ_{Rayl}, and pair production σ_{pp}. Other minor processes, such as photo-nuclear scattering, should in principle be included in the total cross section, but are conventionally excluded as being negligible[5]. Since Rayleigh scattering is small and tends to peak in the forward direction, it is sometimes not included in the total cross section to define attenuation.

The quantity

$$\mu_o(E) \equiv N\sigma_{tot}(E)$$

is the *linear (total) attenuation coefficient*, with dimensions of cm^{-1}, so that $I(x) = I_o\exp(-\mu_o x)$. When one specifies distance penetrated in a material of density ρ (gm/cm^3) in terms of the mass penetrated, as ρx (gm/cm^2), it is convenient to define the *mass (total) attenuation coefficient*

$$\mu_o/\rho \ \ (cm^2/gm),$$

so that $I(x) = I_o\exp(-(\mu_o/\rho)\rho x)$. The linear attenuation coefficient μ_o is the total cross section per unit volume of material, and the mass attenuation coefficient μ_o/ρ is the total cross section of a gram of material, i.e. the total bulk cross section; it is the quantity plotted in Figure (2.53). The *mean-free-path* in a material against total scattering is $1/\mu_o = 1/N\sigma_{tot}$, expressed here in cm, or ρ/μ_o in gm/cm^2. The mean free path against a single process, say Compton scattering, is $1/N\sigma_C > 1/N\sigma_{tot}$.

The phrase "or density of scattering centers" above allows for compounds or mixtures of elements. The scattering center may then be, instead of a single element, a molecule, like H_2O, or a crystal cell, like NaCl, or any repeated unit of several elements in an arbitrary mixture. In this case each of σ_{pe}, σ_C, σ_{Rayl}, and σ_{pp} is the cross section for scattering from that scattering center, for example $\sigma_C = 2\sigma_C(H) + \sigma_C(O)$.

Energy transferred to the target material: kerma

Neutral particles (photons or neutrons) passing through matter are referred to as *indirectly-ionizing* particles. Charged particles (electrons, protons, ions) are *directly-ionizing*. The obvious reason is that photons or neutrons do not directly ionize the material. They do so only after interacting with an atom and kicking out an electron (or recoil target nucleus), and that moving charged particle then ionizes by direct ionization and excitation stopping power.

Thus the process by which an indirectly ionizing particle deposits energy in a target material is a two step process. In the first step, the neutral (indirectly ionizing) particle, in the present case a photon, interacts

---

[5] As mentioned previously, our Compton cross section, σ_C is what Evans [Ev55] calls the *collision* cross section, $_c\sigma$.

with an atom and ejects one or more charged particles (directly ionizing particles), and perhaps a secondary neutral particle (e.g., Compton scattered photon). The charged particles, in the present case one or more electrons, are ejected with some kinetic energy. In the second step, those charged particles deposit much of their energy directly in the target by ionization and excitation collisions with target atoms (by collisional stopping power).

The quantity *kerma*, or the *energy-transfer coefficient* which is directly related to it, is introduced to parameterize the first step. The quantity *dose*, or the directly related *energy absorption coefficient*, is introduced to parameterize the second step [ICRU80; Ca85].

The first step, the initial ejection of charged particles, takes place at some small volume of interest in the target medium. The second step, the ionization energy loss of those charged particles, occurs over some distance beyond the first volume, distributed over the ranges of the produced electrons. Dose does not occur at the same point at which kerma occurs.

Here we summarize the energy transfer from an incident photon beam to the target material.

In Section 2.4 on the Photo-Electric Effect we mentioned the energy-transfer coefficient and kerma appropriate to that effect. Of course, Compton scattering and pair production also create charged particles in the target material and deposit energy.

In a beam of photons of energy E (MeV), number fluence φ (photons/cm^2) the number of photo-electric interactions per gm in an elemental target of atom number density N, density ρ (gm/cm^3), atom mass density $N_g=N/\rho$ (atoms/gm) is

$$\sigma_{pe}(E)N_g\varphi \quad \text{(photo-electric interactions/gm)}$$

Each interaction ejects a kinetic energy $f_{pe}E = E-X$ in electrons, and so the kerma by the photo-electric effect is

$$k_{pe} = f_{pe}E\sigma_{pe}(E)N_g\varphi,$$

or

$$k_{pe} = (E-X)\sigma_{pe}(E)N_g\varphi \quad \text{(MeV/gm)},$$

where X is the average fluorescence X-ray energy per photo-electric absorption event.

Recall the separate quantity

$$\mu_{tr,pe} = f_{pe}\sigma_{pe}N \quad (\text{cm}^{-1})$$

or

$$\mu_{tr,pe}/\rho = f_{pe}\sigma_{pe}N_g = (1\text{-}X/E)\sigma_{pe}N_g \quad (cm^2/gm)$$

was defined as the energy-transfer coefficient (by the photo-electric effect). In general kerma is the energy-transfer coefficient times the photon energy fluence $E\varphi$,

$$k = (\mu_{tr}/\rho)E\varphi \quad (MeV/gm)\,.$$

In general, the kerma is the sum of the kinetic energies of all charged particles ejected in the neutral particle interaction. Here, with photons incident, these charged particles are electrons. For incident neutrons, the kerma is the sum of the kinetic energies of the recoil nucleus, plus protons, plus α particles, plus ... that may exit the interaction. Kerma is the kinetic energy of directly-ionizing radiation resulting from the interaction of indirectly-ionizing radiation with a material target.

In Compton scattering of a photon of energy E, each Compton electron would have an average energy $f_C E$ if the photon scattered from a free electron (f_C is plotted vs. E in Figure 2.24). Its actual energy is reduced by its atomic binding energy E_B. E_B is recovered as kinetic energy of more electrons if the atom relaxes by ejecting Augers. But E_B appears as more photons if the atom relaxes by fluorescence. As E_B depends on the shell from which the photon scattered, it is simpler to parameterize with the average energy X of fluorescence photons per Compton scattering, and the average energy E' of the Compton scattered photon. The scattered photon continues on to some (relatively) distant point. The kerma by Compton scattering is therefore

$$k_C = (E\text{-}E'\text{-}X)\sigma_C(E)N_g\varphi \quad (MeV/gm).$$

Energy-transfer coefficients can be defined separately for the Compton effect and for pair-production, for example,

$$\mu_{tr,C}/\rho = (1 - (E'+X)/E)\sigma_C N_g \quad (cm^2/gm)$$

is the mass energy-transfer coefficient appropriate for Compton scattering. Kerma by Compton scattering is $k_C = (\mu_{tr,C}/\rho)E\varphi$.

In pair production from the nucleus, an energy $E\text{-}2mc^2$ appears as kinetic energy of the electron and positron. Thus the kerma due to nuclear pair production is

$$k_{ppn} = (E\text{-}2mc^2)\sigma_{ppn}(E)N_g\varphi \quad (MeV/gm),$$

where σ_{ppn} is the nuclear pair production cross section.

Pair production from atomic electrons (triplet production) is similar except that fluorescence X-rays are again possible. The kerma due to electronic pair production is

$$k_{ppe} = (E\text{-}2mc^2\text{-}X)\sigma_{ppe}(E)N_g\varphi \quad (MeV/gm),$$

where σ_{ppe} is the electronic pair production cross section, and X is the average fluorescence X-ray energy.

In Rayleigh scattering the photon leaves no energy behind, and so produces no kerma.

Together, all photon interactions produce a kerma

$$k_{tot} = k_{pe} + k_C + k_{ppn} + k_{ppe} \qquad \text{(MeV/gm)} \tag{2.51}$$

The total kerma per unit fluence (*specific kerma*) is

$$\begin{aligned} k'_{tot} &\equiv \frac{k_{tot}}{\varphi} \\ &= [(E-X)\sigma_{pe} + (E-E'-X)\sigma_C + (E-2mc^2)\sigma_{ppn} + (E-2mc^2-X)\sigma_{ppe}]N_g \qquad \text{(MeV-cm}^2\text{/gm)} \end{aligned} \tag{2.52}$$

Here, the X in each process is different, as it depends on the distribution of electron shells with which the photon interacted, and must be evaluated separately for photo-electric absorption, Compton scattering, and electronic pair production. While units indicated are MeV-cm^2/gm, kerma per unit fluence is equally often expressed in erg-cm^2/gm, or rad-cm^2 (=rad per photon/cm^2). 1 rad ≡ 100 erg/gm. SI unit purists must use J-m^2/kg = Gy-m^2; 1 Gy ≡ 1 Gray ≡ 1 J/kg ≡ 100 rad.

Kerma is a point quantity, being the photon energy immediately transferred to kinetic energy of charged particles in a small volume, in the limit as the volume becomes infinitesimally small. Therefore only the first photon interaction in that volume is included in its definition. For example, the subsequent photo-electric absorption of a Compton-scattered photon is not included. All energy in scattered photons is treated as "non-local" and is not included in the definition of kerma.

Even though not all the kinetic energy of charged particles released in the material gets deposited locally (i.e., not all kerma turns into dose, partly due to non-ionizing Bremsstrahlung energy loss), kerma is useful because, unlike dose, it is independent of target geometry and is directly related to basic cross sections. It is also an approximate upper limit to dose; except for attenuation and finite electron range effects discussed below, dose is never larger than kerma.

Kerma in a compound or mixture of elements is the simple additive sum of its constituents, by weight fraction. If a compound consists of elements i and j, in weight fractions w_i and w_j, and k'_i and k'_j (MeV-cm^2/gm) are the specific kermas in each element separately then the kerma in the compound is

$$k' = w_i k'_i + w_j k'_j .$$

As discussed below, the dose in a compound does not add so simply.

Photon fluence-to-kerma conversion factors

As kerma depends only on basic cross sections, it is a function only of photon energy E for a given elemental target material. Photon kerma as a function of E for several elements is shown in Figure (2.55) and for selected semiconductors in Figure (2.56). It is shown as a function of Z for several energies in Figure (2.57). As was the case for cross sections, it may be displayed for all elements as contours in Z-E space. Figure (2.58) shows photon kerma in the elements. The units chosen, rad(element) per unit photon fluence (here taken as 10^9 photon/cm^2), are the units in which one commonly specifies dose. These curves are the photon *fluence-to-kerma* conversion functions. To the extent that kerma is the same as dose, they are also the *fluence-to-dose* conversion functions, or the *material response function*, giving energy deposited in any element for incident photons of any energy and any fluence.

The figures show that at E = 1 MeV, all elements from Z=2 to about 60 experience approximately 4.5×10^{-10} rad per photon/cm^2. Conversely, it requires some 2.2×10^9 photons/cm^2 of 1 MeV to deliver 1 rad to any element with Z<60 (except H). Higher Z experiences a slightly higher kerma, up to about 8×10^{-10} rad per photon/cm^2. At 0.8 to 4 MeV, for all elements, the responsible process is Compton scattering. At a fixed photon energy E below a few MeV, the response function increases somewhat as Z increases. The reason is two-fold. First, the bulk cross section increases as Z increases, Figure (2.53), because at high Z the larger photo-electric cross section becomes non-negligible compared with the Compton cross section. Second, the average photon energy converted to electron energy in the Compton effect is less than or of order E/2, whereas for the photo-electric effect it is essentially E. For example, at the Cs^{137} line, E = 0.662 MeV, the cross section rises from about 0.08 cm^2/gm at low Z to 0.14 at high Z (Figure 2.53), not quite factor of 2. But the kerma per unit fluence increases by more, from 0.3 to 1 rad per 10^9 photons/cm^2, due to the increased fraction of photon energy converted to kerma as the photo-electric effect becomes relatively more important at higher Z.

Energy deposited in the target material: Dose

Once the first step has been completed, the photon has ejected electrons (and possibly positrons) from parent atoms. The kinetic energy in those electrons and positrons is the kerma. As the electrons move they lose their energy along their track length to collisional excitation and ionization, and to Bremsstrahlung. The energy lost per gram of target material to excitation and ionization (collisional stopping power) is taken to be "deposited locally", and is the *dose*. Since the loss to Bremsstrahlung is non-zero, dose is apparently less than kerma. But since the electrons move away from their point of origin, the dose occurs at points different from where the original kerma occurs. This may allow dose, as a point function of position, occasionally to exceed kerma, even in a uniform medium (see following section).

While the spatial distribution of dose and kerma may differ, their spatial integrals would be equal if no energy were lost to Bremsstrahlung. Energy lost to Bremsstrahlung prevents dose from equaling kerma, even when integrated over all positions. In pair production, the positron loses energy by ionization and excitation just as the electron does, usually before annihilating with another electron. So except for positron Bremsstrahlung, its full kinetic energy also is part of the dose.

Let g be the fraction of an electron's energy eventually lost to photon emission during the course of its

slowing down to rest. In first approximation, g is just the Bremsstrahlung *radiative yield* Y_R, discussed in Chapter 3, being the fraction of energy lost to Bremsstrahlung radiation from an energetic electron. Positron annihilation in flight is a small correction to g [Hi92]. Another correction comes from how one treats energy lost to atomic relaxation fluorescence photons following electron collisional (excitation and ionization) energy losses with atoms. There seems to be no universal agreement as to whether the energy of these fluorescence photons should or should not be included in dose [ICRU80, Hu95], but for consistency their energy should be excluded as well. The compilation by Hubbell and Seltzer [Hu95] has the best accounting of photon energy.

For any target material, then, the *energy-absorption coefficient* μ_e is smaller than the *energy-transfer coefficient* μ_{tr} by g

$$\mu_e = (1-g)\mu_{tr} \quad (\text{cm}^{-1}) \ .$$

Likewise, the *mass energy-absorption coefficient* μ_e/ρ is related to the mass energy-transfer coefficient μ_{tr}/ρ by

$$\mu_e/\rho = (1-g)\mu_{tr}/\rho \quad (\text{cm}^2/\text{gm}) \ .$$

The dose is the mass energy-absorption coefficient times the photon energy fluence $E\varphi$,

$$\text{dose} = (\mu_e/\rho)E\varphi \quad (\text{MeV/gm})$$

or the dose per unit fluence (the *specific dose*),

$$\text{dose}/\varphi = (\mu_e/\rho)E \quad (\text{MeV-cm}^2/\text{gm}) \ .$$

This definition of dose, in terms of μ_e, parallels that of kerma in terms of μ_{tr}. It is valid more conceptually than in detail in a specific application because of the above caveat that, because of electron range, dose occurs at a different point from where kerma occurs.

In addition, if the target is made of thin layers of different materials, kerma occurring in one layer may cause dose in another layer as the electrons move. That other layer may have a much different energy transfer coefficient and a different electron stopping power from the first layer. Thus dose also depends on problem geometry. Therefore, due to angular scattering of electrons and complicated materials geometry, in principle the only way to accurately compute dose in a realistic problem is by a photon-electron transport calculation, for example a Monte Carlo simulation.

Kerma and dose at a material interface

Figure (2.59) sketches a side view of photons entering a uniform slab of material from vacuum. The photons may interact with any atoms along the way, so kerma occurs immediately near the surface; kerma at

a point is directly proportional to beam fluence and material density at that point. As the beam proceeds, attenuation reduces its fluence (and its kerma) exponentially. But the *dose* at shallow depth d near the surface is due only to those electrons produced in the preceding thin layer $0<x<d$ (and back-scattered electrons, which we here ignore). There are few of these, so the dose for small x is small. It builds up linearly with increasing depth d as kerma adds more electrons. Dose saturates at a depth equal to the range R_{max} of the most energetic electron. At greater depths than that electrons are ejected anew from atoms at about the same rate at which previous electrons come to rest, causing a "steady state" balance between kerma and dose. The balance is not quite equal, however, because the local dose at depth d is due to electrons created back to $d-R_{max}$, where intensity and kerma were greater. Thus at a given depth it is possible for dose to exceed kerma. Usually, R_{max} is much less than the beam attenuation length (or mean-free-path), so dose closely approximates kerma. For example, in Si, the mean-free-path of a 1 MeV γ-ray is about 16 gm/cm^2, while R_{max} of a 1 MeV electron is less than 0.6 gm/cm^2. At γ-ray energies ($\gtrsim$1 MeV), Compton electrons are generally energetic enough ($\gtrsim$0.5 MeV) and produced more nearly in the forward direction so that their back-scattering is a small correction. At X-ray energies, however, where photo-electric absorption dominates, electrons are produced in the backward hemisphere almost as much as in the forward hemisphere, and of lower energy so that scattering is more important. Then electron backscatter is not negligible.

The term *charged particle equilibrium* is introduced as the condition for dose to equal kerma. It means that electrons must be ejected from their parent atoms uniformly over a distance R_{max}. It does *not* merely mean that a new charged particle enters the (infinitesimal) volume of inquiry whenever one leaves it; rather, the stopping power of the exiting particle must equal that of the entering particle (which effectively means their energies must be equal) in order for the dose to be compensated. When charged particle equilibrium holds, dose equals kerma.

The dose profile depicted in Figure (2.59) holds only when the preceding medium is vacuum. If, say, the medium were air, then photo-electrons and Compton electrons produced in the air would enter the slab at $x=0$, and dose at $x=0+\epsilon$ would be higher than shown.

A second, common situation occurs at the interface between two materials, as sketched in Figure (2.60), where charge particle equilibrium is clearly violated. Material 1 and material 2 are each taken to be slabs thin compared with the photon mean-free-path, so beam attenuation can be neglected, and the photon fluence is a constant through both slabs. Likewise, the kerma is a constant in material 1, and constant, at a different value, in material 2. As they are of different Z, the mass energy-transfer coefficients μ_{tr}/ρ and kermas of the two materials are different, and so the kerma is discontinuous across the interface, as indicated by the two different levels in the figure. Farther than an electron range from the interface the dose is also constant and equal to the kerma.

The figure is drawn for the case $\mu_{tr}/\rho(2) > \mu_{tr}/\rho(1)$, so that kerma is greater in material 2 than in 1. Some of the electrons produced in 2 near the interface scatter back into 1, adding to the dose there. Other electrons are produced in 1 near the interface and move into 2. Together, these make the dose near the interface in 1 greater than its distant, constant value, and that in 2 near the interface less than its distant, constant value. This scattering tends to smooth out the discontinuity in dose, while leaving the discontinuity in kerma. The

electron number flux across the interface is, of course, continuous. Thus the dose itself would be exactly continuous if the electron stopping power were the same in both media. Since the stopping powers are not equal, a small discontinuity in the dose results. The sketch is drawn for the case that the stopping power in material 1 is greater than that in material 2, so the dose in 1 at the interface is greater than that in 2. If the stopping power in 1 were smaller than in 2, the dose in 1 at the interface would be less than that in 2.

Clearly, while kerma depends only on material cross sections, dose depends as well on material geometry and electron transport. Thus, no plots of dose vs Z and/or E can be prepared comparable to those of kerma vs Z and/or E.

Since the fraction g of energy lost to radiative processes depends on the elements in the target material, the dose in a compound material is not the simple weight-fraction additive sum that kerma is. Dose in one element is computed using a radiative yield Y_R appropriate only to that element.

Attenuation, Energy-Transfer, and Energy-Absorption

Photon beam attenuation is due to the total cross section σ_{tot}, with attenuation rate $\sigma_{tot}N_g$ (cm^2/gm). The energy transfer rate μ_{tr}/ρ is smaller than attenuation due to energy scattered out in the form of other photons. The energy absorption rate μ_e/ρ is smaller than the energy transfer rate because of Bremsstrahlung and other radiative losses.

A pictorial way of seeing the flow of energy from the incident photons to final deposition, due to each process, photoelectric, Compton, Rayleigh, and pair production, has been suggested by J. H. Hubbell of NIST [Hu77, Hu99b].

The Hubbell Diagram, Figure (2.61), depicts photons entering from the left and interacting with a target material via one of the processes. The upward-branching arrows depict energy going off after the interaction in photons, leaving the "local" deposition region; these photons are either the scattered incident photon, Bremsstrahlung, fluorescence, or from positron annihilation. All processes together contribute to beam attenuation. All but coherent Rayleigh scattering contribute some energy transfer and deposition. After scattering of the incident photon and rapid fluorescence, but before Bremsstrahlung, is the energy-transfer coefficient μ_{tr}. After losses to Bremsstrahlung and positron annihilation in-flight is the actual energy absorption, μ_e.

Older literature [Ev55] considers only the energy of first scattered photons to be removed from the photon beam, the remainder being deposited, and refers to the resulting coefficient as the "mass absorption coefficient", μ_a. Modern treatments account for energy lost from the charged particles to Bremsstrahlung, fluorescence photons, and positron annihilation radiation before attributing the remainder to being deposited; the result is the mass energy-absorption coefficient μ_e.

As an example, Figure (2.62) shows the attenuation and energy-transfer coefficients, μ_a/ρ and μ_{tr}/ρ respectively, for photons in Si and in Pb, from 100 eV to 100 MeV. As the fluorescence yield in Si is small,

there is little difference between the two coefficients at the K-edge. The difference is significant in high-Z elements, as seen in Pb. The energy absorption coefficient μ_e/ρ is not shown in the figure. It is smaller than μ_{tr}/ρ only at very high energies ($\gtrsim$100 MeV) when the radiative yield of produced electrons and positrons becomes significant.

2.10 ELECTRON FLUX FROM PHOTON FLUX. THE "1% RULE"

Most of the effects on target materials of the passage of photons are due to dose, the energy deposited by the photons. But some targets, notably pixellated semiconductor devices such as charge-coupled devices (CCDs), or focal plane arrays (FPAs), are sensitive to the passage of individual electrons through the pixels, even one energetic electron through one pixel. Actually, this sensitivity is a matter of dose, but only the dose left by electrons that pass through a pixel (whose sensitive volume may be only microns thick) and create electron-hole pairs. In addition to their energy deposition *per se*, one is interested in the number of electrons that pass per cm^2, for that determines noise. Therefore one is interested in the number of electrons, not merely their dose, that are created by an incident photon beam.

Electrons are created from a photon beam by photoelectric absorption, by Compton scattering, and by pair production. In common situations involving nuclear γ rays with energies on the order of an MeV, these electrons are usually Compton electrons.

In a material of atom number density N, the rate at which incident photons of energy E and flux $f_\gamma = f_\gamma(E)$ (photons/cm^2/sec) interact by process i [i = pe (photo-electric absorption), C (Compton scattering), or pp (pair production)] is

$$\eta_i \equiv \text{number of interactions of process } i \text{ per cm}^3 \text{ per sec} = \frac{f_\gamma}{\lambda_i} \ , \tag{2.53}$$

where $\lambda_i = 1/N\sigma_i$ is the mean free path for process i, and $\sigma_i(E)$ is the cross section for that process.

Electrons are produced with some energy distribution, but with average energy E_{ei} when created by process i. Electrons with energy E_{ei} have a range $R = R(E_{ei})$ against their total stopping power in the medium. In steady state, therefore, the flux of electrons is obtained by integrating their production rate over a distance equal to their range,

$$\text{electrons/cm}^2\text{/sec by process } i \equiv f_{ei} = \eta_i R = N\sigma_i f_\gamma R = (R/\lambda_i) f_\gamma \ .$$

f_{ei} is the omni-directional flux of electrons caused by process i, the flux of interest for the ionization subsequently caused by the electrons. This expression for f_{ei} assumes that there is material an electron range R before the point of interest to create the electrons that arrive at the point. That is, we assume charged particle equilibrium. As the range of a 1 MeV electron is less than 0.8 gm/cm^2 in all materials (< 0.3 cm Al, or 6.4 m STP air), charged particle equilibrium will indeed often hold in practical situations. At a depth $x < R$ in a material at a vacuum-matter interface, with the photons entering from vacuum, the electron flux f_{ei}

depends on x approximately as $f_{ei} = \eta_i x$.

(We are discussing the full flux of omni-directional electrons and positrons. But if one wanted the electromagnetic current of the electrons, that is, their net flux in the original direction of the photons rather than their omni-directional flux, R must be replaced by the *mean forward* range R_m of electrons against multiple scattering in the electron original direction of motion, times a factor $\langle\cos\theta\rangle$ for the average of the cosine of their production angle in process i. Then the electromagnetic current density is $-e$ times the flux of electrons crossing a plane normal to the incident photon momentum:

$$\text{Electromagnetic current density} = -e\,(R_m\langle\cos\theta\rangle/\lambda_i)\,f_\gamma\,,$$

where e is the magnitude of the electron charge. As will be seen in Chapter 3, R_m may be as small as $R/2$ or smaller. And for the photo-electric effect, electrons are ejected nearly perpendicular to the incident photon direction, so the directed electromagnetic flux $(R_m\langle\cos\theta\rangle/\lambda_i)\,f_\gamma$ is much smaller than the omnidirectional flux $(R/\lambda_i)f_\gamma = f_{ei}$. At energies where the Compton effect dominates, $\langle\cos\theta\rangle \approx 1$, and the electromagnetic current density is smaller than the omnidirectional electron flux only because $R_m < R$. Pair production contributes, of course, to the omni-directional flux of ionizing particles, but does not contribute to the electromagnetic current as no net charge is displaced. The recoiling struck electron in electronic pair production has very little energy, and so contributes negligibly. Thus, of the three processes it is primarily Compton scattering that contributes to the electromagnetic current.)

Returning to the complete flux, the total cross section is $\sigma_{tot} = \sigma_{pe} + \sigma_C + \sigma_{pp}$, and the omni-directional electron flux is

$$f_e = \Sigma_i f_{ei} = f_{e\,pe} + f_{e\,C} + f_{e\,pp} = N[\sigma_{pe} R(E_{e\,pe}) + \sigma_C R(E_{e\,C}) + \sigma_{pp} R(E_{e\,pp})]f_\gamma\,.$$

The cross section for each process is weighted by the electron range at the average energy $E_{e\,pe}$, $E_{e\,C}$, or $E_{e\,pp}$ appropriate for that process.

The dependence of f_e on photon energy E can be estimated. Photon energies above 100 keV are primarily of interest. The electron energy E_e is roughly proportional to the photon energy E. The electron range R is roughly proportional to E_e^2 for E_e less than a few hundred keV, is roughly proportional to E_e up to about 10 MeV, and increases only logarithmically above 10 MeV (due to Bremsstrahlung). The photo-electric cross section is roughly proportional to $1/E^3$. Thus $f_{e\,pe}$ scales between $1/E$ and $1/E^2$ when $0.1 < E < 1$ MeV. For Compton scattering, σ_C is only slowly decreasing with E up to ~ 1 MeV; at higher energies it drops off roughly as $1/E$. Thus $f_{e\,C}$ increases with E when below ~ 1 MeV, and then tapers off to be nearly independent of E above 10 MeV. The pair production cross section approaches a constant above several tens of MeV, while the electron range continues to increase; thus $f_{e\,pp}$ continues to increase roughly linearly with E.

The ratio of electron flux $f_{e\,i}$ to incident photon flux f_γ is

$$\xi_i = f_{e\,i}/f_\gamma = R/\lambda_i = N\sigma_i R.$$

When $E \sim 1$ MeV (and so the Compton effect dominates), this ratio is often of order 10^{-2} for most materials;

$$f_e \approx 0.01 f_\gamma \qquad (E \sim 1 \text{ MeV})$$

The Compton electron flux is about 0.01 times the photon flux. This is the origin of the name "The 1% Rule". But the ratio differs substantially from 0.01 at other energies. For example as E increases from 0.1 to 10 MeV, E_e and R increase by more than 2 orders of magnitude, while σ_C decreases by only 1 order of magnitude. Thus the ratio continues to increase. Above 10 MeV, where pair production dominates, the pair production cross section saturates, but E_e and R continue to increase, similarly increasing the ratio. A better rule can be constructed.

The 1% Rule

From the previous estimates of the scaling behavior of $f_{e\,pe}$, $f_{e\,C}$, and $f_{e\,pp}$ with E, the ratio

$$\xi_E = f_e / E f_\gamma$$

is more nearly constant with increasing E than the ratio f_e/f_γ itself. The quantity

$$\xi_E \equiv f_e / E f_\gamma = N[\sigma_{pe} R(E_{e\,pe}) + \sigma_C R(E_{e\,C}) + \sigma_{pp} R(E_{e\,pp})]/E, \qquad (\text{MeV}^{-1})$$

that is, the ratio of the electron number flux f_e to the photon energy flux Ef_γ, turns out to be nearly independent of E over a wide range of E.

Figures (2.63) to (2.67) show the ratios $\xi = f_e/f_\gamma$ and $\xi_E = f_e/Ef_\gamma$ in air, Silicon, Germanium, InSb, and $Hg_{1-x}Cd_xTe$ with x=0.2, together with the contribution to ξ_E from Compton scattering. In Si the Compton effect dominates from 0.2 to 10 MeV, and above that energy the Compton contribution to ξ_E drops off, but pair production keeps the ratio up near 0.01. Below about 0.2 MeV, most electrons are created by photo-electric absorption. In Ge, Compton scattering dominates only from about 0.4 to 4 MeV. In both Si and Ge, ξ itself is close to 0.01 only near 1 MeV. Some values are given in Table 2.1.

The numbers for GaAs are essentially the same as for Ge, due to the proximity of atomic numbers. Differences arise only immediately near X-ray edges.

In these results, the positron from pair production has been included, for it ionizes much as an electron does. Thus f_e is really the flux of electrons and positrons[6]. At 30 MeV in Ge, where $\xi_E = 0.0199$, the positron flux is very nearly equal to the electron flux, and it happens that the ratio of each to photon energy flux is very nearly exactly 0.01 MeV^{-1}.

---

[6] Positrons ionize at about the same rate as electrons, and usually come to rest before annihilating. Positron annihilation in-flight is a small correction. See, e.g., Heitler [He54], or Berger and Seltzer [Be82].

TABLE 2.1. Electron/photon flux ratios for several photon energies. ξ is dimensionless. ξ_E is in MeV^{-1}.

Photon Energy (MeV)	Air		Si		Ge or GaAs		InSb		$Hg_{0.8}Cd_{0.2}Te$	
	ξ	ξ_E	ξ	ξ_E	ξ	ξ_E	ξ	ξ_E	ξ	ξ_E
0.1	1.11e-4	1.11e-3	5.31e-4	5.31e-3	7.48e-3	7.48e-2	2.20e-2	2.20e-1	1.58e-2	1.58e-1
0.5	3.44e-3	6.87e-3	3.85e-3	7.70e-3	5.15e-3	1.03e-2	8.98e-3	1.80e-2	1.70e-2	3.40e-2
0.6616 (Cs^{137})	5.65e-3	8.54e-3	6.27e-3	9.48e-3	7.51e-3	1.14e-2	1.06e-2	1.61e-2	1.74e-2	2.63e-2
0.8	7.68e-3	9.60e-3	8.46e-3	1.06e-2	9.75e-3	1.22e-3	1.25e-2	1.57e-2	1.86e-2	2.32e-2
1	1.06e-2	1.06e-2	1.16e-2	1.16e-2	1.31e-2	1.31e-2	1.56e-2	1.56e-2	2.08e-2	2.08e-2
1.1732 (Co^{60})	1.31e-2	1.12e-2	1.42e-2	1.21e-2	1.59e-2	1.35e-2	1.82e-2	1.55e-2	2.30e-2	1.96e-2
1.3325 (Co^{60})	1.53e-2	1.15e-2	1.66e-2	1.25e-2	1.83e-2	1.38e-2	2.07e-2	1.55e-2	2.51e-2	1.89e-2
2	2.34e-2	1.17e-2	2.57e-2	1.28e-2	2.80e-3	1.40e-3	3.10e-2	1.55e-2	3.55e-2	1.77e-2
3	3.28e-2	1.09e-2	3.75e-2	1.25e-2	4.23e-2	1.41e-2	4.85e-2	1.62e-2	5.56e-2	1.85e-2
5	4.83e-2	9.67e-3	5.90e-2	1.18e-2	7.44e-2	1.49e-2	9.23e-2	1.85e-2	1.08e-1	2.16e-2
10	8.26e-2	8.26e-3	1.13e-1	1.13e-2	1.71e-1	1.71e-2	2.30e-1	2.30e-2	2.72e-1	2.72e-2
20	1.50e-1	7.48e-3	2.28e-1	1.14e-2	3.86e-1	1.93e-2	5.35e-1	2.67e-2	6.26e-1	3.13e-2
30	2.18e-1	7.26e-3	3.46e-1	1.16e-2	5.97e-1	1.99e-2	8.21e-1	2.74e02	9.54e-1	3.18e-2
50	3.54e-1	7.08e-3	5.77e-1	1.15e-2	9.84e-1	1.97e-2	1.32	2.63e-2	1.51	3.02e-2
100	6.75e-1	6.75e-3	1.08	1.08e-2	1.735	1.74e-2	2.22	2.22e-2	2.49	2.49e-2
200	1.20	6.02e-3	1.81	9.04e-3	2.703	1.32e-2	3.31	1.65e-2	3.63	1.82e-2

For photon energies $E > 100$ MeV, the corresponding electron (and positron) energies are above ~ 50 MeV (mostly from pair production), and their range exceeds ~ 20 gm/cm^2. In practical devices, charged particle equilibrium is much less likely to hold at these energies, and the actual ratio of (electron+positron) flux to photon flux will likely be less than in the table or the figures.

The Compton cross section (cm^2/gm) is only slightly smaller for high Z elements than for low Z. The electron range (gm/cm^2) is only slightly larger in high Z elements than in low Z. Thus the Compton contribution to ξ or to ξ_E is nearly independent of Z, as can be seen by comparing air with HgCdTe.

The photoelectric cross section near 100 keV is some two orders of magnitude larger for $Z \approx 80$ than for $Z \approx 8$. Thus the Photoelectric contribution to ξ or to ξ_E is two orders of magnitude greater in HgCdTe than in air or Si.

The pair production cross section is several times larger for high Z than for low Z. Thus above several MeV, the ratios ξ and ξ_E are several times larger in HgCdTe than in air or Si. These dependencies on Z can be seen in the figures from air to HgCdTe.

Thus, *The 1% Rule* may be taken as the observation that the ratio ξ_E of electron (+ positron) omni-directional *number* flux to photon *energy* flux remains near 0.01 MeV^{-1} over a wide range of energies, assuming charged particle equilibrium. In Si, the ratio is between ~0.9 and 1.3 % for all energies in $0.6 \lesssim E$ (MeV) $\lesssim 200$. In Ge it is between 1 and 2 % over the same energies.

As mentioned, charged particle equilibrium becomes valid only at a depth beyond the range of the most energetic electrons. Due to relatively long electron range, this condition is stressed in practice in a single medium for high photon energies, where Compton and/or pair production dominate. For the case $E \approx 1$ MeV, typical electron energies are ~ 0.5 MeV. The range of a 0.5 MeV electron is approximately 0.25 gm/cm^2 in most materials. In Si, therefore, the table and figures for the 1% rule are not strictly applicable above 1 MeV until one reaches depths of more than 0.1 cm. However, equally often in practice the target is not directly exposed to photons through vacuum. Instead the photons must penetrate some other solid before striking the target material, such as an Al or stainless steel housing, or air, etc. The table and figures are applicable in the chosen target material if that material is preceded by a thickness of other matter equal to the range of the most energetic electrons produced [near 1 MeV that is about 0.2 gm/cm^2 or more of Aluminum or other material]. To the extent that the target material of interest is surrounded by sufficient columnar mass density of other matter the table and figures will be approximately correct, since the ratios ξ and ξ_E are only slowly varying with atomic number.

2.11 SOURCES of CROSS SECTION DATA

Sources of Photon Cross Section Data

The two principal photon-atom cross section databases have been compiled by NIST and by LLNL. Both are available at no cost on the web. Both are for unpolarized incident photons only, and contain no polarization data. (It is possible for polarized photons to follow from unpolarized incident photons, for example in Rayleigh scattering near 90°. The NIST and LLNL compilations provide no information for applications involving incident or outgoing polarized photons.)

NIST cross sections may be found in the XCOM data base at the NIST physics reference data site, http://physics.nist.gov/PhysRefData/Xcom/Text/XCOM.html. All cross sections on the elements (photo-electric, Rayleigh, Compton, nuclear and electronic pair production) are tabulated at incident photon energies from 1 keV to 10^5 MeV. Any compound or mixture may be entered, and its cross sections will be returned

over the same energies. The incoherent scattering function and the coherent scattering form factors are provided not directly in XCOM, but in another tabulation called FFAST, also on the NIST site [Ch95b], so angular distributions can be constructed. The databases are updated periodically. [Sa88] summarizes almost all of the data to 1988.

Over the years NIST has developed a series of Monte Carlo transport codes primarily for the transport of photons and electrons, under the generic name ETRAN. ETRAN algorithms form the basis for a number of later codes, such as CYLTRAN, ACCEPT, Sandia's SANDYL, TIGER and its outgrowth ITS (Integrated Tiger Series), and so forth [Se88]. Electron energies are typically 1 keV to 1 GeV. The ETRAN-based codes provide the transporting and sampling algorithms; various cross section databases may be used.

The LLNL photon cross section database is the Evaluated Photon Data Library (EPDL), updated every few years. The current version, EPDL97, is from 1997. This compilation contains all cross sections on the elements at photon energies from 1 eV to 10^5 MeV (the previous version, from 1989, started at 10 eV). In addition to the total cross sections (integrated over solid angle) as a function of incident photon energy, the incoherent scattering function and coherent scattering form factors are given, allowing one to construct angular distributions (as were used to construct the plots in this chapter). In addition, partial photo-electric cross sections for ionization from individual electron shells are given.

EPDL97 is documented in [Cu97], and the format of its files in [Pe02]. Both documents are included on the distribution CD-ROM, and are separately available as discussed below.

The EPDL97 data library is stored in ASCII text documents, readable by almost any editor on any computer, with the numbers arrayed in one of two formats, that of the ENDF library (six columns per line), or that of the ENDL library (two columns per line). The ENDL format is being phased out in favor of the more popular ENDF format[7]. These are summarized separately below. On the other hand, the NIST site presents on-line columnar data that can be downloaded immediately into any text file or spreadsheet.

The EPDL compilation of photon cross sections is available in the ENDF *and* ENDL formats via any one of the following four sites:

- National Nuclear Data Center, Brookhaven National Laboratory, http://www.nndc.bnl.gov/nndc/endf/
- Los Alamos National Laboratory, http://t2.lanl.gov/data/atomic.html
- The International Atomic Energy Agency, Vienna, http://www-nds.iaea.org/epdl97/.
- The International Nuclear Energy Agency, Paris, http://www.nea.fr/.

---

[7] The ENDF format is now the de facto world standard for tabulating cross sections. It was originally devised by BNL to tabulate neutron cross sections. Meanwhile LLNL had been compiling electron and photon cross sections in their own ENDL-format library. Most of the electron and photon data in ENDL has been transcribed to ENDF format. But the ENDF format has no provision for a few quantities; they remain only in ENDL format. Examples are photo-atomic excitation cross sections and the average energy of outgoing particles.

The site http://www.llnl.gov/cullen1/ serves as a portal to most of the above four sites.

Sources of General Nuclear and Particle Data

Although it departs from the current topic of photons, we digress to present sources of data of more general interest.

Commonly needed material data include

- Data on particle interactions with atoms and nuclei (photo-atomic and electro-atomic cross sections, neutron cross sections, angle and energy distributions, etc.)
- Radioactive nuclear decay data
- Fission product yields

The international network for compiling, maintaining, and making available these and related data is comprised of four primary centers:

- The U.S. National Nuclear Data Center (NNDC) at Brookhaven National Laboratory (BNL), Brookhaven, NY, http://www.nndc.bnl.gov/
- The International Atomic Energy Agency (IAEA), Vienna, Austria, http://iaeand.iaea.or.at/
- The International Nuclear Energy Agency (NEA), headquartered in Paris, France, http://www.nea.fr/
- The Russia Nuclear Data Center (Institute of Physics and Power Engineering, IPPE), Obninsk, Russia. http://www.rssi.ru/IPPE/

Other locations, primarily the

- Los Alamos National Laboratory T2 site, http://t2.lanl.gov/

maintain access to most of these data as well. In addition,

- The U.S. Idaho National Engineering and Environmental Laboratory (INEEL) maintains radioactive decay gamma spectroscopy data, http://www.inel.gov/, http://id.inel.gov/gamma/.

- The U.S. National Institute of Standards and Technology (NIST) does not maintain a *nuclear* database, but does provide photon and charged particle atom interaction data, and its own measurements of radioactive nuclide half lives, http://physics.nist.gov/PhysRefData/.

Particle cross section data for photon, electron, protons, heavier ions, and neutron projectiles, and particle decay data, often but not always from ENDF, are available then at five main organizations:

LANL; NNDC; IAEA; NEA; NIST

at their web sites listed above.

Most sites that provide particle data do so in three major categories:

1. Raw experimental data
2. Evaluated data
3. Bibliography of experimental measurements

A typical user will be interested in category 2, a collection of "best" experimental measurements and calculations that have been reviewed and stand as "recommended" values. Experts will be interested in categories 1 and 3.

Over the years, several countries have produced many nuclear data libraries. Most are accessible through the NEA or IAEA at the above web sites. The list here is incomplete. All are in ENDF-6 format unless otherwise specified.

GENERAL PURPOSE LIBRARIES

BROND Russian (and FSU) evaluated neutron data library.

CENDL Chinese Evaluated Neutron Data Library.

ENDF/B-VI US evaluated nuclear data library. The library is divided into the following sublibraries; incident neutron data (general purpose library), radioactive decay data, fission yields data, thermal scattering law data, photo-atomic interaction data, electro-atomic data, incident charged-particle data, activation data, and dosimetry data.

JEFF The Joint Evaluated Fission and Fusion File is an evaluated library produced via an international collaboration of Data Bank member countries. Supercedes outdated JEF compilation.

JENDL Japanese Evaluated Neutron Data Library.

SPECIAL PURPOSE LIBRARIES

ADL Russian activation data library. The library contains excitation functions of reactions on targets for neutron energies up to 20 MeV. The library is in a psuedo ENDF-6 format - i.e. generally follows ENDF formatting rules, but with some modifications to allow description of reactions leading to metastable states.

EADL The Evaluated Atomic Data Library of the Lawrence Livermore National Laboratory, USA, in the ENDL format. It contains evaluated atomic subshell and relaxation data for isolated neutral atoms, including fluorescence yields, subshell parameters (e.g. binding energies), both radioactive and non-radioactive transition probabilities, and energy deposition terms.

EAF The European Activation File is designed for activation, transmutation and gas-production calculations. The file, in EAF format, contains data on neutron-induced reactions on stable and unstable targets.

EEDL The Evaluated Electron Interaction Data Library of the Lawrence Livermore National Laboratory, USA.

EFF The European Fusion File contains data for 80 materials of interest for fusion neutronic design calculations, from H to Bi^{209}. The library format conforms mostly to the legal ENDF-6 format, but there are deviations.

EPDL The Evaluated Photon Interaction Data Library of the Lawrence Livermore National Laboratory, USA.

FENDL A comprehensive nuclear data library for fusion applications, developed by an international effort coordinated by the IAEA Nuclear Data Section. Sub-libraries exist for activation (FENDL/A), decay (FENDL/D), dosimetry (FENDL/DS), fusion (FENDL/C), transport applications (FENDL/E) and validation (VALIDATION).

IRDF The International Reactor Dosimetry File. Contains neutron cross section data for reactions used for reactor dosimetry by foil activation. It also contains radiation damage cross-sections for a few materials in the older ENDF-V format.

JENDL-ACT Japanese library of activation reactions.

MENDL The Medium Energy Nuclear Data Library, a neutron reaction data library for nuclear activation and transmutation at intermediate energies (up to 100 MeV). Generally follows ENDF formatting rules, but with different MT numbers.

UKFY The UK fission product yield evaluated data

UKHEDD UK Heavy Element Decay Data file. Contains evaluations for 125 heavy element nuclide of interest in nuclear fuel cycle calculations, including some spontaneous fission data.

UKPADD The UK activation product decay data library. Contains radioactive decay data for 328 activation products (including some fission products).

IAEA Photonuclear data. Photo-excitation, photo-absorption, photo-neutron production, photo-fission, etc., cross sections. Available at http://iaeand.iaea.or.at/photonuclear/, provides the Russian BOFOD library (from IPPE, Obninsk, Russia), Russian EPNDL library (from CDFE, Moscow), Chinese (CNDC), Japanese (JENDL), South Korean (KAERI) and U.S. (LANL) photo-nuclear data libraries, with evaluated, recommended values.

These and others may be accessed through the NEA, http://www.nea.fr/.

The ENDF data library and its format

One of the major data evaluations is the U.S. Evaluated Nuclear Data File library (ENDF), a massive compilation of atomic and nuclear cross sections and nuclear decay rate data. It was originally designed by the National Nuclear Data Center (NNDC) at Brookhaven National Laboratory for recording neutron cross section data. Over the decades it has expanded to include other projectiles. Data are updated periodically; the current version is ENDF/B-VI.

An introduction to ENDF is available on line [LA98]. To quote from it:

> ENDF-format libraries are computer-readable files of nuclear data that describe nuclear reaction cross sections, the distributions in energy and angle of reaction products, the various nuclei produced during nuclear reactions, the decay modes and product spectra resulting from the decay of radioactive nuclei, and the estimated errors in these quantities.
>
> ENDF-format libraries are intended to be used for a wide variety of applications that require calculations of the transport of neutrons, photons, and charged-particles through materials, the enumeration of the interactions of this radiation with the materials and their surroundings, and the time evolution of the radioactivity associated with the nuclear processes.
>
> Examples of uses for ENDF-based libraries include fission and fusion reactor calculations, shielding and radiation protection calculations, criticality safety, nuclear weapons, nuclear physics research, medical radiotherapy, radioisotope therapy and diagnostics, accelerator design and operations, geological and environmental work, radioactive waste disposal calculations, and space travel calculations.

The ENDF library now includes as projectiles photons, electrons, neutrons, protons, and alpha particles. It is continually updated and expanded. The library containing cross sections for incident photons is called the Evaluated Photon Data Library (EPDL), and the data base for incident electrons is the Evaluated Electron Data Library (EEDL).

After excitation or ionization of atoms by photon or incident electron collisions, the atom may de-excite by X-ray emission (fluorescence) and/or other electron emission (Auger or Coster-Kronig). Probabilities for these atomic relaxation modes are tabulated in a separate library, the Evaluated Atomic Data Library (EADL).

EPDL includes cross sections for photo-ionization from individual atomic subshells, but it does not

tabulate photo-excitation cross sections. The latter are contained separately in the Evaluated Excitation Data Library (EXDL). Compiled there, in addition to excitation cross sections, are fluorescence yields, Auger yields, Coster-Kronig transition probabilities, etc. EXDL is distributed with EPDL97, but maintained as a separate file of data, in order to simplify its use in applications. At present, EXDL is available only in the older ENDL format. This format is documented in LLNL report [Pe02], and libraries in that format are included with the complete EPDL library.

The library containing cross sections for incident neutrons or protons or alpha particles has no separate name, and is simply known as ENDF.

Structure of the ENDF format

This discussion addresses all incident projectiles, not just photons. ENDF data files are nuclear data evaluated (category 2 above) by the Cross Section Evaluation Working Group. They are kept as computer-readable ASCII files. The ENDF *format* refers to the way numbers are arranged on the records in the file. The ENDF layout format has become the one of choice world-wide for almost all nuclear reaction cross section data and photo-atomic data. In this format, every record is 80 characters wide. Numerical data are presented in point-wise pairs (for example, energy–cross section), three pairs (six numbers) to a line, consuming 66 of the 80 columns. 300 data points fit on 100 rows. The numerical data are preceded by rows identifying the element, what process the following data are for (whether it is the coherent scattering cross section *vs* incident photon energy; a form factor *vs* momentum transfer, etc.), interpolation algorithms, etc. The ENDF format has been documented by members of the Cross Section Evaluation Working Group in [McL01]; this document has come to be known as "ENDF-102".

To parameterize all possible interactions, one must specify the incident projectile, the target, the kind of data one is working with (a total cross section vs energy, a differential cross section, decay data, etc.), and the specific reaction of interest (e.g., $Al^{27}(n,np)Mg^{27}$, etc.). In ENDF these four quantities are controlled by four numerical parameters, NSUB, MAT, MF, and MT, as follows.

The entire ENDF library is divided into sub-libraries, one for each incident particle. More precisely, there may be several sub-libraries for a given projectile; for example for incident photons there is one sub-library for photo-nuclear data, one for photo-induced fission product yields, and one for photo-atomic interaction data (this latter is known separately as EPDL). A Fortran parameter, NSUB, is defined to identify the sub-library. For example, EPDL for photo-atomic cross sections is NSUB=3.

A target material is identified by a four-digit integer variable given the name MAT (Fortran), ranging from 1 to 9999. For any projectile, target materials may be either individual nuclear isotopes or elements in their natural isotopic compositions, or in some cases other mixtures of isotopes. To accommodate all possibilities, the assignment conventions of the MAT numbers may be only partially transparent (and the numbering convention allows for two excited isomeric nuclear states of nuclides). The first two of the four digits in MAT are the element atomic number. The last two identify the isotope or the natural element. The two isotope identification digits do not necessarily correspond to atomic number or neutron number. An

element Z in its natural isotopic composition has MAT number 100Z; MAT for natural Fe is 2600. The lightest stable isotope is assigned number MAT = 100Z+25; MAT = 2625 for $_{26}Fe^{54}$. The (stable) isotope $_{26}Fe^{57}$ has MAT number 2634. The list of all MAT numbers can be found in the format document ENDF-102 referenced above.

For a given projectile and target, one must specify the class of information desired about that projectile on that material, such as a reaction cross section as a function of incident projectile energy, or angular distributions for emitted particles, or neutron resonance parameters, etc. Each of these quantities was originally kept in a separate file; but now each quantity is assigned an identifying integer variable MF; the "F" for file and the preceding M to make it a Fortran integer, harmonious with the M in MAT. The two-digit MF variable ranges from 1 to 99. For a reaction cross section as a function of incident projectile energy, MF=3; neutron resonance parameters are in the file MF=2; angular distribution for emitted particles are in MF=4, etc. While earliest compilations had each MF value in a separate file, today all MF values are included in a single, much larger file for a given target material. A class of data for a given MF is still loosely referred to as a "file".

For a given projectile, target, and quantity of interest, one must specify a particular reaction of interest, or the *type* of quantity desired. This is identified by the three-digit "type" variable MT. It ranges from 1 to 999. MT=2 is the total elastic scattering cross section; MT=18 is total projectile-induced fission cross section; MT=102 is the neutron radiative capture cross section, and is defined only for incident neutrons. In the early days, each type of quantity was kept in a certain section of a file. Today a particular reaction is still referred to as a "section" of a "file", meaning a particular MT in a particular MF part of the complete file for that material.

Thus: The projectile is specified by NSUB, the chosen sub-library (e.g., EPDL97 for a photon)
The target material is specified by MAT (e.g., MAT=1300 for natural Al)
The quantity desired is specified by MF (e.g., MF=3 for a cross section vs. energy)
The particular type of reaction for that quantity (i.e., the specific cross section) is specified by MT (e.g., MT=522 for photo-electric cross section)

Every ENDF file contains the number NSUB in the first few lines. Every record of every ENDF file contains the numbers MAT, MF, and MT in columns 67–75, and a 5-digit record sequence number in columns 76-80.

Some special numbers are set aside for incident photons or electrons. For example, MT=522 is the photo-electric absorption cross section, meaningful only for incident photons; MT=540 is the cross section for photo-electric ionization from the M_3 ($3p^{3/2}$) subshell, and so forth.

With some exceptions, most (but not all) cross sections and processes of interest can be made to fit into these ENDF conventions, and are tabulated in the library.

The first few MF numbers in the ENDF format are defined as follows:

MF	Description of File Contents (MF number)
1	General information
2	Resonance parameter data
3	Reaction cross sections
4	Angular distributions for emitted particles
5	Energy distributions for emitted particles
6	Energy-angle distributions for emitted particles
7	Thermal neutron scattering law data
8	Radioactivity and fission-product yield data
9	Multiplicities for radioactive nuclide production
10	Cross sections for radioactive nuclide production
12	Multiplicities for photon production
13	Cross sections for photon production
14	Angular distributions for photon production
15	Energy distributions for photon production
23	Photo- or electro-atomic interaction cross sections

The definitions of all MF values is given in document ENDF-102 [McL01].

With some exceptions the MT numbers can be broken down approximately as follows:

MT	Description of Reaction Types (MT numbers)
10 - 100	reactions in which at least 1 neutron is emitted
10 - 49	One or more neutrons, plus at least one other particle, are produced
50 - 91	Just one neutron is produced, with residual nucleus left in excited state
101 - 150	reactions in which no neutron is in the final state
151 - 200	resonance region information
201 - 450	quantities derived from the basic data, such as particle production cross sections, average energies, etc.
451 - 599	miscellaneous quantities, such as fission nubar, charged particle stopping powers, etc., and photon cross sections.
600 - 891	particle production with residual nucleus in excited state
600 - 649	proton is produced, with residual nucleus left in excited state
650 - 699	deuteron is produced, with residual nucleus left in excited state
700 - 749	triton is produced, with residual nucleus left in excited state
750 - 799	He^3 is produced, with residual nucleus left in excited state
800 - 849	α particle is produced, with residual nucleus left in excited state

Specific MT values are too numerous to list here. Full descriptions are in document ENDF-102 [McL01]. In addition, the first records of every ENDF data file contain descriptive text, and include MF and MT definitions for all the data quantities in that file.

ENDF Preprocessing and Postprocessing Codes

ENDF stores basic data in a rather compressed form. Further processing may be necessary to obtain the desired quantity. In neutron reactions, for example, cross sections in the resonance region are not stored as energy–cross section pairs; rather the resonance parameters are given. To get the cross section vs energy the resonance parameters must be expanded.

One should use the preprocessing codes PREPRO2002 to prepare the raw data in the basic ENDF data files. For all projectiles (i.e., for all ENDF data files) the PREPRO codes check for and correct internal inconsistencies, make sure partial cross sections add up to the proper total, check for negative cross sections, etc. A capability for combining elements into compounds and mixtures is provided. For neutrons, it also

expands resonance parameters to produce point-wise cross sections as a function of neutron energy, and Doppler broadens the cross sections to any specified temperature. PREPRO is available at no cost through the major organizations listed above, for example at the IAEA: http://iaeand.iaea.or.at/ndspub/endf/prepro/.

A more comprehensive post-processing group of codes is NJOY, which provides extensive capabilities for manipulating ENDF files and data. NJOY is not free; authorized users may obtain it for a fee through the

Radiation Safety Information Computational Center, http://www-rsicc.ornl.gov/rsicc.html

or at the

NEA Data Bank at http://www.nea.fr/.

NJOY introductory documentation is freely available through Los Alamos National Laboratory: http://t2.lanl.gov/njoy/, and http://t2.lanl.gov/codes/.

Extracting or Plotting a Cross Section from an ENDF file

It is often convenient to have cross section data in simple parallel column format, rather than in the compressed ENDF format which minimizes the number of records in a file.

There are several ways to extract a cross section from an ENDF file, short of writing one's own code to read the file.

- Most sites (especially LANL T2 and NNDC) permit downloading ENDF data automatically extracted in parallel column format, usually six or ten columns wide.

- A utility program LISTEF, written by C. L. Dunford at BNL-NNDC, extracts all data from an ENDF file and expands it into parallel columns. A version of this code is included in the CD-ROM accompanying this book.

- To extract 1-dimensional data only (i.e., a cross section vs energy, but not a differential cross section as a function of incident particle energy and outgoing particle angle) one can use the simple code ENDF1D included on the CD-ROM.

- The NEA maintains a free, very useful utility, *Janis*, which can extract, display, and compare data.

Plots of cross sections are available at the LANL-T2 site. The NEA Janis routine also produces plots. The LLNL Monte Carlo transport codes TART and EPIC, discussed presently, include a very nice display package, EPICSHOW, to plot photon, electron, light ion, and neutron cross sections.

The Evaluated Photon Data Library in ENDF format

After the digression on general data, we now again restrict attention to incident photons, and discuss the EPDL data base. Due to the popularity of the ENDF format, the EPDL library, originally in ENDL format, has been made available in ENDF format. In that format it contains the following quantities:

- Photo-ionization cross sections from individual electron sub-shells (K, L_1, L_2, L_3, M_1, M_2, etc.);
- For each subshell, the photo-ionization edge energy, and the fluorescence yield
- Atomic photo-ionization cross section (as distinct from photo-excitation), being the sum of all sub-shell photo-ionization cross sections;
- Coherent (Rayleigh) scattering cross section;
- Incoherent (Compton) scattering cross section;
- Nuclear-field, electron-field and total pair production cross sections;
- Total cross section (=sum of photo-electric, coherent, incoherent, nuclear pair, and electronic pair);
- Incoherent scattering function $S(q)$, from which one can construct the incoherent differential cross section;
- Coherent scattering form factor $F(q)$;
- Real and imaginary parts of coherent anomalous scattering factors $f_1(E)$ and $f_2(E)$, from which, together with $F(q)$, one can construct the coherent differential cross section.

Functions of incident photon energy E [that is, all quantities except $S(q)$ and $F(q)$] are given for energies from 1 eV to 100 GeV. As reaction identifiers in the ENDF format were established long ago with no idea that the ENDL library would ever be transcribed to it, some parameters in ENDL format could not be carried over. Thus the EPDL library in the ENDL format still contains some quantities not in the ENDF format.

The ENDL data library and its format

The Evaluated Nuclear Data Library has been compiled over many years by LLNL, starting in the late 1950's. It has been documented in many paper reports, carrying the general number UCRL 50400, but recently has moved to electronic form. The Evaluated Photon Data Library, EPDL, is only one part of ENDL. ENDL also contains electron-atom cross sections and energy loss (EEDL), atomic relaxation data (EADL), and atomic excitation data (EXDL).

The EPDL97 data base in its original ENDL format contains all the quantities put in ENDF format (above) plus the following additional quantities on all 100 elements:

- Average energy of outgoing particles (e.g., average Compton electron energy, or average positron and electron energies following pair production as a function of incident photon energy)

- Average energy left in the residual atom following photo-electric absorption. From this and the average energy of outgoing particles one can construct the energy transfer and kerma.

- Photo-excitation cross sections, as well as photo-ionization cross sections.

LLNL also has constructed a Monte Carlo electron-photon transport code, EPIC, using the EPDL data base, and a Monte-Carlo neutron-photon transport code TART. TART dates from the 1970's, spearheaded largely by E. F. Plechaty, but the current versions of EPIC and TART were written by Dermott E. ("Red") Cullen [http://www.llnl.gov/cullen1/]. TART is distributed by RSICC at ORNL, and EPIC should be publicly available soon. Provided with the TART code, in addition to neutron cross sections, is the EPDL database at a reduced set of energies, suitable for plotting. A beautiful, fast plotting routine, EPICSHOW, is included, enabling one to quickly view all major and minor cross sections as a function of energy, and print them out in tabular form at the included energies. Forthcoming versions of EPICSHOW should include all energies of the original ENDL database.

Comparison of NIST and LLNL Photon Data

Experimental measurements do not exist for all interaction processes on all elements at all energies. Cross section databases must therefore be compiled from what data do exist and from calculations. These calculations are continually being improved, using more and more sophisticated atomic structure models. In addition, such calculations are required for photon interaction cross sections on ions in their ground states, or on neutral atoms and ions in excited states, for which there are few if any measurements. These latter cross sections are needed, for example, for astrophysical and laboratory plasma applications.

Therefore databases, even for neutral atoms, can differ based upon those experiments and calculations in which the compilers have faith and choose for their foundation. Each database represents one possible interpretation of the available data and computations.

Even within NIST, two different compilations below about 400 keV, XCOM and FFAST, each developed for different purposes, may differ in total cross section by several percent [NISTb]. In general, however, we have found EPDL97 and XCOM to agree in the total cross section and in each major cross section (that process which is dominant at a given energy) to better than about 1%.

In addition to the comparison of Rayleigh scattering angular distribution in Figures (2.15) and (2.16), we mention here a quick comparison of angle-integrated cross sections between the two major compilations, LLNL EPDL97 and NIST XCOM.

In general the two data sets agree to significantly better than 1% on total cross section (sum of photo-electric, coherent, incoherent, and pair production). This means that at any one energy, the two compilations for the dominant cross section at that energy also agree as well. But the lesser cross sections differ by more. As an example, Figure (2.68) shows both compilations on Aluminum. The solid lines are the EPDL97 data, shown here, as in Figure (2.4), from 10 eV to 100 GeV. The dots are the NIST data, which are given on the NIST web site from 1 keV to 100 GeV. Below about 30 keV the photo-effect dominates, and the two compilations agree very well on that cross section. But the Rayleigh cross section at low energies disagree considerably, at least near X-ray edges. The NIST XCOM model does not yet fully account for the

anomalous scattering which causes significant, sometimes wild, variations in the coherent cross section near edges.

Likewise, above a few hundred MeV, the Compton cross sections disagree by an ever increasing amount, growing to nearly 5% at tens of GeV. Thus if an application requires accurate cross sections for a non-dominant process, such as Compton scattering at hundreds of MeV, or Rayleigh scattering below tens of keV, the user must inquire more deeply as to which data compilation is the more nearly correct for that process at those energies. Table 2.3 shows numerical comparisons from the two main libraries at a few energies.

Both databases are continually being updated. Web sites should be checked for the latest release.

TABLE 2.3. Numerical comparison of photo-atomic cross sections in Aluminum from the LLNL EPDL97 data base and the NIST online XCOM database. Cross sections in barn/atom. EPDL97 tabulates cross sections to 7 significant figures, NIST tabulates them to 3 significant figures. EPDL numbers here have been rounded to 4 significant figures.

MeV	Photoelectric		Rayleigh		Compton		Total Pair Prod		Total	
	EPDL	NIST	EPDL	NIST	EPDL	NIST	EPDL	NIST	EPDL	NIST
1e-3	5.297e4	5.30e4	7.952e1	1.01e2	6.398e-1	6.39e-1			5.305e4	5.31e4
1e-2	1.145e3	1.14e3	2.577e1	2.47e1	4.765e0	4.74e0			1.175e3	1.17e3
1e-1	8.240e-1	8.25e-1	5.944e-1	5.93e-1	6.220e0	6.22e0			7.638e0	7.64e0
1e0	1.184e-3	1.18e-3	6.451e-3	6.44e-3	2.743e0	2.75e0	0.0	0.0	2.751e0	2.75e0
1e1	4.331e-5	4.33e-5	6.463e-5	6.45e-5	6.628e-1	6.65e-1	3.736e-1	3.73e-1	1.036e0	1.04e0
1e2	3.875e-6	3.87e-6	6.463e-7	6.45e-7	1.066e-1	1.08e-1	1.020e0	1.02e0	1.127e0	1.13e0
1e3	3.830e-7	3.83e-7	6.463e-9	6.45e-9	1.453e-2	1.52e-2	1.343e0	1.35e0	1.358e0	1.36e0
1e4	3.827e-8	3.82e-8	6.463e-11	6.45e-11	1.835e-3	1.92e-3	1.417e0	1.42e0	1.419e0	1.42e0
1e5	3.823e-9	3.82e-9	6.463e-13	6.45e-13	2.216e-4	2.32e-4	1.428e0	1.43e0	1.429e0	1.43e0

Other Data Sources

Links to photon-atom cross section data can be found at the Lawrence Berkeley National Laboratory Center for X-Ray Optics sites: http://www-cxro.lbl.gov/optical_constants/, and http://www-cxro.lbl.gov/optical_constants/web.html. Various tabulations of form factors and scattering functions can be found at these sites.

As mentioned, current work on elastic photon-atom scattering is compiled at http://www-phys.llnl.gov/Res

earch/scattering/elastic.html.

Other available data sources are summarized in [Cu97].

Photon Related Data

The Lawrence Livermore National Laboratory Evaluated Atomic Data Library, EADL, contains data to describe the relaxation of an ionized atom back to neutrality following ionization by photons or electron collisions. Fluorescence photons and Auger (and Coster-Kronig) electron transitions are presented.

The LLNL Evaluated Excitation Data Library, EXDL, contains data describing the decay of photo-excited atoms.

These data libraries (EPDL, EADL, EXDL) and their documentation are available from the Radiation Safety Information Computational Center at Oak Ridge National Laboratory, or from the International Atomic Energy Agency, http://www-nds.iaea.org/epdl97/.

2.12 LARGE CONTOUR PLOTS

Four large, color contour plots (11"×17") are available that graph useful photon parameters. They are in high resolution pdf format on the accompanying CD (and would require a printer capable of handling 11"×17" paper), or may be obtained separately on paper from the publishers. They are:

Total photon cross section. Photoelectric + Rayleigh (≡"elastic"≡"coherent") + Compton (≡"Incoherent") + Pair Production.

- *Total photon cross section in barns/atom.* (1 barn ≡ 10^{-24} cm^2). A smooth function of Z and E.

- *Total photon cross section in cm^2/gram.* $\sigma(\text{cm}^2/\text{gm}) = (N_A/A)\cdot 10^{-24}\,\sigma(\text{barn/atom})$, where N_A = Avogadro's number, A = element atomic weight. While σ(barn/atom) is smooth, contours are jagged here because $A(Z)$ is a jagged function of Z.

The Compton cross section σ_C, and the major part of charged particle stopping power, are proportional to the number of electrons in the material. The number of electrons per gram, $(Z/A)N_A$, is proportional to Z/A. Since Z/A =1 for H, but ~1/2 for other elements, σ_C(cm^2/gm) in H is about twice σ_C in He. This fact would cause contour lines to bunch near $Z = 1$. To avoid this problem, the H cross section graphed in cm^2/gm is 1/2 the actual H cross section. All other elements are graphed at their correct value. The same ploy is used on graphs of charged particle stopping powers. To illustrate this point, another (fifth) graph is included in which H is plotted at its correct value; on it H and He are obscured.

▪ ***Mean free path against total scattering*** (gm/cm^2) ≡ $1/\sigma(cm^2/gm)$. This duplicates information in the previous graph. However displayed contour values are not always the inverse of those on the $\sigma(cm^2/gm)$ graph, and so are not in the same position. Therefore the two graphs allow more precise interpolation than one graph alone.

▪ ***Photon number fluence to kerma conversion factor***. Units of rad(element) per 10^9 photons/cm^2. For example, in Si (Z=14) at 1 MeV the graph shows that 10^9 photons/cm^2 release 0.45 rad(Si), or it takes $10^9/0.45 = 2.2\times10^9$ photons/cm^2 to deposit 1 rad(Si) in the form of electron kinetic energy. Dose is geometry dependent and must be calculated separately; dose equals kerma under "charged particle equilibrium".

2.13 DATA ON THE CD-ROM

Although EPDL97 contains cross sections down to 1 eV, we have included on the CD-ROM cross sections only at energies above 100 eV. There are several reasons:

- The libraries EPDL, EEDL, EADL, and EXDL have been compiled by LLNL to be a self-consistent set for use in electron-photon transport codes. In this application, self-consistency is more important than absolute accuracy. (Hence, some photo-electric edges differ from other standard compilations). The libraries are not intended to be accurate cross sections for arbitrary applications. Nevertheless, the cross sections at the energies presented are believed to be reliable for free atoms.

- Notwithstanding applications to atomic gases, as mentioned in Section 2.1, free atom cross sections at low energies give inaccurate results in applications in solids, in liquids, and in diatomic or molecular gases.

- EPDL97 cross sections at low energies were really compiled and intended only to support calculations of coherent anomalous scattering factors for use in electron-photon transport calculations, not as true, evaluated atom cross sections for arbitrary application.

- Documentation [Cu97] blatantly states, "Between 10 and 100 eV it is neither safe nor accurate to use these data" in arbitrary applications. And below 10 eV the warnings are even more stern.

- Users desiring cross sections below 100 eV can get them by actually downloading EPDL97 from one of the sources listed above. The pain of this chore may encourage them actually to read the documentation, wherein is sufficient warning about the data's uncertainties. Were the low energy cross sections provided on the CD-ROM accompanying this book, the temptation to use them would be too great to prevent their use in inappropriate applications.

Paraphrasing the discussion in [Cu97], above about 1 keV the cross sections appear to be reliable and safe to use. From 100 eV to 1 keV, the experimental and theoretical cross section data contain, of course, some uncertainties. But in this energy span their application appears to be limited only by that uncertainty, at least in non-condensed *atomic* media. In non-condensed *molecular* media, the cross sections are again

inappropriate due to level shifts from interactions with neighboring atoms. In condensed media their application is further limited by interactions with neighboring atoms, as per the caveats in Section 2.1. While the LLNL group chose to include the low energy data anyway in EPDL97, hoping some numbers would be better than none (and requesting user feedback), the NIST group has chosen to present numbers in XCOM only above 1 keV. Another difference between the two compilations is that numerical cross section values are presented in EPDL97 to 7 significant figures, while the NIST tabulation presents them to 3 significant figures. Recall the purpose of the EPDL cross section set is for use in electron-photon transport calculations, and is designed to be consistent with electron cross sections in the separate EEDL electron-atom cross section database.

The cross sections in the NIST and EPDL97 data bases are for photons incident on a single, isolated, cold atom. Cross sections are different, of course, in condensed media, as discussed at the beginning of this chapter. Differences in *K* and *L* edge energies between gas phase and in a solid are compiled by Deslattes, et al [De03].

In spite of the reservations about the use of free atom cross sections below a few hundred eV discussed in Section 2.1, we have chosen to present numbers down to 100 eV in the hopes that the reader will apply them responsibly. That we have chosen to use the LLNL EPDL97 numbers rather than NIST XCOM numbers is in no way to be construed as a technical judgment about the correctness of one set over another. Rather, it is because it is only EPDL97 that has a consistent set both below and above 1 keV. Above 1 keV, one should feel just as free and secure using the NIST cross sections.

As documented in [Cu97] the partial cross sections are to be interpolated "log*x*-log*y*", i.e., power-law interpolation between tabulated points. The energies at which the cross sections are tabulated in the CD-ROM files are chosen to adequately resolve energy dependence.

The included data are:

- Fluorescence yields of K-shell and average fluorescence yields of L-shell and M-shell for all elements.

- Fluence-to-kerma (essentially fluence-to-dose) conversion functions in all elements as a function of photon energy.

- Photo-atomic cross sections in all elements as a function of photon energy (both in units of barn/atom and in cm^2/gm):
  - Total photo-electric ionization cross section (from all shells)
  - Coherent scattering (Rayleigh elastic scattering) cross section
  - Incoherent scattering (Compton scattering) cross section
  - Cross section for pair production from the nucleus
  - Cross section for pair production from atomic electrons
  - Total pair production cross section (nuclear + electronic)
  - Total cross section (photo-electric + coherent + incoherent + pair production)

REFERENCES

Åb85 T. Åberg, J. Tulkki, "Inelastic X-Ray Scattering Including Resonance Phenomena", Chapter 10 in Crasemann, ed. [Cr85].

Ba72 W. Bambynek, B. Crasemann, R.W. Fink, H.-U. Freund, H. Mark, C.D. Swift, R.E. Price, P.Venugopala Rao, "X-Ray Fluorescence Yields, Auger, and Coster-Kronig Transition Probabilities", *Rev. Mod. Phys.* **44**(4): 716-813 (1972)

Be53 H.A. Bethe and J. Ashkin, "Passage of Radiations Through Matter", in E. Segre, ed., *Experimental Nuclear Physics*, Vol. 1, J. Wiley (1953)

Be67 J. A. Bearden and A. F. Burr, *Rev. Mod. Phys.* **39**(1): 125 (1967)

Be79 J. Berkowitz, *Photoabsorption, Photoionization, and Photoelectron Spectroscopy*, Academic Press (1979)

Be82 M. J. Berger and S. M. Seltzer, *Stopping Powers and Ranges of Electrons and Positrons*, 2nd Edtition, NBS publication NBSIR 82-2550-A (December 1982).

Be93 P.M. Bergstrom, Jr., T. Surić, K. Pisk, R.H. Pratt, "Compton scattering of photons from bound electrons: Full relativistic independent-particle-approximation calculations", *Phys. Rev.* **A 48** (2): 1134-1162 (1993)

Be97 P.M. Bergstrom and R.H. Pratt, "An Overview of the Theories Used in Compton Scattering Calculations," *Radiat. Phys. Chem.* **50**: 3-29 (1997).

Bi99 E. Biémont, Y. Frémat, P. Quinet, "Ionization Potentials of Atoms And Ions From Lithium to Tin (Z=50)", *Atomic Data and Nuclear Data Tables* **71**(1):117-146 (January 1, 1999)

Ca85 G.A. Carlsson, "Theoretical Basis for Dosimetry", Chap. 1 in *The Dosimetry of Ionizing Radiation*, Vol. 1, K.R. Kase, B.E. Bjärngard, F.H. Attix, eds., Academic Press (1985)

Ch95a C.T. Chantler, "Theoretical Form Factor, Attenuation and Scattering Tabulation for Z=1-92 from E = 1-10 eV to E = 0.4-1.0 MeV", *J. Phys. Chem. Ref. Data* **24**(1): 71 (1995)

Ch95b FFAST: NIST X-Ray Form Factor, Attenuation, and Scattering Tables, http://physics.nist.gov/PhysRefData/FFast/Text/cover.html

Ch95c C.T. Chantler, "Erratum on Theoretical Form Factor, Attenuation and Scattering Tabulation for Z=1-92 from E = 1-10 eV to E = 0.4-1.0 MeV", [*J. Phys. Chem. Ref. Data* **24**(1): 71 (1995)]. http://physics.nist.gov/PhysRefData/FFast/Text/erratum.html

Ch98 B.K. Chatterjee and S.C. Roy , "Tables of Elastic Scattering Cross Sections of Photons in the

Energy Range 50 keV to 1500 keV for All Elements in the Range 13<Z<104", *J. Phys. Chem. Ref. Dat.* **27**(6): 1011 (1998)

Ch00 C.T. Chantler, "Detailed Tabulation of Atomic Form Factors, Photoelectric Absorption and Scattering Cross Section, and Mass Attenuation Coefficients in the Vicinity of Absorption Edges in the Soft x-Ray (z=30-36, z=60-89, E=0.1 keV-10 keV), Addressing Convergence Issues of Earlier Work", *J. Phys. Chem. Ref. Data* **29**(4) (2000)

Cr85 B. Crasemann, ed., *Atomic Inner-Shell Physics*, Plenum Press (1985)

Cu95 D.E. Cullen, "A Simple Model of Photon Transport", *Nucl. Instr. Meth. Phys. Res.* **B 101**: 499-510 (1995)

Cu97 D.E. Cullen, J.H. Hubbell, L. Kissel, "EPDL97: The Evaluated Photon Data Library, '97 Version", UCRL--50400, Vol. 6, Rev. 5 (September 19, 1997)

Da52 C.M. Davisson, R.D. Evans, "Gamma-Ray Absorption Coefficients", *Rev. Mod. Phys.* **24**: 79 (1952)

De99 A. Derevianko, W.R. Johnson, K.T. Cheng, "Non-dipole Effects in Photoelectron Angular Distributions for Rare Gas Atoms", *Atomic Data and Nuclear Data Tables*, **73**(2): 153-211 (November 1999)

De00 T.P. Devereaux, A.P. Kampf, "A Consistent Picture of Electronic Raman Scattering and Infrared Conductivity in the Cuprates", *Phys. Rev. B* **61**, 1490 (2000)

De03 R. D. Deslatttes, E. G. Kessler, Jr., P. Indelicato, L. de Billy, E. Lindroth, and J. Anton, *Rev. Mod. Phys.* **75**(1): 35 (2003)

Ev55 R.D. Evans, *The Atomic Nucleus*, McGraw-Hill (1955)

Ha58 R. W. Hayward, *Nuclear Electromagnetic Radiations*, Chapter 9-6 in HANDBOOK OF PHYSICS, Ed by E.U. Condon and H. Odishaw, McGraw-Hill, New York (1958)

He54 W. Heitler, *The Quantum Theory of Radiation*, 3rd edition, Oxford Univ. Press (1954)

He93 B.L. Henke, E.M. Gullikson, and J.C. Davis. "X-ray interactions: photo-absorption, scattering, transmission, and reflection at E=50-30000 eV, Z=1-92", *Atomic Data and Nuclear Data Tables*, **54** (no.2):181-342 (July 1993)
These tables are available at http://www-cxro.lbl.gov/optical_constants/asf.html.

Hi92 P.D. Higgins, F.H. Attix, J.H. Hubbell, S.M. Seltzer, M.J. Berger, C.H. Sibata, "Mass Energy-Transfer and Mass Energy-Absorption Coefficients, Including In-Flight Positron Annihilation for Photon Energies 1 keV to 100 MeV", National Institute of Standards and Technology, Report

NISTIR 4812 (1992)

Hu77 J.H. Hubbell, "Photon Mass Attenuation and Mass Energy-Absorption Coefficients for H, C, N, O, Ar, and seven mixtures from 0.1 keV to 20 MeV", *Radiat. Res.***70**: 58-81 (1977)

Hu89 J.H. Hubbell, "Bibliography, and Current Status of *K*, *L*, and Higher Shell Fluorescence Yields for Computations of Photon Energy-Absorption Coefficients", National Institute of Standards, Report NISTIR 89-4144 (August 1989)

Hu94 J.H. Hubbell, P.N. Trehan, N. Singh, B. Chand, D. Mehta, M.L. Garg, R.R. Garg, S. Singh, S. Puri "A Review, Bibliography, and Tabulation of *K*, *L*, and Higher Atomic Shell X-Ray Fluorescence Yields", *J. Phys. Chem. Ref. Data*, **23**(2): 339-364 (1994). Tables 4, 5, 6, and 7 of this article contain certain errors.

Hu95 J.H. Hubbell, S. Seltzer, "Table of X-ray Mass Attenuation Coefficients and Mass Energy-Absorption Coefficients from 1 keV to 20 MeV for Elements Z=1 to 92 and 48 Additional Substances of Dosimetric Interest", National Institute Of Standards and Technology, Report NISTIR 5632 (May, 1995)

Hu99a J.H. Hubbell, "An Examination and Assessment of Available Incoherent Scattering S-Matrix Theory, also Compton Profile Information, and Their Impact on Photon Attenuation Coefficient Compilations", National Institute of Standards Report NISTIR 6358 (July 1999)

Hu99b J.H. Hubbell, "Review of Photon Interaction Cross Section Data in the Medical and Biological Context", *Phys. Med. Biol.***44**:R1-R22 (1999)

IAEApn Recommended photo-nuclear cross sections: http://iaeand.iaea.or.at/photonuclear/

ICRU69 International Commission on Radiation Units and Measurements, Report 13, "Neutron Fluence, Neutron Spectra and Kerma" (September 15, 1969)

ICRU80 International Commission on Radiation Units and Measurements, Report 33, "Radiation Quantities and Units" (1980)

Ka98 S. Kahane, "Relativistic Dirac-Hartree-Fock Photon Incoherent Scattering Functions", *Atomic Data and Nuclear Data Tables* **68**(2):323-347 (March 1, 1998)

Ki85 L. Kissel, R.H. Pratt, "Rayleigh Scattering: Elastic Photon Scattering by Bound Electrons", Chapter 11 in Crasemann, ed. [Cr85]

Kn00 G.F. Knoll, *Radiation Detection and Measurement*, 3rd edition, J. Wiley (2000)

Kr79 M.O. Krause, "Atomic Radiative and Radiationless Yields for K and L Shells", *J. Phys. Chem. Ref. Data*, **8**(2): 307-322 (1979)

LA98 Los Alamos National Laboratory report LA-UR-98-1779, http://t2.lanl.gov/endf/title.html

LLNL D.E. Cullen, EPICSHOW module in the TART code, summarizing cross sections.

Ly85 D.W. Lynch, "Interband Absorption–Mechanisms and Interpretation", Chapter 10 in [Pa98] Vol.1

McL01 V. McLane, ed., "ENDF-102, Data Formats and Procedures for the Evaluated Nuclear Data File ENDF-6", National Nuclear Data Center, Brookhaven National Laboratory, Report BNL-NCS-44945-01/04-Rev. (Revised April, 2001).
Available at: http://www.nndc.bnl.gov/nndcscr/documents/endf/endf102/

Mi85 S. S. Mitra, "Optical Properties of Nonmetallic Solids for Photon Energies below the Fundamental Band Gap", Chapter 11 in [Pa98] Vol. 1

Ne66 R. G. Newton, *Scattering Theory of Waves and Particles*, McGraw-Hill (1966)

NIST http://physlab.nist.gov/PhysRefData/Xcom/Text/XCOM.html

NISTb http://physics.nist.gov/PhysRefData/XrayNoteB.html

NIST20 NIST X-ray Photoelectron Spectroscopy (XPS) Database, (NIST Standard Reference Database 20) http://srdata.nist.gov/xps/

nndc National Nuclear Data Center http://www.nndc.bnl.gov/

Pa98 E. D. Palik, ed., *Handbook of Optical Constants of Solids*, Academic Press, Vol. 1: 1985, Vol. 2: 1991, Vol.3: 1998.

Pe02 S.T. Perkins, D.E. Cullen, "ENDL Type Formats for the LLNL Evaluated Atomic Data Library, EADL, for the Evaluated Electron Data Library, EEDL, and for the Evaluated Photon Data Library, EPDL", LLNL Report UCRL-ID-117796, Rev. 1 (May 17, 2002)

Pl75 E. F. Plechaty, D. E. Cullen, and R. J. Howerton, "Tables and Graphs of Photon Interaction Cross Sections from 1 keV to 100 MeV drived from the LLL Evaluated Nuclear Data Library", LLNL Report UCRL-50400, Vol 6, Revision 1 (October 31, 1975)

Pu95 S. Puri, B. Chand, D. Mehta, M.L. Garg, N. Singh, P.N. Trehan, "K and L Shell X-Ray Fluorescence Cross Sections", *Atomic Data and Nuclear Data Tables* **61**(2):289-311 (November 1, 1995)

Qu72 P. Quittner, *Gamma-ray spectroscopy: with particular reference to detector and computer evaluation techniques*, Hilger (1972)

Qu91 M. R. Querry, D. M. Wieliczka, and D. J. Segelstein, "Water (H_2O)", pp. 1059–1078 in [Pa98] Vol. 2.

Sa31 F. Sauter, *Ann. Phys. (Paris)* **11**: 454 (1931)

Sa88 E.B. Saloman, J. H. Hubbell, J. H. Scofield, "X-Ray Attenuation Cross Sections for Energies 100 eV to 100 keV and Elements Z=1 to Z=92", *Atom. Dat. Nuc. Dat. Tables* **38** (1):1-197 (January 1988)

Se88 S.M. Seltzer, "An Overview of ETRAN Monte Carlo Methods", Chapter 7 in *Monte Carlo Transport of Electrons and Photons*, ed. by T.M. Jenkins, W.R. Nelson, and A. Rindi, Plenum Press, New York (1988)

Sh64 S. M. Shafroth (ed), *Scintillation Spectroscopy of Gamma Radiation*, Gordon & Breach (1964)

Si65 K. Siegbahn, *Alpha, Beta and Gamma Ray Spectroscopy*, Elsevier Science Ltd. (1965)

Sm85 D. Y. Smith, E. Shiles, and Mitio Inokuti, "The Optical Properties of Metallic Aluminum", pp. 369–406 in [Pa98] Vol. 1.

Te97 M.L. Ter-Mikaelyan, "Simple atomic systems in resonant laser fields", *Physics–Uspekhi* **40** (12) 1195-1238 (1997) [Full text at: http://ufn.ioc.ac.ru/abstracts/abst97/abst9712.html]

Tr01 M.B. Trzhaskovskaya, V.I. Nefedov, V.G. Yarzhemsky, "Photoelectron Angular Distribution Parameters for Elements Z=1 to Z=54 in the Photoelectron Energy Range 100-5000 eV", *Atomic Data and Nuclear Data Tables*, **77**(1):97-159 (January 1, 2001)

Ts74 Yung-Su Tsai, "Pair production and bremsstrahlung of charged leptons", *Rev. Mod. Phys.* **46**(4): 815 - 851 (October, 1974)

Wa93 J.H. Wang, R.P. Sagar, H. Schmider, V.H. Smith, "X-Ray Elastic and Inelastic Scattering Factors for Neutral Atoms Z = 2-92", *Atomic Data and Nuclear Data Tables* **53**(2):233-269 (March 1, 1993)

Wi58 J.G. Winans and E.J. Seldin, "Fluorescence and Phosphorescence", Part **6**, Chapter 7 in E.U. Condon and H. Odishaw, eds., HANDBOOK OF PHYSICS, McGraw-Hill (1958)

Wi77 B. Williams, ed., *Compton Scattering*, McGraw-Hill (1977)

FIGURES FOR CHAPTER 2

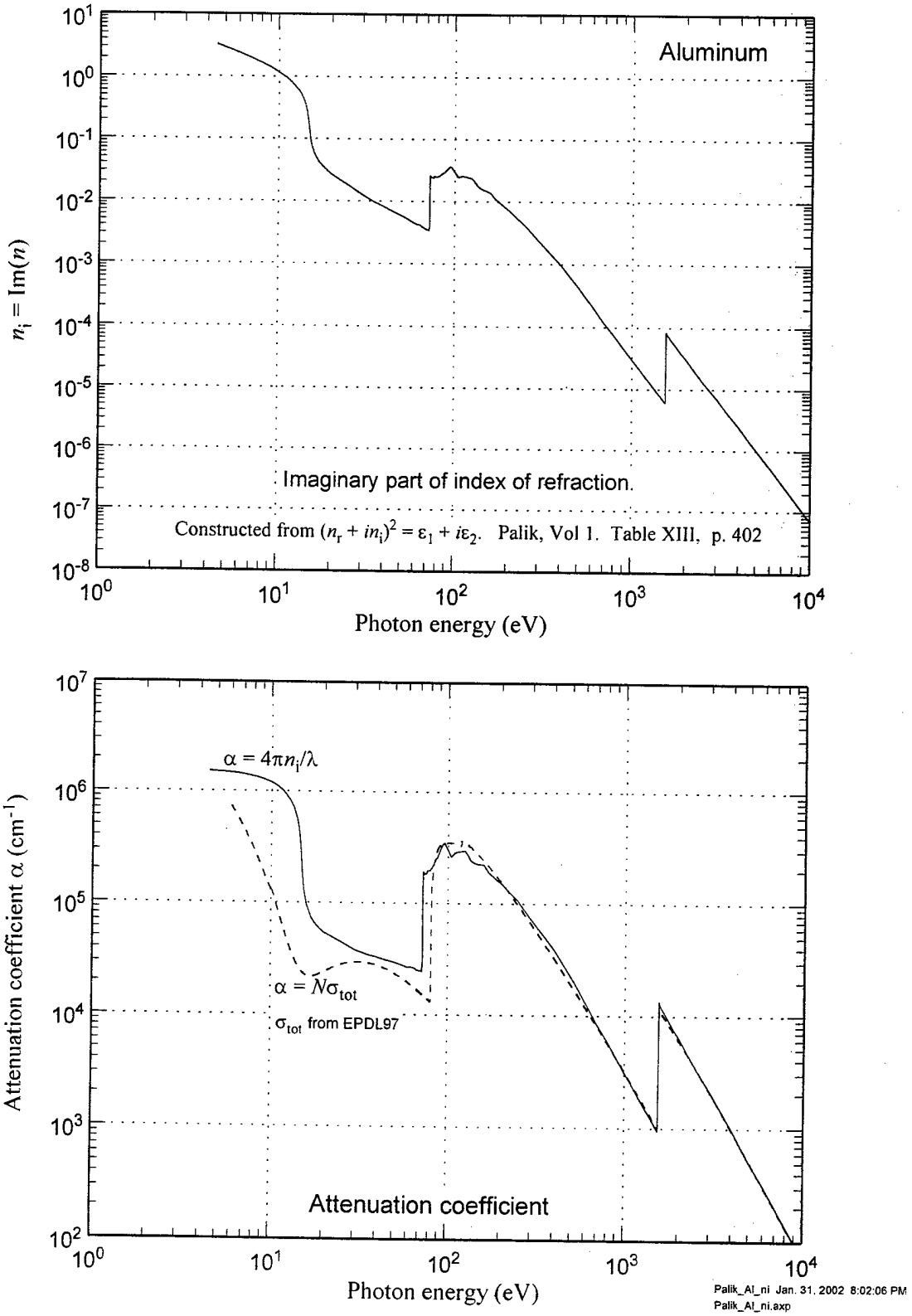

Figure 2.1 Comparison of Al attenuation data (from [Pa98], Vol. 1) with that expected from free atom cross sections (from EPDL97).

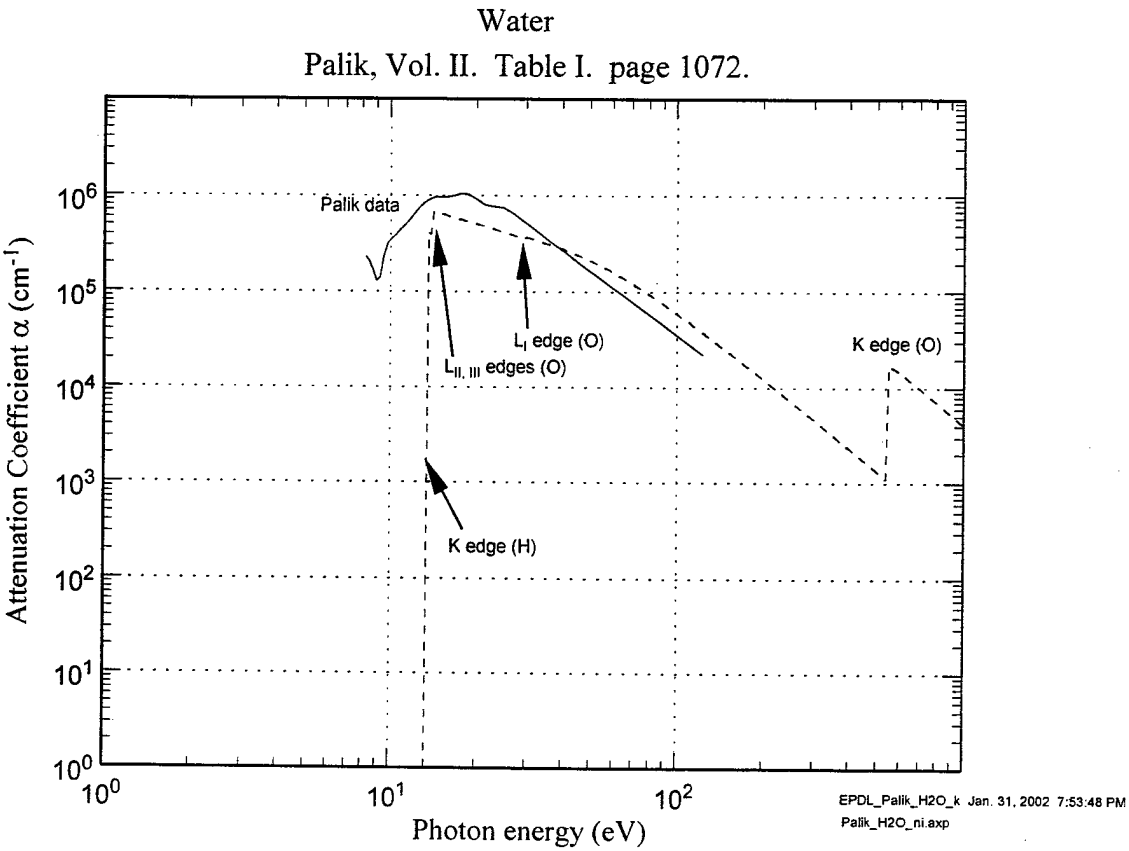

Figure 2.2 Comparison of water attenuation data (from [Pa98], Vol. 2) with that expected from free atom cross sections.

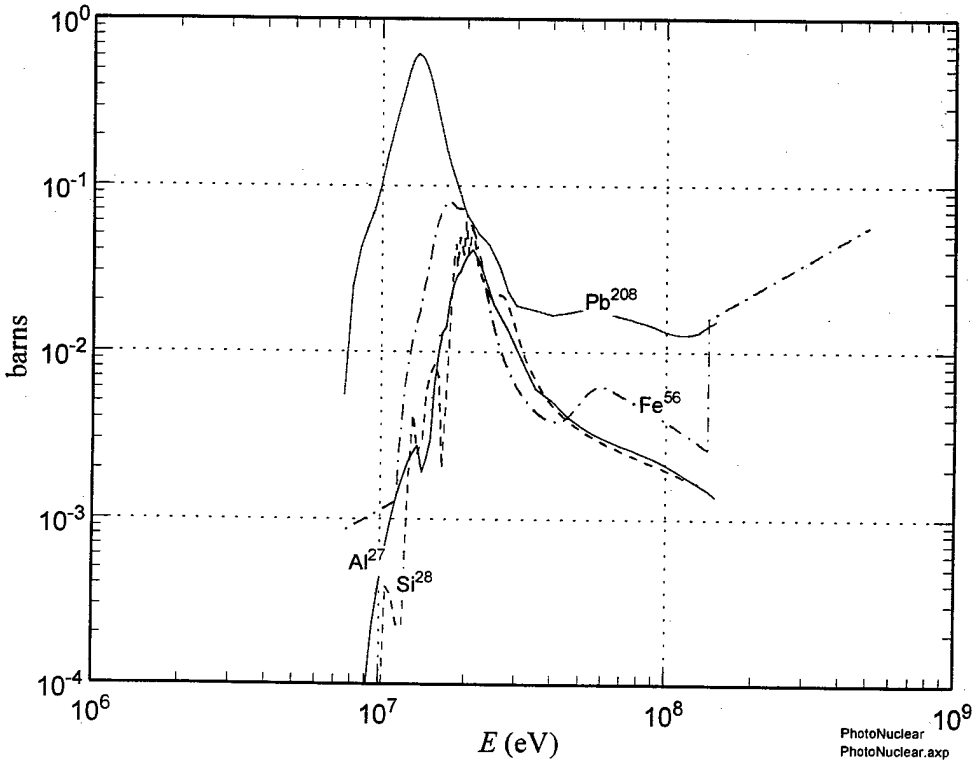

Figure 2.3. Total non-elastic photo-nuclear cross sections on four isotopes. Data from: http://iaeand.iaea.or.at/photonuclear/recommended/

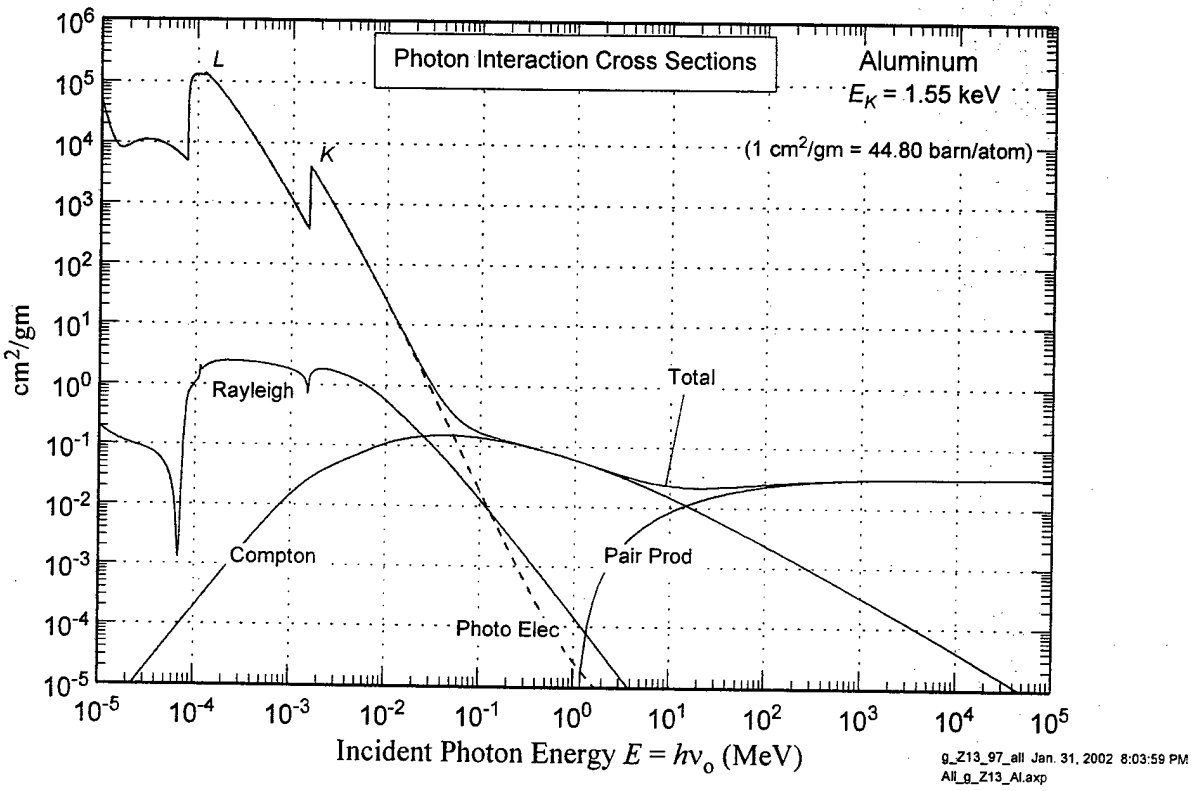

Figure 2.4 Photon interaction cross sections on an isolated, cold Aluminum atom. Data from Lawrence Livermore National Laboratory Evaluated Photon Data Library (EPDL97). This data base extends down to 1 eV.

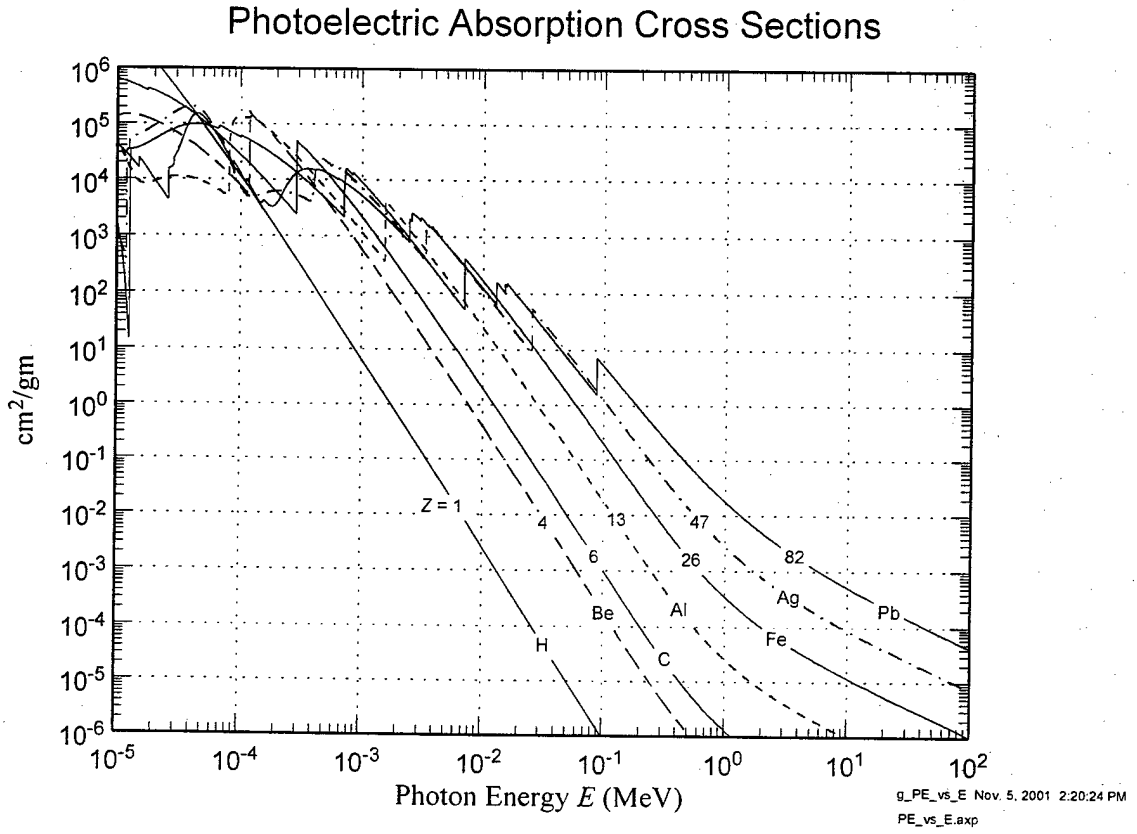

Figure 2.5 Photoelectric absorption cross section on several elements as a function of incident photon energy $h\nu_0$. Data from LLNL EPDL97.

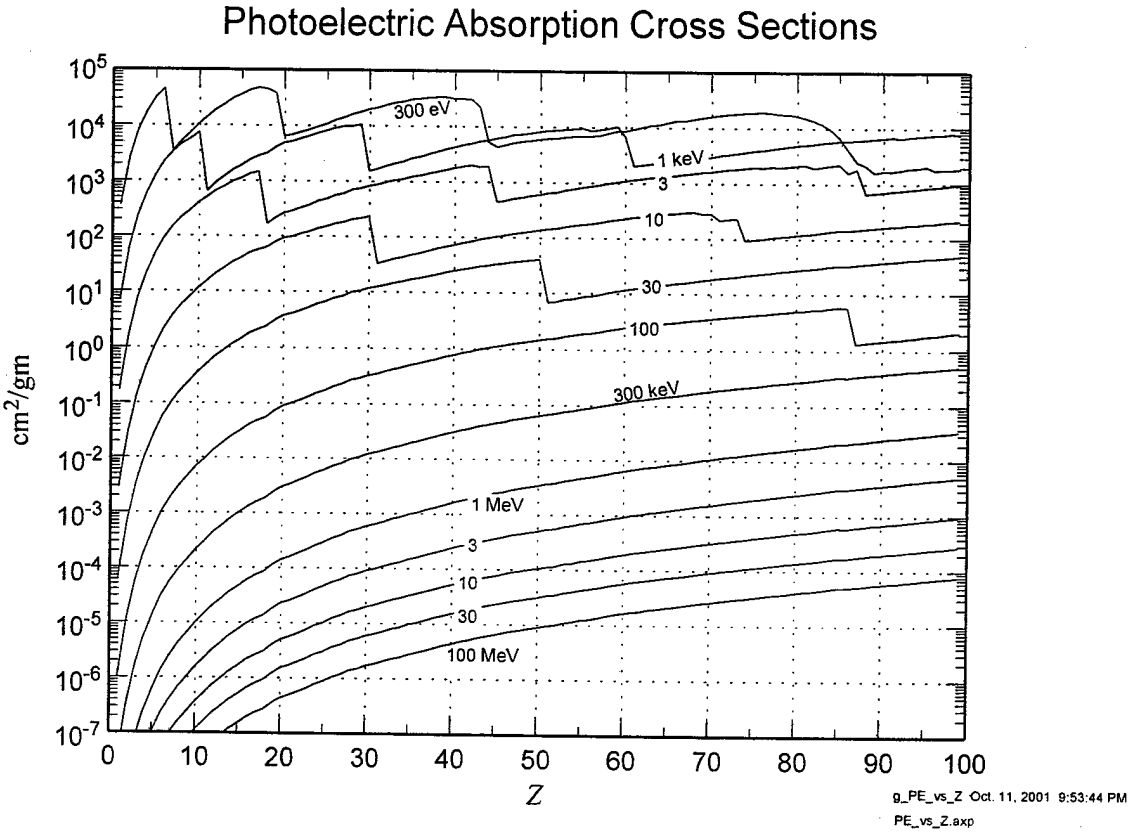

Figure 2.6 Photoelectric absorption cross section at several energies as a function of atomic number Z. Data from LLNL EPDL97.

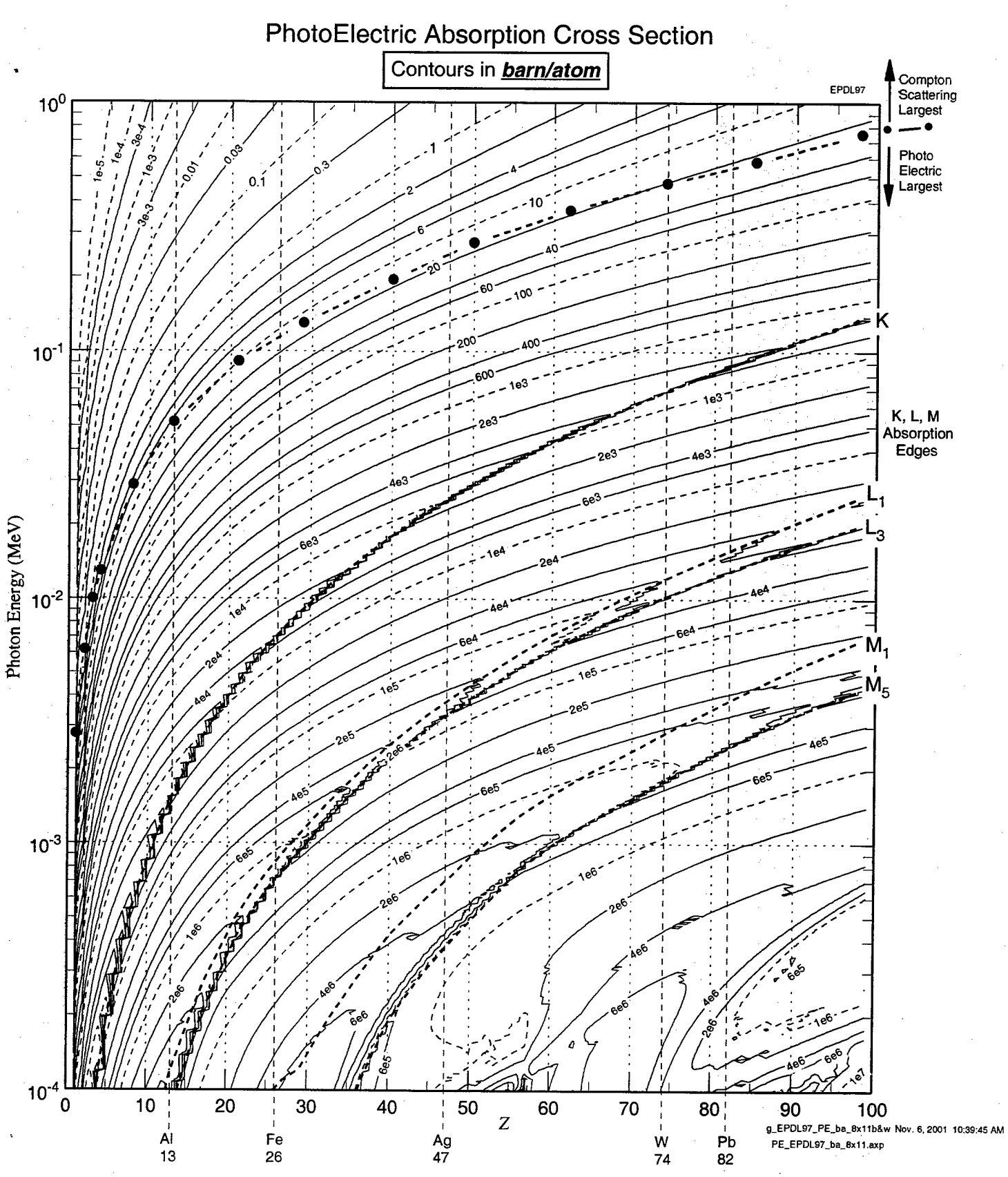

Figure 2.7 Contours of photoelectric absorption cross section in all elements, from $E \equiv h\nu_o$ = 100 eV to 1 MeV. In barn/atom. Data from LLNL EPDL97.

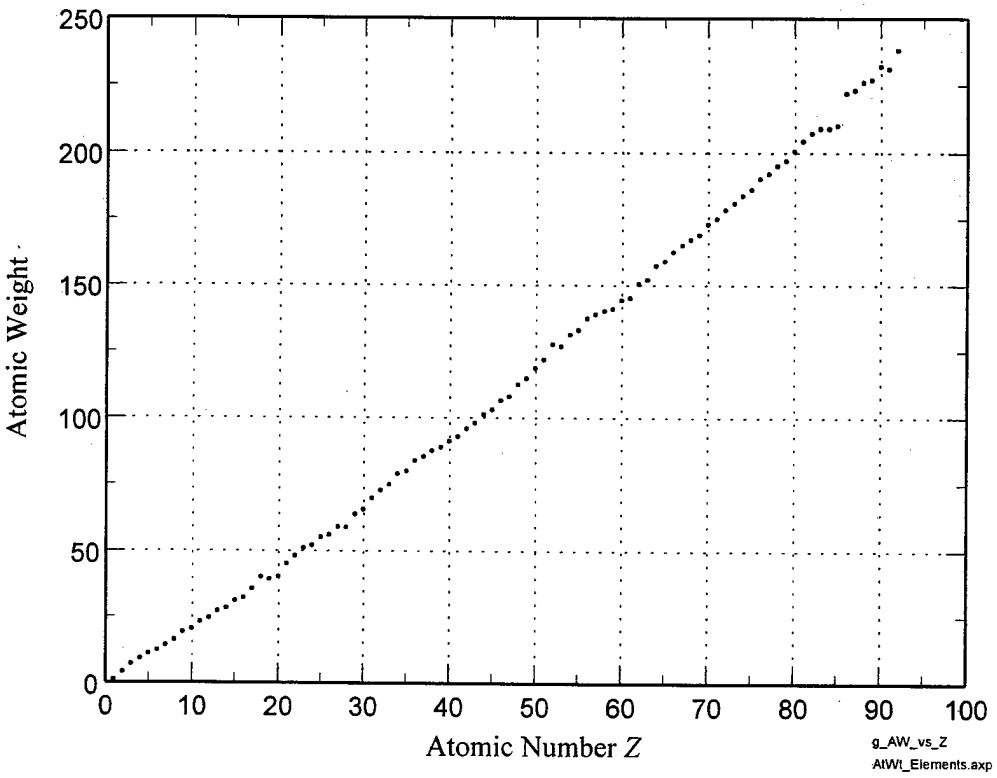

Figure 2.8 Atomic Weight of the elements, naturally occurring isotopic abundances. Data from http://physics.nist.gov/PhysRefData/Compositions/

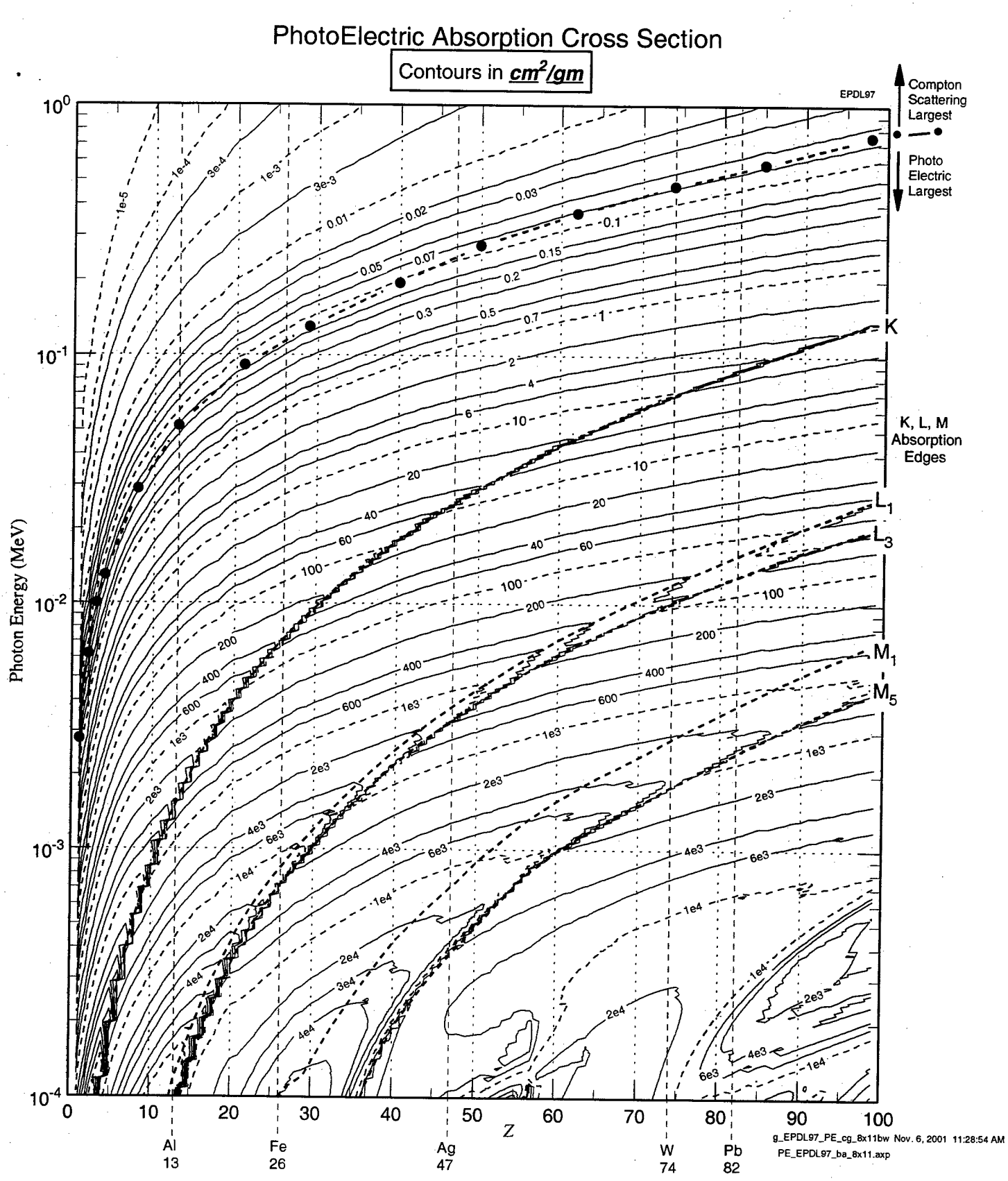

Figure 2.9 Contours of photoelectric absorption cross section in all elements, from $E \equiv h\nu_o$ = 100 eV to 1 MeV. In cm²/gm. Data from LLNL EPDL97.

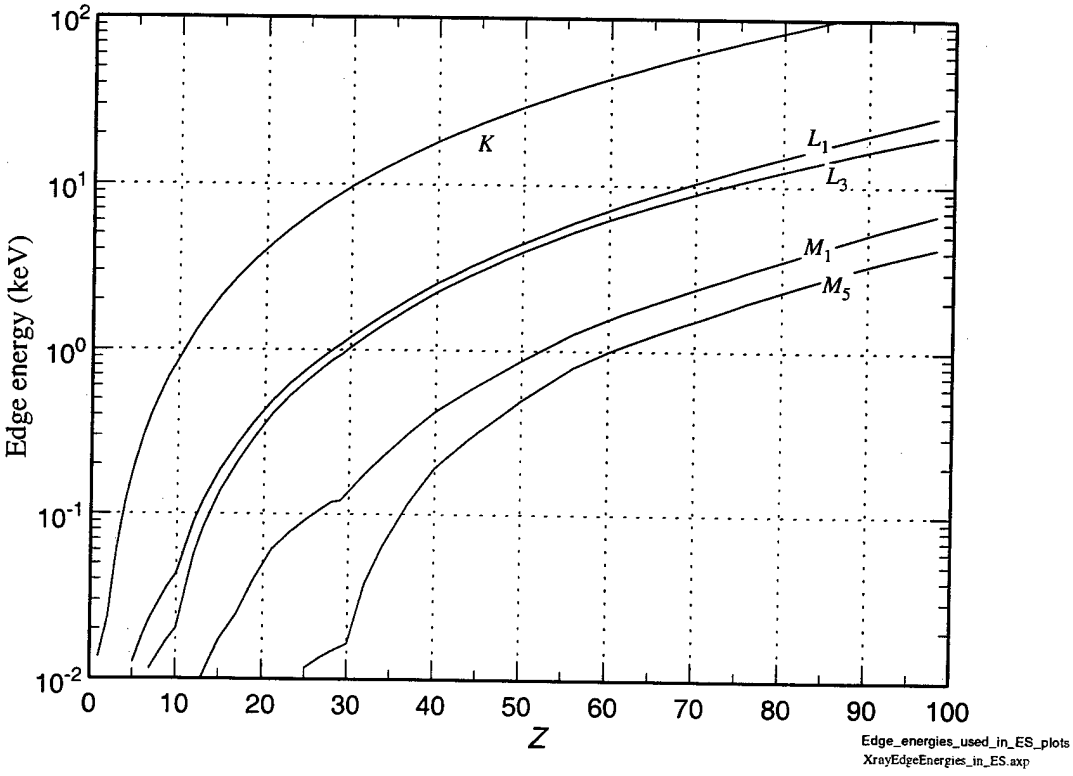

2.10 X-ray Edge Energies in the elements.
Data from LLNL TART98 Epicshow module.

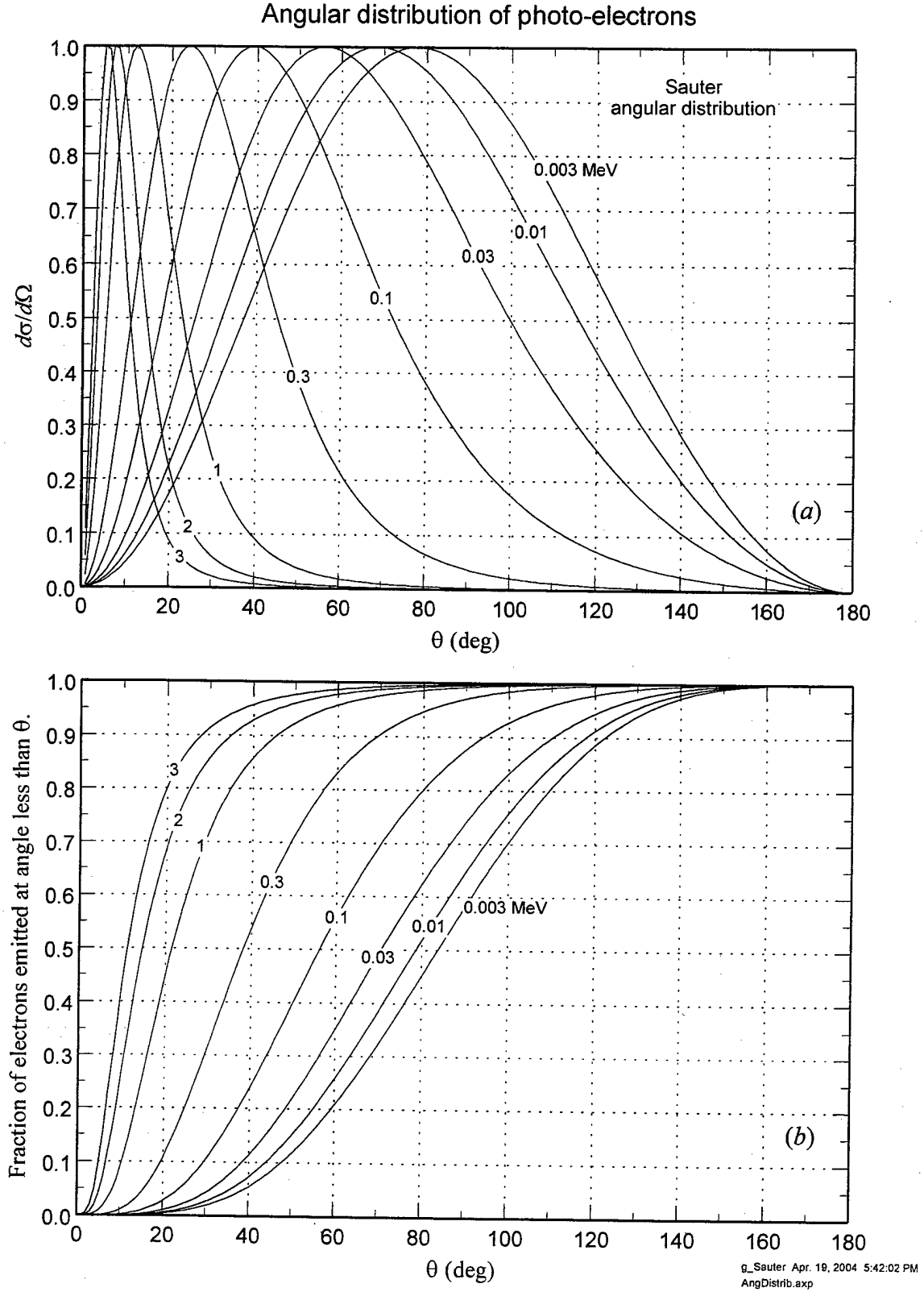

Figure 2. / / Angular distribution of photo-electrons, according to the calculations of Sauter [Sa31] (see also [Da52]). Above a few tens of keV the angular distribution is significantly shifted forward. (*a*) the solid angle distribution $\sim d\sigma/d\Omega$, normalized to unit maximum. (*b*) fraction of photo-electrons ejected at less than polar angle θ.

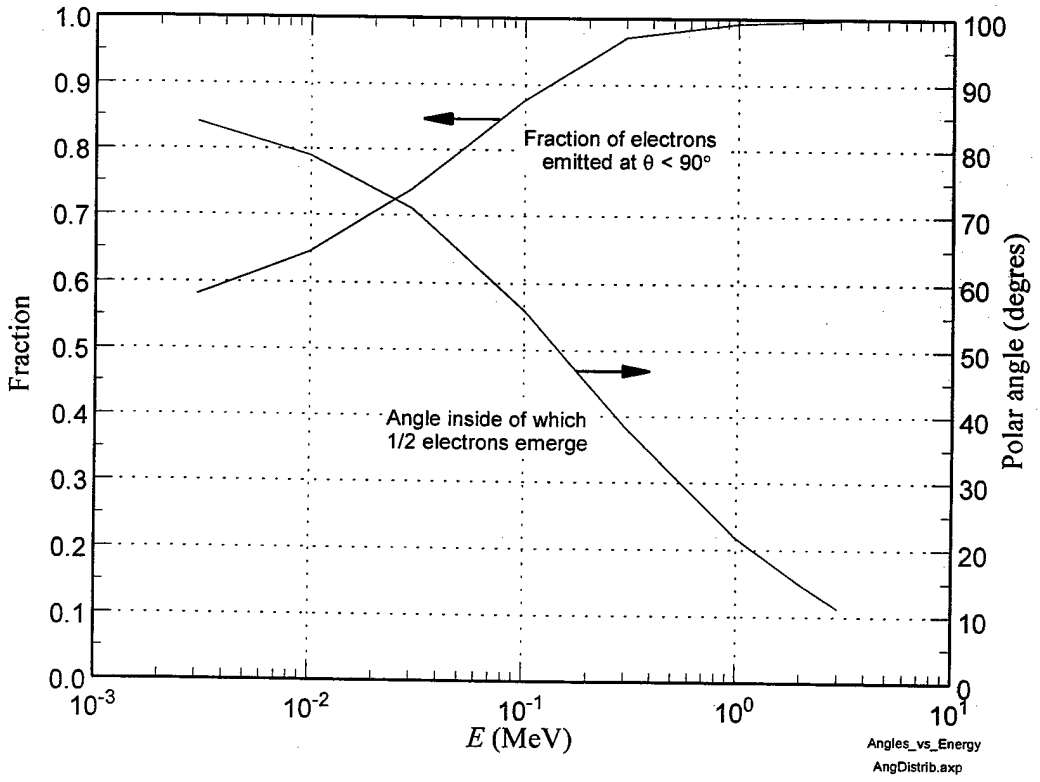

Figure 2. 12 Summary angles for electron emission in photo-electric absorption. Binding energy is ignored; photon energy = electron energy, so that the abscissa represents either one.

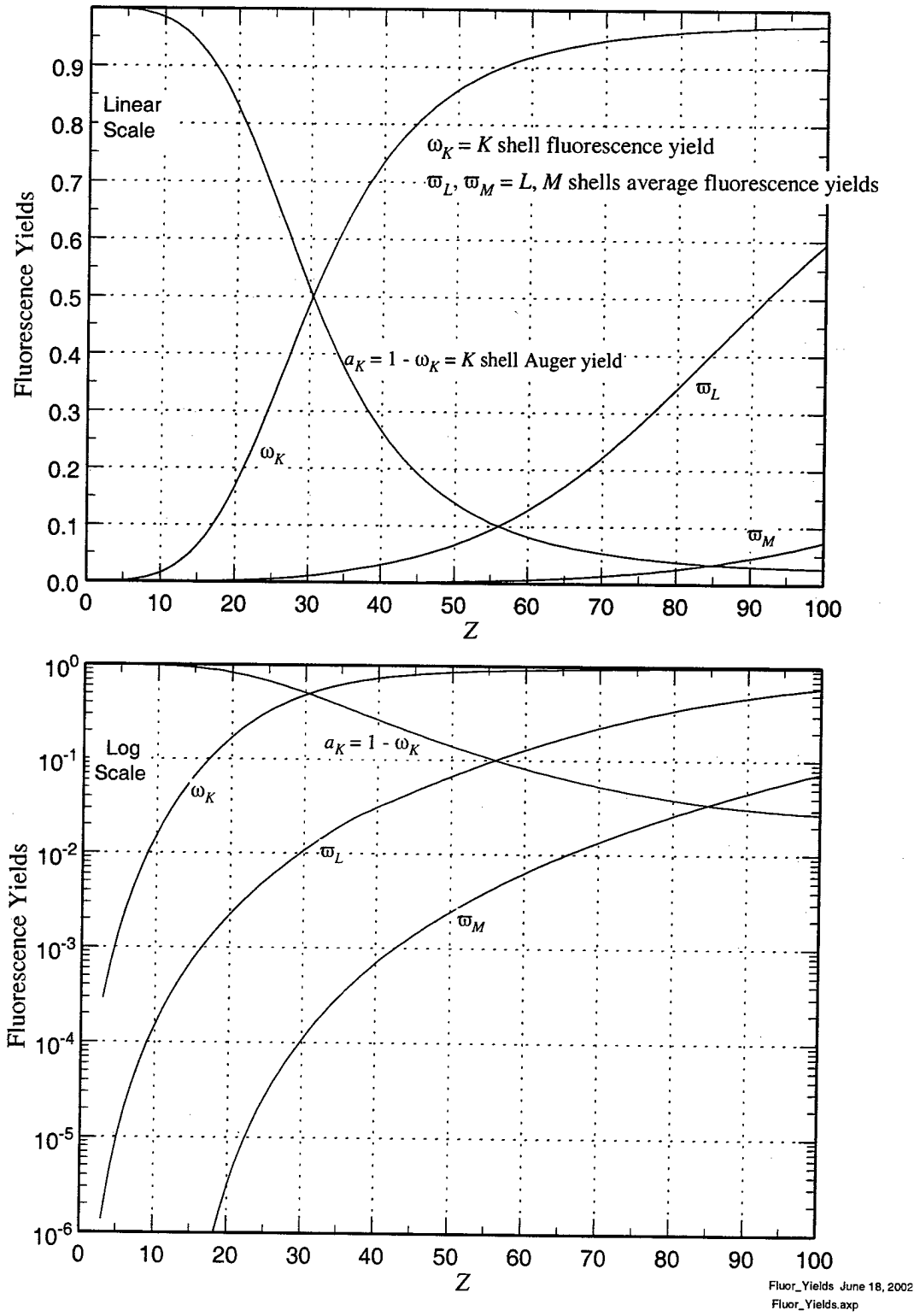

Figure 2.13 *K, L, M* - Shell Fluorescence Yields. Data from [Hu89].

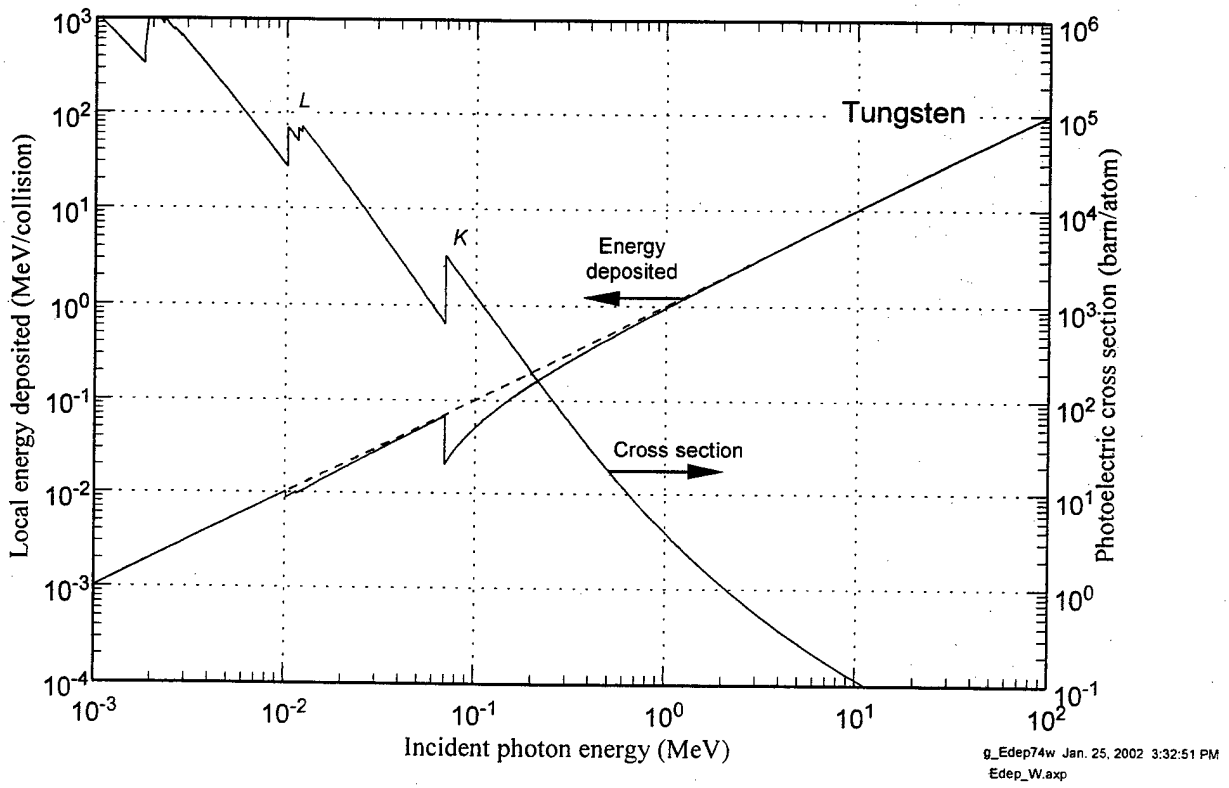

Figure 2.14

Energy deposition in Tungsten by photoelectric absorption as a function of incident photon energy. The right hand scale shows the photoelectric absorption cross section in barn/atom. The *K* and *L* edges are indicated on the curve. The dashed line is the incident photon energy; it would be the energy deposited were it not for fluorescence. Accounting for fluorescence, the solid line is the energy left in the material in the form of kinetic energy of electrons, and is the actual energy deposited "locally". The difference from the incident energy is released as characteristic X-rays. With incident energy just above the K edge the fluorescence X-rays have energy just below the K edge, and a mean free path in the material some 4.2 times as long as the incident photons. Data from TART98 EPICSHOW module.

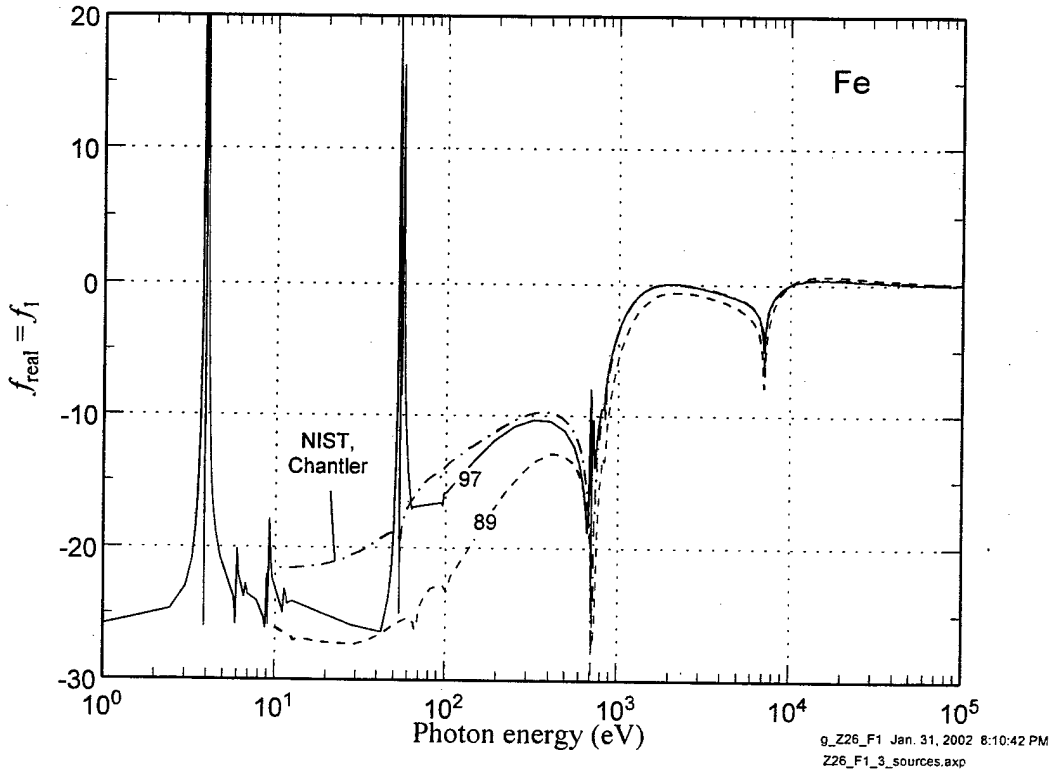

Comparison of three recent compilations of anomalous scattering factor f_1 in Fe. EPDL97 extends down to 1 eV. NIST (Chantler) and EPDL89 start at 10 eV.

2.15 (a)

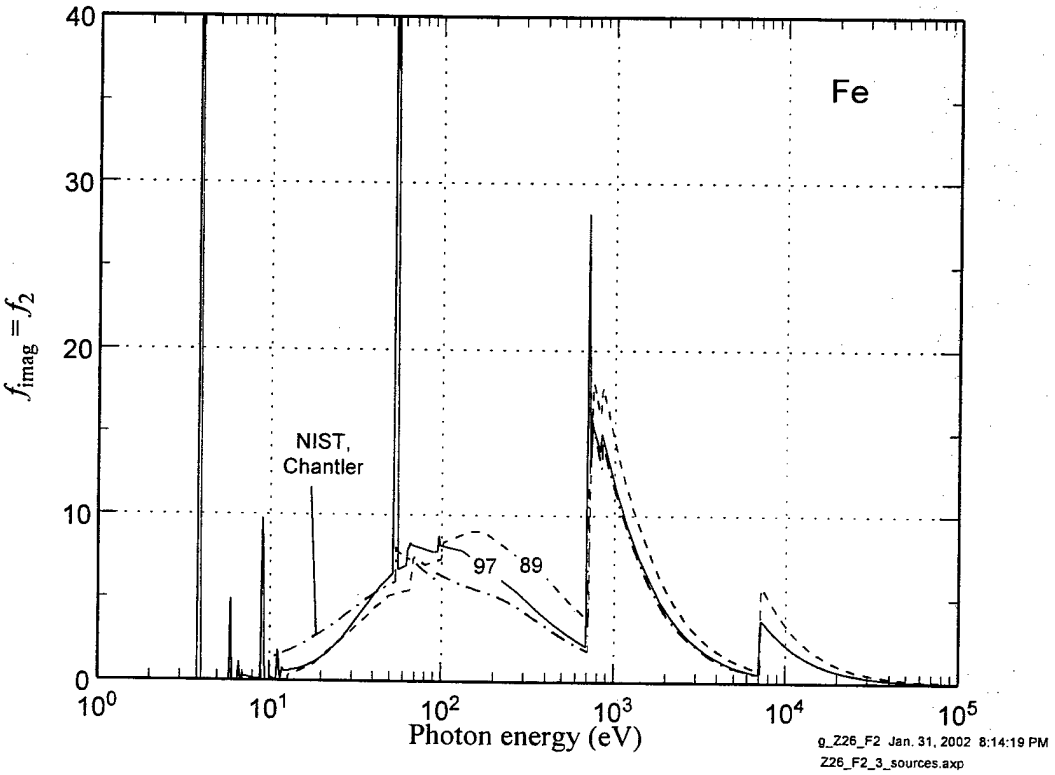

Comparison of three recent compilations of anomalous scattering factor f_2 in Fe. EPDL97 extends down to 1 eV. NIST (Chantler) and EPDL89 start at 10 eV.

2.15 (b)

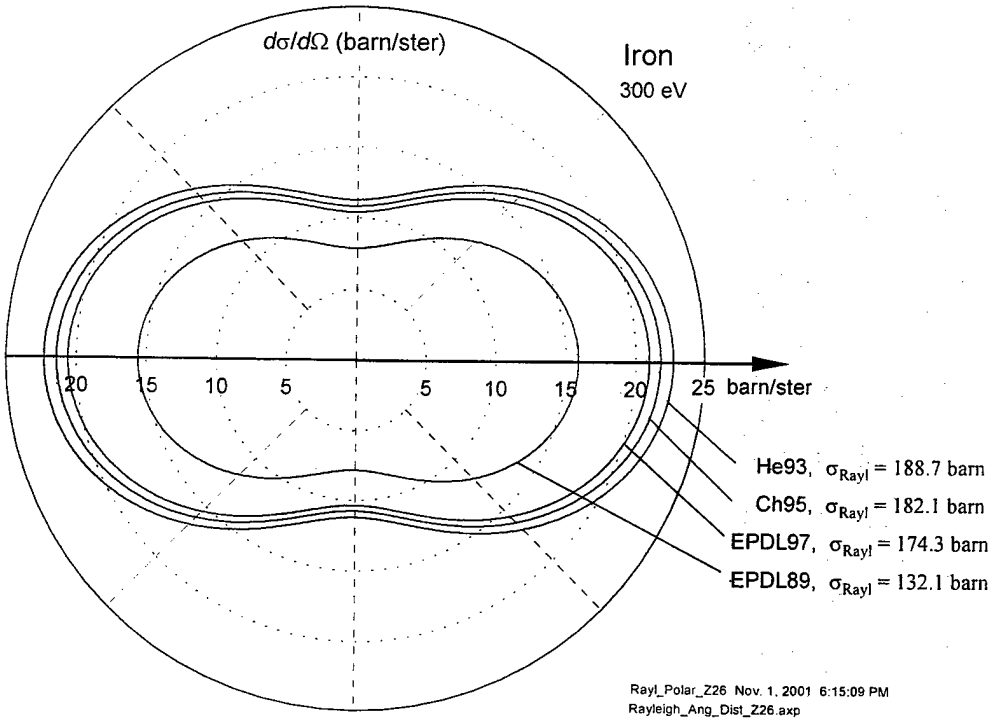

Figure 2.16 Illustrating variations in recent compilations of Rayleigh scattering angular distribution and total cross section, on Fe at incident photon energy of 300 eV. This plot was constructed from the form factors $F(q), f_1$, and f_2 compiled in the cited references, using Eq(2.19). Ch95 is from [Ch95a] and [Ch95b].

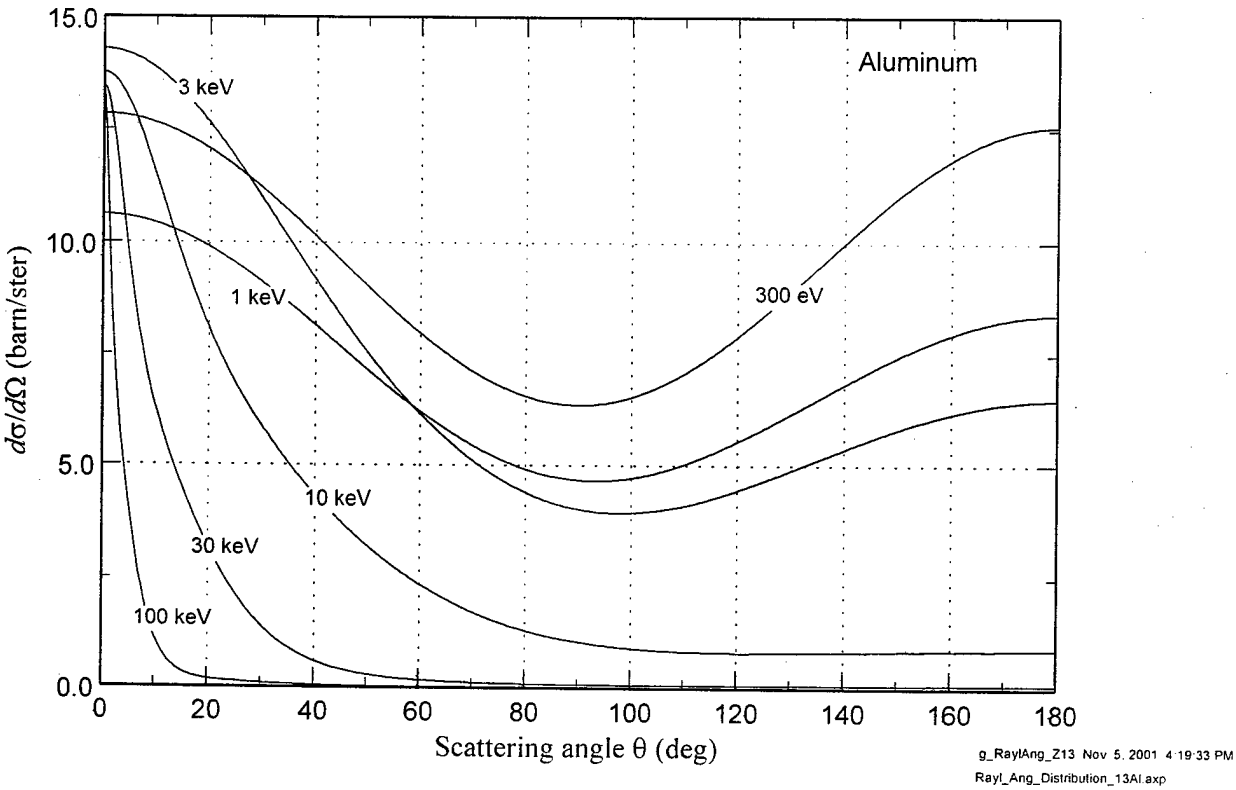

Figure 2.17 Coherent (Rayleigh) scattering angular distribution on atomic Aluminum. Data from EPDL97.

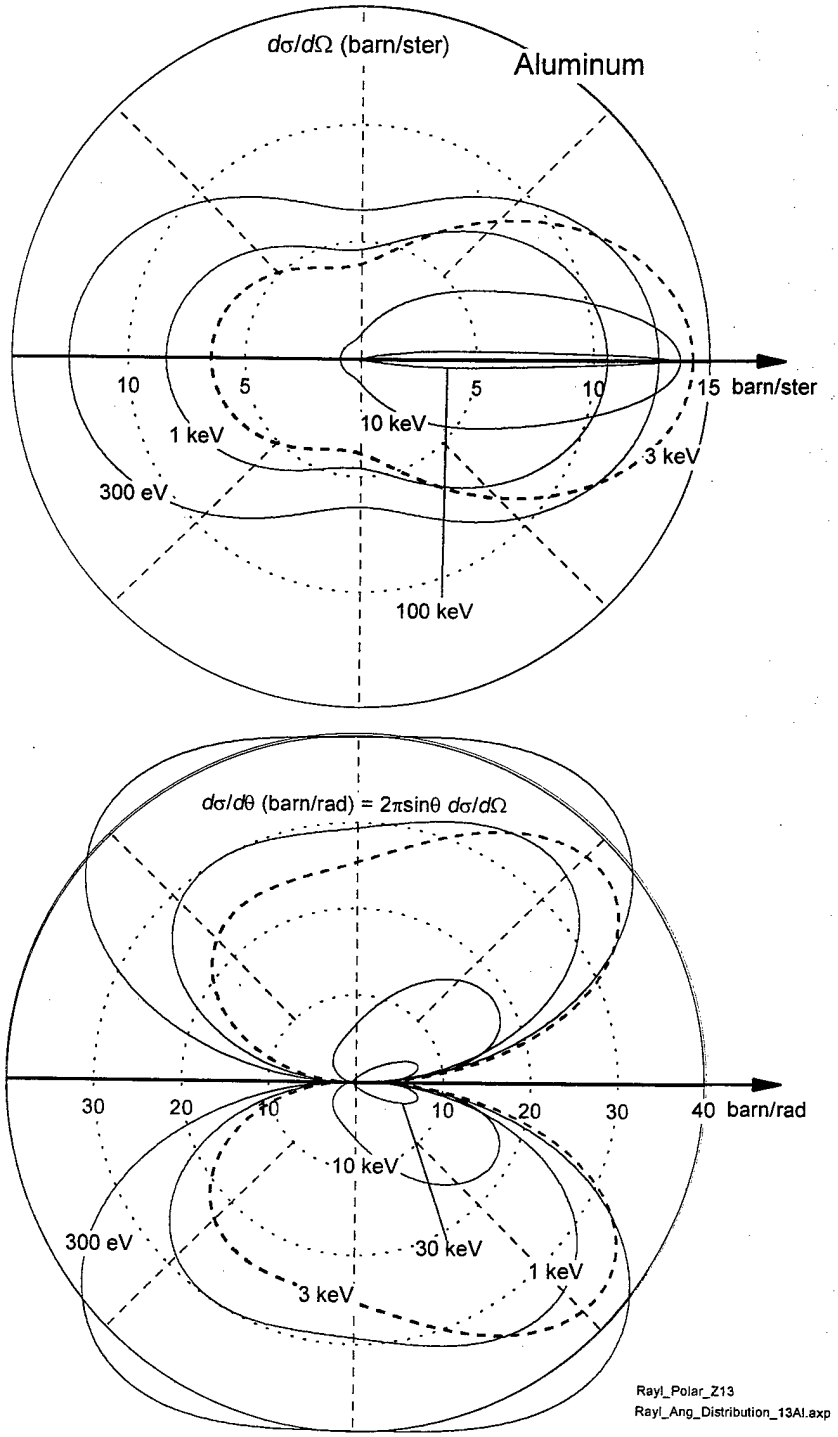

Figure 2.18 Angular distribution of coherent (Rayleigh) scattering on atomic Aluminum. Upper panel: $d\sigma/d\Omega$ (barn/ster). Lower panel: $d\sigma/d\theta$ (barn/rad) = $2\pi\sin\theta d\sigma/d\Omega$. Data from EPDL97

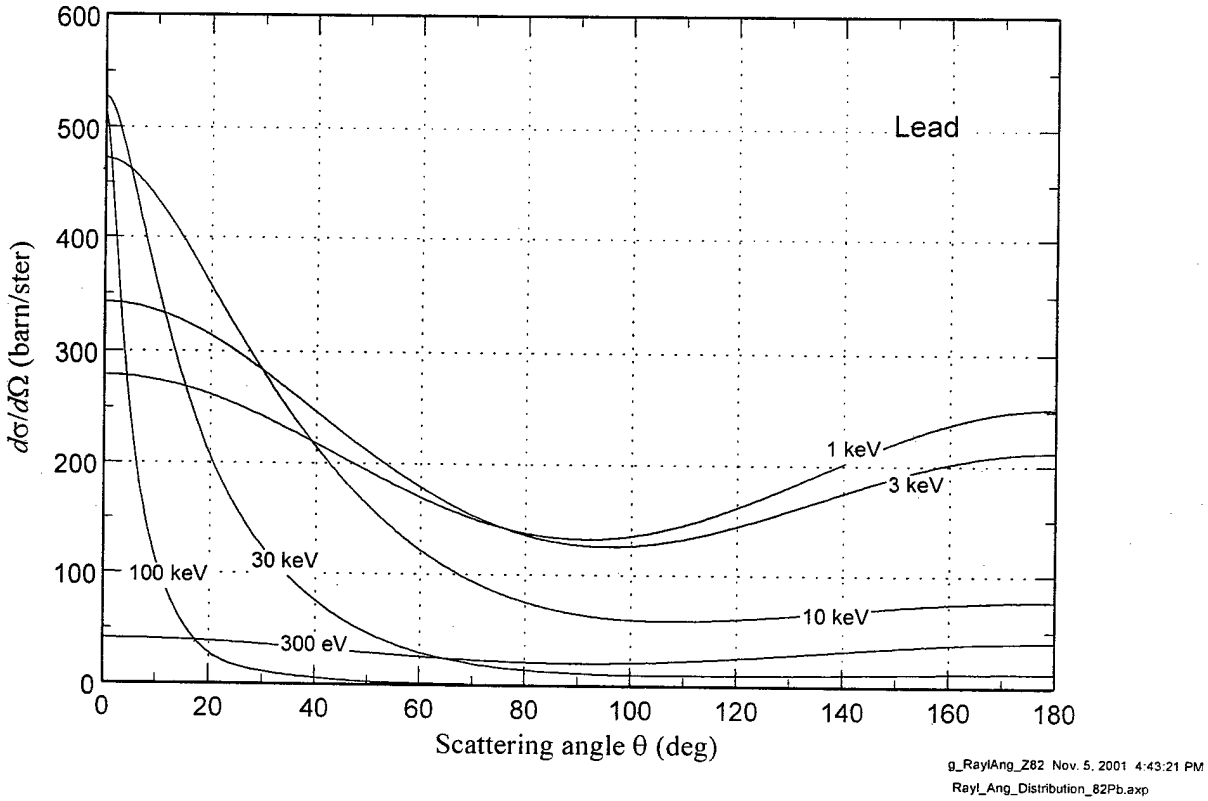

Figure 2.19 . Coherent (Rayleigh) scattering angular distribution on atomic Lead. Data from EPDL97.

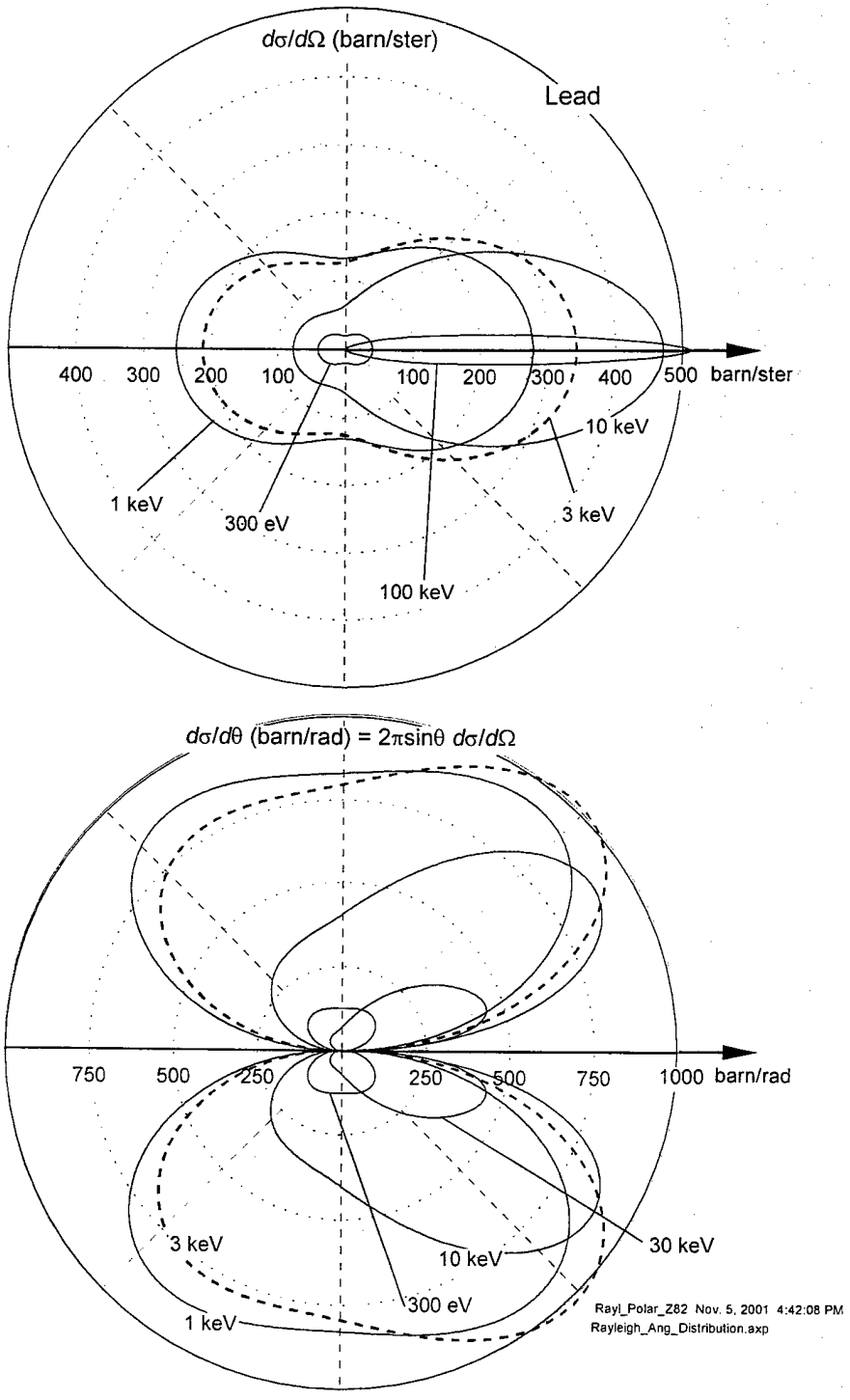

Figure 2.20 Angular distribution of coherent (Rayleigh) scattering on atomic Lead. Upper panel: $d\sigma/d\Omega$(barn/ster). Lower panel: $d\sigma/d\theta$(barn/rad) = $2\pi\sin\theta\, d\sigma/d\Omega$. Data from EPDL97.

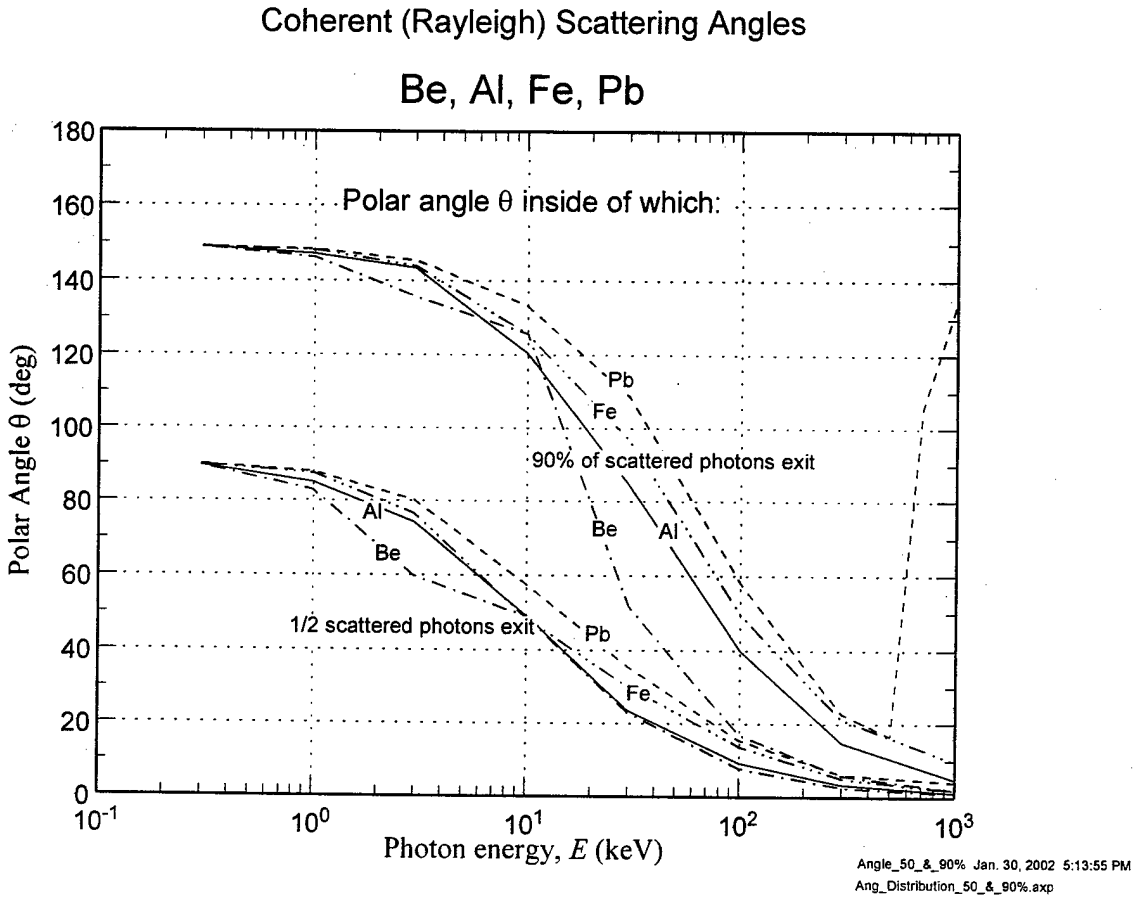

Figure 2.21

Concentration of coherent Rayleigh scattering in the forward direction at high energy and low Z. In Be at 100 keV 50% of photons scatter at less than 7.5°, and 90% scatter at less than 17°. Data from EPDL97. (In Pb above 500 keV, in spite of sharp forward peaking, there is small scattering at all angles, and 90% does not accumulate until more than 100°)

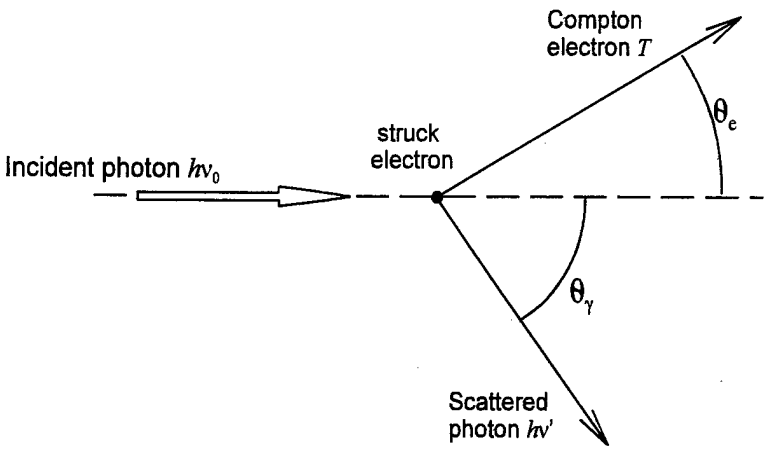

Figure 2.22. Angle definitions for Compton scattering

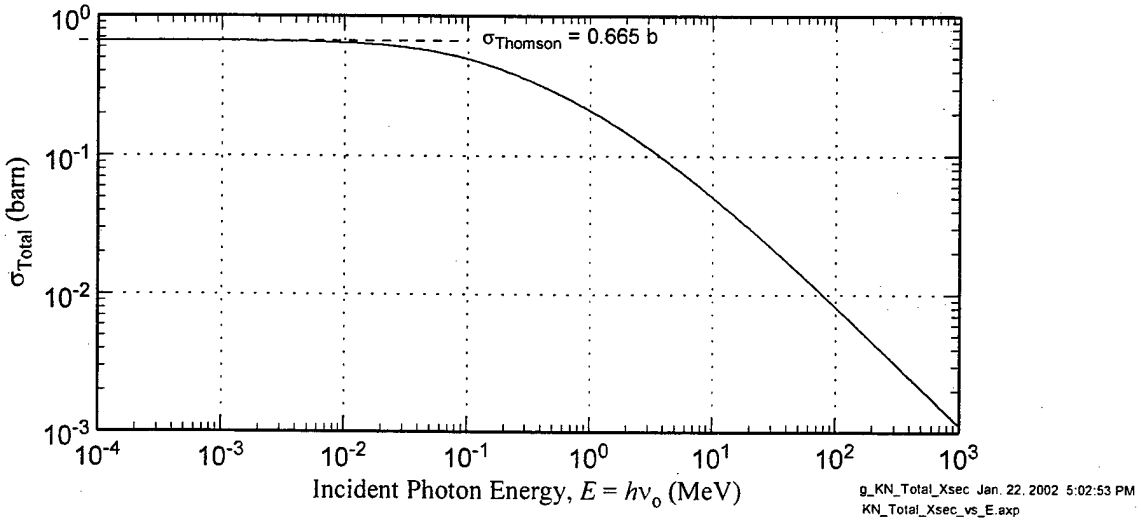

Figure 2.23 Klein-Nishina cross section on a free electron.

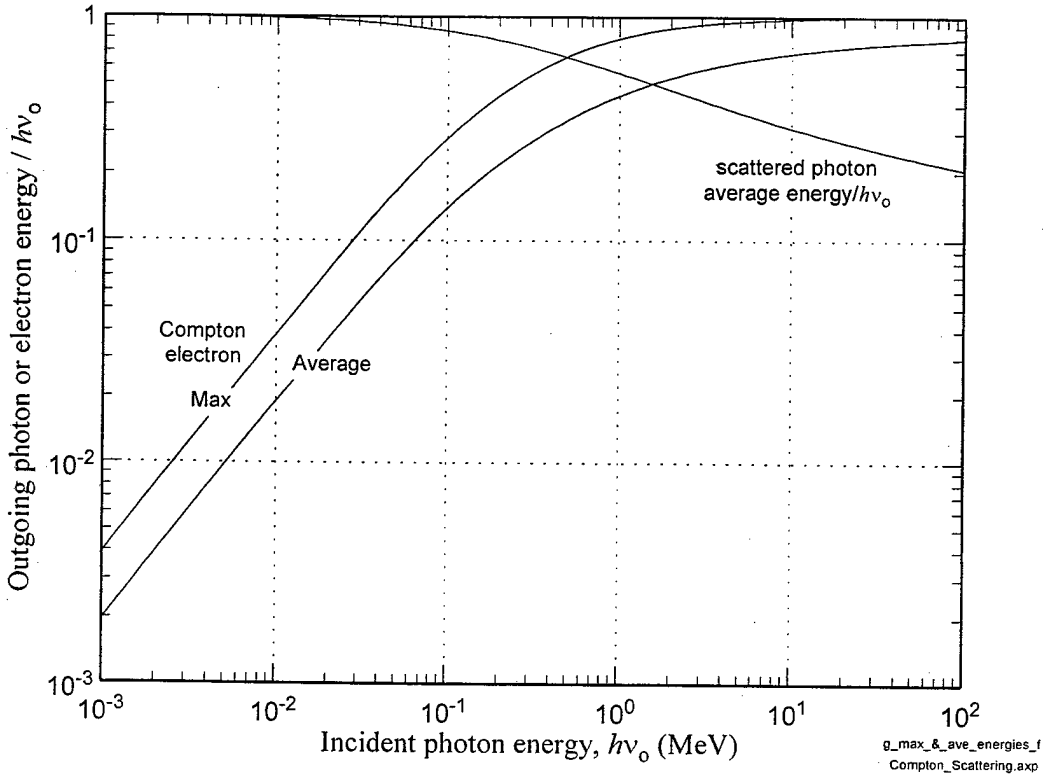

2.24

Figure . Average and maximum energies of Compton electron, and average energy of scattered photon, normalized to incident photon energy $h\nu_o$.

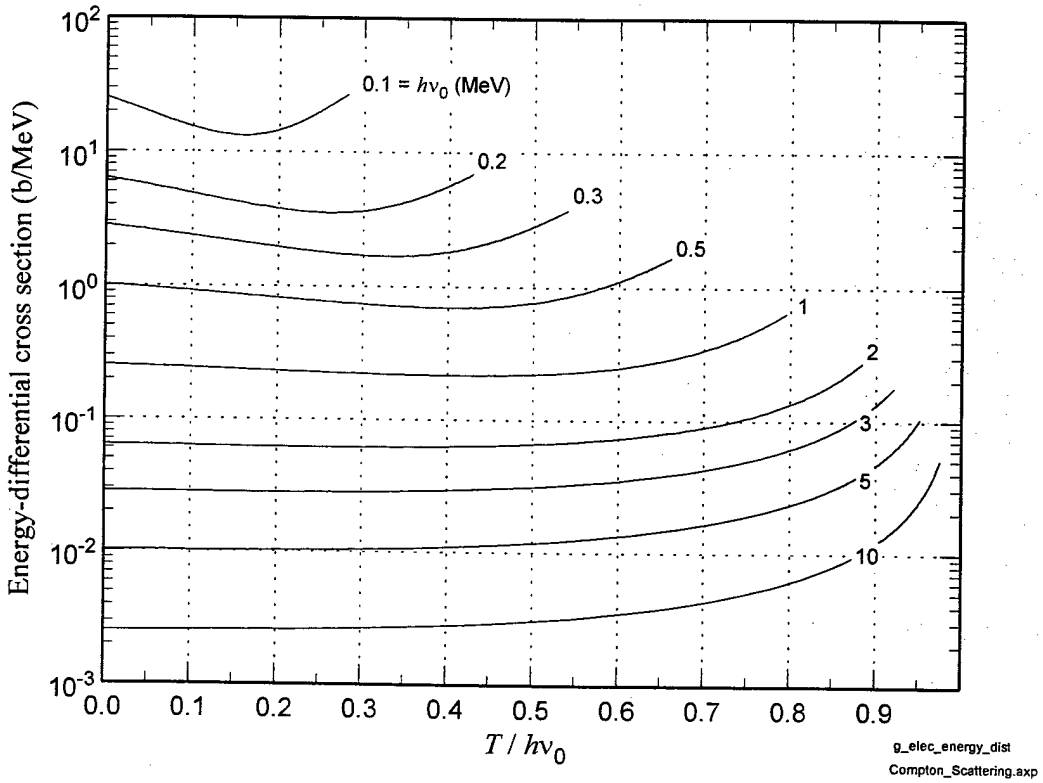

Figure 2.25 Compton electron energy distribution for Compton scattering from a free electron.

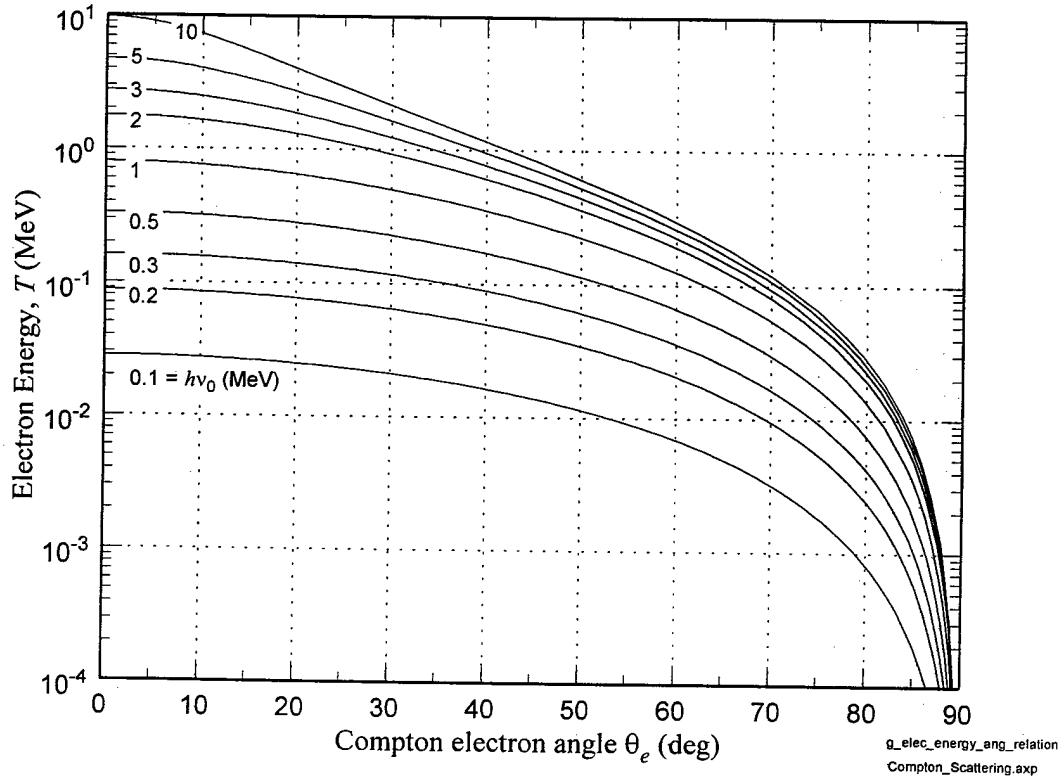

Figure 2.26 Compton electron energy *vs* outgoing angle θ_e.

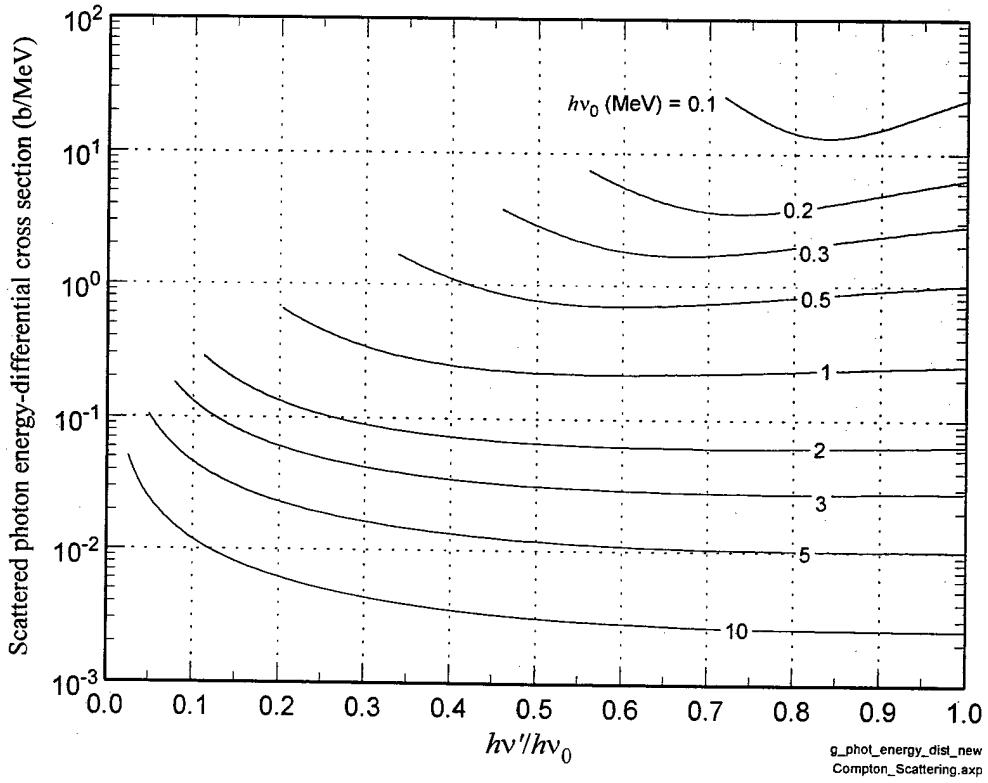

Figure 2.27 Scattered photon energy distribution.
Compton scattering on a free electron.

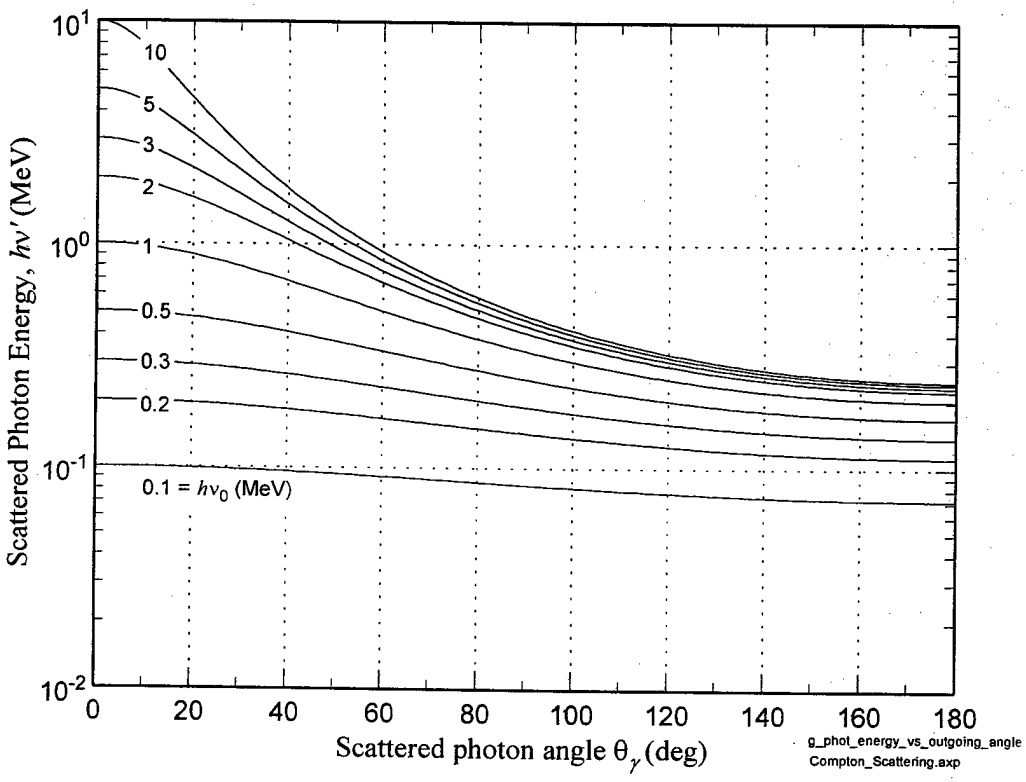

Figure 2.28 Scattered photon energy *vs* outgoing angle θ_γ.
Compton scattering on a free electron

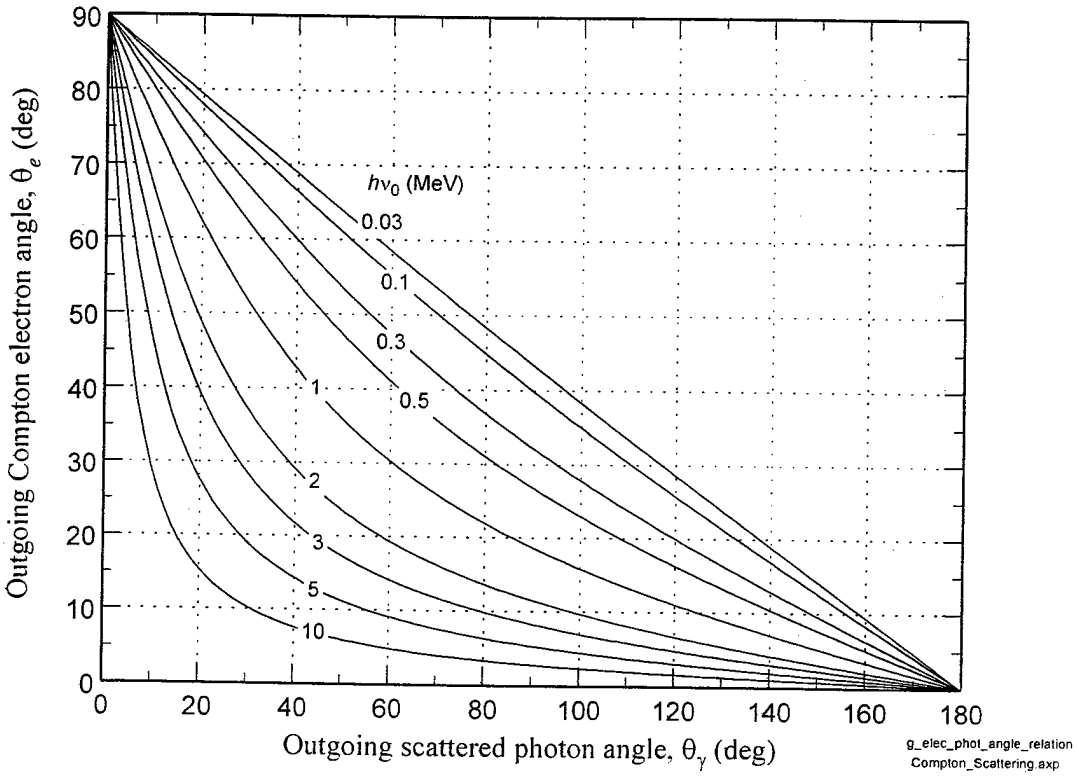

Figure 2.29 . Compton electron angle of emission *vs* scattered photon angle.

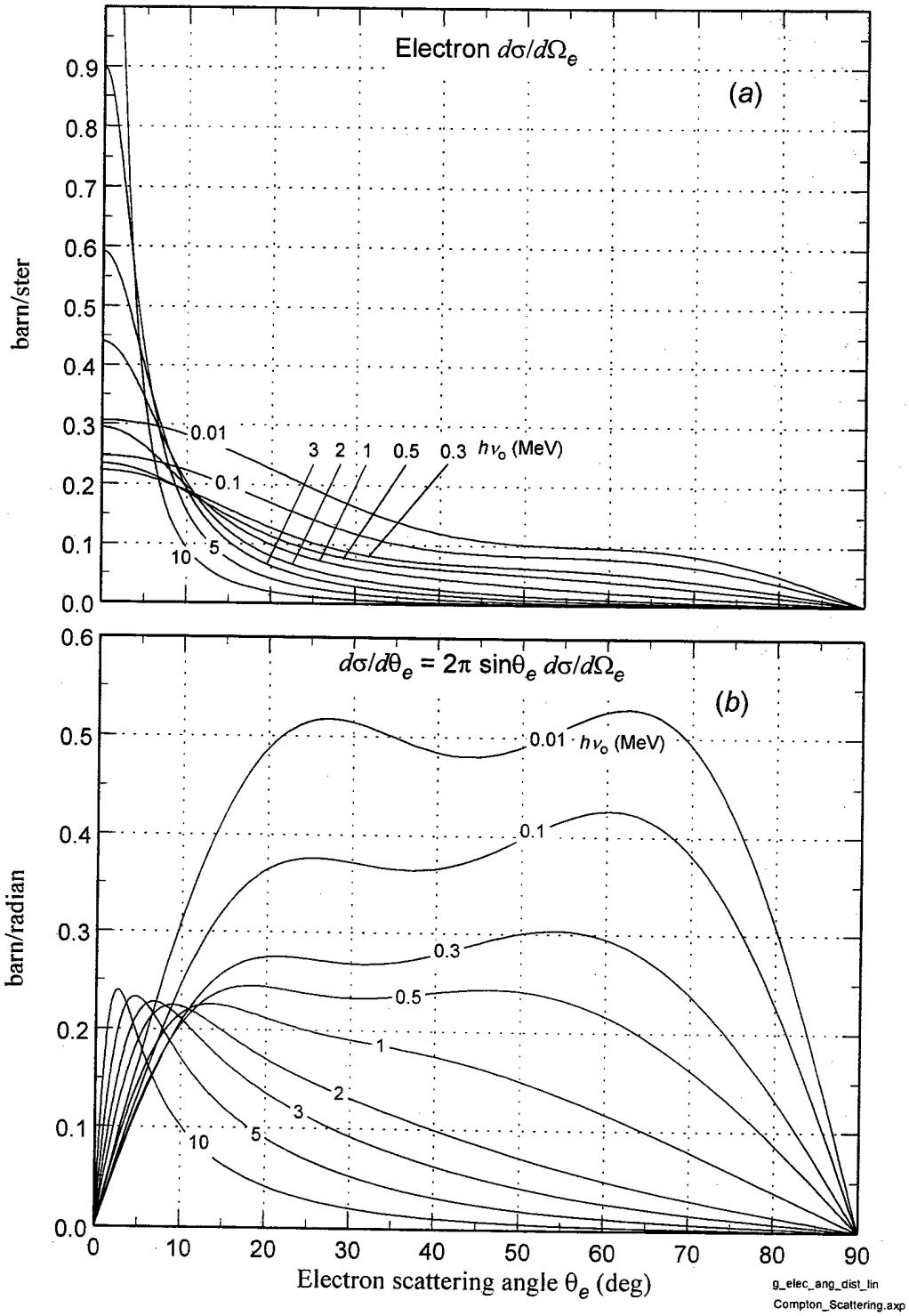

2.30 Compton electron differential scattering cross section on a free electron *vs* outgoing electron polar angle θ_e.

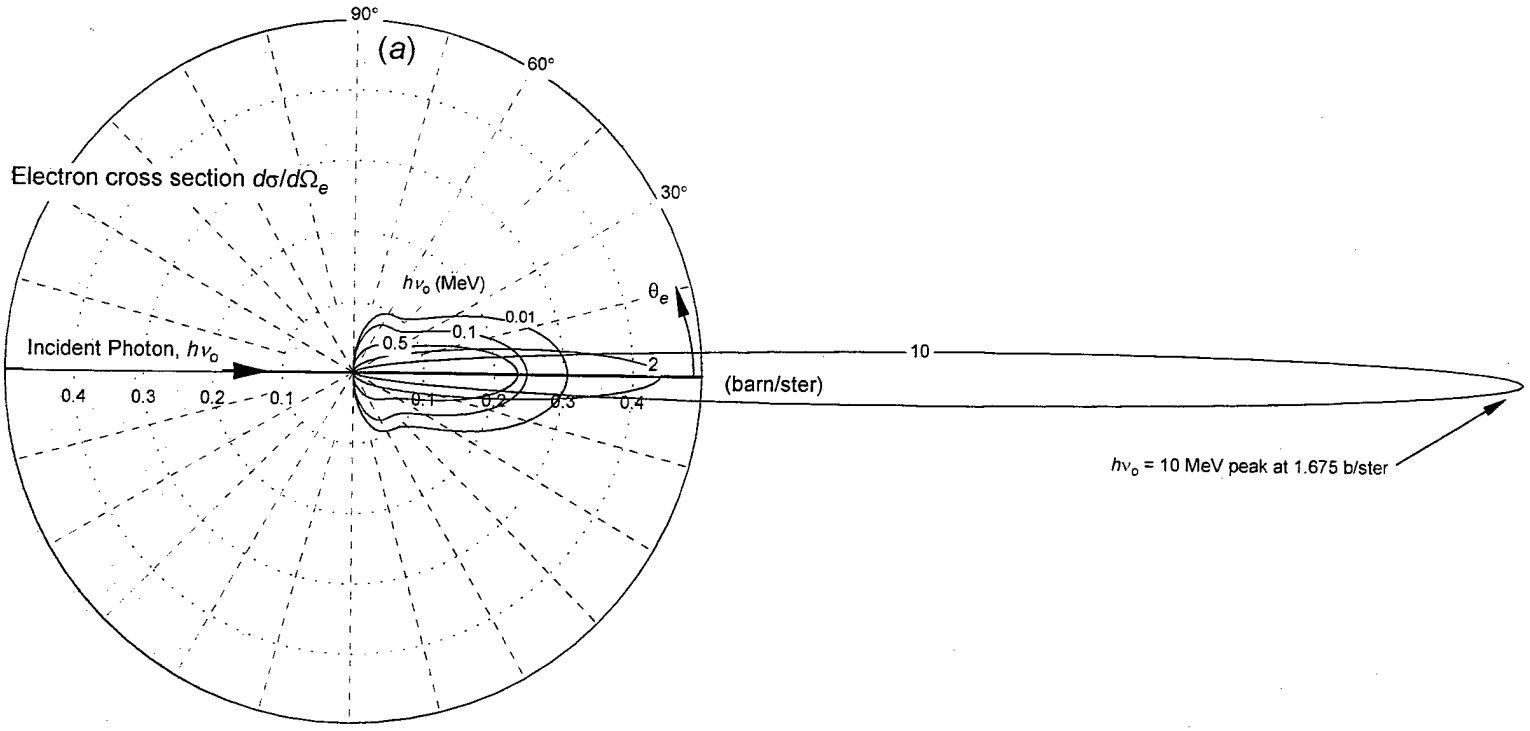

(*a*) Electron differential scattering cross section, per unit solid angle, $d\sigma/d\Omega_e$ as a function of electron scattering angle θ_e.

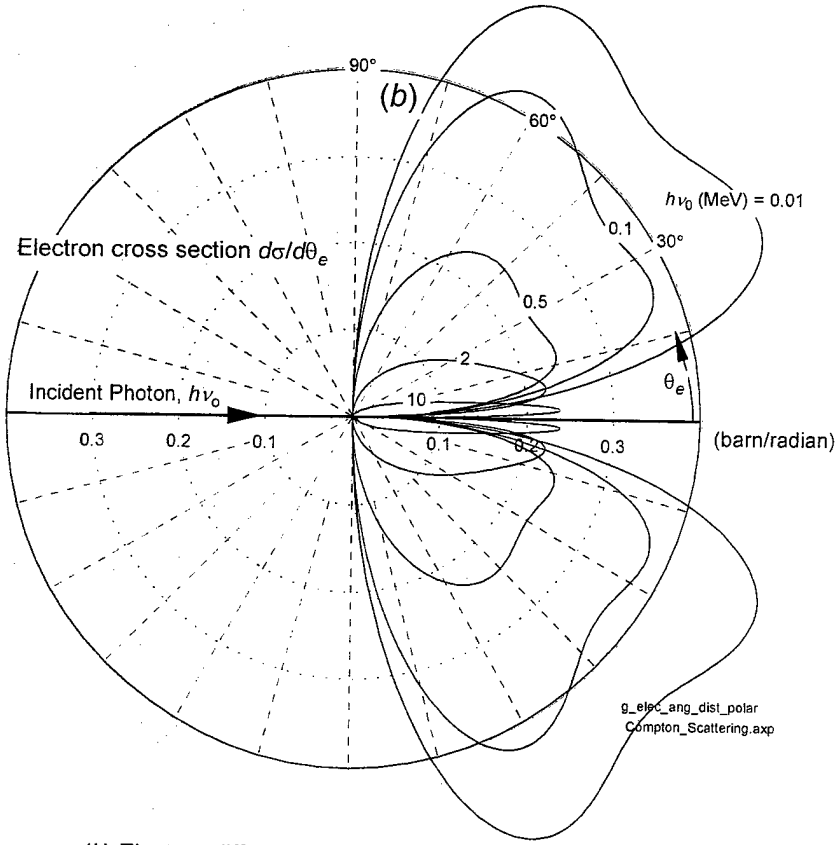

(*b*) Electron differential scattering cross section, per unit polar angle, $d\sigma/d\theta_e$ as a function of electron outgoing angle θ_e , $= 2\pi\sin\theta_e \, d\sigma/d\Omega_e$

Figure 2.31 . Compton electron angular distribution.

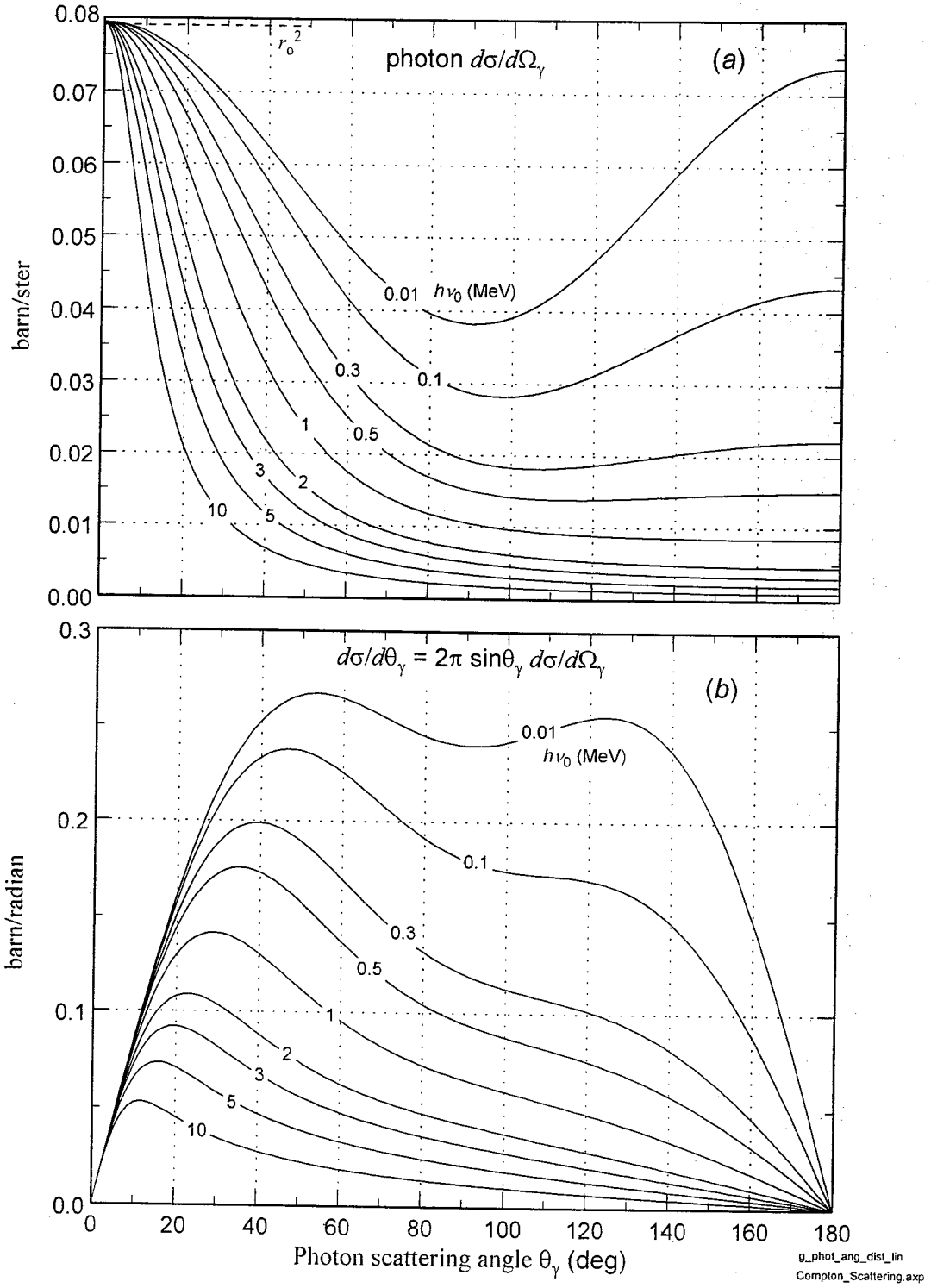

Figure . Compton scattered photon differential cross section on a free electron *vs* scattering angle.

2.32

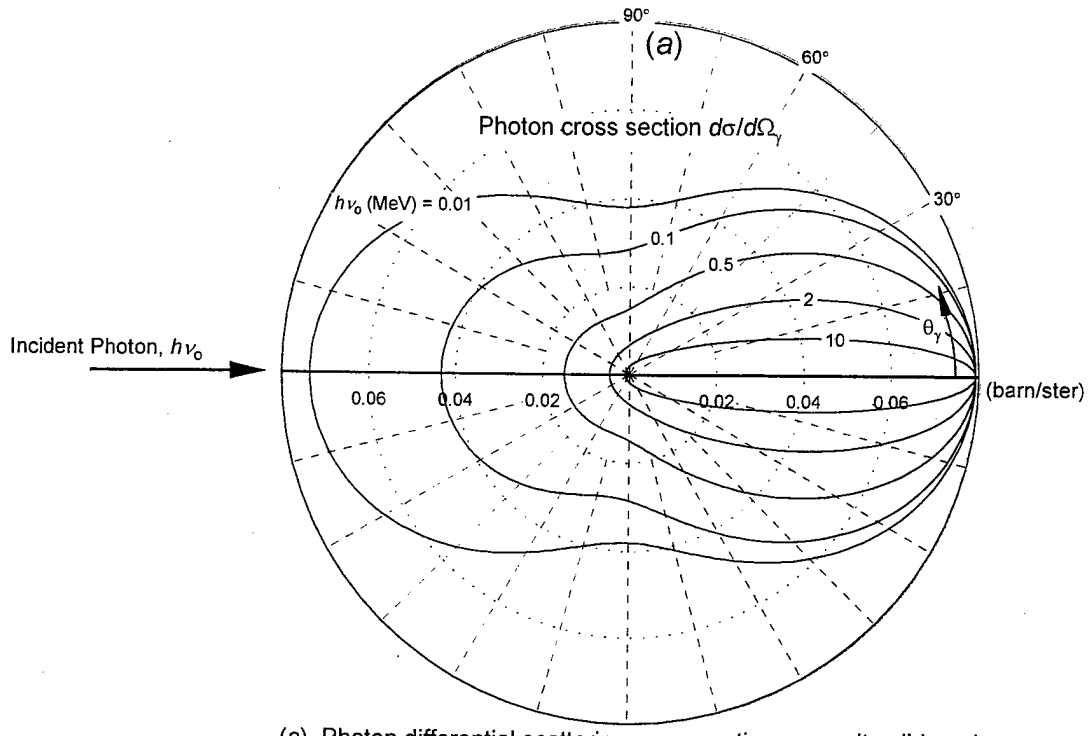

(a) Photon differential scattering cross section, per unit solid angle, $d\sigma/d\Omega_\gamma$ as a function of scattering angle θ_γ.

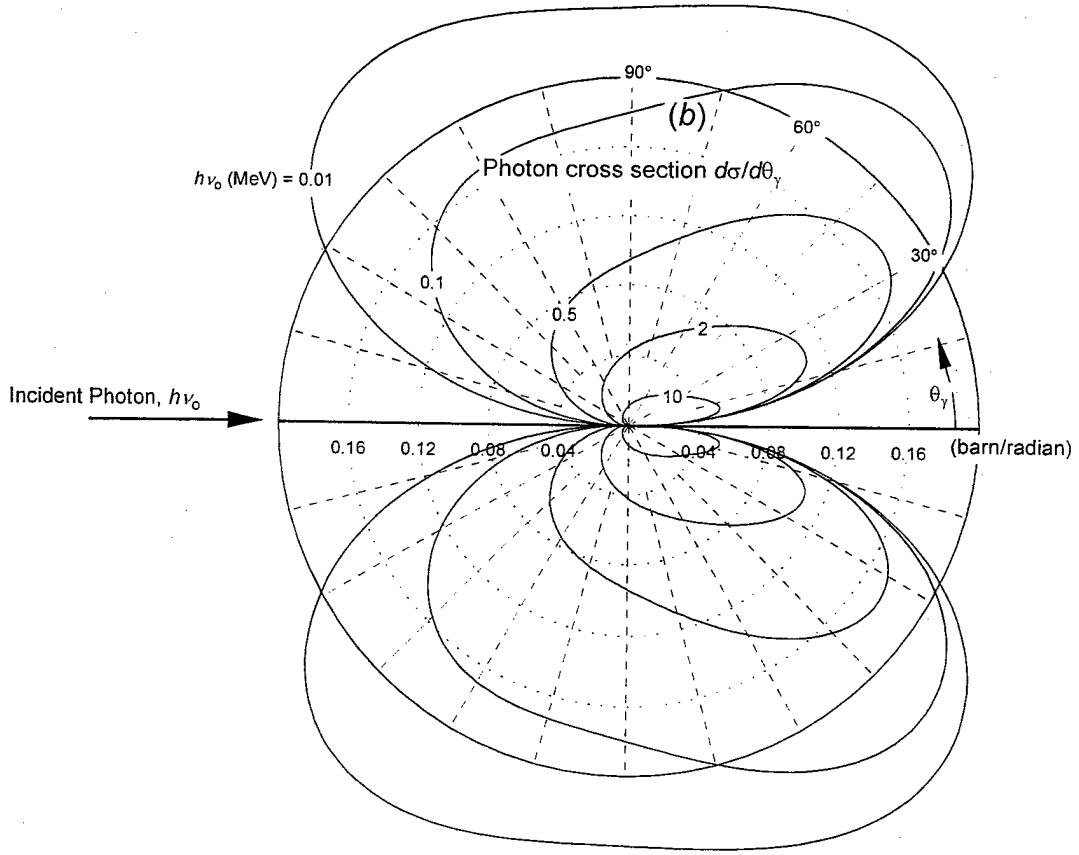

(b) Photon differential scattering cross section, per unit polar angle, $d\sigma/d\theta_\gamma$ as a function of scattering angle θ_γ. $= 2\pi\sin\theta_\gamma \, d\sigma/d\Omega_\gamma$.

g_phot_ang_dist_polar
Compton_Scattering.axp

Figure . Angular distribution of scattered photon in Compton scattering from a fee electron.

2.33

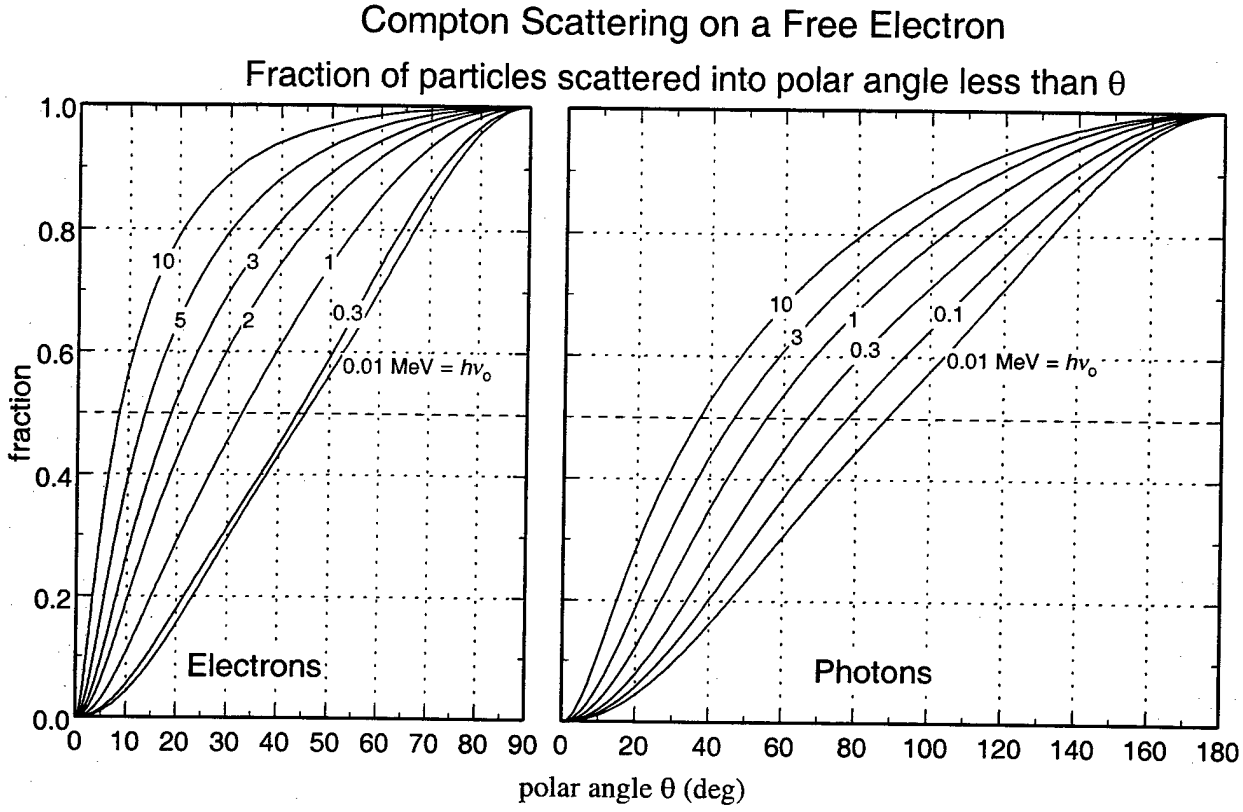

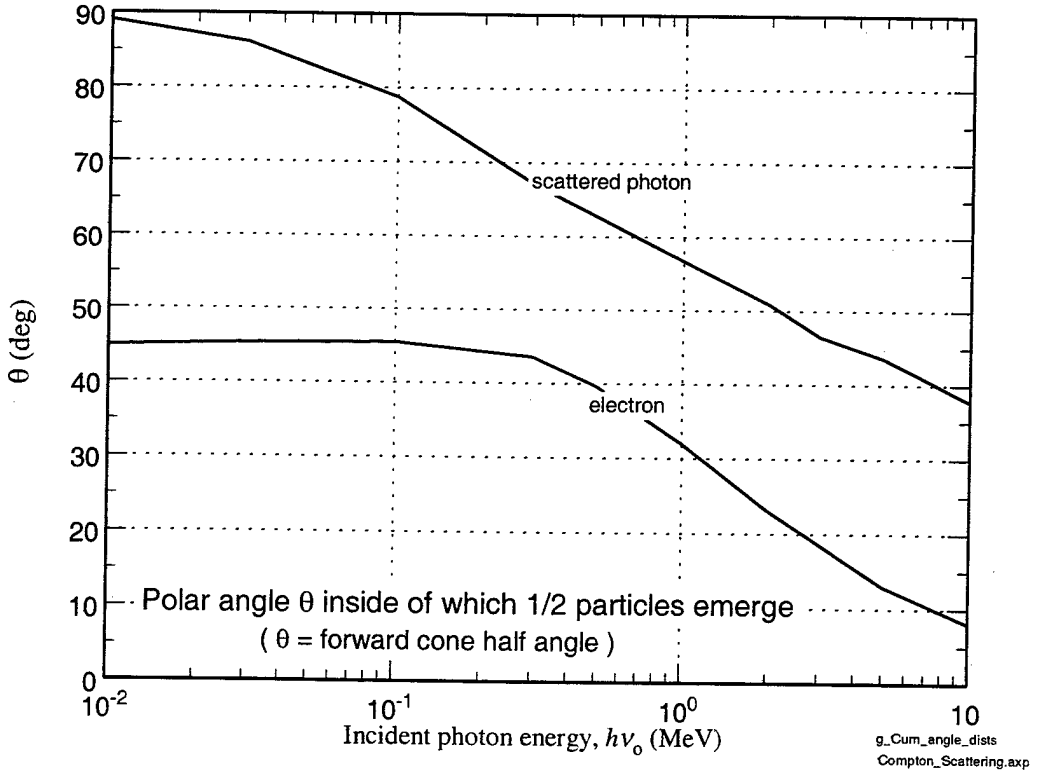

Figure 2.34 . Compton scattering cumulative angular distributions.

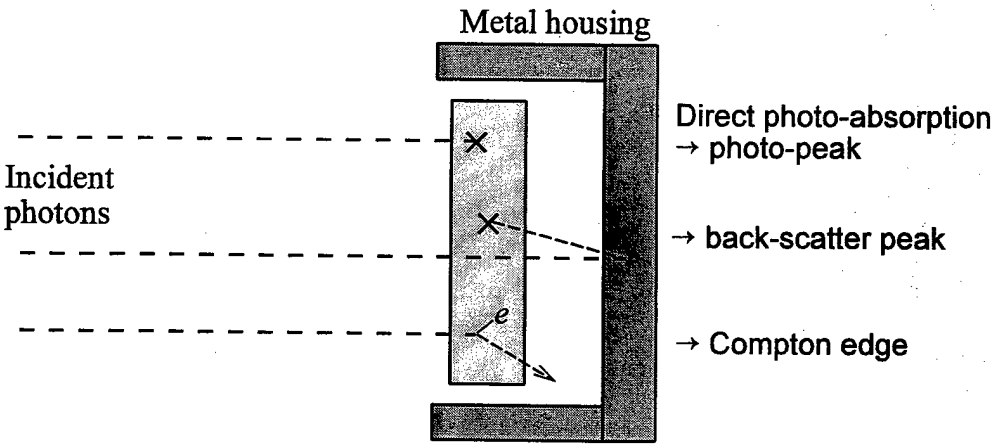

35

Figure 2. Illustrating three kinds of photon interactions in a crystal gamma detector. The upper photon is directly absorbed by the photo-electric effect; all its energy is deposited in the crystal (except possibly for fluorescence X-rays), contributing to the photo-peak. The center photon passes through the crystal and Compton scatters through a large angle from the housing; the scattered photon is absorbed in the crystal, leading to the back-scatter peak. The lower photon undergoes a Compton scattering in the crystal; the electron stops in the crystal contributing its energy to the Compton shoulder.

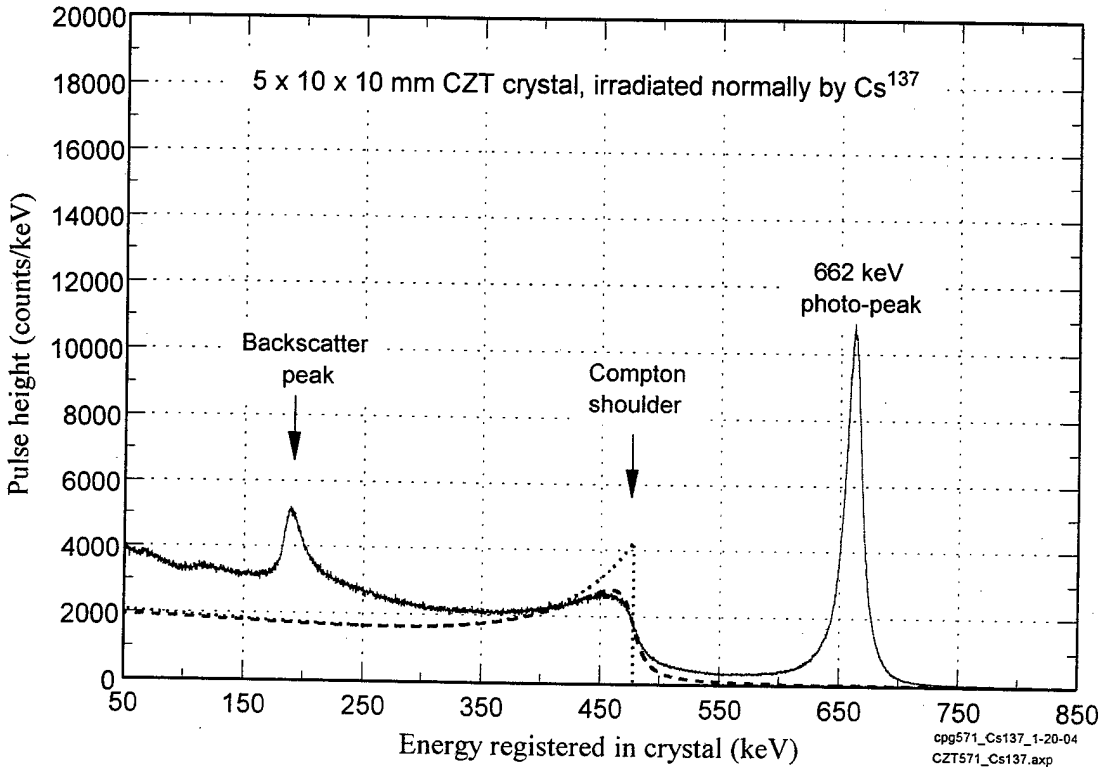

Figure 2. 36 Gamma ray spectrum measurement of a Cs^{137} source in a CdZnTe crystal. The main Cs peak at 661.6 keV is pronounced. The Compton shoulder is clear at T_{max} = 477 keV. The backscatter peak is near a minimum energy of $h\nu'(180°)$ = 184 keV. The data include ambient environmental background noise. The dotted curve is the ideal Compton electron spectrum, with a sharp cutoff at T_{max}. The dashed curve is after broadening by a detector resolution function with FWHM = 18 keV. Data courtesy of John Baker, Mission Research Corporation.

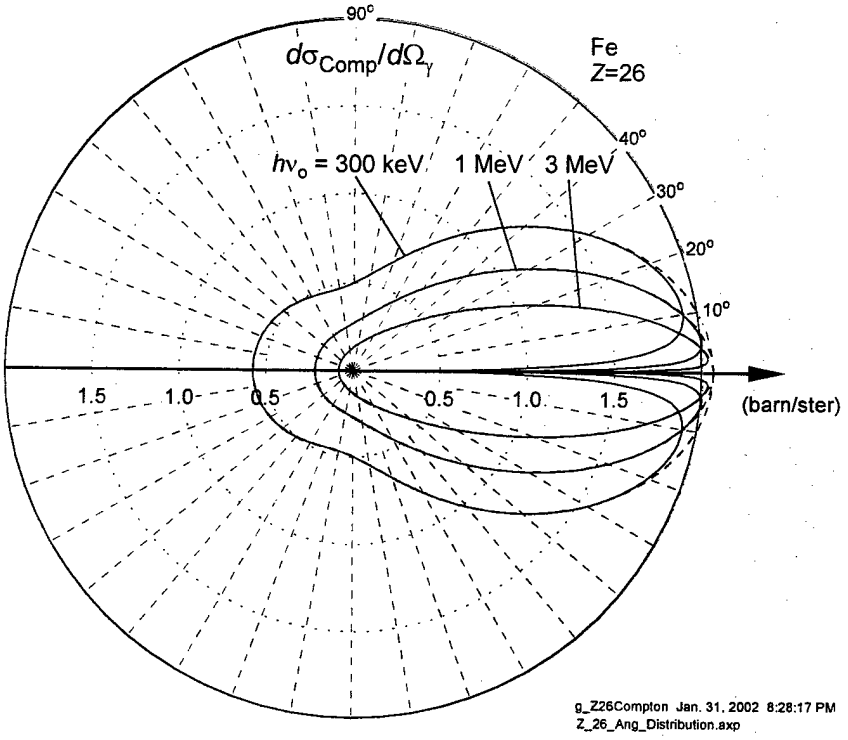

Figure 2.37 Compton differential cross section for the scattered photon on atomic Fe at three incident energies. Solid lines are computed from Eq(2.22) using data on $S(q)$ from EPDL97. Dashed lines are $Zd\sigma_{KN}/d\Omega$.

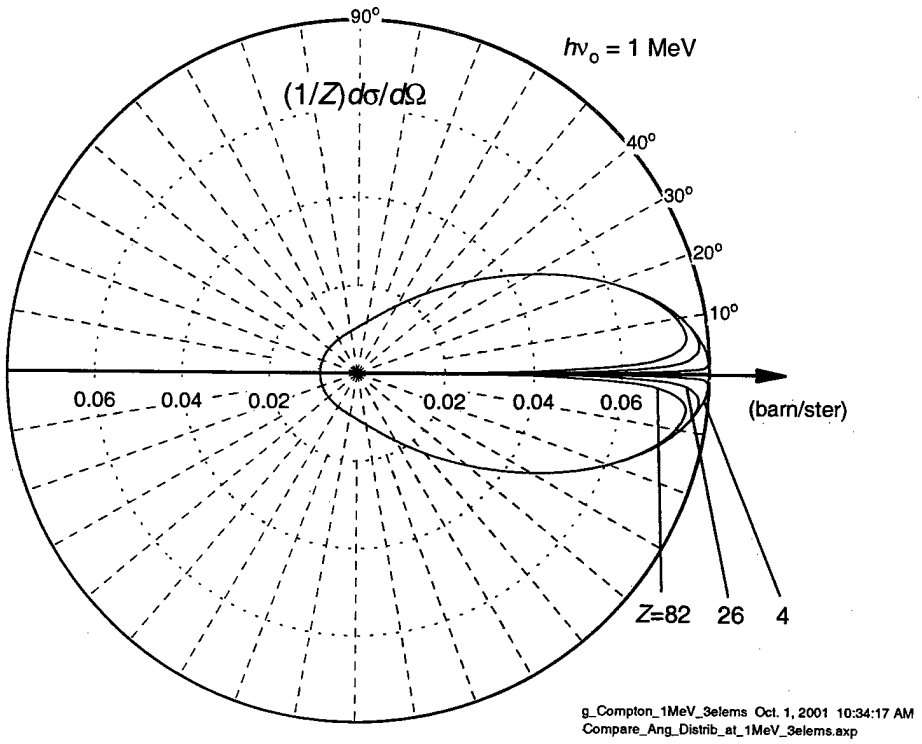

Figure 2.38. Compton differential cross section (for the scattered photon), divided by the atomic number Z, on Be, Fe, and Pb at 1 MeV incident energy.

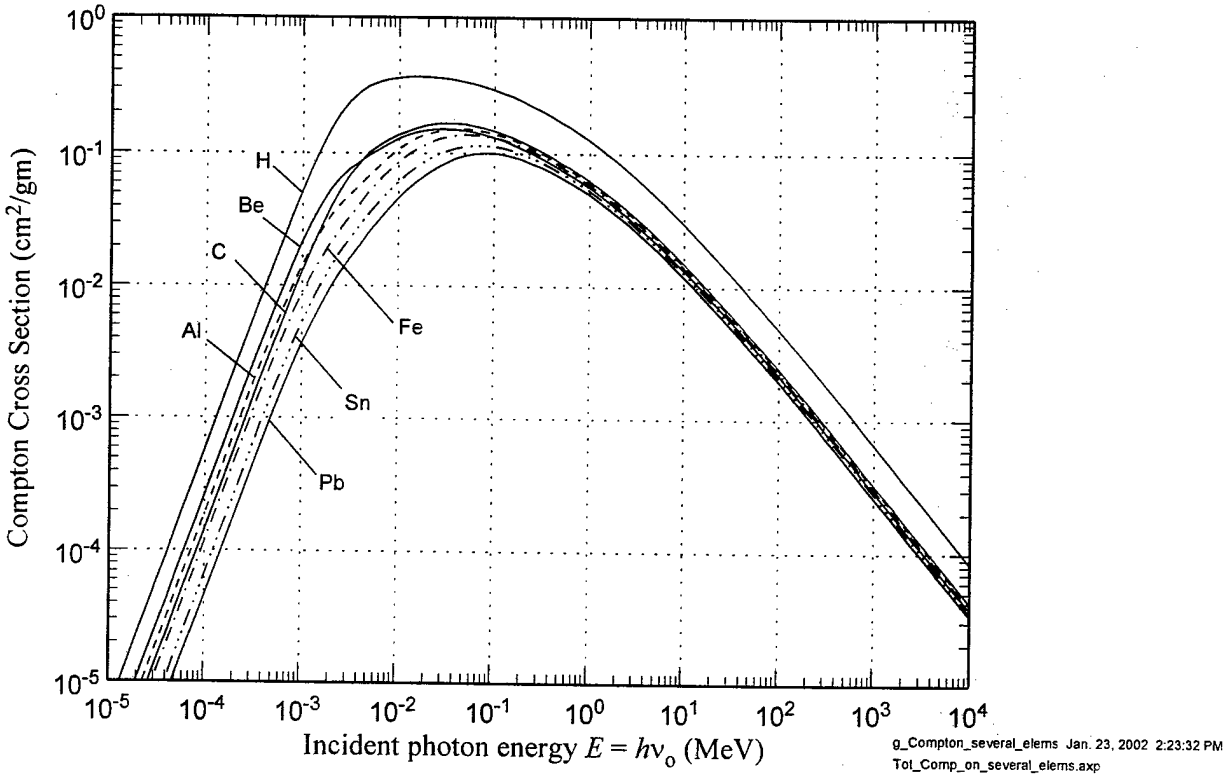

Figure 2.39 Total Compton cross section on several elements, cm^2/gm. Data from EPDL97.

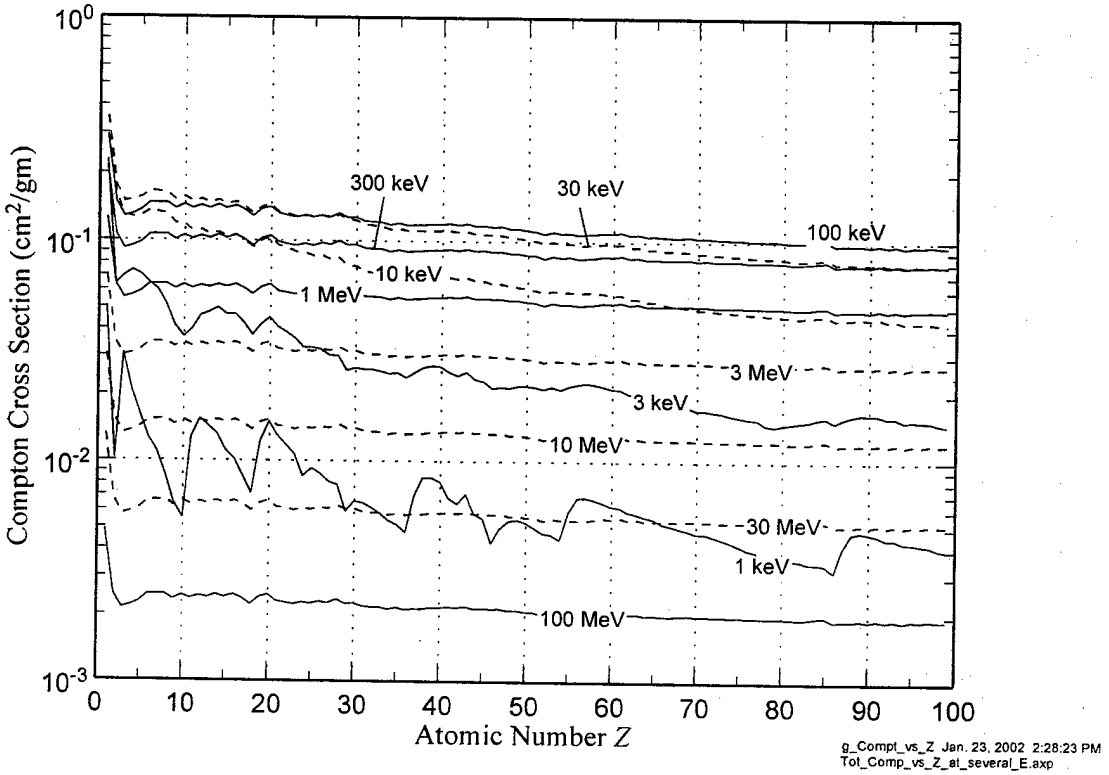

Figure 2.40 Total Compton cross section for all elements at several energies, cm^2/gm. Data from EPDL97.

Compton Cross Section

Contours in ***barn/atom***

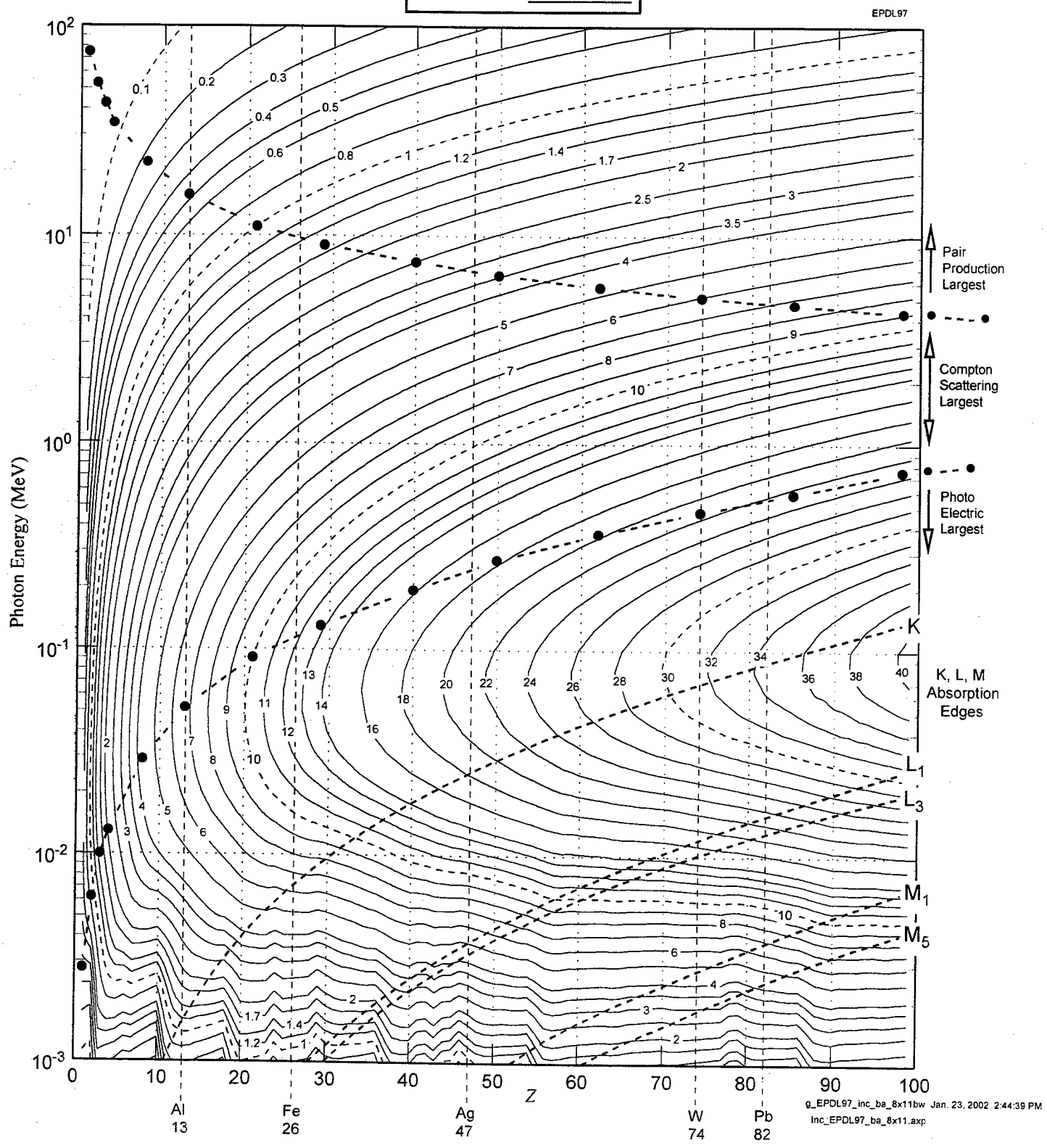

Figure 2.41 Contours of Compton cross section in all elements, from $E \equiv h\nu_0$ = 1 keV to 100 MeV. In barn/atom. Data from LLNL EPDL97.

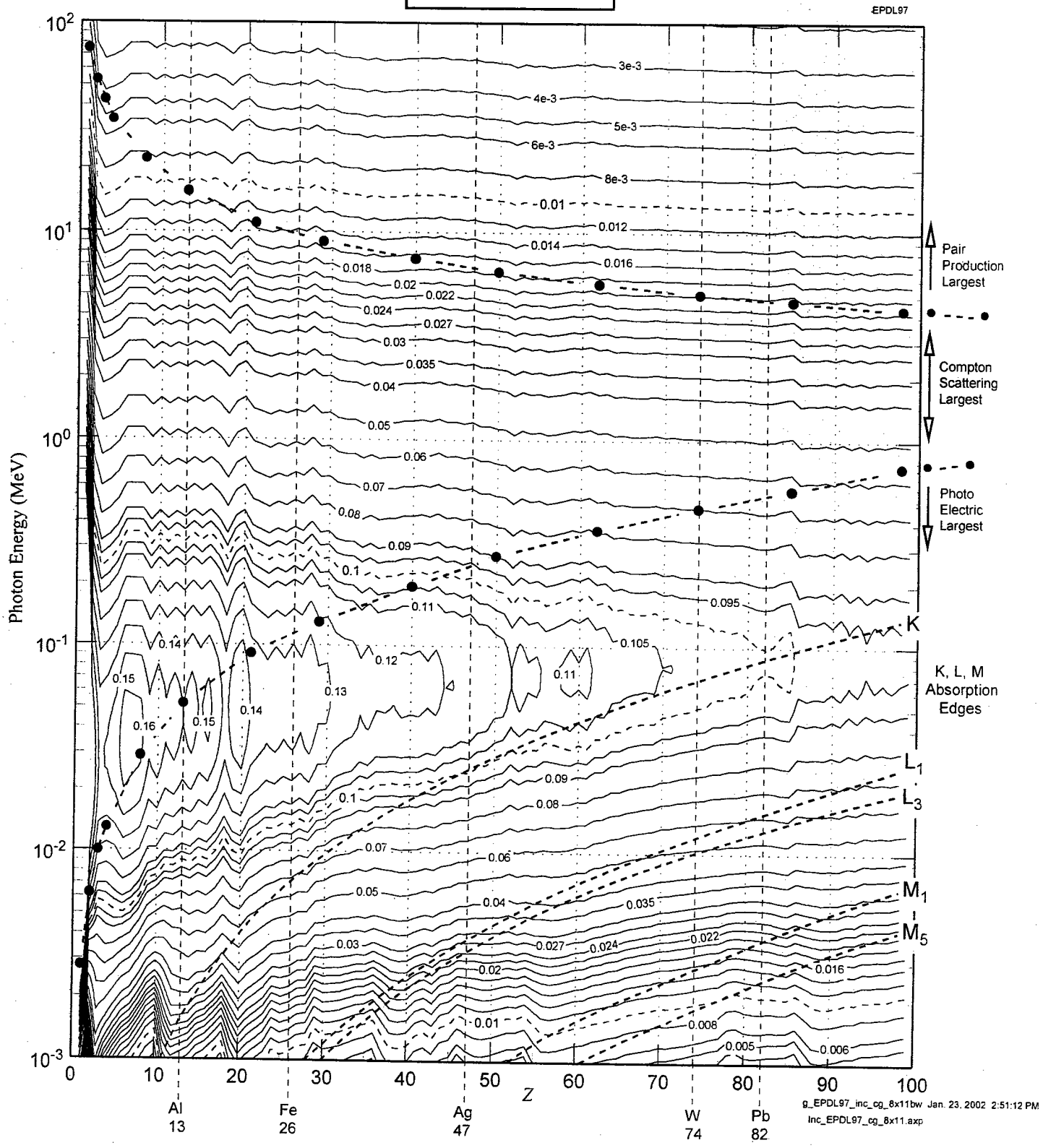

Figure 2.42 Contours of Compton cross section in all elements, from $E \equiv h\nu_0 = 1$ keV to 100 MeV. In cm^2/gm. Data from LLNL EPDL97.

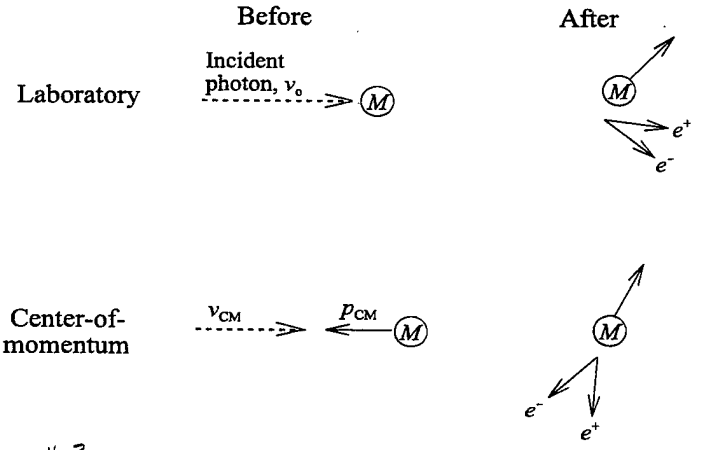

2.43

Figure ~~2.41~~. Pair production by a photon in the Coulomb field of a charged particle of mass *M*. Depicted before and after the interaction, and as seen in the laboratory and in the center-of-momentum frames of reference.

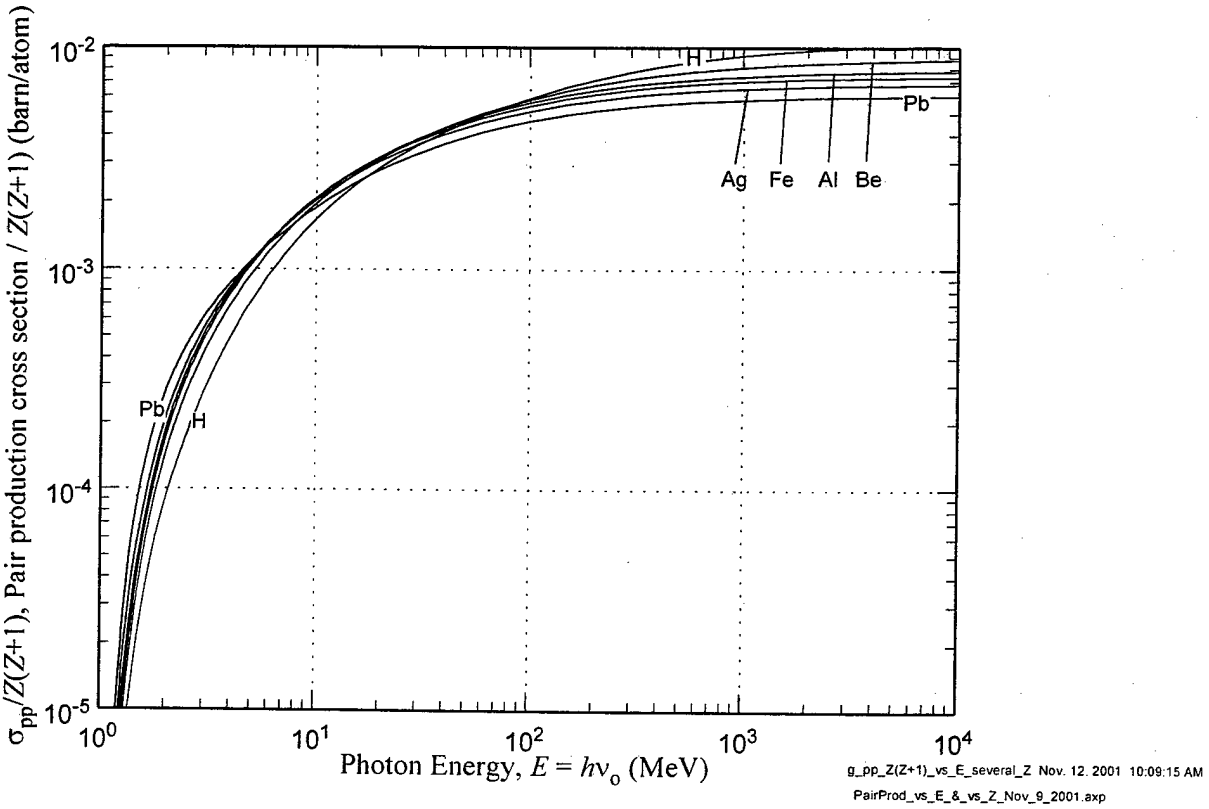

Figure 2.44

The total (nuclear plus electronic) pair production cross section divided by Z(Z+1) in several elements. Cross section in barn/atom. Between the lightest and heaviest elements, at high energies, the cross section departs from proportionality to Z(Z+1) by about a factor of 2. Data from EPDL97.

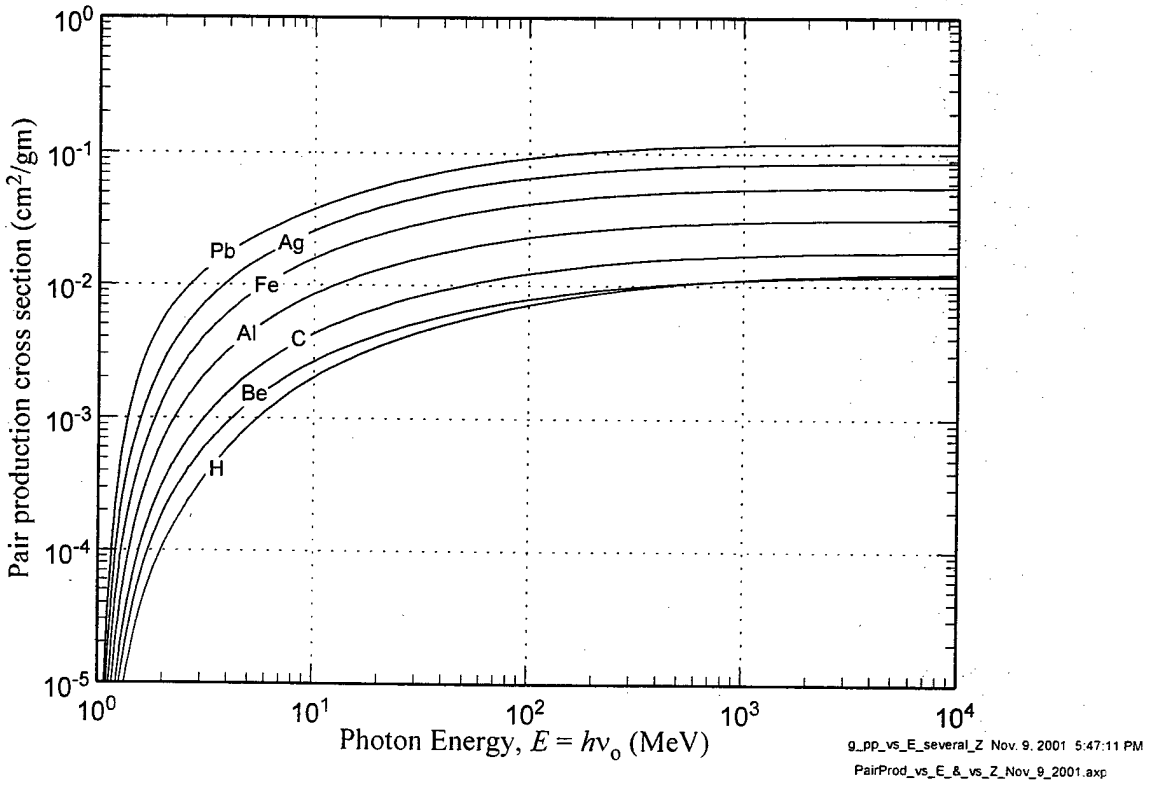

Figure 2.45 . Total (nuclear plus electronic) pair production cross section for selected elements *vs* incident photon energy, in cm^2/gm.

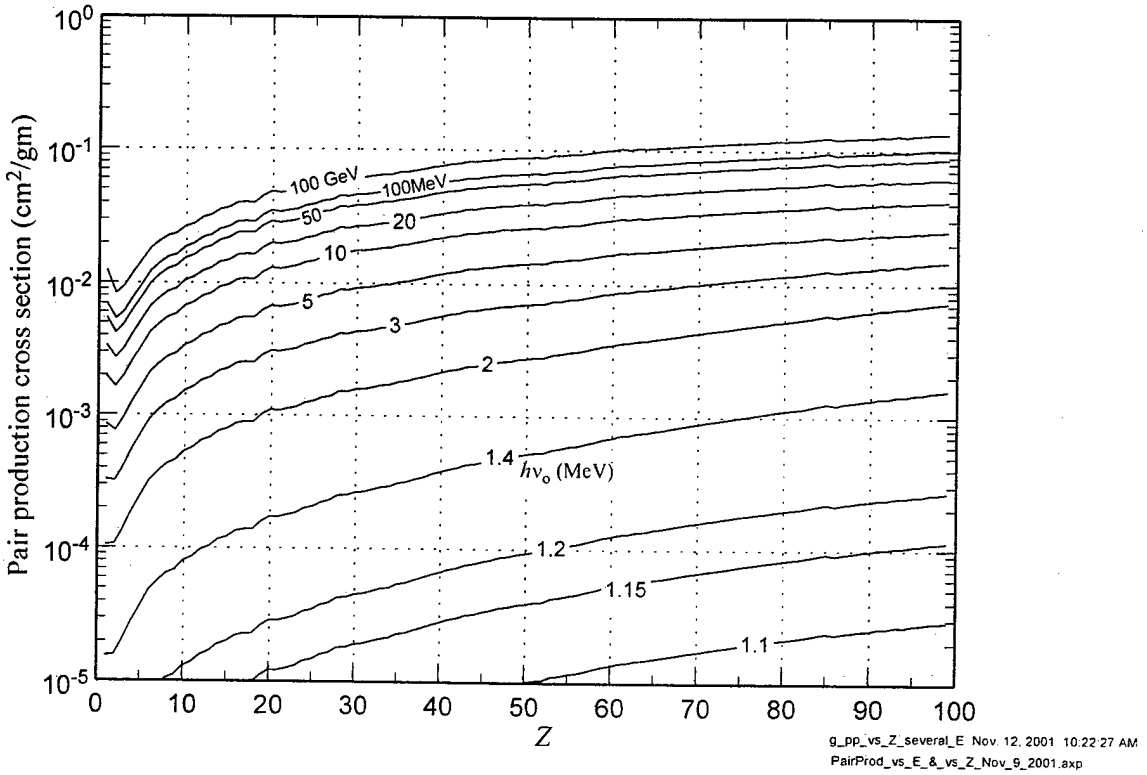

Figure 2.46 . Total (nuclear plus electronic) pair production cross section for selected incident photon energies *vs* Z, in cm^2/gm.

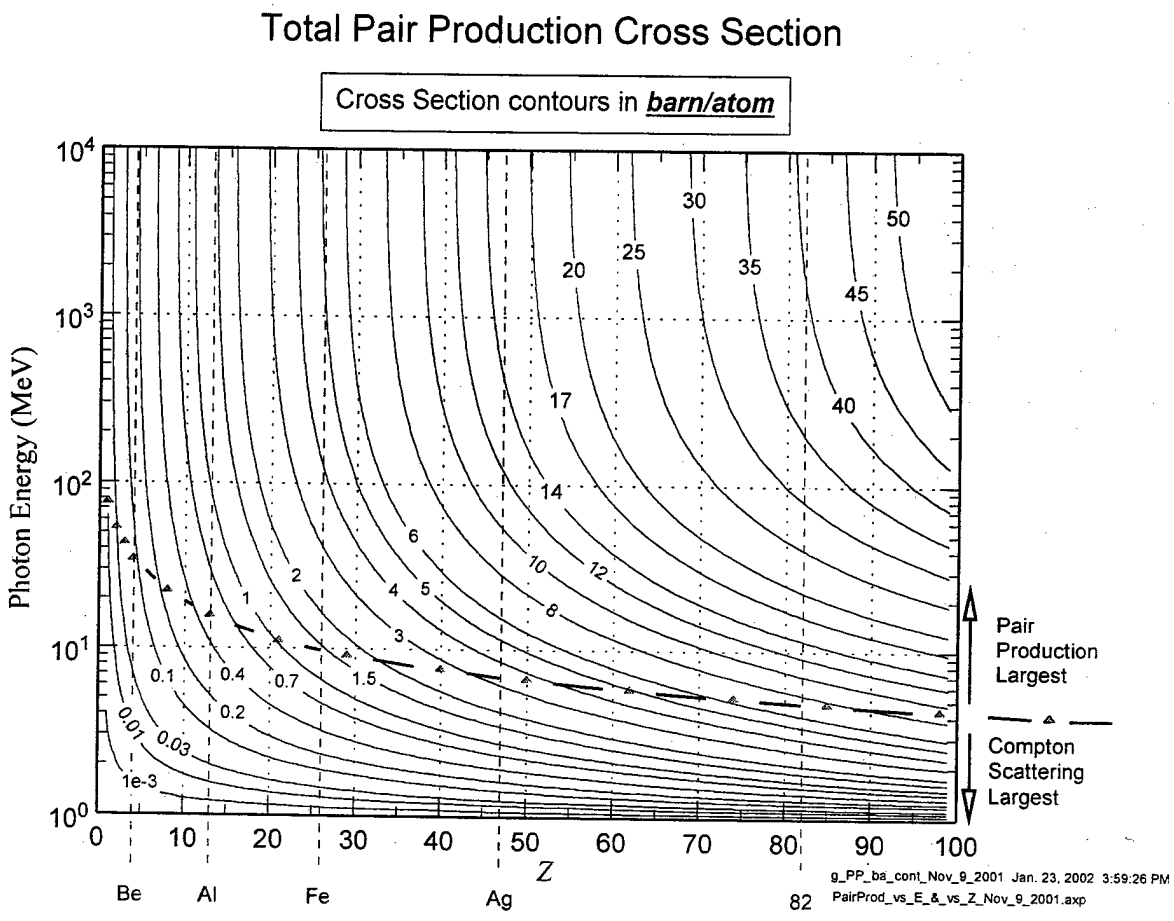

Figure 2.47 . Contours of total (nuclear plus electronic) pair production cross section vs incident photon energy and Z, in barn/atom.

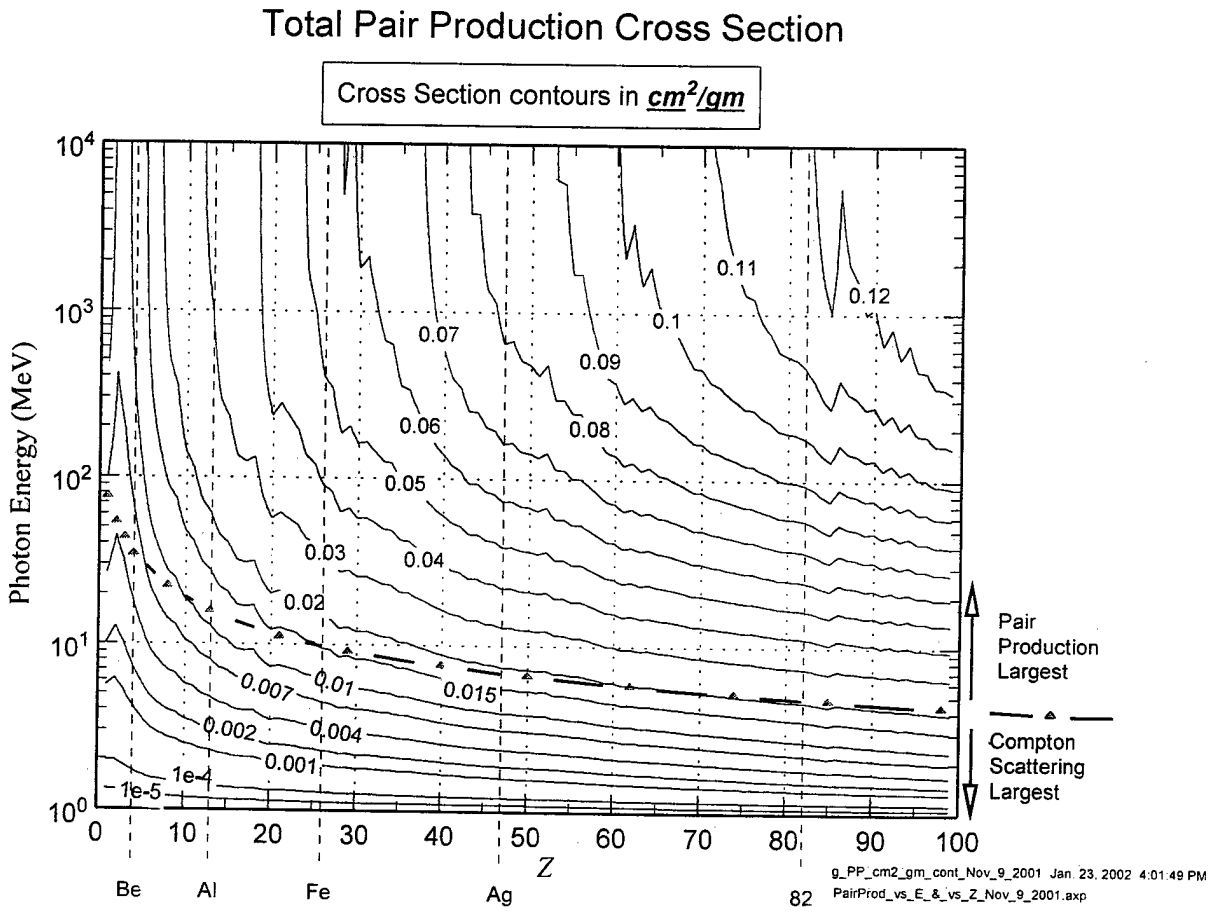

Figure 2.48 . Contours of total (nuclear plus electronic) pair production cross section vs incident photon energy and Z, in cm^2/gm.

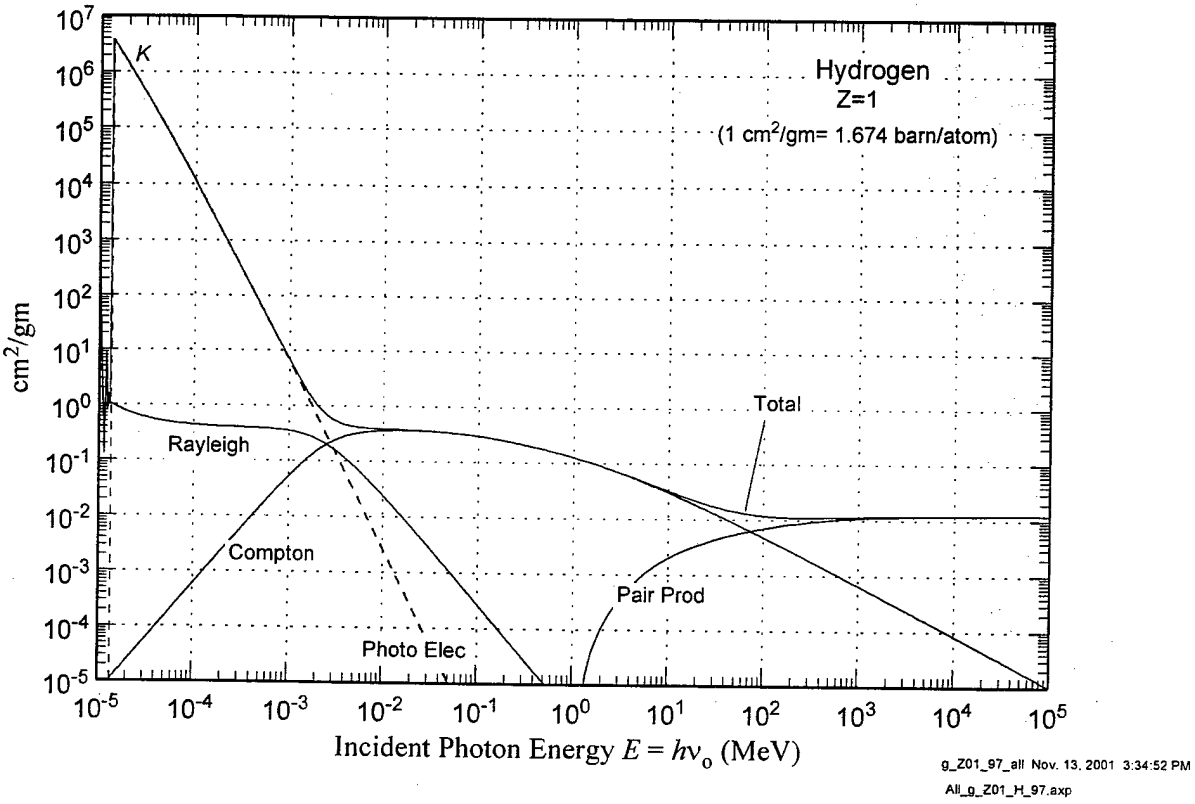

Figure 2.49 H

Photon interaction cross sections on an isolated, cold Hydrogen atom. Data from Lawrence Livermore National Laboratory Evaluated Photon Data Library (EPDL97).

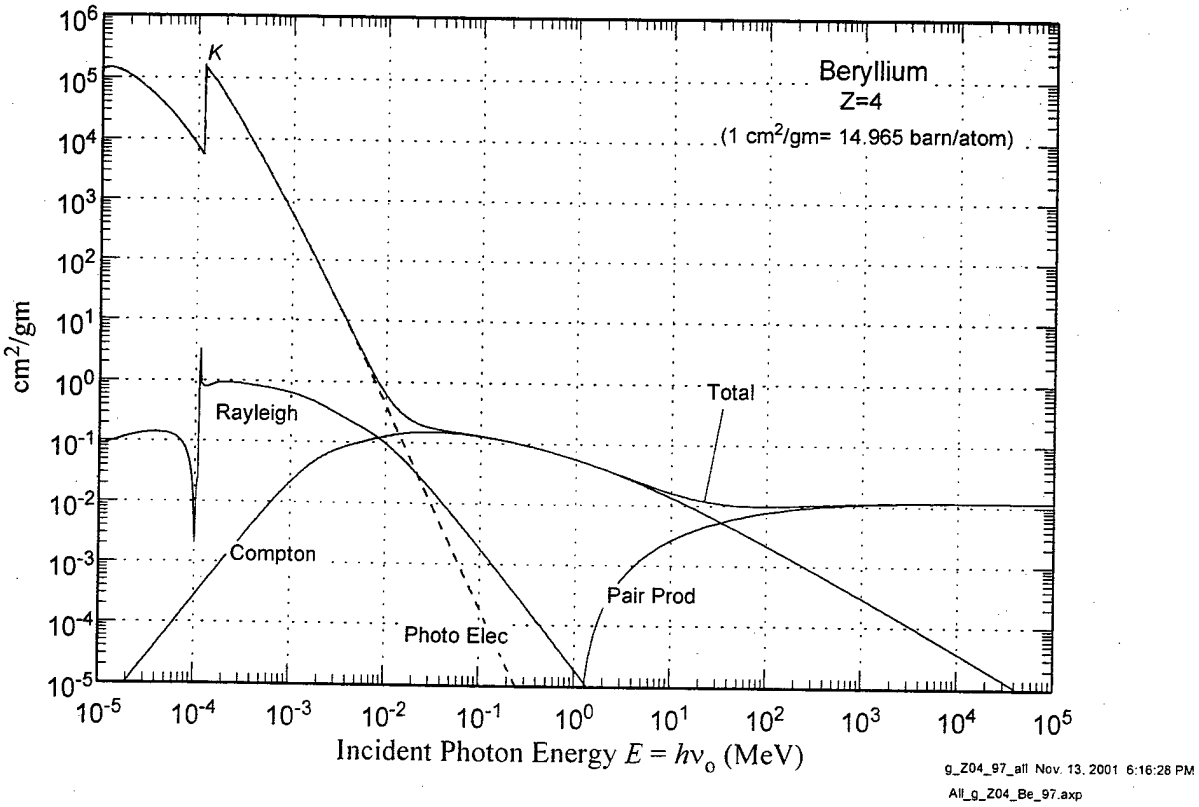

Figure 2.49 Be

Photon interaction cross sections on an isolated, cold Beryllium atom. Data from Lawrence Livermore National Laboratory Evaluated Photon Data Library (EPDL97).

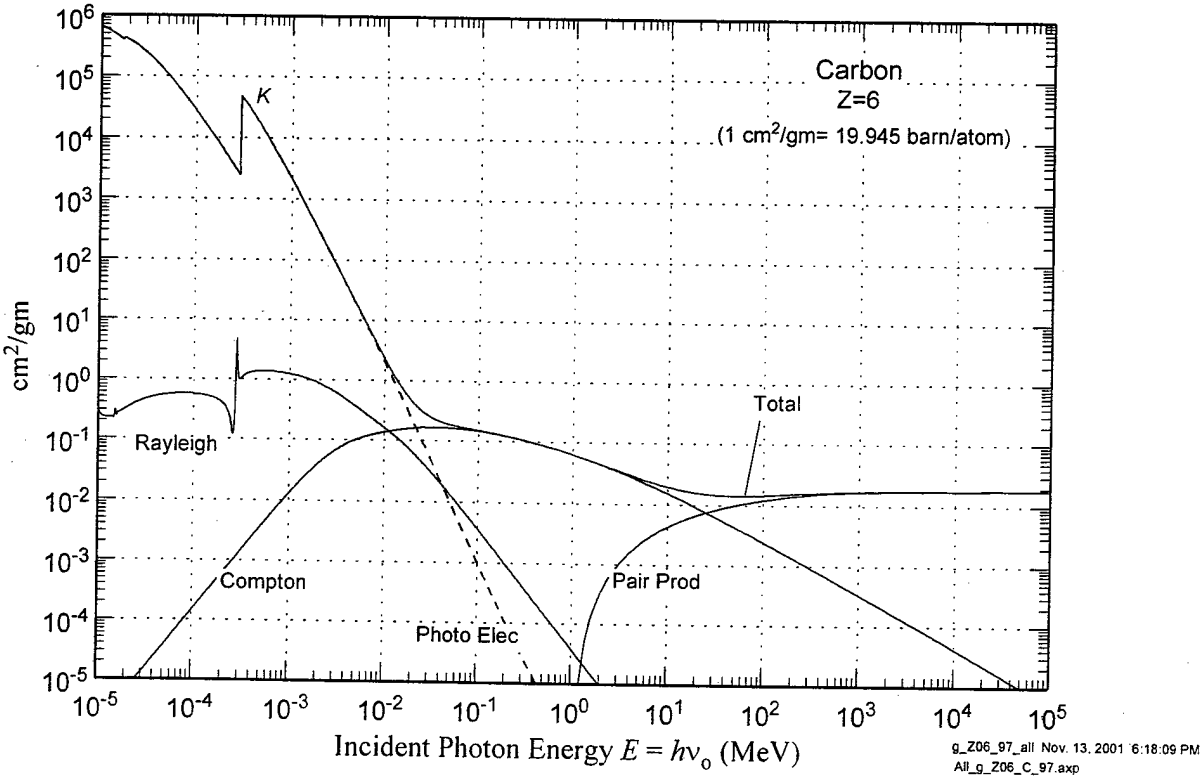

Figure 2.49 C Photon interaction cross sections on an isolated, cold Carbon atom. Data from Lawrence Livermore National Laboratory Evaluated Photon Data Library (EPDL97).

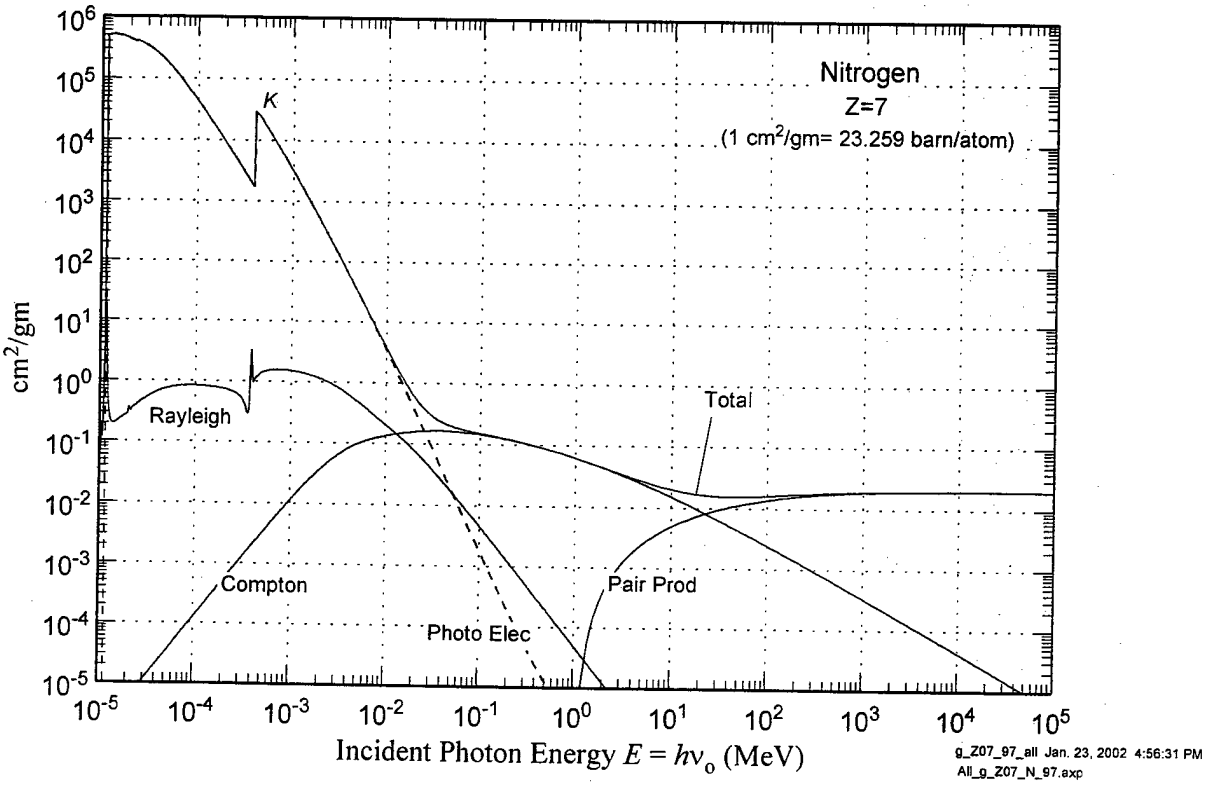

Figure 2.49N

Photon interaction cross sections on an isolated, cold Nitrogen atom. Data from Lawrence Livermore National Laboratory Evaluated Photon Data Library (EPDL97).

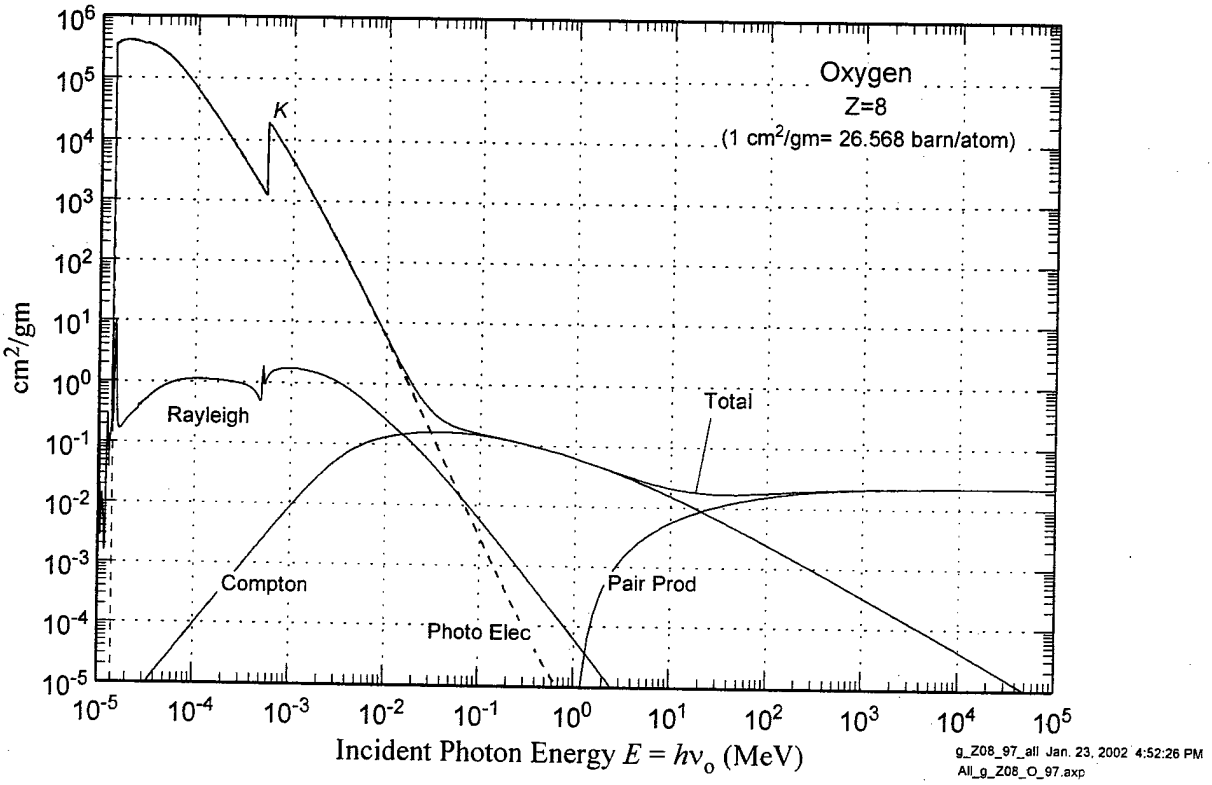

Figure 2.490 Photon interaction cross sections on an isolated, cold Oxygen atom. Data from Lawrence Livermore National Laboratory Evaluated Photon Data Library (EPDL97).

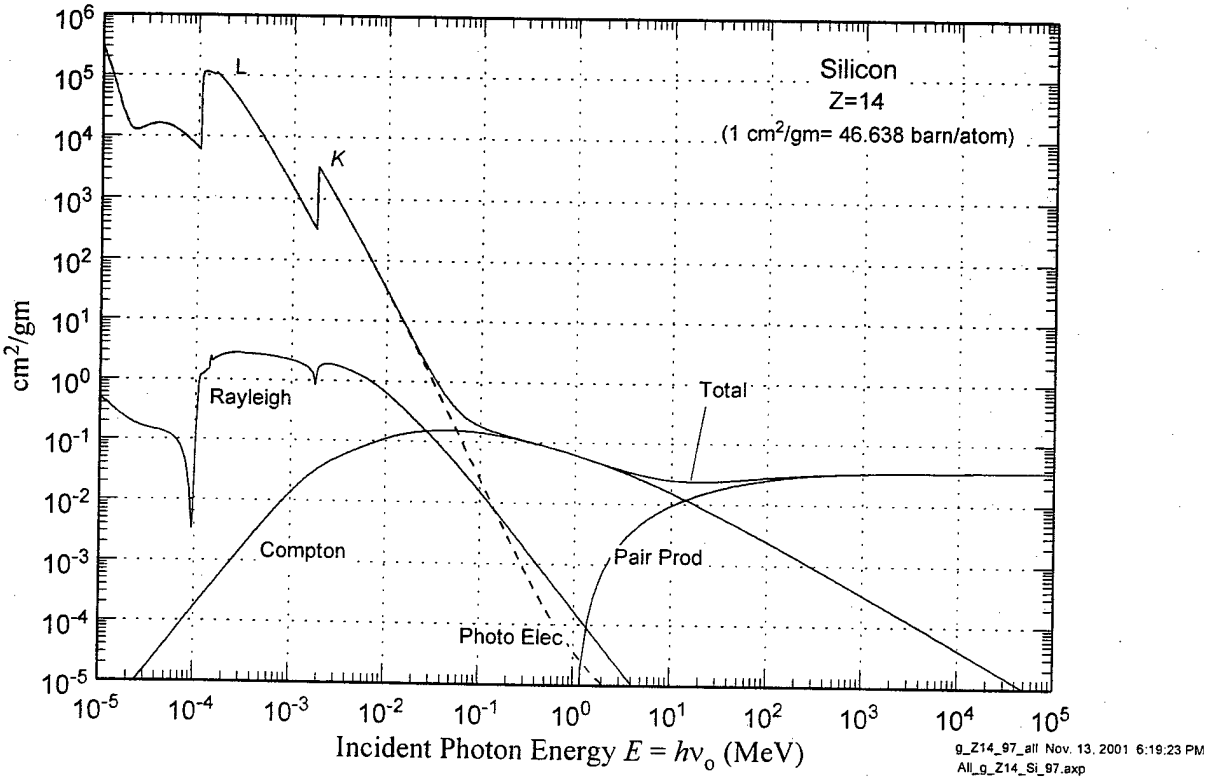

Figure 2.49 Si

Photon interaction cross sections on an isolated, cold Silicon atom. Data from Lawrence Livermore National Laboratory Evaluated Photon Data Library (EPDL97).

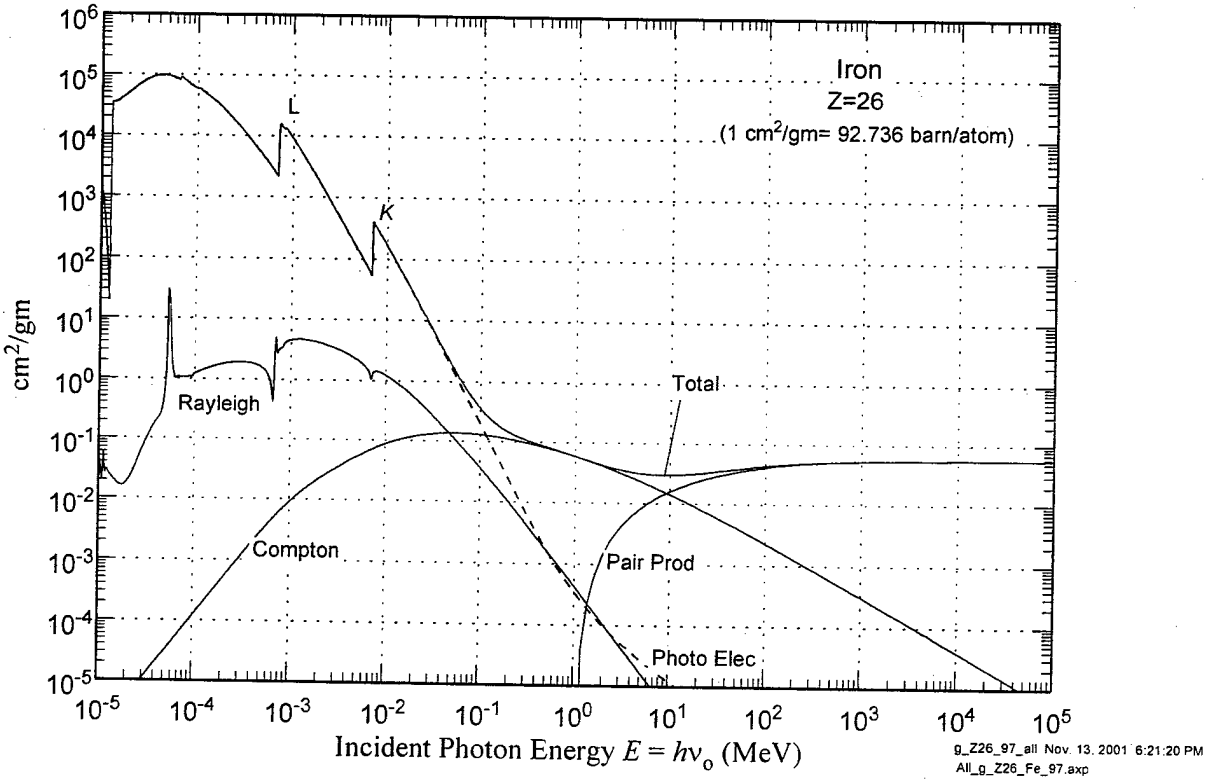

Figure 2.49 Fe

Photon interaction cross sections on an isolated, cold Iron atom. Data from Lawrence Livermore National Laboratory Evaluated Photon Data Library (EPDL97).

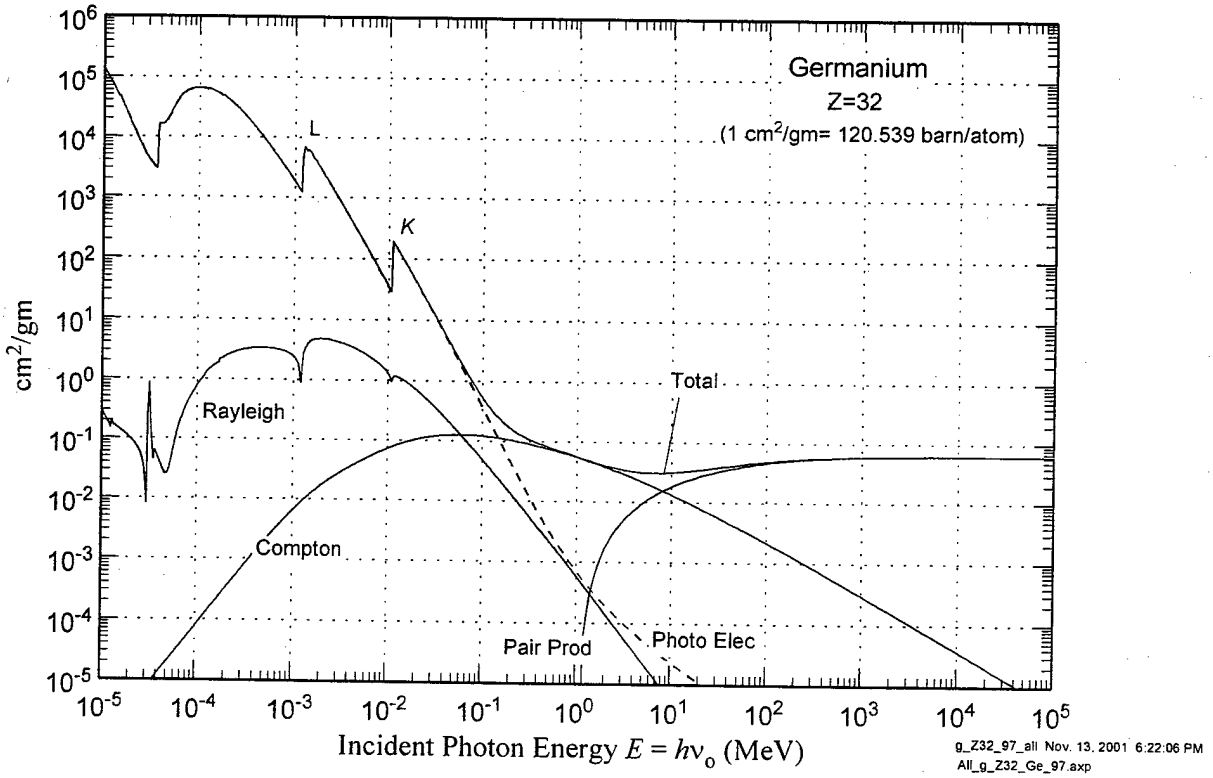

Figure 2.49 Ge

Photon interaction cross sections on an isolated, cold Germanium atom. Data from Lawrence Livermore National Laboratory Evaluated Photon Data Library (EPDL97).

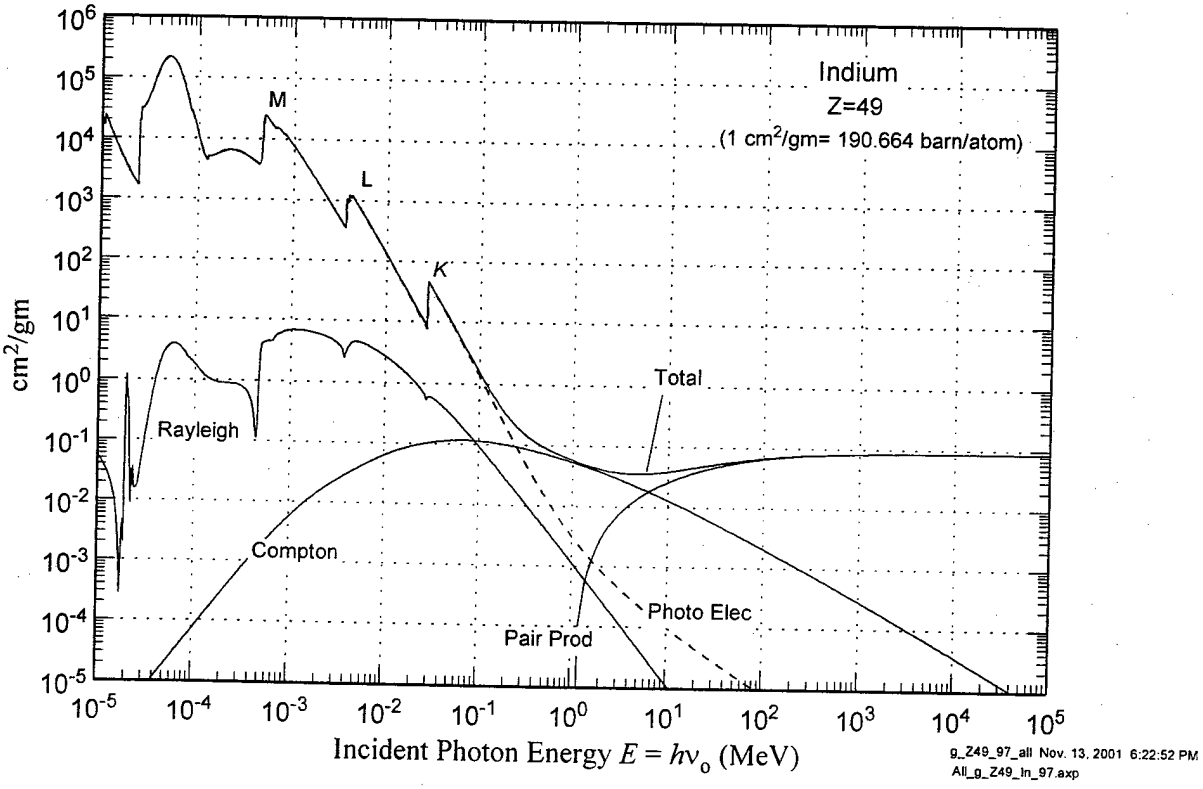

Figure 2.49 In

Photon interaction cross sections on an isolated, cold Indium atom. Data from Lawrence Livermore National Laboratory Evaluated Photon Data Library (EPDL97).

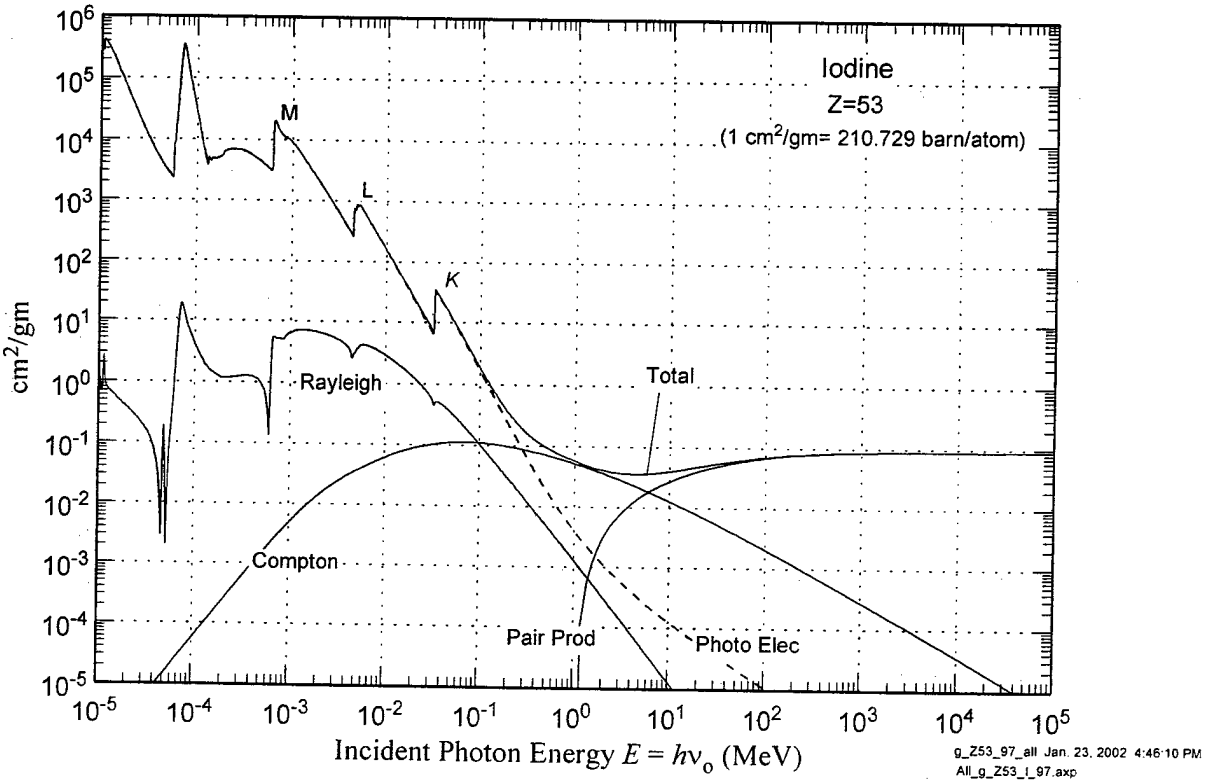

Figure 2.49 I — Photon interaction cross sections on an isolated, cold Iodine atom. Data from Lawrence Livermore National Laboratory Evaluated Photon Data Library (EPDL97).

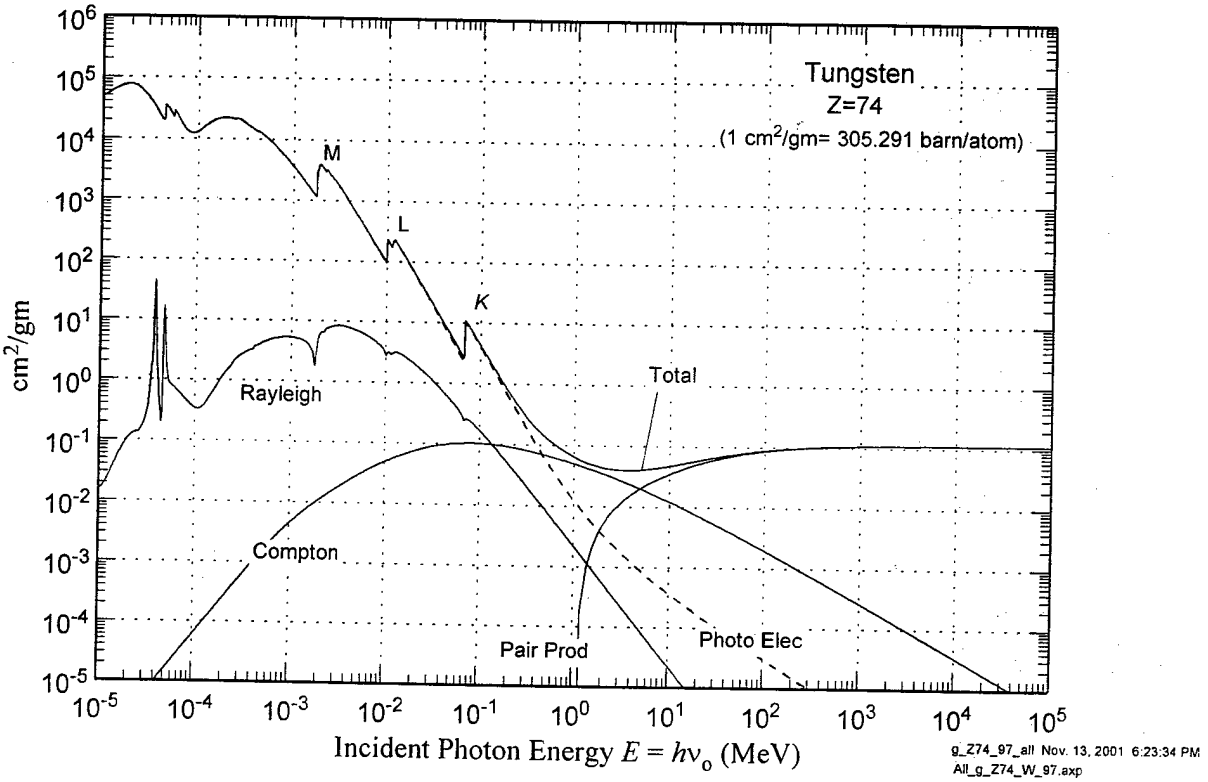

Figure 2.49 W Photon interaction cross sections on an isolated, cold Tungsten atom. Data from Lawrence Livermore National Laboratory Evaluated Photon Data Library (EPDL97).

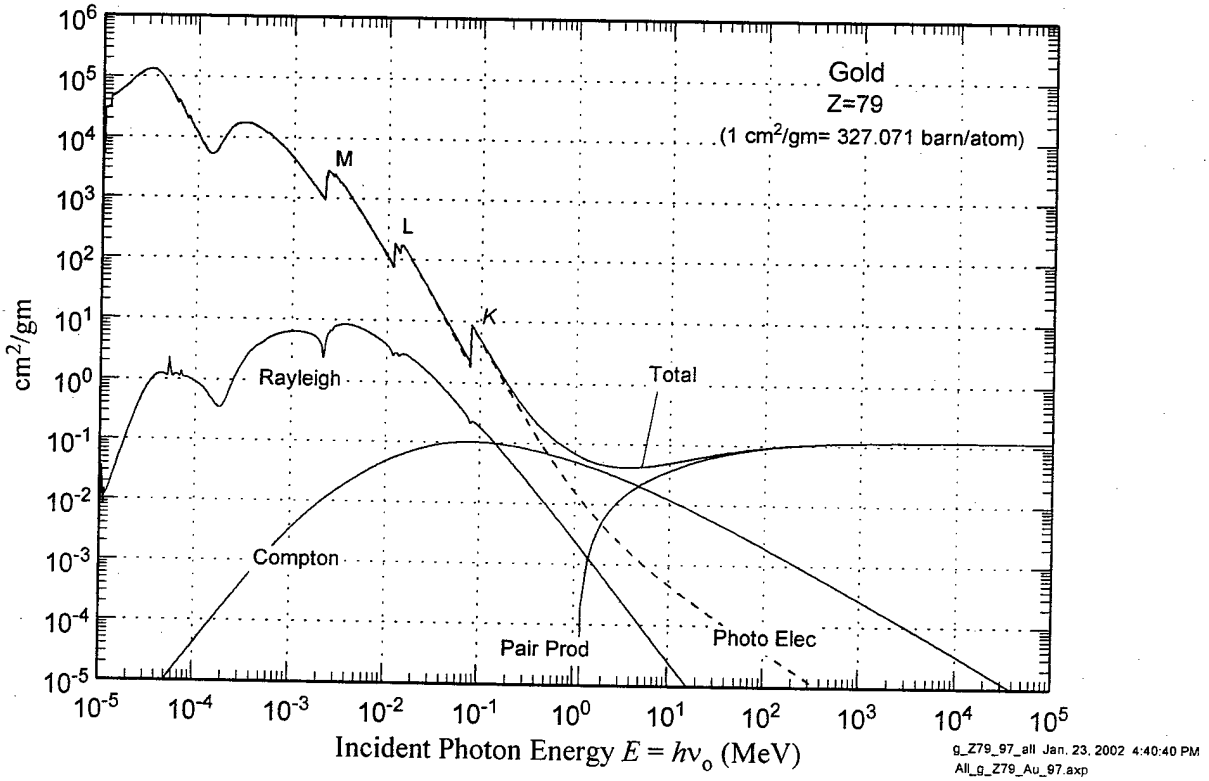

Figure 2.49 Au

Photon interaction cross sections on an isolated, cold Gold atom. Data from Lawrence Livermore National Laboratory Evaluated Photon Data Library (EPDL97).

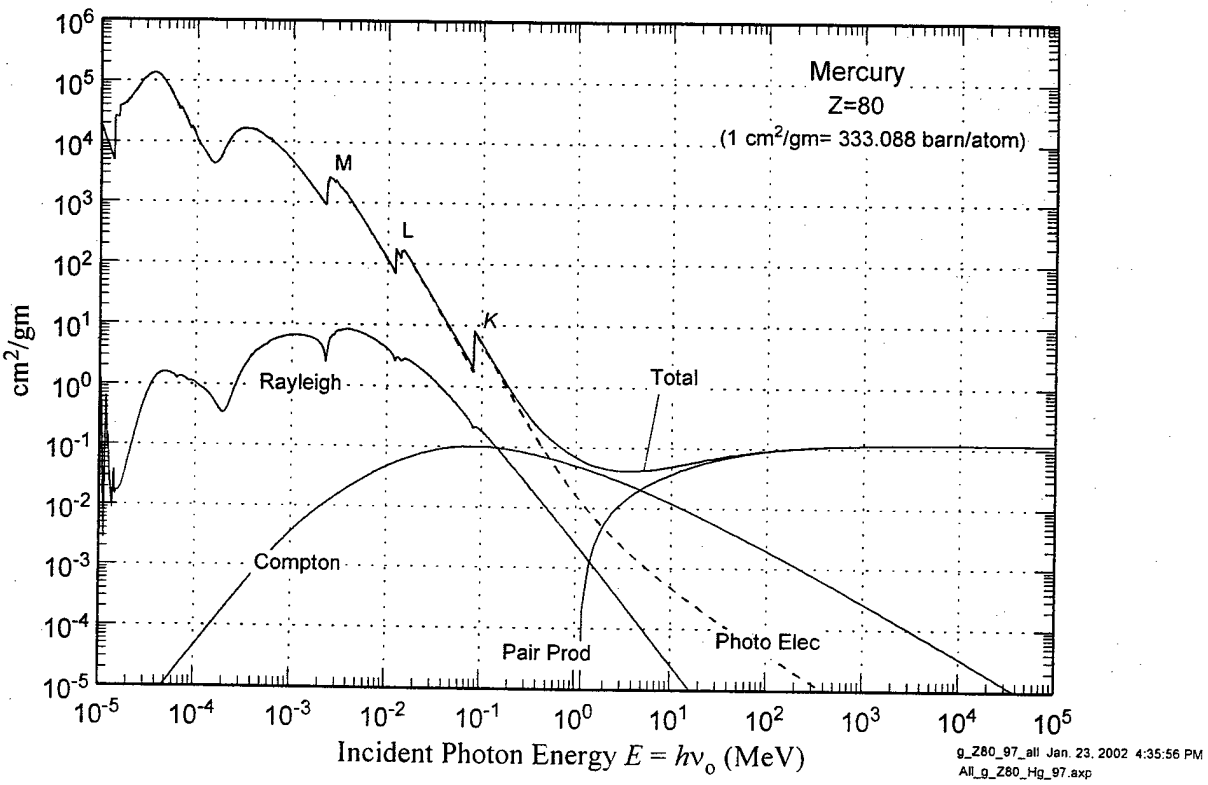

Figure 2.49 Hg — Photon interaction cross sections on an isolated, cold Mercury atom. Data from Lawrence Livermore National Laboratory Evaluated Photon Data Library (EPDL97).

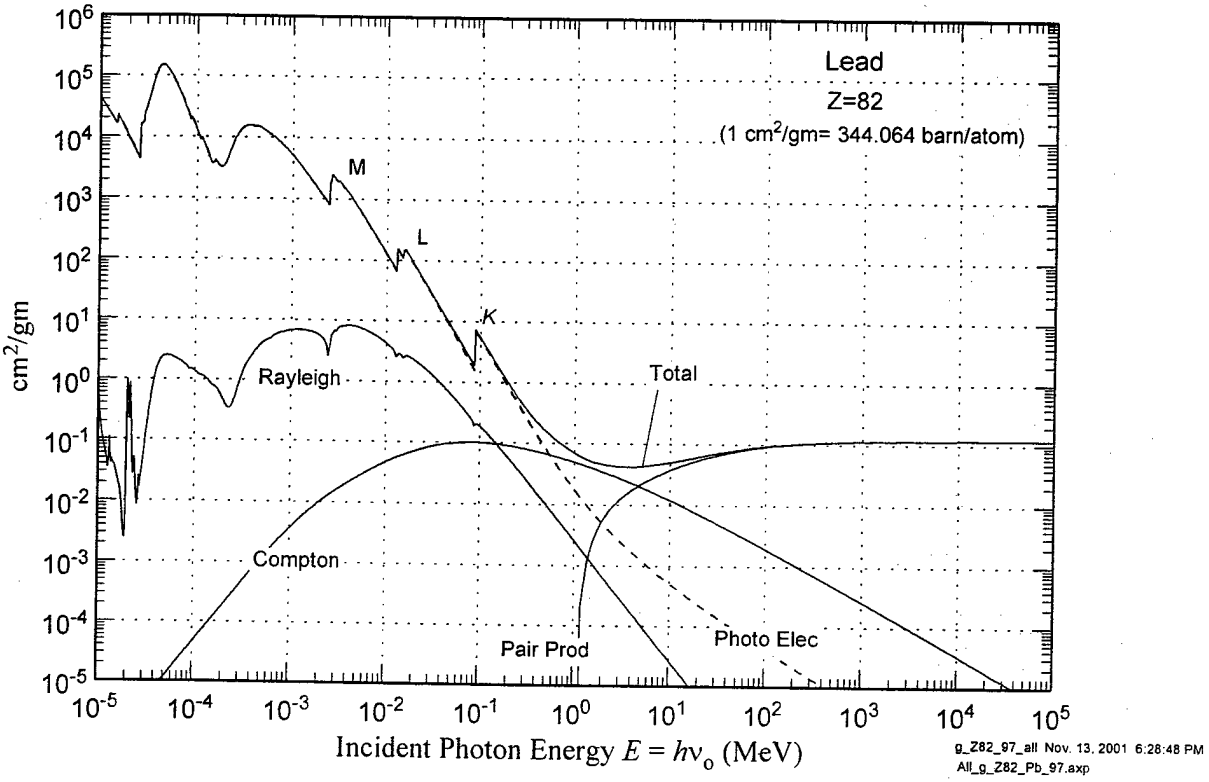

Figure 2.49 Pb

Photon interaction cross sections on an isolated, cold Lead atom. Data from Lawrence Livermore National Laboratory Evaluated Photon Data Library (EPDL97).

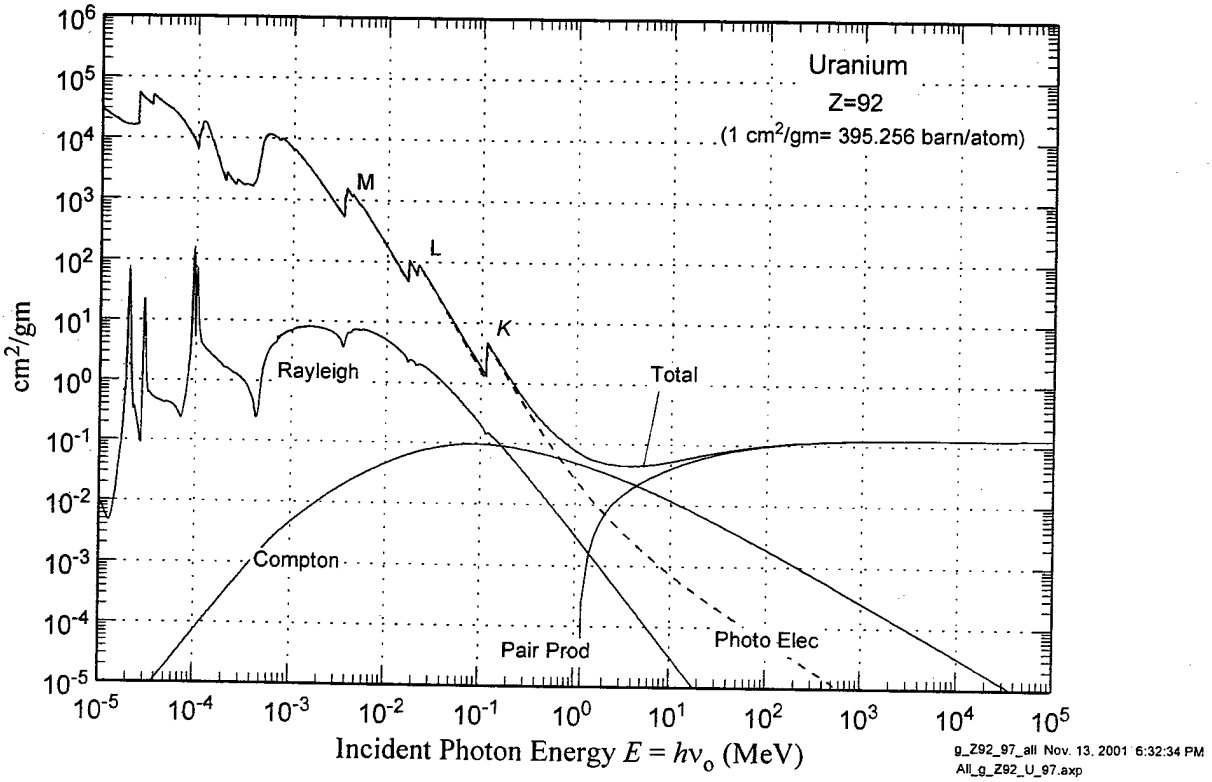

Figure 2.49 U — Photon interaction cross sections on an isolated, cold Uranium atom. Data from Lawrence Livermore National Laboratory Evaluated Photon Data Library (EPDL97).

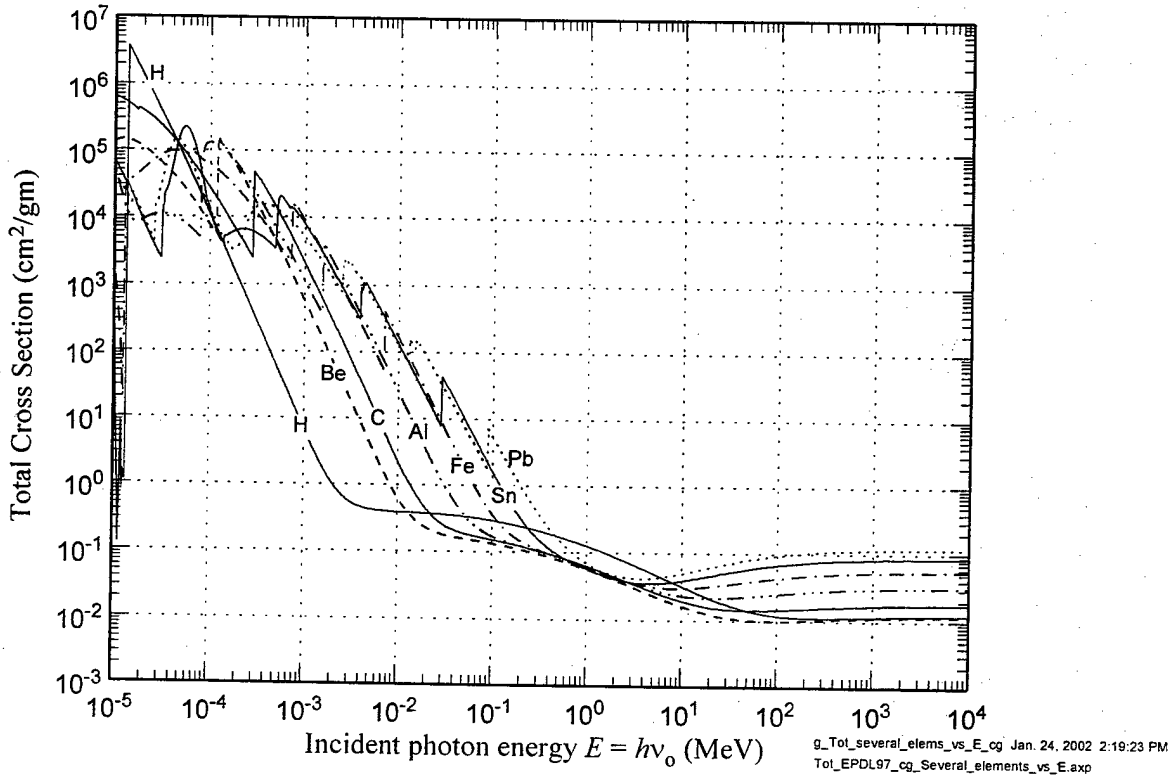

Figure 2.50 Total Photon Interaction cross section (including coherent) on several elements, cm^2/gm. Data from EPDL97.

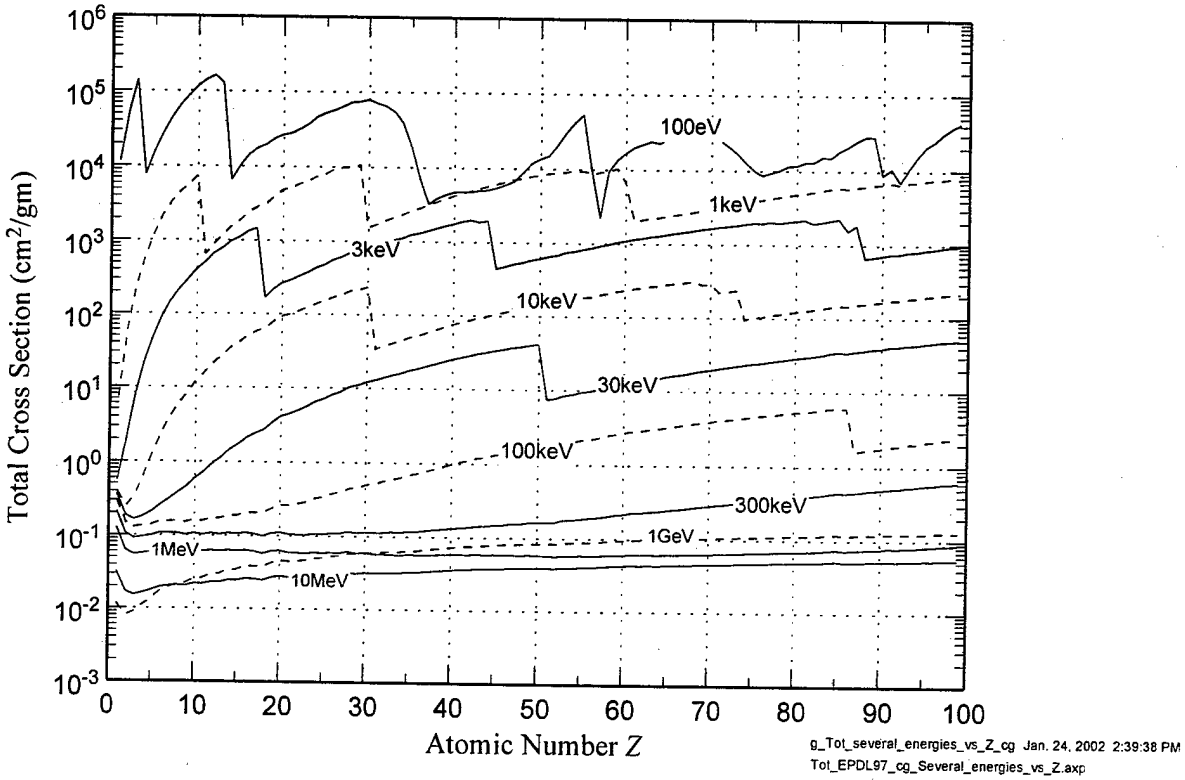

Figure 2.51 Total Photon Interaction cross section (including coherent) at several energies on all elements. cm^2/gm. Data from EPDL97.

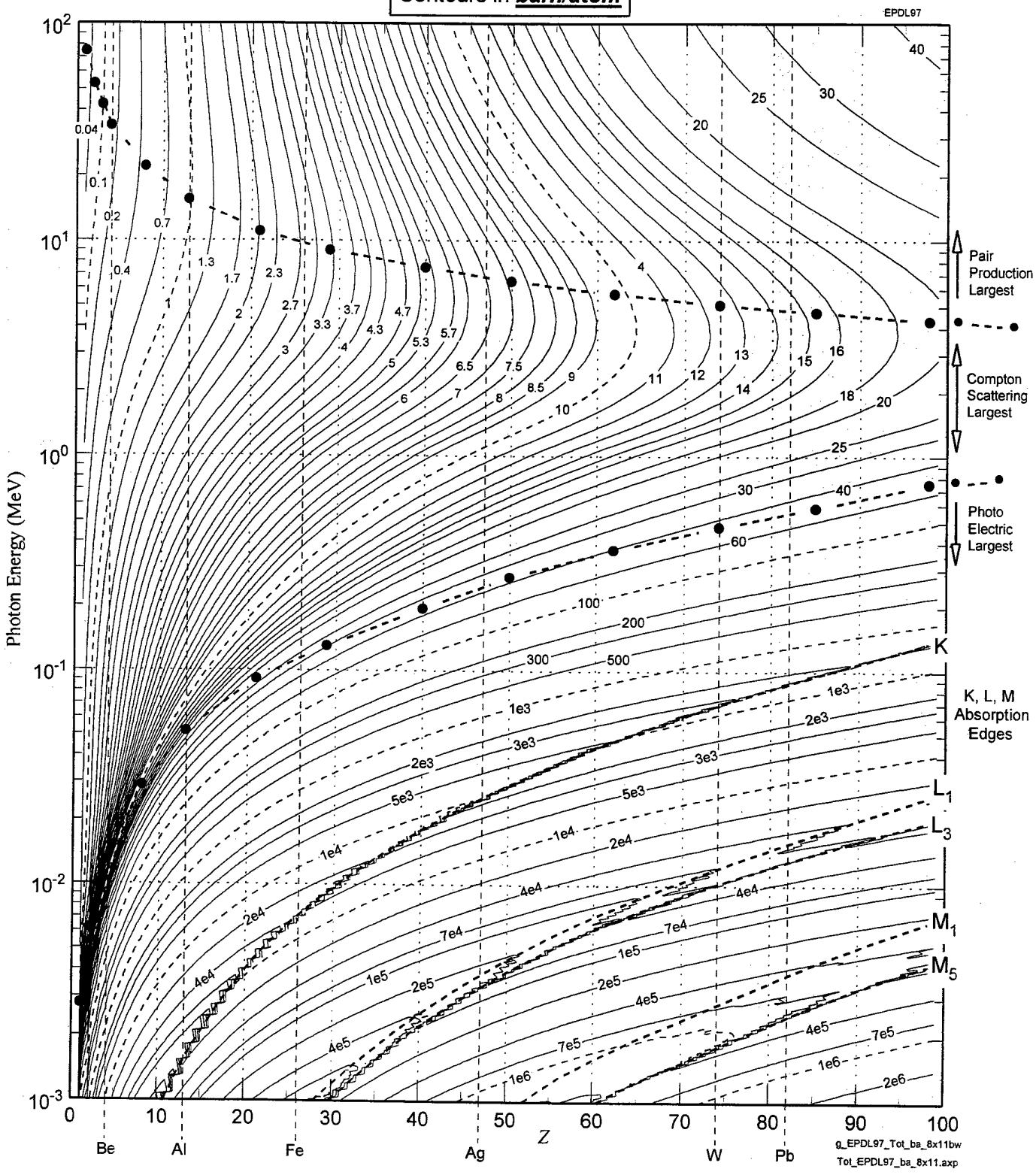

Figure Contours of total photon cross section in all elements, from $E \equiv h\nu_0 = 1$ keV to 100 MeV. In barn/atom. Data from LLNL EPDL97.

2.52

Total Photon Interaction Cross Section (including coherent)

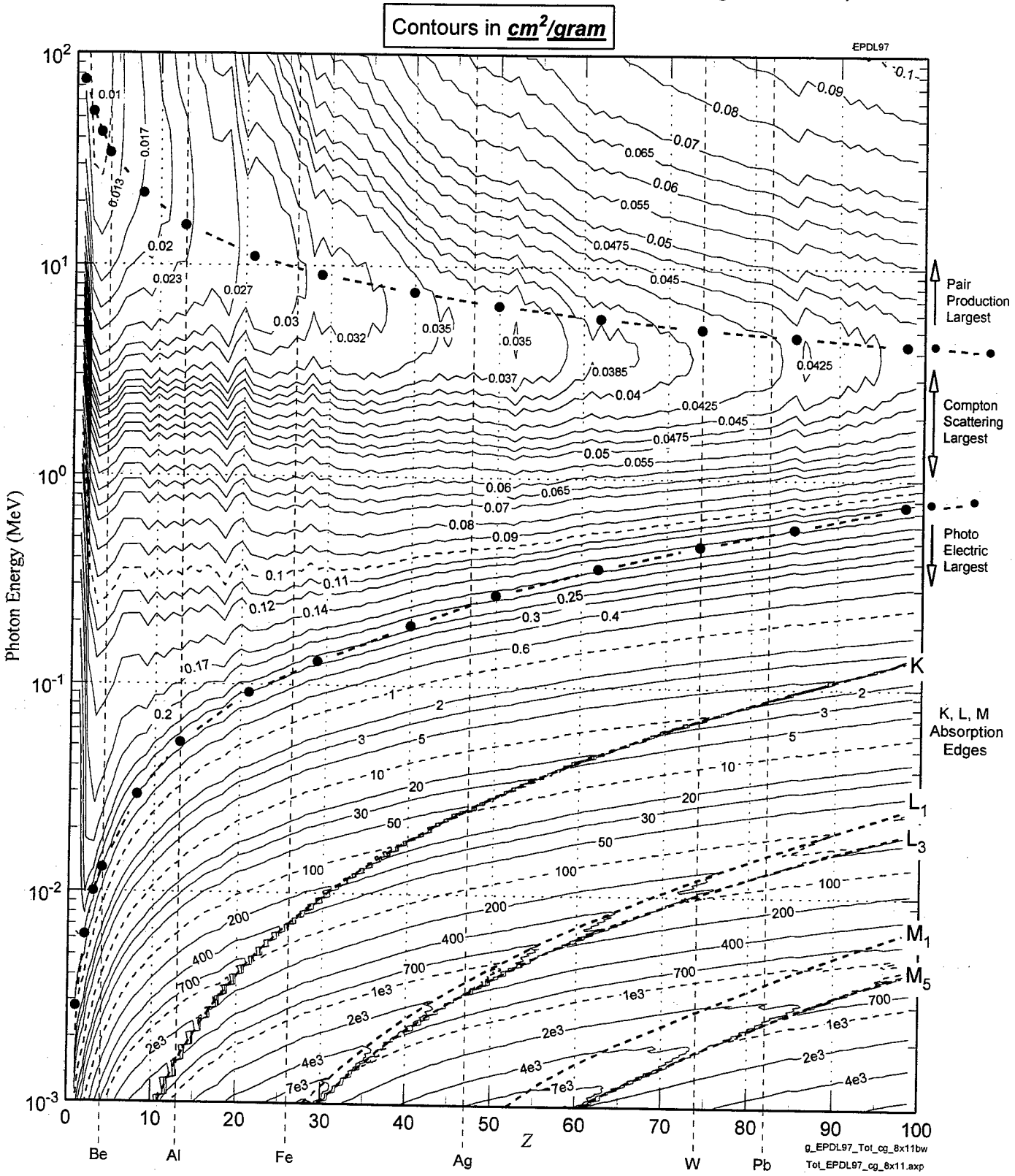

Contours of total photon cross section in all elements, from $E \equiv h\nu_0 = 1$ keV to 100 MeV. In cm^2/gram. Data from LLNL EPDL97.

Photon Mean-Free-Path Against Total Scattering (including coherent)

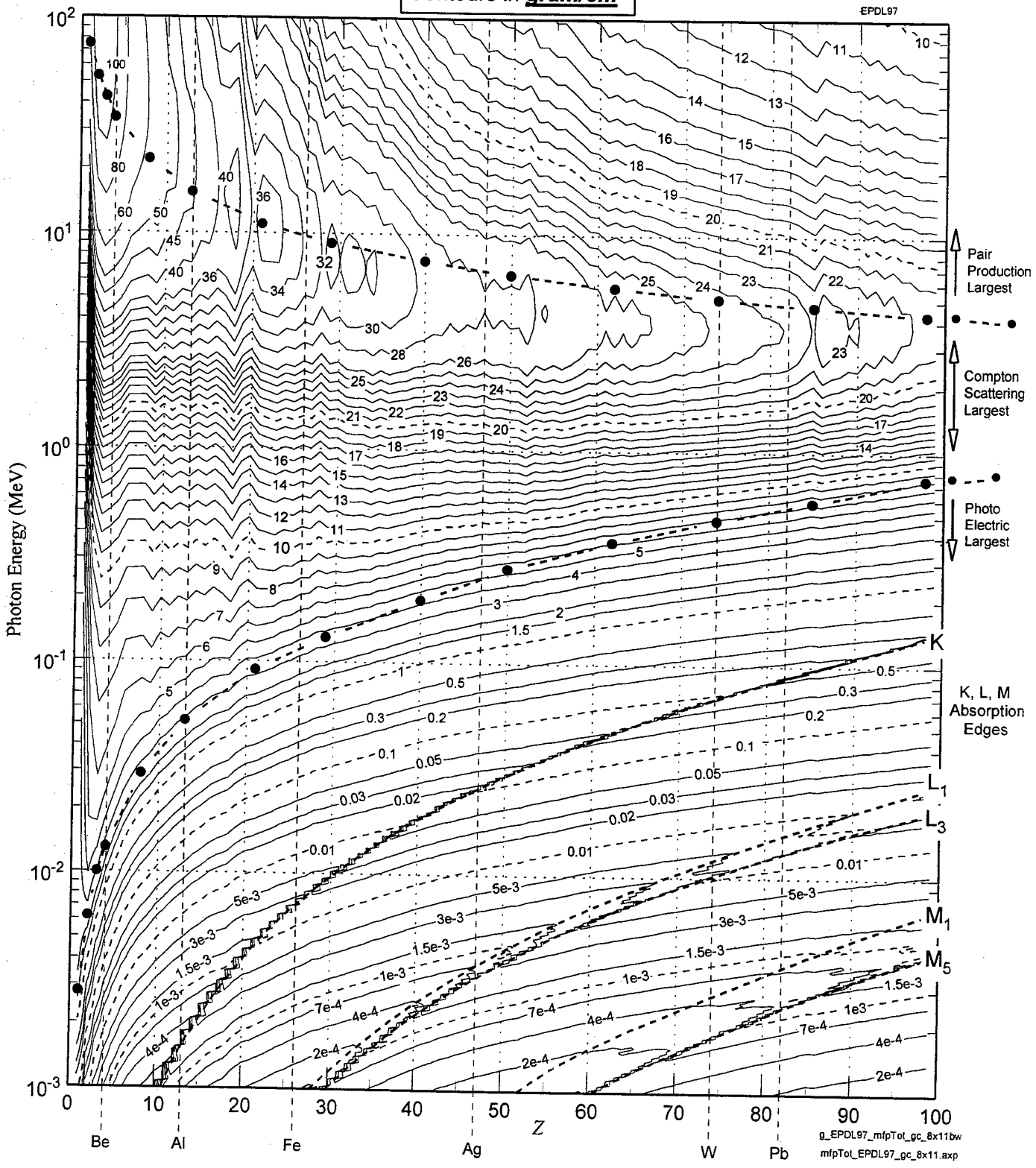

Contours of photon mean free path against total scattering in all elements, from $E \equiv h\nu_o$ = 1 keV to 100 MeV. In gram/cm^2. Data from LLNL EPDL97.

2.54

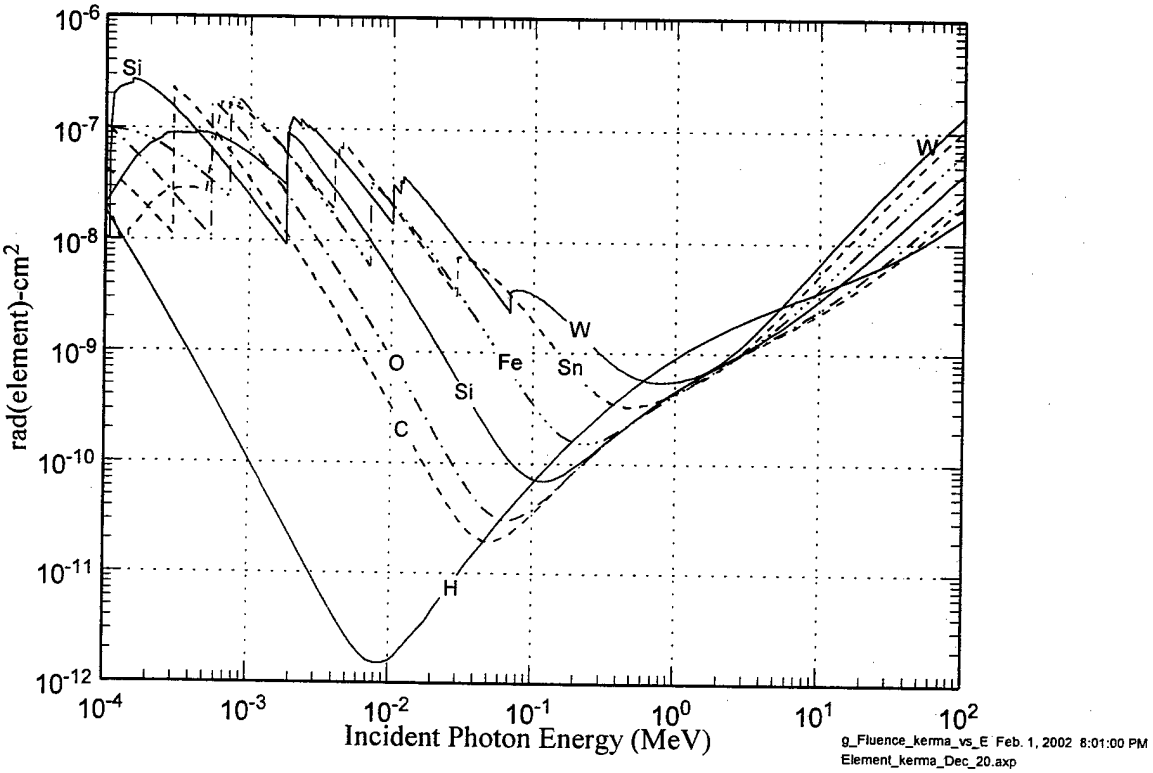

Photon number-fluence to kerma conversion factor for several elements, as a function of incident photon energy. Units are rad(element) per photon/cm^2. At 2 MeV in almost all elements except H, about 1.3E9 photons/cm^2 delivers 1 rad.

2.55

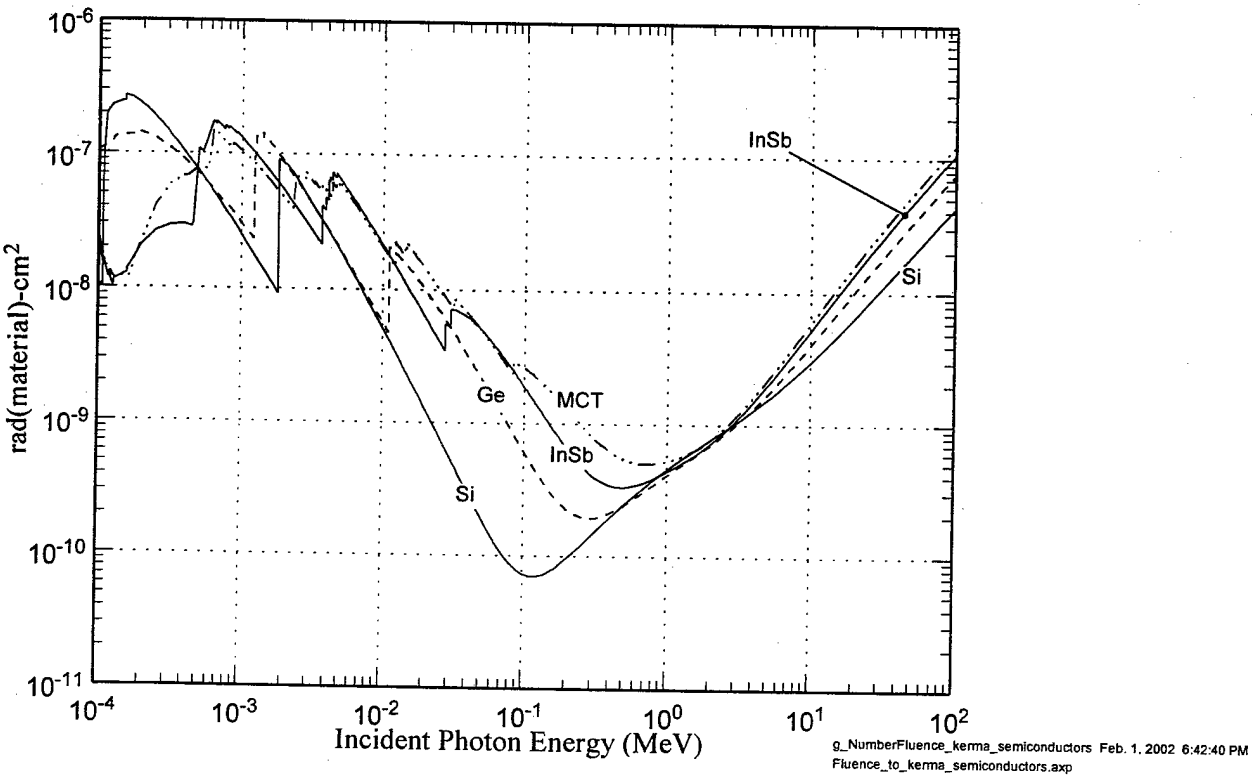

Photon number-fluence to kerma conversion factor for four semiconductor materials. Units are rad(material) per photon/cm^2. GaAs differs only slightly from Ge. MCT is $Hg_{0.8}Cd_{0.2}Te$.

2.56

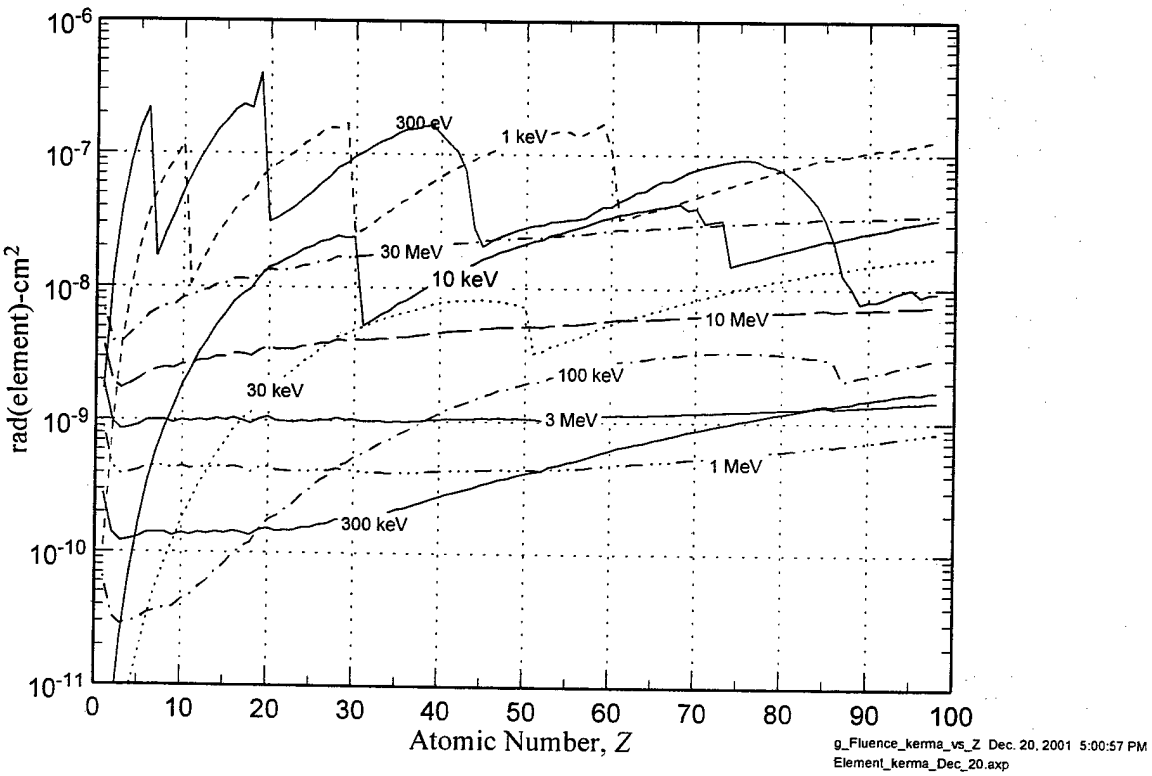

Figure 2.57 . Photon number fluence to kerma conversion factor for all elements at selected energies. Units are rad(element) per photon/cm^2.

Total Photon Fluence-to-kerma conversion factor. Z = 1-98.

Contours in ***rad(element) per 10^9 photons/cm^2***

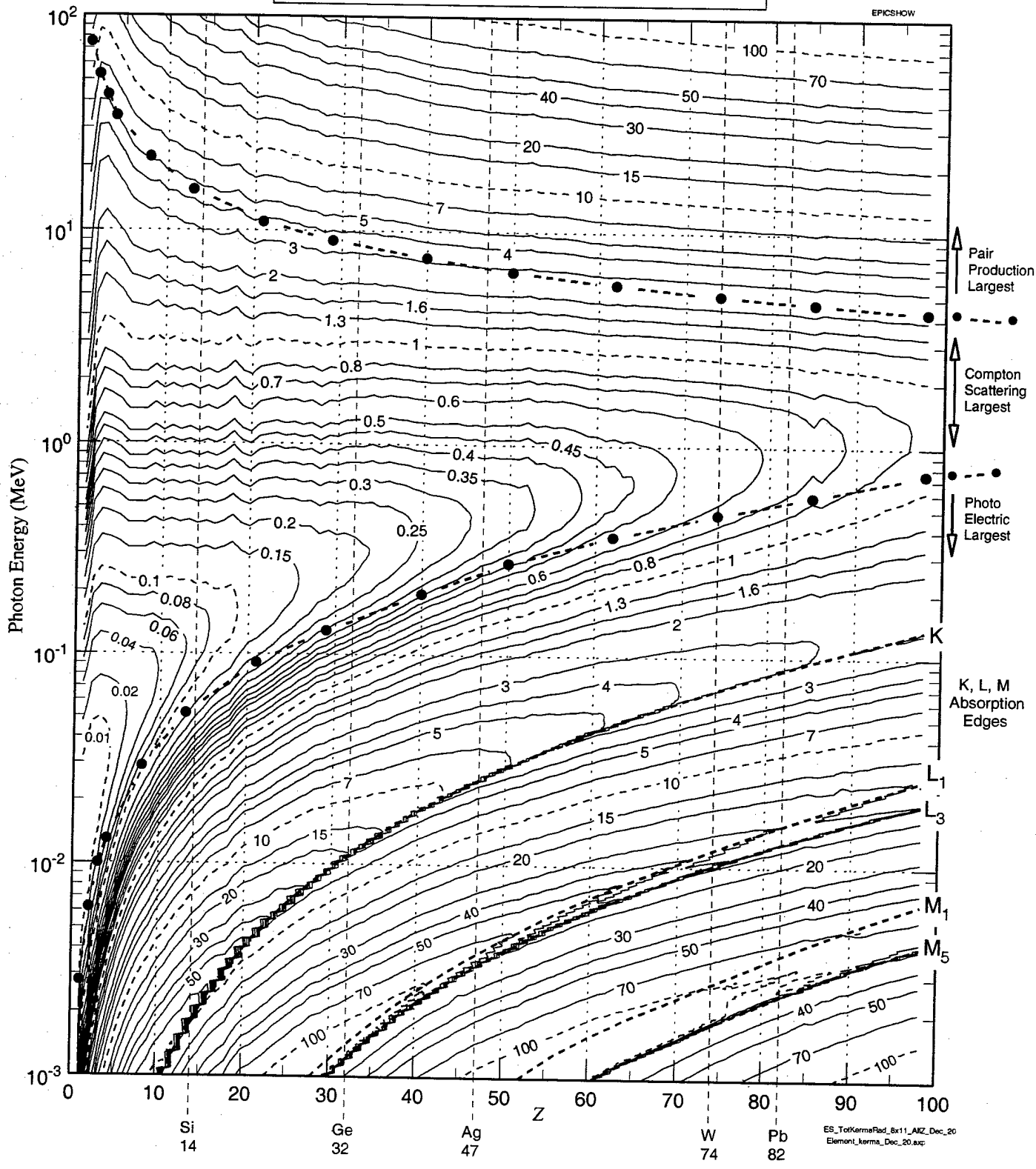

Figure 2.58 Contours of Photon number-fluence to kerma conversion factor in all elements, from $E \equiv h\nu_o$ = 1 keV to 100 MeV. In rad(element) per 10^9 photon/cm^2. 1 rad = 100 erg/gram.

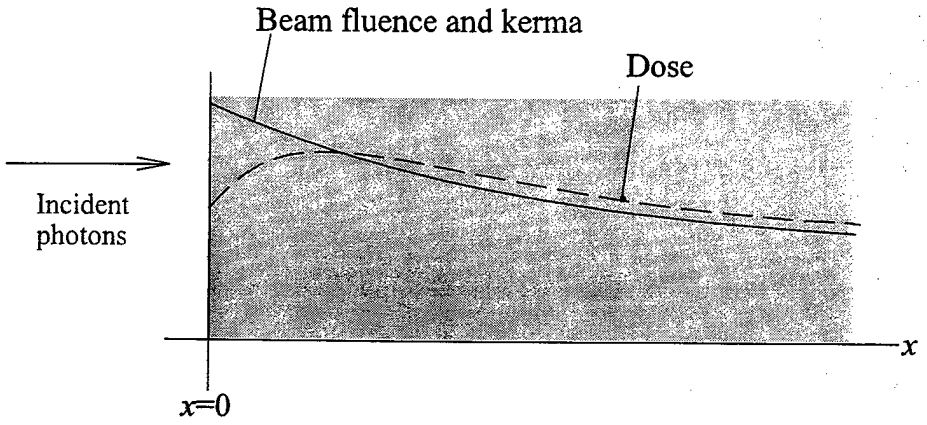

Figure 2.59 . Illustrating photon beam entering matter from vacuum. Photon fluence and kerma attenuates exponentially. Dose may build up to slightly exceed kerma. Adapted from [ICRU69].

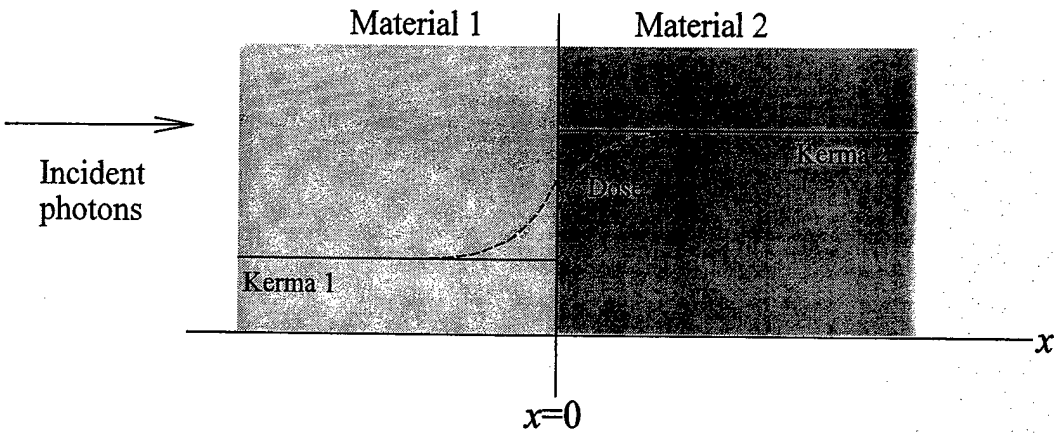

Figure 2.60 . Illustrating photon beam entering matter of two thin layers of two different materials. Photon fluence is assumed to be constant throughout. Kerma in material 1 is constant, and kerma in 2 is constant. Dose spreads out over the interface due to finite electron range and scattering. Adapted from [ICRU69].

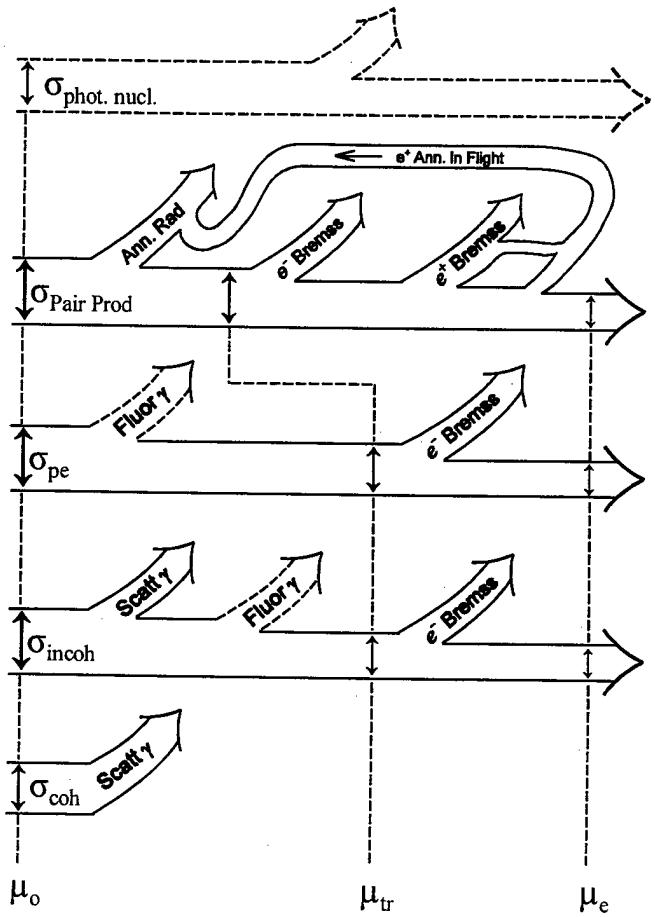

2.61

Figure ~~2.59.~~ Hubbell diagram depicting contributions by each of the five possible interactions to the attenuation coefficient μ_o, the energy transfer coefficient μ_{tr}, and the energy absorption coefficient μ_e. Energy escaping the "local" region by photons is indicated by upward going arrows. In pair production, energy lost to Bremsstrahlung from positrons is reduced because some positrons annihilate in flight. Adapted from [Hu77, Hu99b].

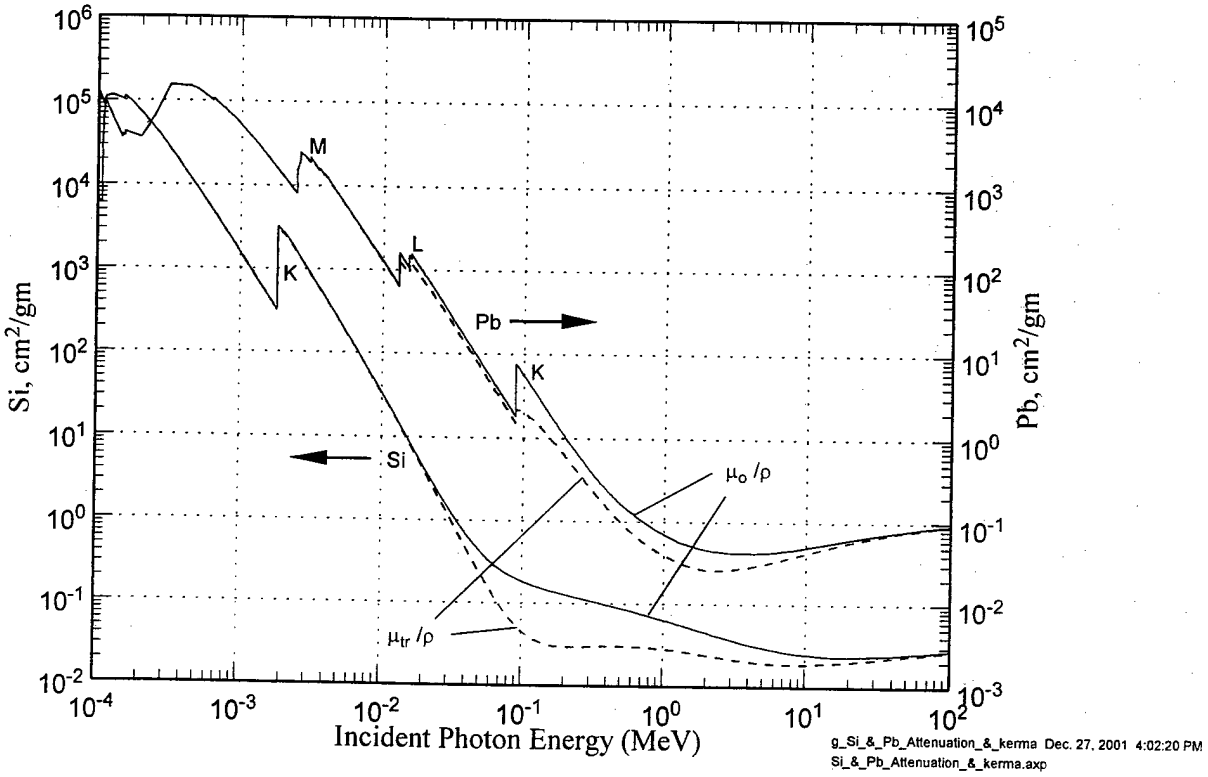

Figure 2.62 . Total attenuation coefficient, μ_o/ρ, (=total cross section per gm), and energy-transfer coefficient μ_{tr}/ρ in Si and in Pb. cm^2/gm.

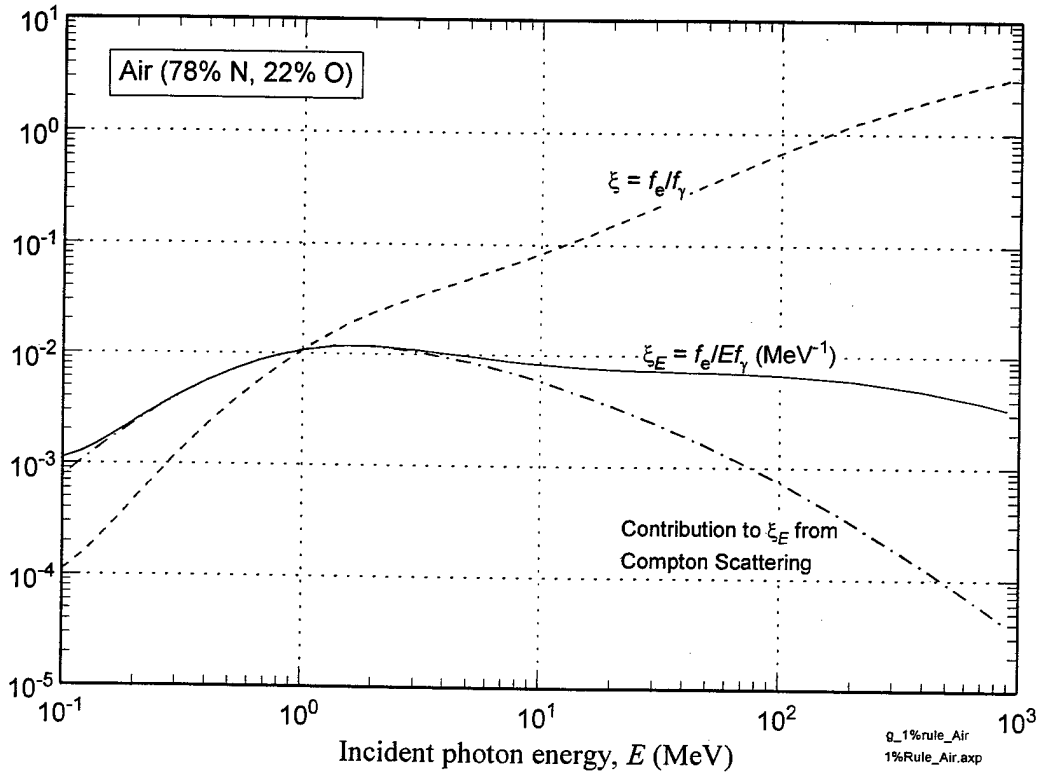

The "1% Rule" in air, the ratio of omni-directional electron and positron flux f_e [(electrons+positrons)/cm^2/sec due to photo-electric, Compton, and pair production] to photon number flux f_γ (ξ) or to photon energy flux Ef_γ (ξ_E). Assumes charged particle equilibrium.

2.63

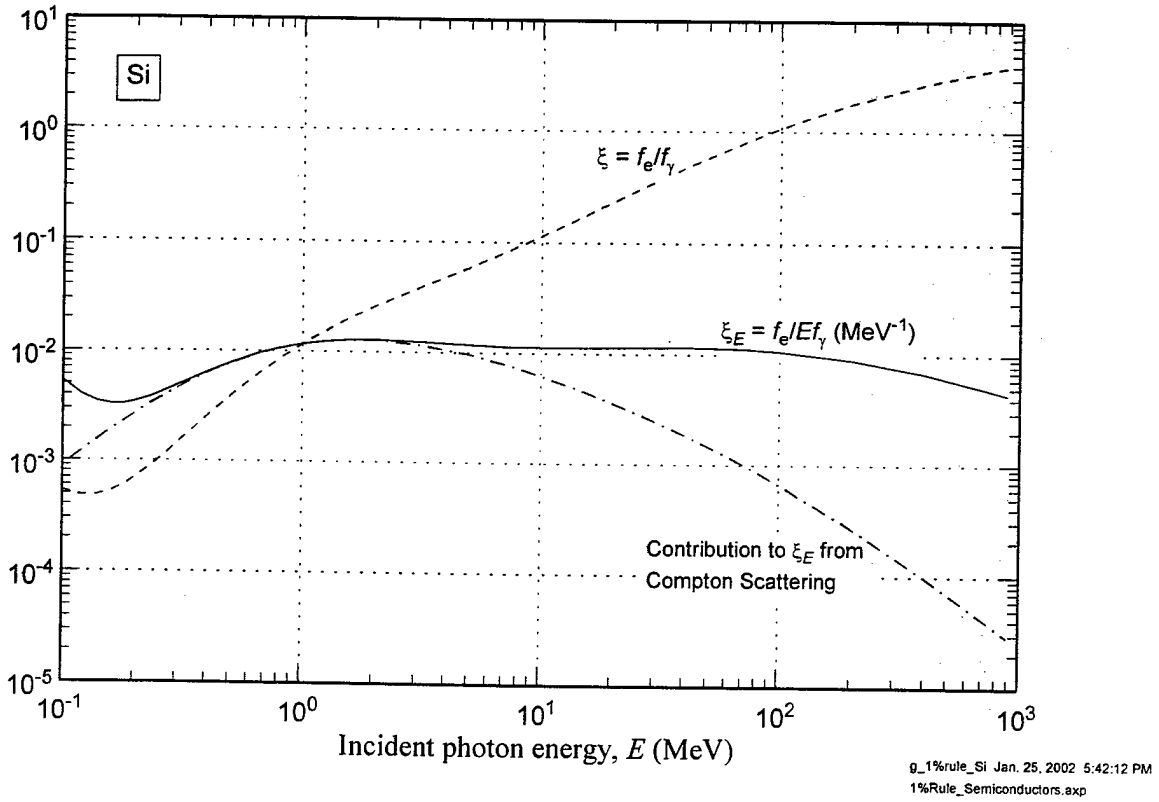

Figure 2.64 The "1% Rule" in Si. Assumes charged particle equilibrium, and includes positron flux from pair production

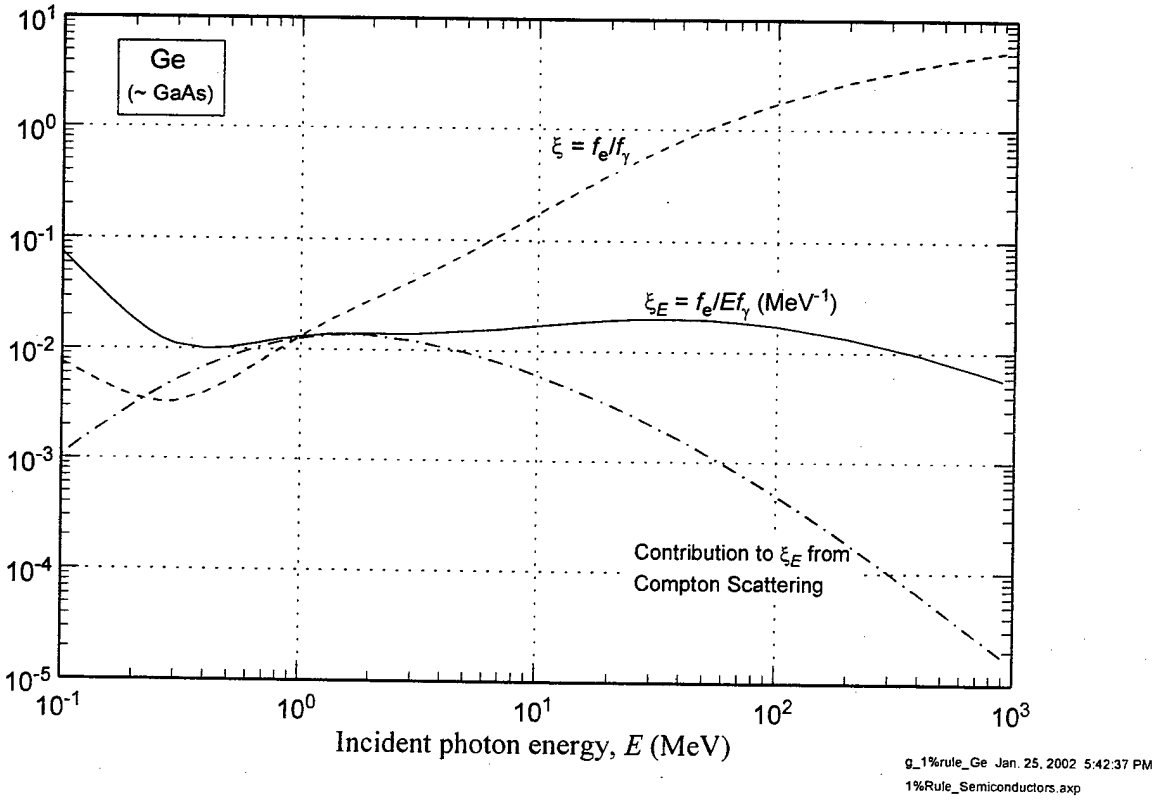

Figure 2.65

The "1% Rule" in Ge. Assumes charged particle equilibrium, and includes positron flux from pair production. GaAs is essentially the same, due to the proximity in Z.

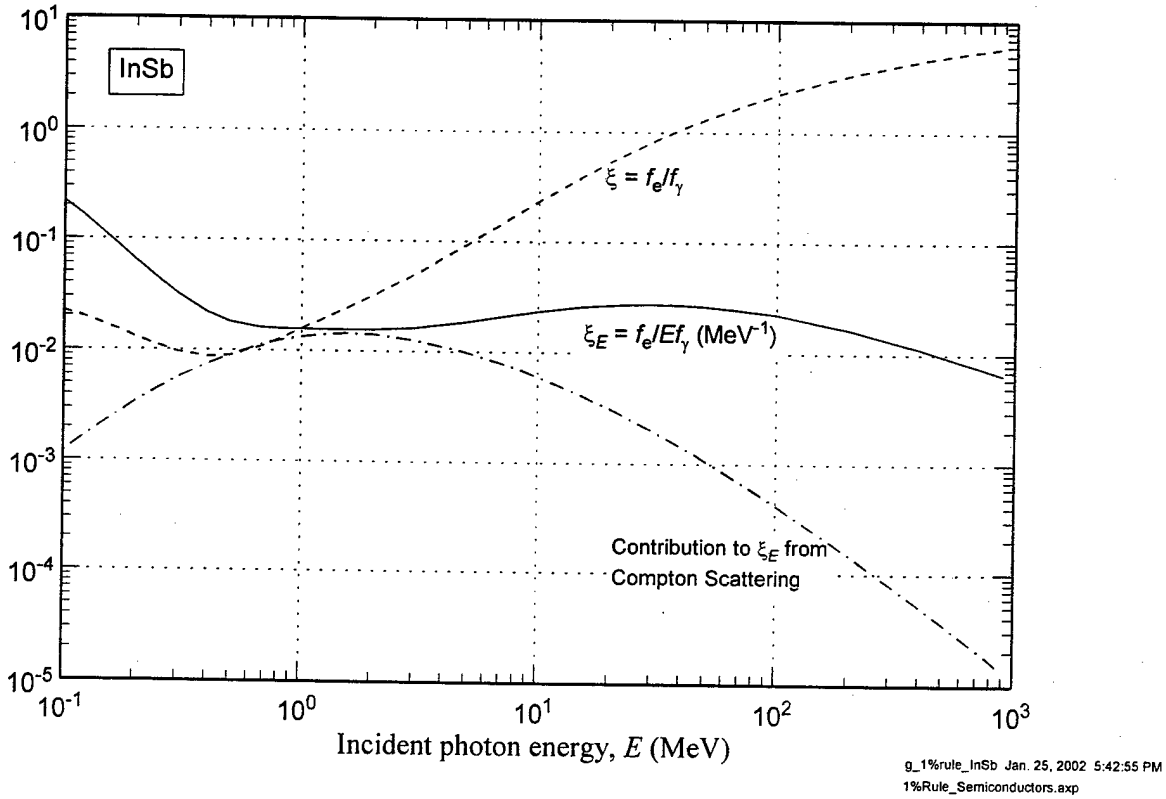

Figure 2.66 The "1% Rule" in InSb. Assumes charged particle equilibrium, and includes positron flux from pair production

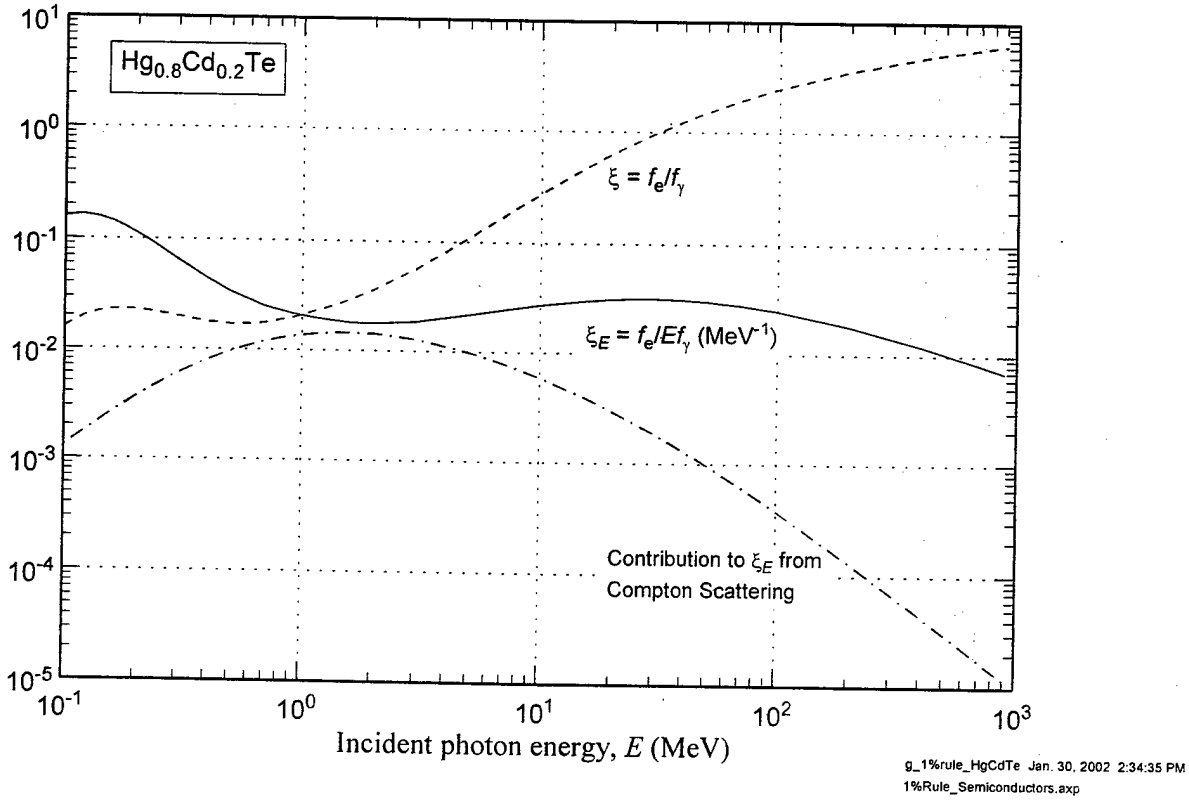

Figure 2.67

The "1% Rule" in $Hg_{1-x}Cd_xTe$ for x=0.2. Assumes charged particle equilibrium, and includes positron flux from pair production. Results are not very sensitive to x near x=0.2.

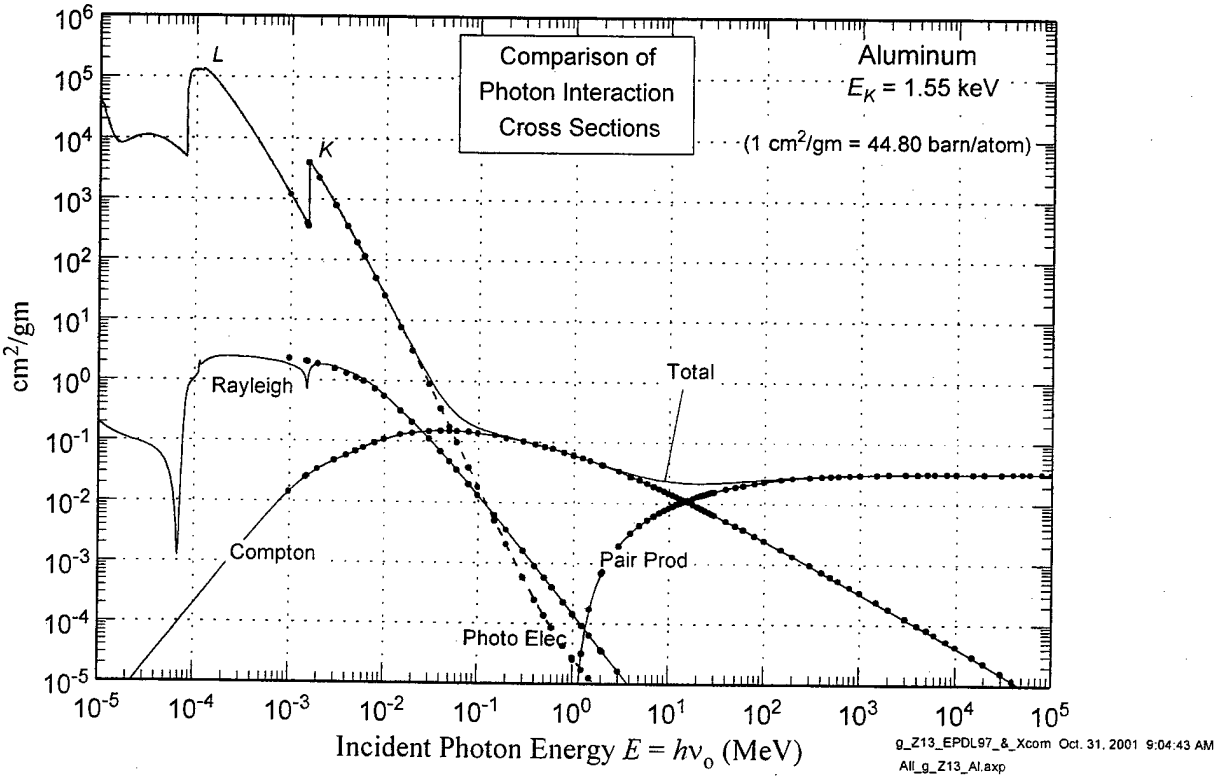

Figure 2.68 Comparison of cross section databases. Solid lines: EPDL97. Dots: NIST XCOM.